EGGSHELL CATALYST FOR HYDROCARBON SYNTHESIS:
KINETIC MODELING AND REACTOR PERFORMANCE

by

Enzo Peluso

Department of Chemical and Biochemical Engineering
Faculty of Engineering Science

Submitted in partial fulfillment
of the requirements for the degree of
Master of Engineering Science

Faculty of Graduate Studies
The University of Western Ontario
London, Ontario
August, 1998

ABSTRACT

The synthesis of middle distillate hydrocarbons via Fischer-Tropsch (FTS) is a process strongly influenced by intra-catalyst mass transport limitations. This is due to the slow diffusion of high-molecular-weight paraffins inside the catalyst pores.

The present study considers "eggshell" catalysts reducing transport restrictions and therefore increasing reaction rates and C_5^+ selectivity. Cobalt-zirconium eggshell catalysts were prepared, characterised and tested for the production of heavy paraffinic oils via FTS. A standard (uniformly impregnated) catalyst was also considered as a reference. Characterization was performed using BET surface area, Temperature Programmed Reduction (TPR), Atomic Adsorption (AA), and Optical Microscopy. Reaction testing was developed in an internally recycled Berty reactor at 210 °C and 1.52 MPa, using a stoichiometric feed of $H_2/CO = 2.0$ with a gas hourly space velocity (GHSV) of about 350 h^{-1}. Evaluation of eggshell catalysts revealed a higher carbon monoxide conversion (per metal site) than the standard catalyst. There were also significant gains in product hydrocarbon distribution within the C_{10}-C_{20} paraffin hydrocarbon range.

Following this, the effect of various operating conditions such as temperature, pressure, GHSV and H_2/CO inlet ratio on the eggshell Co-Zr catalyst performance was evaluated. It was found that the type of catalyst selected and the operating conditions have an important effect on CO conversion, product selectivity and hydrocarbon distribution. On this basis a

suitable kinetic model was developed. This kinetic model was further applied to the simulation of a multi-tubular fixed-bed reactor for converting synthesis gas via FTS process.

The FTS is a highly exothermic reaction requiring efficient heat removal. The present study considers the Pseudo-adiabatic operation (PO), a new mode of operation for multi-tubular fixed-bed catalytic reactors. With this end in view, a one-dimensional pseudo-homogeneous model was solved numerically for various reactant and coolant temperatures, coolant and reactant flows and total pressures. Two characteristic regimes were identified: a) temperatures showing a maximum at a finite axial reactor position (hot spots inside the unit or MFARP), b) temperature always increasing with the axial reactor coordinate (PO). Simulation results demonstrate that the PO is a viable operation regime for a FTS based on the use of an "eggshell" catalyst.

DEDICATION

"Discovery is not only finding new things but looking at old things with new eyes"

Dedico esta tesis a mi familia, mi esposa Carmen y a mis hijos Alexander y Andrés. Sin ellos todo esto no hubiera sido posible y más aún sin su apoyo y esfuerzo no hubiese tenido el mismo sentido. Quiero además dedicar esta tesis a mis padres Salvador y Margarita mis maestros en la vida. A ellos estoy infinitamente agradecido.

ACKNOWLEDGMENTS

I wish to express my sincere gratitude to Prof. H. I. de Lasa for giving me the opportunity to complete graduate studies under his supervision. His support, advice and patience during all these years are really appreciated.

Special thanks must also go out to Souheil Afara for his constant presence and his motivation to help other people.

Also I want to express my thanks to all the fellow graduate students, past and present, for their friendship and their support.

Sincere thanks to the staff of Mechanical shop of Engineering Science, everyone in Engineering Stores, and the staff of the Engineering Library, and in particular, Eva, Mary and Teresa for their constant and valuable help.

And at last but not the least, I like to express my sincere gratitude to INTEVEP S. A, for awarding me the scholarship to perform this program. At INTEVEP special thanks go out to Dr Daysi Rojas, Dr Maria di Marco and Dr Magdalena Ramirez for their support and help. Final words of thanks for all the people at INTEVEP who encouraged us to take this adventure.

TABLE OF CONTENTS

LIST OF TABLES

LIST OF FIGURES

LIST OF APPENDICES

NOMENCLATURE

		[-]
a	Kinetic parameter	[depends on rate model]
A	ρ_b P M/(u_s ρ_g) parameter used by the one-dimensional model (equation 3.21)	[Mpa ($kg_{cat.}$) $kmol^{-1}$ m^{-1}
AA	Atomic Adsorption	[-]
A_p	Area of the peak (chromatograph)	[-]
ARF	Calibrated TCD response factor	[area/mole]
ASF	Anderson-Schultz-Flory distribution	[-]
b	Adsorption-desorption equilibrium constant	[depends on rate model]
B	(-ΔH) ρ_b/(u_s ρ_g c_{pg}) parameter used by the one-dimensional model (equation 3.22)	[$kg_{cat.}$. h K $kmol^{-1}$ m^{-1}]
BET	Brunauer-Emmett-Teller, method for measuring surface area	[-]
Bi	Biot number, B_i = (α_w R)/k_{er}	[-]
c	Adsorption-desorption equilibrium constant	[depends on rate model]
C	2 U/(u_s ρ_g c_{pg} R) parameter used by the one-dimensional model (equation 3.23)	[m^{-1}]
C^0_{CO}	Inlet carbon monoxide concentration	[mol / mol]
C^0_{H2}	Inlet hydrogen concentration	[mol / mol
C_1	Methane	[-]
C_{10}-C_{20}	Hydrocarbon fraction from decane to eicosane	[-]
C_{21}^+	Hydrocarbon fraction with 21 or more carbon atoms	

C_2-C_4	Hydrocarbon fraction from ethane to butane	[-]
C_5-C_9	Hydrocarbon fraction from pentane to nonane	[-]
C_{CO}	Carbon monoxide concentration	[mol / mol
C_{H2}	Hydrogen concentration	[mol / mol
C_i	Hydrocarbon with i carbon atoms	[-]
C_p	Heat capacity	[KJ Kg^{-1} K^{-1}]
CREC	Chemical reactor Engineering Centre (Univ. of Western Ontario)	[-]
d	Adsorption-desorption equilibrium constant	[depends on rate model]
D	$2 \Pi R t_n/(W_c C_{pc})$ parameter used by the one-dimensional model (equation 3.24)	[m^{-1}]
D_{er}	Effective radial diffusivity	[m h^{-1}]
d_p	Diameter of catalytic pellets	[m]
E, E_a	Activation energy	[KJ mol^{-1}]
F	Molar flow	[Kmol/h]
FID	Flame Ionization Detector	[-]
FTS	Fischer-Tropsch synthesis	[-]
GC	Gas Chromatograph	[-]
GHSV	Gas hourly space velocity (STP condition)	[cm^3 cm^{-3} cat h^{-1}]
h_{out}	Heat transfer coefficient, shell side	[KJ m^{-2} h^{-1} K^{-1}]
K	Thermal conductivity	[KJ m^{-1} h^{-1} K^{-1}]

k_1	Propagation step	[-]
k_2	Termination step	[-]
k_A	(pseudo) adsorption equilibrium constant for species A (A= CO or A= H_2)	[depends on rate model]
k_{co}	First-order rate constant for CO conversion	[depends on rate model]
k_{emp}	Empirical rate constant	[depends on rate model]
k_{er}	Effective radial thermal conductivity	[KJ m^{-1} h^{-1} K^{-1}]
Ki	Adsorption-desorption equilibrium constant for i^{th} process	[depends on rate model]
K_o	Frecuency factor	[depends on rate model]
M	Molecular weight (average of the mixture)	Kg/Kmol
MFARP	Maximum at a finite axial reactor position	[-]
n	Carbon number	[-]
N_{PRATER}	Prater number = $(-\Delta H\ C_s\ D_{eff})/(K_{eff}\ T_s)$	[-]
P	Total pressure	[MPa]
p_{CO}	Partial pressure of CO in the reactor	[MPa]
Pe_{mr}	Peclet number for radial dispersion of mass	[-]
p_{H2}	Partial pressure of H_2 in the reactor	[MPa]
P_n	Partial pressure of nitrogen	[mmHg]
P_{no}	Saturation pressure of nitrogen	[mmHg]
PO	Pseudoadibatic operation	[-]

Pr	Prandtl number, $Pr = (Cp_{(i)}\ u_{(i)}) / k_{(i)}$; where i = g, c	[-]
R	Reactor radius	[m]
$-r_{H2+CO}$	Rate of disappearance of hydrogen plus carbon monoxide	mmol/min/g of catalyst
R_1	Gas constant	[Kj/kmol/K]
$-r_{CO}$	Rate of disappearance of carbon monoxide	mmol/min/g of catal
Re	Reynolds number	[-]
STD	Standard deviation	[-]
STP	Standard temperature and pressure	[-]
T	Average temperature for the cross section	[K or °C]
T^*	Temperature at reactor centerline	[K or °C]
t/a	Annual ton.	
T_{av}	Average temperature	[K]
TCD	Thermal Conductivity Detector	[-]
tn	Number of tubes in a multitubular unit	[-]
TPD	Temperature Programmed Desorption	
TPR	Temperature Programmed Reduction	[-]
U	Overall heat transfer coefficient	[KJ h^{-1} m^{-2} K^{-1}]
u_s	Superficial velocity	[m h^{-1}]
V_m	Volume of the monolayer of nitrogen	[cm^3]
V_n	Volume nitrogen	[cm^3]

V_{STP}	Volume of nitrogen at standard temperature and pressure	[cm^3]
W	Mass flow rate	[kg h^{-1}]
Wcat	Weight of catalyst	[g]
W_n	Weight fraction of the carbon atoms within chains containing "n" carbon number	[-]
wt%	Percentage by weight	[-]
x	Extent of reaction	[Kmol Kg^{-1} s^{-1}]
z	Axial coordinate	[m]

Subscripts

a	axial
b	bed
c	coolant
g	gas phase
i	reacting species
o	reactor inlet
p	particle
r	radial
tot	tot

Superscripts

a	kinetic parameters, E/R_1 (K)
b	natural logarithm of pre-exponential factor
c_i	surface coverage
d_i	surface coverage
m	reaction order

n	reaction order	
T	Temperature (K)	

Greek Symbols

α_w	heat transfer coefficient near the wall	[KJ m^{-2} h^{-1} K^{-1}]
ρ	density	[Kg m^{-3}]
μ	viscosity	[Kg m^{-1} h^{-1}]
ΔH	enthalpy of reaction	[KJ Kg^{-1} mol^{-1}]
∞	at infinite reactor length, $z \rightarrow \infty$	[-]
α	Chain growth probability	[-]
ΔT	Temperature gradient	[K]

CHAPTER 1

INTRODUCTION

In 1973, the oil crisis prompted considerable world interest in the production of liquid fuels. A major reason for this was the vital importance of reliable supplies of liquid hydrocarbons to the industrialized world. As a result, the Gulf crisis accelerated the search for alternate and economic energy sources.

Coal and natural gas world reserves are far in excess of those of crude oil and this creates an incentive for the conversion of coal and natural gas into transportation fuels.

Because of the vast coal reserves, much attention was initially paid to the development of indirect coal liquefaction, coal gasification followed by hydrocarbon synthesis. However, the high level of capital investment involved and the environmental problems associated with are still major barriers on the commercial application of the process.

On the other hand, natural gas is well known as a clean, efficient energy source. As well the evolution of proven natural world gas reserves, about 4000 trillion cubic meter (Wender, 1996), shows an expected shift towards the use of natural gas as a feedstock for manufacturing transportation fuels and even petrochemicals on a large scale.

Recognition of this situation led to an increased interest in new emerging technologies, which can efficiently convert natural gas into liquids and higher added-value-products. Most of these technologies involve the initial conversion of natural gas into syngas, a mixture of hydrogen and carbon monoxide, followed by additional processes to obtain the desired liquid products.

The principal uses of syngas are given in Figure 1.1. The major commercial, near commercial and potential commercial chemical uses of syngas are outlined in Figure 1.2.

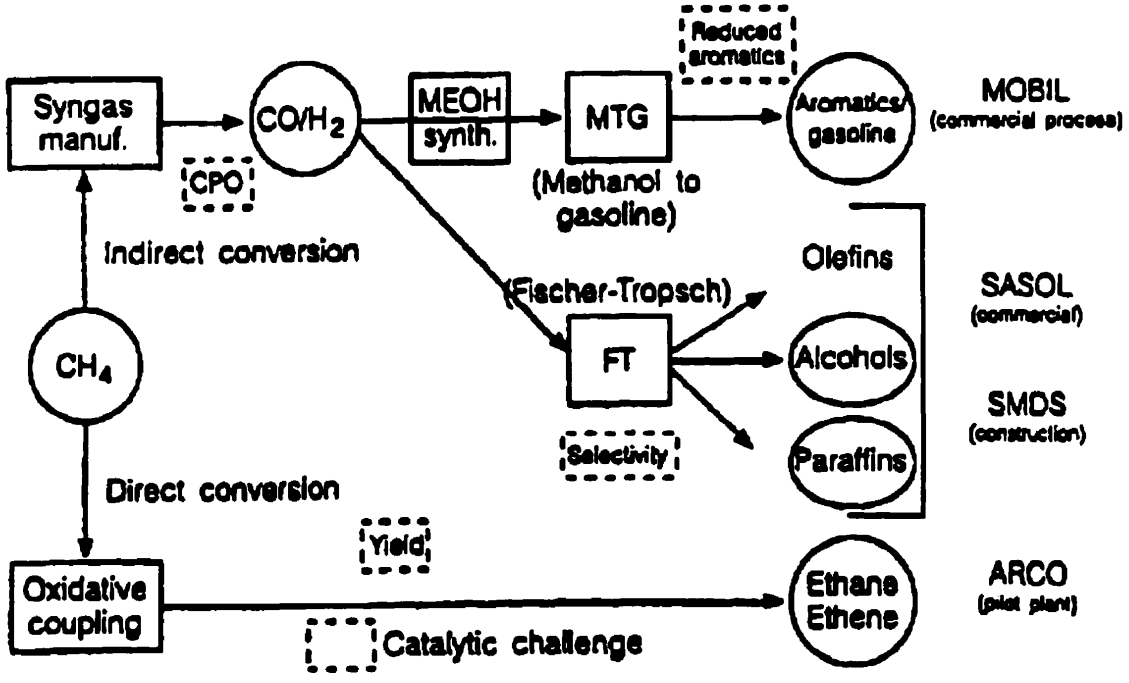

Figure 1.1. Principal commercial uses of synthesis gas (Maxwell and Naber, 1992)

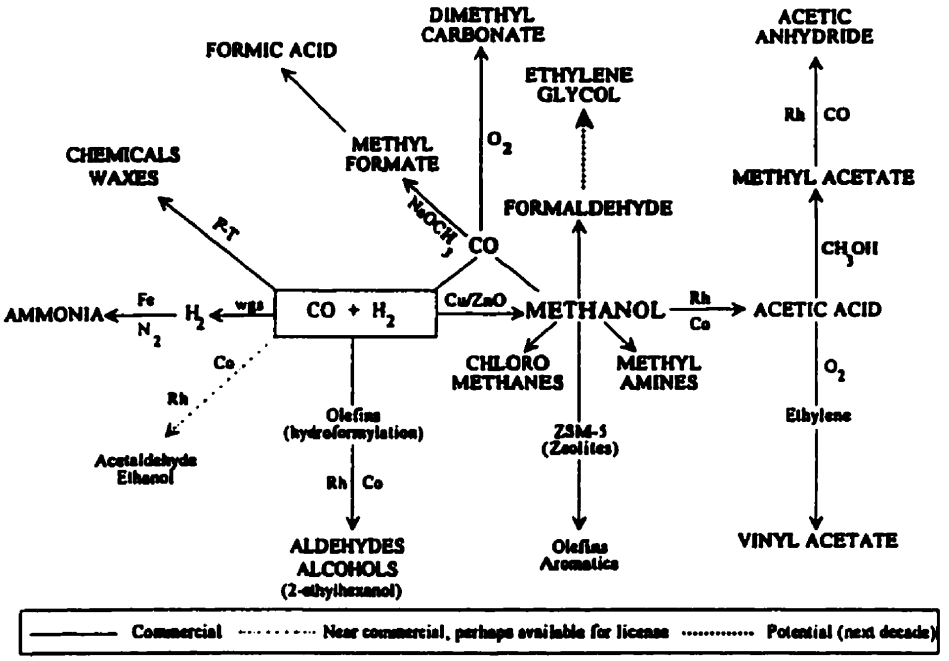

Figure 1.2. Commercial, near commercial and potential chemicals from synthesis gas (Wender, 1996)

For more than sixty years, hydrocarbons synthesis via FTS has been considered as an attractive technological option for fuel production. Following the 1973 and 1987 oil crises, FTS has been revitalized given it provides one of the best alternatives for clean fuels (Siri *et al*, 1993).

The FTS is usually carried out using iron, cobalt or ruthenium catalysts. In cases where Fischer-Tropsch has been used at the industrial scale, iron (or cobalt) is the essential catalyst component. Hydrocarbons are formed by a chain growth mechanism, which follows the Anderson-Schultz-Flory (ASF) distribution.

It has to be mentioned that recent developments, in the Fischer-Tropsch technology, are focused on the production of high molecular, straight chain waxes, which in turn can be hydrocracked to products in the middle distillate range. A key element in this innovation is the development of new and more active cobalt catalysts (Wender, 1996).

It has been apparent that, in the Fischer-Tropsch synthesis conducted in the solid-catalyzed gas-phase reaction system (fixed bed/gas phase reactors), the iron (or cobalt) based catalysts operate under diffusion limitations. This is presumably due to the formation of condensed hydrocarbons. This condensed phase fills the pores of the catalyst and limits intraparticle mass transfer (Post *et al.*, 1989). Liquid diffusivities are typically 10^3 to 10^4 times smaller than gas diffusivities (Reid *et al.*, 1987).

Several experimental studies (Iglesia *et al.*, 1991; Sie *et al.*, 1991 and Post *et al.*, 1989) describe the role of transport restrictions on FTS. These studies indicate that transport limitations influence considerably hydrocarbon synthesis rates and selectivity with two major diffusional effects identified: a) slow removal of reaction products from catalyst pellets, b) delayed arrival of reactants to the catalytic sites.

Thus, design of catalysts able to prevent or minimize these effects is a most interesting research subject. Eggshell catalysts, where the active metal (Fe or Co) is located preferentially near the outer pellet surface can be a solution to this problem. The eggshell catalyst reduces the severity of

these transport limitations and leads to higher synthesis rates and C_5^+ selectivity. Note that the benefits of non-uniform intrapellet site (catalytic site) distributions have been previously reported for other catalytic reactions (Lee and Aris, 1984; Iglesia *et al.*, 1995).

Another important matter concerning FTS is given by the very exothermic character of this reaction taking place in a relatively narrow temperature range (Senden *et al.*, 1992). So, when the FTS is conducted in a solid-catalyzed gas-phase reaction system, the FTS is accompanied by local overheating of the catalyst. Local overheating of the catalysts may lead not only to catalyst deactivation but also to an increase in methane selectivity (Adesina, 1996). Thus, an efficient and rapid system for the removal of the large heat of reaction ($-\Delta H = -(165 - 240)$ kJ/mol) is a major factor in the design of FTS reactors.

Some of the earliest FTS processes employed a multitubular fixed bed reactor with a hot gas recycle, similar to those employed for ammonia production. These reactors usually have "hot spots", which may lead to "runaway" reactions producing catalyst attrition and carbon deposition.

A mode of operation for exothermic reactions the so-called Pseudoadiabatic Operation has been developed in order to control, in multitubular fixed bed reactors, runaway behavior (de Lasa *et. al.*, 1982).

The Pseudoabatic Operation (PO) is a mode of operation for packed-bed catalytic reactors where a gradual increase of the axial reactor

temperature takes place while the reactor is being cooled concurrently. This reactor design was invented by UWO researchers (de Lasa, 1990; de Lasa, 1987; de Lasa, *et al.*, 1986; Soria Lopez *et al.*, 1981) and successfully tested for methanol-to-gasoline (MTG) reaction (de Lasa, *et al.*, 1989; Ravella, *et al.*, 1989; Ravella, 1987; Ravella, and de Lasa 1987b; Ravella, and de Lasa, 1987a) and for the conversion of synthesis gas into gasoline range products (Simard *et. al.*, 1991; and Simard, 1991).

This type of operation has demonstrated intrinsic advantages, such as a) better control of temperature distribution, b) thermal symmetry (all tubes in the multitubular unit have the similar temperature profile), c) less parametric sensitivity, and d) adequate product distribution.

Given these facts it is the goal of this study to examine the suitability of the PO reactor for FTS using eggshell catalysts. Kinetics models, to be used in the simulation, are going to be the ones developed in the context of the present research.

CHAPTER 2

SCOPE OF THE RESEARCH

A main goal for this thesis is the demonstration of the viability of the Pseudoadiabatic reactor for the conversion of syngas (carbon monoxide plus hydrogen) into middle distillate hydrocarbons (C_{10}-C_{20}) using a Fischer-Tropsch Synthesis catalyst based on the eggshell design.

With this end in view the present thesis was organized as follows:

- Selection and Development of the appropriate catalytic materials for FTS.

  It was expected this task should include the methods for preparation and characterization of the selected eggshell catalysts based on cobalt/zirconium supported on silica.

- Study of the influence of operating conditions on the performance of the eggshell cobalt-zirconium catalyst using a Berty reactor.

  It was planned that this reaction testing could provide information about CO conversions, product and hydrocarbon distribution. It was also envisioned that this data could help clarify the ability of the eggshell catalyst to yield

significant fractions of paraffinic hydrocarbons in the middle distillate range (C_{10}-C_{20}).

- Design and development of an experimental plan. Kinetic Modelling.

  There was expectation that the experimental plan of the present study was going to be suitable for the development of a kinetic expression adequate for the calculation of reaction rates and reaction rate parameters for eggshell catalysts.

- Computer modelling of the pseudo-adiabatic reactor using an egg shell catalyst.

  For this topic of the study, there was the intent that a numerical simulation of a continuous fixed bed catalytic reactor based on a pseudo-homogenous model was going to confirm the value of the pseudo-adiabatic regime for FTS. It was also part of this plan to incorporate kinetic models, also developed in the present study, as main tools for reactor modelling and reactor simulation.

CHAPTER 3

LITERATURE SURVEY

3.1. Introduction

The conversion of synthesis gas to hydrocarbons (higher paraffin) has been extensively covered in the technical literature during the last fifteen years. In this respect, particular emphasis has been given to the matters concerning the Fischer-Tropsch synthesis (FTS) process in fixed bed catalytic reactors.

In the first section of this literature review, the Fischer-Tropsch synthesis (FTS), its selectivity problems and the Fischer-Tropsch processes will be briefly reviewed. Following this, the important questions of reactor configuration, non-adiabatic reactor designs and the specific pseudoadiabatic reactor will be discussed. Finally, a review on the modeling and on the simulation of a fixed-bed reactor under pseudoadiabatic operation will be presented.

3.2. Historical Background

The Fischer-Tropsch (FT) process was the first one used to convert syngas to liquid fuels in a commercial scale. In 1902, Sabatier and Senderens reported the synthesis of methane from carbon monoxide and hydrogen in the presence of nickel and cobalt catalysts. In 1913, BASF obtained patents for the manufacture of liquid hydrocarbons from synthesis gas at high pressure, mostly on oxide catalysts. In 1923 Franz Fischer and

Hans Tropsch synthesized higher hydrocarbons using iron and cobalt at low pressure. Several countries, including England, Japan and United States, initiated studies on the Fischer-Tropsch Synthesis (FTS) as early as 1926 (Wender, 1996).

In 1931, Fischer and K. Meyers developed Ni-ThO_2-Kieselguhr and Co-ThO_2-kieselguhr catalysts for FTS. From 1935 to 1945 the FTS was operated commercially in Germany using Co catalysts. It was found that the best performance of the catalysts was achieved when the reactor was operated in the middle pressure range, 0.5-2.0 KPa. After World War II, cobalt catalysts were replaced however, with alkalized iron catalysts for economic reasons (Anderson, 1984).

The manufacture of FT products, in Germany, during World War II, reached a maximum development in early 1944, mainly in the form of motor fuels. After the war the process was further developed and especially on its medium-pressure version using fixed-bed reactors (ARGE). In 1950, a fluidized-fixed bed process for the FTS, developed by Hydrocarbon Research, was installed in Texas. Syngas was obtained by reforming natural gas. The plant operated only briefly as the increase in natural gas prices made it uneconomical (Anderson, 1984).

At about the same time, in South Africa, the Sasol FT plants were built and their commercial operation started in 1955. Two types of reactor

were used: ARGE fixed-bed and Kellog's circulating-fluid bed reactors (Anderson, 1984).

The oil crisis of 1973 initiated quite a number of new developments to convert unconventional feedstocks to hydrocarbon products. As a result of that, in the late 1970s Sasol started building two new plants, which became operational in the early 1980s.

In 1985, Shell announced the development of a two-step process for middle distillate synthesis (SMDS). In the first step, the Fischer-Tropsch synthesis was carried out in a fixed-bed reactor using a cobalt based catalyst. The FTS was operated under conditions where production of higher hydrocarbons (waxes) were favoured. The second step was a mild, trickle-flow hydrocracker handling the wax fraction and producing middle distillates (Sie *et al.*, 1991).

In New Zealand, a methanol plant operating on natural gas and based on Mobil's MTG technology (Mobil methanol-to-gasoline) came on stream in 1985. First the syngas produced from natural gas is converted to methanol. Following this, methanol is transformed into gasoline via the MTG process (Wender, 1996).

3.3. Synthesis Gas Conversion into Higher Paraffins.

Synthesis gas (syngas), a mixture of hydrogen and carbon monoxide, can be manufactured mainly from coal, natural gas and petroleum. Syngas is, at the present time, increasing its importance as a source of environmentally clean

fuels and chemicals. Different alternatives have been considered for the effective utilization of syngas: methanol manufacturing and FTS (Wender, 1996).

The Fischer-Tropsch synthesis is essentially a polymerization process. Perhaps a better definition is to consider FT as an oligomerization, since in most cases the average molecular weight of the product is not very high. Carbon-carbon bonds are formed between C atoms proceeding from carbon monoxide, under the influence of hydrogen and a metal catalyst. This also leads to the formation of water by an elimination reaction.

Without willing to provide a detailed discussion of the reaction mechanism, the main reaction of the Fischer-Tropsch (FT) synthesis may be represented as:

$$n\,CO + 2n\,H_2 \rightarrow (-CH_2-)_n + n\,H_2O \qquad (3.1)$$

Proper selection of catalysts (iron, cobalt, nickel, and ruthenium) and reaction conditions, yields a variety of products such as: paraffins, olefins, and oxygenates (alcohols, aldehydes, ketones, acids, and esters) (Röper, 1983).

Fischer-Tropsch liquids obtained using cobalt catalysts can be considered equivalent to very paraffinic natural petroleum fractions. However, the FTS products are not a so complex mixture. Straight chain saturated aliphatic molecules and mono-olefins are typical FTS constituents with alcohols, fatty acids, and other oxygenated compounds representing less than 1% of the total liquid product (Kirk-Othmer, 1986).

The molecular weight distribution of FTS products can be described with relatively simple equations, originally developed for polymerization processes. These equations consider the probability of chain growth and chain termination (Snel, 1987). Röper (1983) postulated a mechanism in which after each incorporation of a C_1 monomer, derived from CO, a further propagation step may occur. These two steps, propagation and termination, may occur with different rate constants, k_1 and k_2, as illustrated bellow:

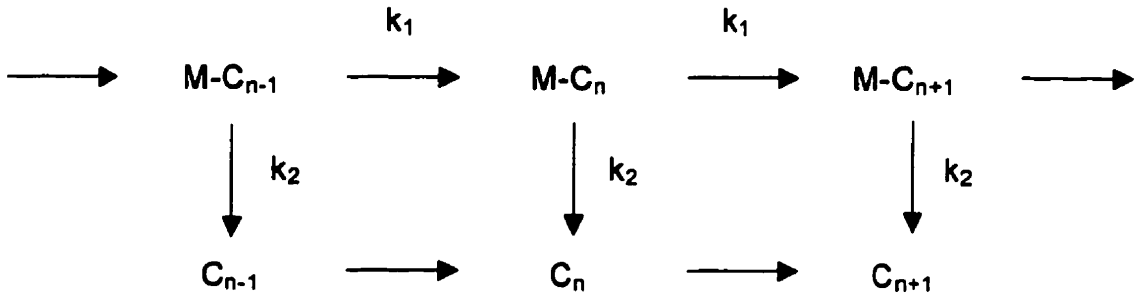

In this simplified scheme it is assumed that under steady-state conditions, k_1 and k_2 are independent of chain length with C_1 being the monomer inserted (Röper, 1983).

Under these conditions the carbon-number distribution of FT products can be described by the so-called Anderson-Schultz-Flory (ASF) distribution in which W_n, fraction of molecules having n carbon atoms, decreases according to a geometric progression.

$$W_n = n(1-\alpha)^2 \alpha^{n-1} \qquad (3.2)$$

Note that the distribution function (Eq. 3.2) contains a simple α parameter which is equal to $k_1/(k_1+k_2)$.

Moreover, Eq. (3.2) can also be written in the logarithmic form as:

$$\log\frac{W_n}{n} = n\log\alpha + \log\frac{(1-\alpha)^2}{\alpha} \qquad (3.2a)$$

Therefore, the slope of a plot of log (Wn/n) versus "n" gives the "log α" or α, the chain growth probability (Iglesia *et al.*,1992). This relationship is illustrated in Fig. 3.1 for a variety of industrial catalysts.

It is important to mention that the ratio k_1/k_2, which can be obtained from the slope log α of Fig 3.1, provides an indication of the distribution of molecular weights synthesized. If $k_1 << k_2$, $\alpha \rightarrow 0$ and correspondingly (– log α) is very large, then essentially low molecular weight products such as methane or C_2-C_4 are formed. On the other hand, if $k_1 \approx k_2$, $\alpha \rightarrow$ ½ and (– log α) is in the middle range. This yields oligomers with a wider distribution, e.g. C_1....C_{15}. Finally, if $k_2 << k_1$, then $\alpha \rightarrow 1$, and (– log α) $\rightarrow$ 0. In this last case the reaction produces a very wide distribution including high molecular weight products like paraffinic oils and waxes.

An important consequence of the sequential chain-growth mechanism is that is not possible to exclusively synthesize a paraffin of a particular carbon number or to synthesize a paraffin fraction of a specified narrow range of chain lengths (refer to Fig. 3.2). The only exceptions to this

rule are the single-carbon products methane and methanol, which can be obtained with high selectivity.

It is important to mention that once the α parameter or (-log α) is set, the whole product distribution is determined (Röper, 1983).

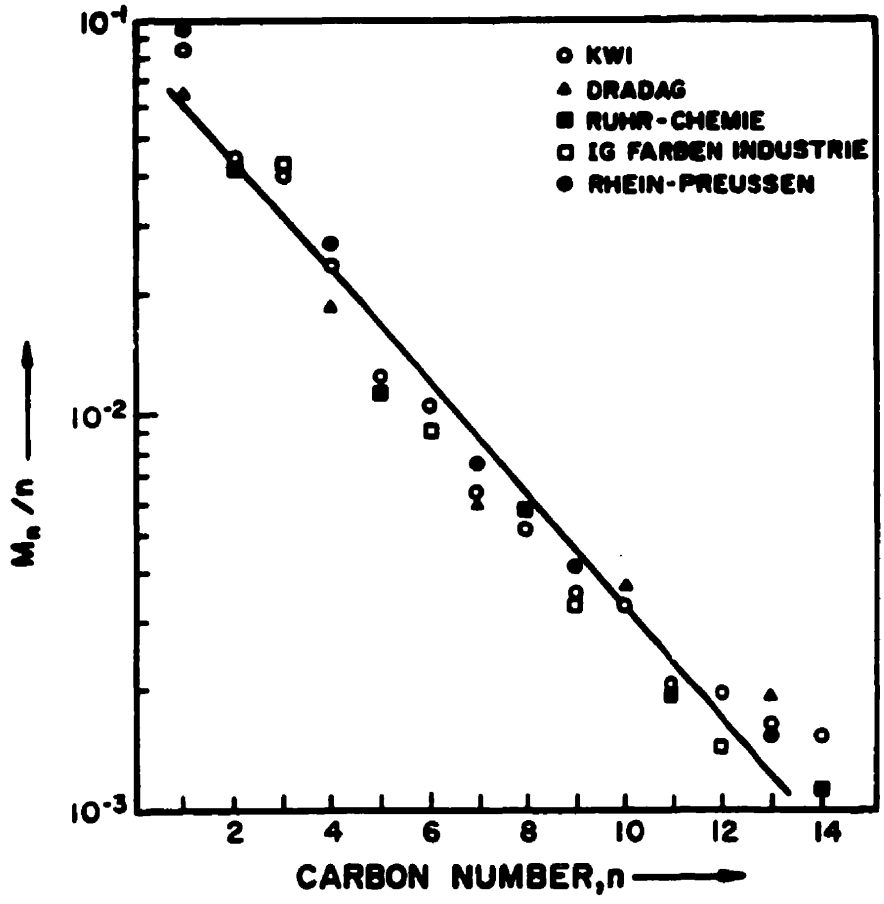

Figure 3.1. Product distribution found for industrial catalysts tested under FTS conditions (Röper, 1983).

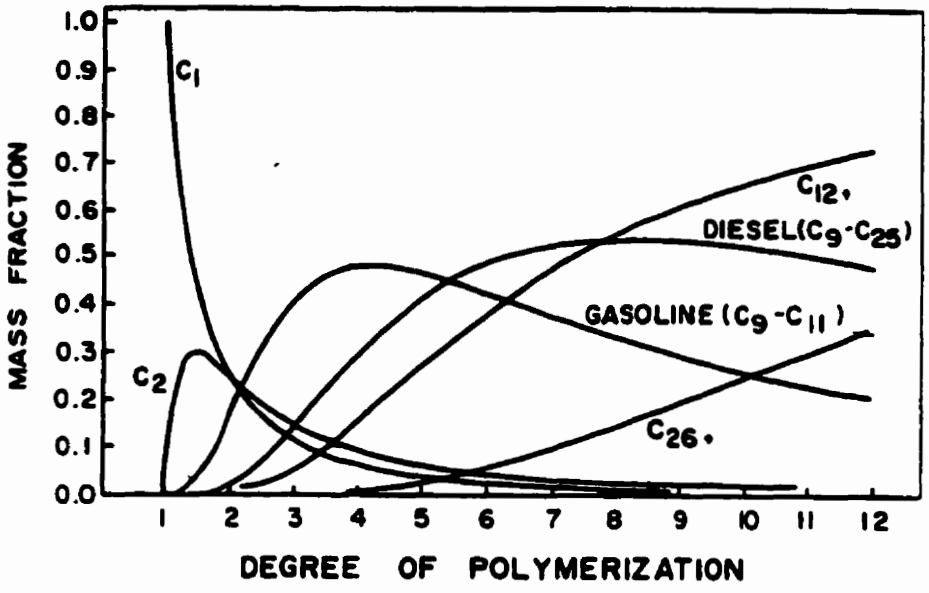

Figure 3.2. Selectivity limitations on Fischer-Tropsch synthesis as determined by the ASF distribution function (Röper, 1983).

Thus, the FT reaction invariably gives rise to a product, which is a complex mixture of light and heavy hydrocarbons. However, this product distribution can be changed within the constraints of this model (ASF model) by the appropriate choice of catalyst, reactor and operating conditions. Therefore, the value of the "α" parameter can be shifted, and accordingly different hydrocarbon product ranges can be obtained.

As illustrated in Fig. 3.3, it is possible to obtain, using different catalytic formulations and operating conditions, α-values varying from 0.71 to 0.93.

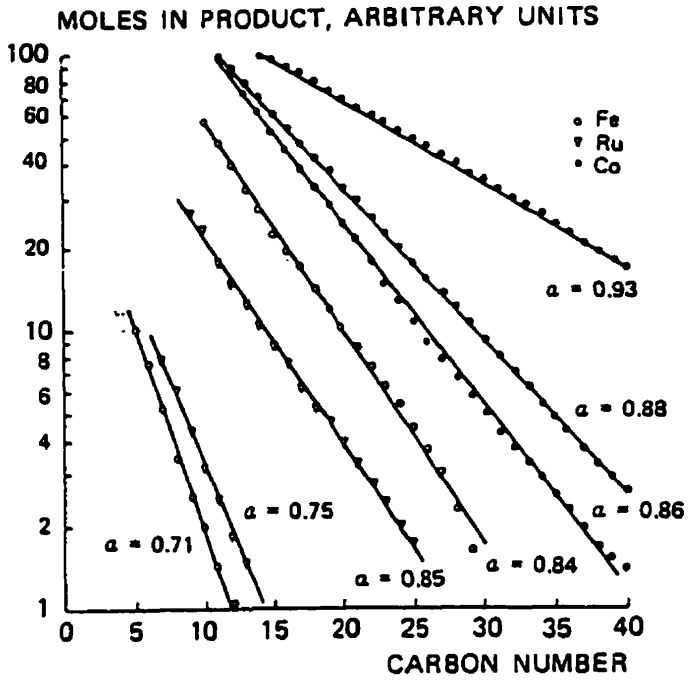

Figure 3.3. Typical carbon number distributions for various catalytic systems and operating conditions. (Sie *et al.*, 1991).

Deviations from the ASF distribution are possible if secondary reactions, such as cracking on acidic supports or insertion of product olefins into the growing chain, occur. This behavior (Fig. 3.4) has been explained considering two possible types of catalytic sites leading to different hydrocarbon chain formation, each one with a slightly different value of the chain growth probability (Huff and Satterfield, 1984). As a result superposition of distributions with different α parameters creates a deviation from the classical ASF.

Recently, using Ru (and Co) catalysts, a non-ASF distribution has been associated to diffusional problems. It is believed that the transport-limited

removal of α-olefins from catalyst pellets enhances re-adsorption rates (Iglesia *et. al*, 1991). In this respect, it has been suggested that the long chains α-olefins are re-adsorbed with only a negligible amount of the short α-olefins following re-adsorption steps. All this yields a net chain growth probability, which is higher for high carbon numbers and causes as a result a larger C_{10}^{+} selectivity than the ones predicted by a simple ASF distribution (Kuipers *et al.*, 1995).

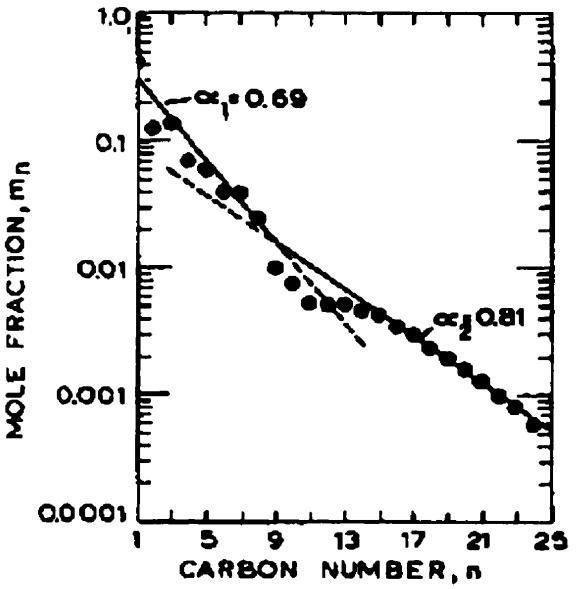

Figure 3.4. ASF distribution for a nitride fused-iron catalyst (Huff and Satterfield, 1984)

3.4. General Aspects of the Fischer-Tropsch synthesis

3.4.1. Stoichiometry and Thermodynamics

A large number of reactions occur during FTS. These reactions can be represented by a number of stoichiometric equations whose relative importance depend on catalysts used and reaction conditions adopted (Röper, 1983).

Hydrogenation of carbon monoxide in the presence of cobalt or ruthenium catalysts can be represented by eq (3.3). Note that the hydrocarbon synthesis is generally accompanied by the production of water:

$$CO+2H_2 \rightarrow -(CH_2)-+H_2O \qquad (\Delta H_{R(227\,^{\circ}C)} = -165\ kJ) \qquad (3.3)$$

In the presence of iron catalysts, however, carbon dioxide formation becomes more significant,

$$2CO+H_2 \rightarrow -(CH_2)- + CO_2 \qquad (\Delta H_{R(227\,^{\circ}C)} = -205\ kJ) \qquad (3.4)$$

In practice, eqs (3.3) and (3.4) are linked via the water gas shift reaction:

$$CO + H_2O \rightarrow CO_2 + H_2 \qquad (\Delta H_{R(227\,^{\circ}C)} = -40\ kJ) \qquad (3.5)$$

Linear combination of eqs. (3.3), (3.4) and (3.5), gives two equations as follows:

$$3CO+ H_2O \rightarrow -(CH_2)- + 2CO_2 \qquad (\Delta H_{R(227\,^{\circ}C)} = -245\ kJ) \qquad (3.6)$$

$$CO_2+3\ H_2 \rightarrow -(CH_2)- + 2\ H_2O \qquad (\Delta H_{R(227\,^{\circ}C)} = -125\ kJ) \qquad (3.7)$$

Eq (3.6) describes the hydrocarbon synthesis from carbon monoxide and water vapor, also known as Kölbel-Engelhardt synthesis, while eq (3.7) represents the hydrogenation of carbon dioxide.

Morever, the undesired formation of methane and carbon deposition (Boudouard equilibrium) can also contribute to the FT synthesis.

$$CO + 3H_2 \rightarrow CH_4 + H_2O \qquad (\Delta H_{R(227\,^{\circ}C)} = -215\ kJ) \qquad (3.8)$$

$$2CO \rightarrow C + CO_2 \qquad (\Delta H_{R(227\,^{\circ}C)} = -134\ kJ) \qquad (3.9)$$

It is known, however, that in the temperature range commonly used for FT synthesis, the selectivity, found in practice, is quite different from the one expected from thermodynamic calculations (Dry, 1981). Consequently, these reactions are obviously kinetically controlled and the product distribution may be strongly influenced by catalysts selected as well as by reaction conditions adopted.

The synthesis of hydrocarbons from CO and H_2 is, under the usual reaction conditions, a strongly exothermic reaction, generating in the range 146-176 kJ per mole of CO (Storch *et al.*, 1951). Since the product distribution depends significantly on the reaction temperature, heat removal is a very important factor in reactor design. Also, excessive catalyst temperatures can lead to undesirable products, carbon deposition, and catalyst deactivation or even catalyst disintegration.

Anderson (1984) has given an excellent summary of the thermodynamics of the FT synthesis. The following major conclusions can be drawn as follows: a) Methane production is always thermodynamically preferred over reactions producing alcohols, alkenes, and higher alkanes; and b) Selectivity towards these products follows generally the order: alkanes > alkenes > alcohols.

3.4.2. Fischer-Tropsch Mechanisms

A basic problem of the Fischer-Tropsch synthesis is the control of product selectivity and this is closely related to the reaction mechanism. One of the earliest mechanisms proposed in 1926 is the surface carbide hypothesis by

Fischer and Tropsch (Storch, *et al.*, 1951). It was argued that the formation of olefinic and paraffinic hydrocarbons occurs by polymerization of methylene radicals, via hydrogenation of the surface carbides. This mechanism was, however, disregarded given that it cannot explain the hydrocarbon synthesis with catalysts of the iron group (Storch, *et al.*, 1951).

Another mechanism proposed (Vannice, 1975; Storch, *et al.*, 1951) involves surface intermediates of the type RCOH. These species polymerize by hydro-de-condensation to form oxygenated or olefinic and saturated hydrocarbons. Pichler and Schulz in 1970 also suggested another mechanism involving repeated insertion of CO in the metal alkyl bond (Dry, 1996).

In any extent, mechanistic postulations (Zagli, et al., 1979; Dwyer, and Somorjai, 1979; Biloen, et al., 1979; van Barneveld, and Ponec, 1978) consistently support a reaction that starts with CO dissociation. Ponec (1978) and Araki and Ponec (1976) concluded that H_2 and CO are adsorbed dissociatively on the catalyst surface and this is the main route to the formation of methane.

Furthermore, over the last twenty years, with the development of new and sophisticated surface analytical techniques, it appears there is general consensus that carbene ($=CH_2$) species are involved in the chain growth mechanism with CO insertion accounting for the formation of oxygenates (Dry, 1996).

In summary, while there are different possible reaction mechanisms proposed to explain the FTS, the subject still remains controversial. Among these

the most relevant mechanistic formulations are: a) the CH_2 insertion, b) the CO insertion, c) the enolic mechanism, d) the alkoxy mechanism (Adesina, 1996)

However, it is being hypothesized that FTS has to be seen as a network of physical and chemical steps, with the following being suggested: (i) reactant adsorption, (ii) chain initiation, (iii) chain growth, (iv) chain termination, (v) product desorption and (vi) re-adsorption and further reaction. It is important to highlight that chain growth (Fig. 3.5) and termination could proceed in various possible ways with the type of catalyst and process conditions playing an important role.

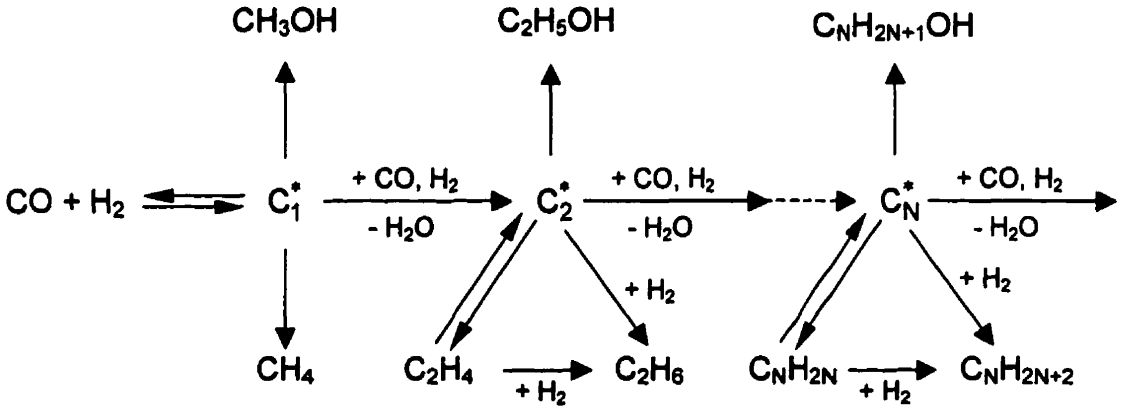

Figure 3.5. Simplified reaction mechanism for Fischer-Tropsch synthesis. (Bub and Baerns, 1980)

While trying to elucidate the reaction steps, a variety of active species have been detected on the surface of the FTS catalysts, namely: C, CO, CO_2, H, HCO, OH, H_2O, O (Sarup, and Wojciechowski, 1989). These species may be all present on the catalyst surface and may be involved in different extents in both the growth and the termination steps. For that reason, it is generally

acknowledged that the surface of a FT catalyst is very complex and it also has a heterogeneous character.

3.4.3. The Kinetic Rate Expression

As stated in the previous sections of this review an appreciable amount of theoretical and empirical evidence has been published on the mechanism of the Fischer-Tropsch synthesis. However, until today a final conclusion has not been reached about a comprehensive reaction kinetics. FTS involves a complex network of reactions with a plurality of reaction parameters (temperature, pressure, synthesis gas composition, catalyst, mass and heat transfer) .

Vannice (1975) has summarized the most important kinetics expressions before 1974. In 1988, Wojciechowski (1988) reviewed major kinetics models. From the analysis of these two reviews, two different general kinetics expressions can be advanced:

a) Power law

$$-r_{CO} = k_{emp} p_{H2}^{m} p_{CO}^{n} \qquad (3.10)$$

b) Langmuir-Hinshelwood-Hougen expression

$$-r_{CO} = \frac{a p_{H2}^{m} p_{CO}^{n}}{\left[1 + \sum_{i=1}^{n} K_i p_{H2}^{c_i} p_{CO}^{d_i}\right]^2} \qquad (3.11)$$

where, k_{emp} in the eq.3.10 represents an empirical rate constant and *m* and *n* the reaction orders with respect to H_2 and CO partial pressures, respectively.

In the case of eq. (3.11), "*a*" and "K_i" are kinetics and adsorption equilibrium constants respectively. Parameters *m* and *n* are related to the molecularities of the rate-determining step and c_i and d_i represent the surface coverage related parameters.

Another interesting observation on the kinetic model is the general agreement that the rate-controlling step is a bimolecular surface reaction, as evidenced by the power two in the denominator of the rate equation.

In general, the kinetic data consistently shows that over a wide range of conditions, and with a wide variety of catalysts, the rate of CO conversion in the Fischer-Tropsch reaction displays a linear dependence with respect to the hydrogen partial pressure. The influence of CO partial pressure could vary from negative (-1) to mildly positive (0.5) or positive (1) with this order depending in some cases on the H_2/CO ratio.

Thus, there is a diversity of reaction orders and this may be partially assigned to the different specific surface area of the catalysts studied, in many cases not measured. In addition to this there are differences between laboratories in methodologies for data interpretation and differences on synthesis gas conversion, and catalyst pretreatment. All this makes direct comparison of kinetic models rather difficult.

Proposed rate expressions for FTS display a wide range of mathematical forms and this may be partly the result of the considerable variation in reaction conditions studied. Many of the earlier work, were performed in integral fixed-bed reactors. Integral kinetic data for complex reactions, case of Fischer-Tropsch synthesis, are difficult to be analyzed given the problems of maintaining isothermal conditions. More specifically over cobalt catalysts, a significant number of kinetic studies of the Fischer-Tropsch synthesis have been developed (Storch *et al.*, 1951; Anderson, 1956; Yang *et al.*, 1979; Bub and Baerns, 1980, Pannell *et al.*, 1980;; Rautavuoma and van der Baan 1981; Dixit and Tavlarides 1982; Wojciechowski, 1988; Sarup and Wojciechowski, 1989; Post *et al.*, 1989; Yates and Satterfield 1991; Iglesia *et al.*, 1993). A consistent result, however, is given by the fact that rate equations show that carbon monoxide inhibits the FTS synthesis rate.

3.4.3.1. Power Law Rate Equations

Pannell *et. al.* (1980) studied the Fischer-Tropsch product distribution over cobalt catalysts in a internal recycle reactor. These authors found a power rate equation with the following mathematical form,

$$-r_{CO} = a p_{H2}^{0.55} p_{CO}^{-0.33} \qquad (3.12)$$

In an agreement with this, rate expressions developed by Yang *et.al.* (1979) and Wang (1987) using cobalt-based catalysts postulate the following:

$$-r_{CO} = a p_{H2} p_{CO}^{-0.5} \quad \text{(Yang)} \qquad (3.13)$$

and,

$$-r_{CO} = a p_{H2}^{0.66} p_{CO}^{-0.5} \quad \text{(Wang)} \tag{3.14}$$

Note that in eqs (3.12), (3.13) and (3.14) there is a negative power assigned to the carbon monoxide partial pressure and this suggests, as advanced, inhibition by adsorbed CO.

Furthermore, a kinetic rate equation developed by Post *et. al.*(1989) using a cobalt catalyst on silica,

$$-r_{CO} = k_{CO} p_{H2}^{m} p_{CO}^{n} \tag{3.15}$$

displays a first order in hydrogen gas-phase concentration (m = 1) and zero order in carbon monoxide gas-phase concentration (n = 0). The value of n = 0 suggests that inhibition exactly compensates an expected order of one for CO.

3.4.3.2. Langmuir-Hinshelwood-Hougen Models

A typical example of the Langmuir-Hinselwood-Hougen models is the one of Anderson (1956) where the FTS rate is proportional to the desorption of chains with the concentration of growing chains on the catalyst being empirically related to $p^2_{H2}p_{CO}$:

$$-r_{H2+CO} = k_0 e^{\left(\frac{-E_a}{RT}\right)} \frac{p_{H2}^2 p_{CO}}{\left(1 + b p_{H2}^2 p_{CO}\right)} \tag{3.16}$$

Rautavuoma and van der Baan (1981) studied the kinetics of the Fischer-Tropsch reaction using a cobalt catalyst supported on alumina. These authors

examined five possible rate determining steps. The expression most favoured to fit their data best is the following:

$$-r_{tot} = \frac{a p_{H2} \sqrt{p_{CO}}}{\left(1 + \sqrt{K_{CO} p_{CO}} + \sqrt{K_{H2} p_{H2}}\right)^3} \qquad (3.17)$$

Note that the kinetic rate given by eq. (3.17), is consistent with a mechanism in which the FTS reaction proceeds via CO dissociation and formation of a " $-CH_2-$" surface intermediate with the formation of these surface intermediates as the rate-determining step. This model also allows for hydrogen adsorbed dissociatively, with dissociated CO being however the predominant surface species. Therefore, the term for dissociated H_2 is not included in the denominator of the rate expression:

$$\sqrt{K_{H2} p_{H2}} \leq 1 + \sqrt{K_{CO} p_{CO}} \qquad (3.18)$$

In other published work, Sarup and Wojciechowski (1989) described six different possible mechanisms for the Fischer-Tropsch reaction on cobalt catalysts. Four of the proposed expressions hypothesize that dissociated CO participates in the reaction, while the other two postulate that CO is adsorbed but not dissociated.

In spite of these differences all of the hypothesized reaction mechanisms considered by Sarup and Wojciechowski (1989) involve a bimolecular surface reaction, and thus the denominator of the rate models is consistently squared:

Model 1

$$-r_{CO} = \frac{a\, p_{CO}^{1/2}\, p_{H2}^{1/2}}{\left(1 + b p_{CO}^{1/2} + c p_{H2}^{1/2} + d p_{CO}\right)^2} \qquad (3.19)$$

Model 5

$$-r_{CO} = \frac{a p_{CO}\, p_{H2}^{1/2}}{\left(1 + b p_{CO} + c p_{H2}^{1/2}\right)^2} \qquad (3.20)$$

with: *a*, *b*, *c* and *d* being model-specific temperature-dependent constants.

More specifically, Model 1 (eq. 3.19) requires that the hydrogenation of surface carbon or of surface oxygen be rate limiting. This demands reversibility in the dissociative adsorption of CO. Model 5 (eq. 3.20) however implies reversibility of molecular CO adsorption only. Note that Model 5 (eq. 3.19) appears to be in agreement with the general concept that CO dissociates irreversibly on Fischer-Trospch catalysts. However, based on the experimental data, Sarup and Wojciechowski (1989) state that they were unable to distinguish between Models 1 and 5.

Another kinetic expression, in terms of Langmuir-Hinshelwood-Hougen form, which only contain two adjustable parameters was developed by Yates and Satterfield, 1991 (eq. 3.21). One of these parameters represents a surface rate constant and the other an adsorption coefficient. These authors considered that additional adjustable parameters make the kinetics expression unnecessarily complex without adding to it significant physicochemical information.

$$-r_{CO} = \frac{a p_{CO}\, p_{H2}}{\left(1 + b p_{CO}\right)^2} \qquad (3.21)$$

3.5. Catalyst design and development

A key element in the Fischer-Tropsch processes is the development of active catalysts. A Fischer-Tropsch catalyst usually consists of an active metal, oxide promoter(s) and a support.

3.5.1. Catalyst metals.

As early as 1902 Sabatier and Senderens reported the first catalysts developed for the CO hydrogenation. These authors observed the production of methane over a nickel wire. Subsequent studies showed that Co and Fe were also good metals for FTS. These studies were particularly valuable to demonstrate the production of higher hydrocarbons. Nowadays, it is generally accepted that most of the Group VIII metals have measurable CO hydrogenation activity yielding different product distribution (Adesina, 1996).

It has been observed that the specific activity for CO hydrogenation of Group VII metal can be ranked as follows: Ru > Fe > Ni > Co > Rh > Pd > Pt. However, the average hydrocarbon molecular weight decreased in the following order: Ru > Fe > Co > Rh > Ni > Ir > Pt > Pd (Vannice, 1975). Although several metals are active for the FTS, only iron and cobalt catalysts appear economically feasible on an industrial scale (Biloen and Sachtler, 1981). Moreover, while it has been determined that nickel is very active for FT synthesis, too much methane is formed making Ni unsuitable. On the other hand, Ru is too expensive and this is because of its very limited availability (Dry, 1996).

Regarding Fe-based catalysts one of its main advantages is that iron is relatively cheap, and this was one of the reasons of its selection in pioneering research studies in Germany.

The Fe-based catalysts have to be used, however, at higher pressures than the Co-based catalysts and this implies a major cost in the gas compression system. Additionally, under FT synthesis conditions, Fe readily forms oxides, carbides, nitrides and carbonitrides which are also all active for FT synthesis (Anderson, 1984).

Furthermore, as Fe-based catalysts work at higher temperature than Ni and Co-based catalysts they display a stronger tendency to produce elementary carbon (Boudouart reaction) and this leads to catalyst deactivation. In fact, the formation of Co and Ni carbides is thermodynamically unfavoured at FT synthesis conditions (Adesina, 1996).

Regarding the Fischer-Tropsch reaction with cobalt-based catalysts, reaction products consist of a broad spectrum of linear saturated hydrocarbon molecules containing from 1 to over 40 carbon atoms. It has been established that cobalt is not very active for the water gas shift reaction, (Bruce *et al.*, 1993) and this is in sharp contrast with the performance of iron-based Fischer-Tropsch catalysts. Note that with cobalt catalysts only a small fraction of the water produced is subsequently converted to carbon dioxide.

Under reaction conditions the metallic state has been assumed frequently as essential for the catalysts of the FT synthesis. Also another state (oxydic or

carbidic) may be present and in all these states physisorption and/or chemisorption of the CO or H_2 is possible.

The nature of CO and H_2 adsorption and the resulting interaction on Group VIII metals apparently determine the effectiveness of FTS catalysts. It has been shown that with these metals both CO and H_2 compete for the same sites with CO adsorption being several times stronger than H_2 adsorption (Adesina, 1996).

3.5.2. Supports

The most popular supports for the FT catalysts are silica, alumina, magnesia, titania and zirconia. Recently, zeolites have been incorporated as supports for FT catalysts specially when the target of the synthesis are hydrocarbon fractions rich in light olefins.

Selection of the appropriate support for FT catalysts depend of several factors. Among them basicity, dispersion, electronic modifications and strong-metal support interactions are important parameters that affect their overall performance. In this respect, previous studies (Reuel and Bartholomew., 1984; Bessel, 1995 and Zowtiak and Bartholomew, 1983) demonstrated that different supports significantly influence the morphology, adsorption and activity/selectivity properties of cobalt.

3.5.3. Promoters

Catalyst promoters can be divided into two groups according to their mode of action. In the first group there are oxides, which are difficult to reduce, such as SiO_2, Al_2O_3, ThO_2, and ZnO. These oxides are frequently called structural promoters, since they provide a large surface area and prevent transferring and sintering of the active catalyst.

In the second group, chemical promoters, such as alkalis and their salts can be cited. These promoters work by mechanisms still not clearly understood transfering electrons to the catalysts or even blocking pores (Wender, 1996).

The increment of the activity of FT catalysis caused by the incorporation of promoters have been explained by Ali *et al*, (1995) according to the following functions:

- Promoters enhancing the CO dissociation and the overall rate of synthesis,
- Promoters shifting the selectivity in FT synthesis to higher hydrocarbons,
- Promoters favoring the formation of unsaturated products,
- Promoters affecting selectivity or in other words determining in which extent the FT synthesis of hydrocarbons are accompanied by other reactions.

3.5.4. Preparation method

Fischer-Tropsch catalysts are often prepared by precipitation, impregnation, ion exchange, synthesis from organometallic compounds and

vapour phase deposition in which the metal precursor is loaded onto the support metal (Adesina, 1996). Normally, after support impregnation, catalyst drying and calcination are carried out.

Catalysts activation by reduction of the metal precursor to the metallic phase is required to perform the FT synthesis. Obviously, the interrelations of catalyst composition and preparation conditions determine the activity and selectivity behavior for a given set of process parameters.

Recently, Iglesia and coworkers (1993) have considered a catalyst preparation methodology, where the active metal has a non-uniform distribution into the support. They proposed an eggshell catalyst, in which the active metal is preferentially located near the outer pellet surface.

It is known that transport restrictions are common during the FT synthesis due to the presence of liquid products within the porous support. This phenomenon diminishes the rate of reactant reaching (and product removal) at catalytic sites and consequently controls reaction rates and selectivity. It appears that eggshell catalysts can reduce the severity of these transport restrictions and lead to higher reaction rates and C_5^+ selectivity (Iglesia, et al., 1993).

3.6. Fischer-Tropsch Processes.

3.6.1. Sasol

In 1955, in South Africa, the Sasol 1 plant with a capacity of about 700.000 t/a went into operation. The syngas was produced from coal (Lurgi dry

ash gasifiers) and both fixed bed (Ruhrchemie/Lurgi) and circulating fluidized bed (Kellog) FT reactors were used. The fixed bed tubular reactor, ARGE reactor, still in operation is a multitubular reactor (Figure 3.6a). Each reactor consists of 2050 tubes, 5 cm ID and 12 m long. The heat of reaction is removed by water circulating around the tubes. A precipitated iron catalyst promoted with copper and a potassium salt such K_2CO_3 is used to fill the reactor tubes. The Sasol 1 fixed bed reactors are generally operated at medium pressures (about 2.6 MPa) and 225 °C. About 50% of the products consists of linear waxes which are selectively hydrocracked to diesel (Dry, 1996).

The other type of reactor used in Sasol 1 is an entrained fluidized bed reactor, so-called Synthol reactor (Figure 3.6b). This circulating fluidized bed (CFB) reactor was developed by the Kellog Company. These CFB reactors offer efficient heat transfer and provide higher gas throughputs than fixed bed reactors. Synthol reactors are operated at about 340 °C and 2.5 MPa. The gas fed into the reactor zone entrains the hot catalyst coming from a standpipe. The heat of reaction is transferred to heating coils. Although these CFB reactors have performed very successfully, they are complex to operate. The Synthol reactor produces more light hydrocarbons, more olefins, more oxygenated compounds, more gasoline and less heavy oil and waxes (Wender, 1996).

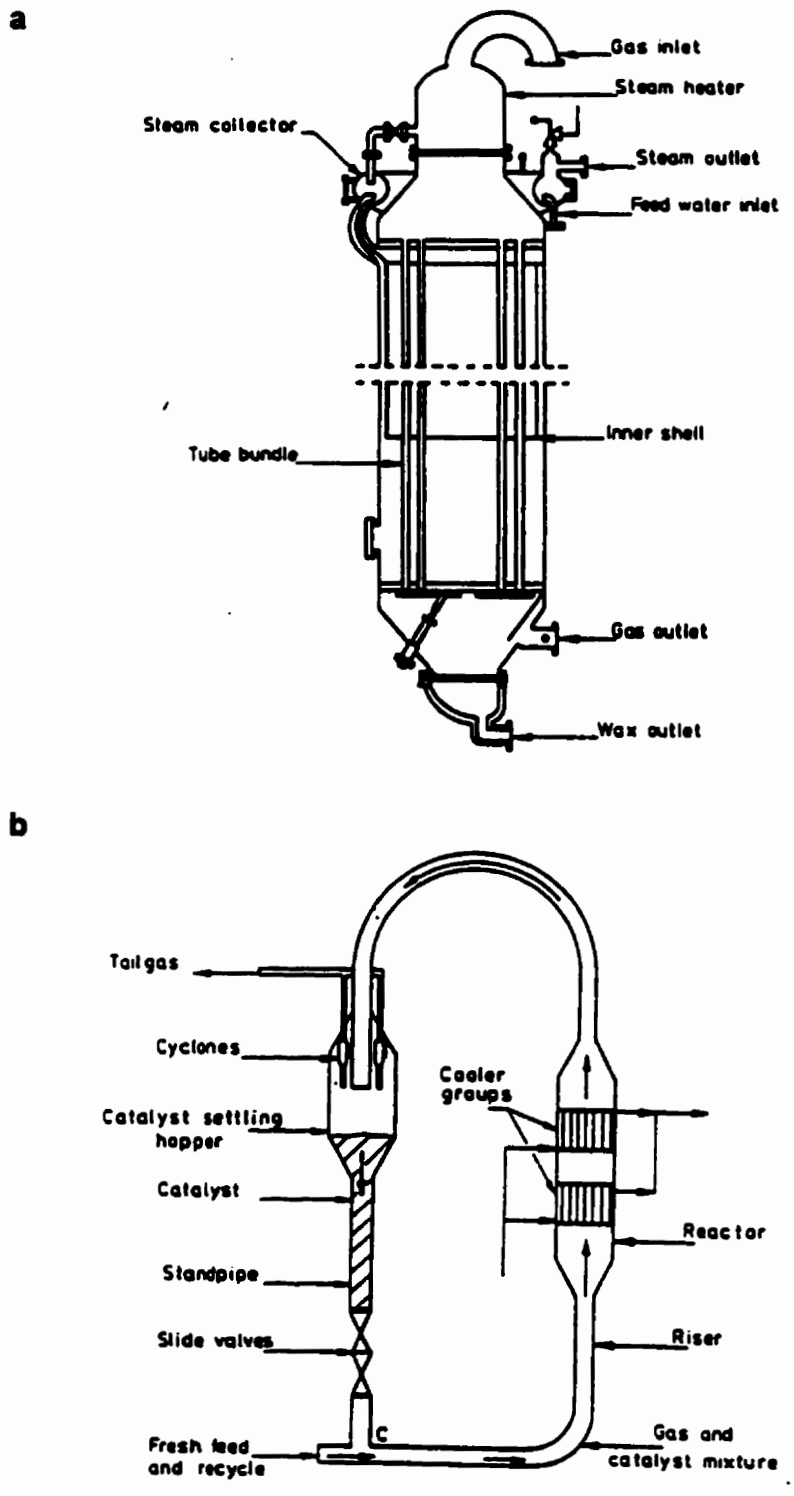

Figure 3.6. **a) Fixed-bed Sasol reactor, b) Synthol reactor (Dry and Hoogendoorn, 1981).**

An alternative to the CFB reactors is a conventional fixed fluidized reactor developed by Sasol (Figure 3.7). This reactor is called the Sasol Advanced Synthol (SAS). The SAS reactor was incorporated into Sasol 1 and 2 plants and used mainly for the production of heavy hydrocarbons. In the SAS reactor, the gas enters the reactor via a distributor and bubbles through the catalyst bed. Note that while the SAS reactor is referred to as "fixed" since in reality the bed, although fluidized, is not transported as in the CFB reactor (Wender, 1996).

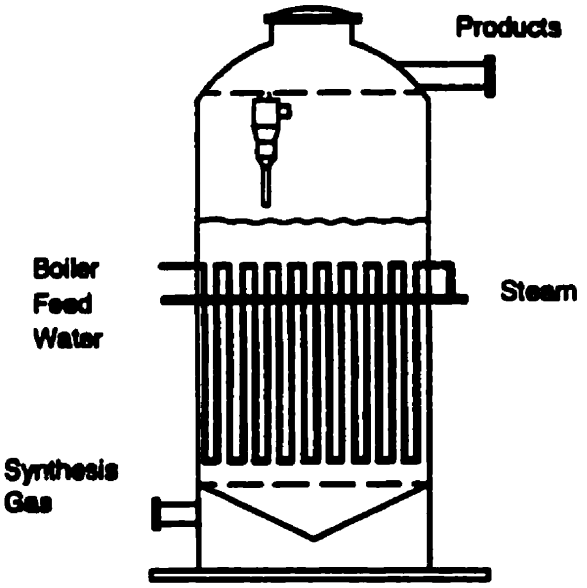

Figure 3.7. Sasol advanced fluidized reactor (Wender, 1996)

A variation of the SAS, as present in Fig. 3.8, is the newest type of reactor incorporated into Sasol units, so-called the SSBP (Sasol Slurry Bed Process). It resembles a SAS reactor except that the catalyst is suspended in a liquid, usually a FT wax. Several advantages has been claimed for this reactor design including

a low pressure drop, isothermal behavior, good scale-up potential, on-line catalysts removal, improved catalysts economy and low turndown ratio (Jager and Espinoza, 1995).

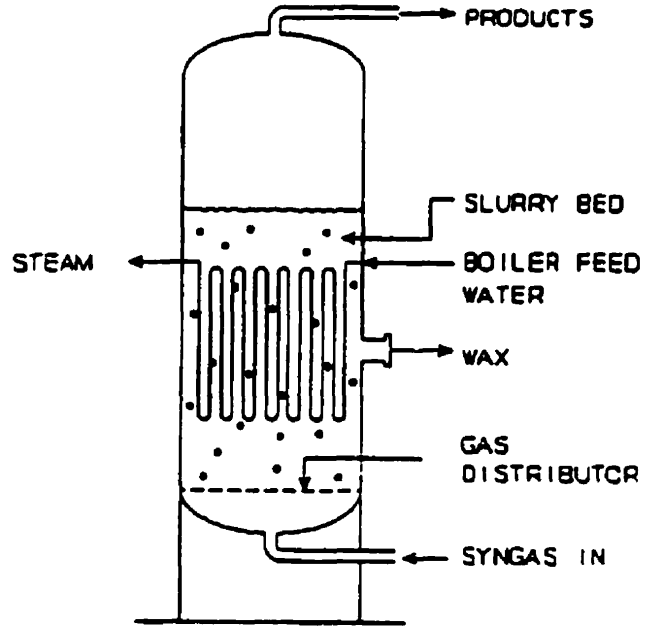

Figure 3.8. Sasol slurry bed reactor (Jager and Espinoza, 1995)

3.6.2. Shell Middle Distillate Synthesis

The Shell Middle Distillate Synthesis (SMDS) process developed by Shell Petroleum International, uses remote natural gas as the feedstock to produces high-quality middle distillates via synthesis gas and a hydrocarbon/cracking step (Senden *et al.*, 1992). The SMDS process consists of three stages: syngas manufacture (SGP), heavy paraffin synthesis (HPS) via the FTS and heavy paraffin conversion (HPC). A simplified flow scheme is given in Figure 3.9.

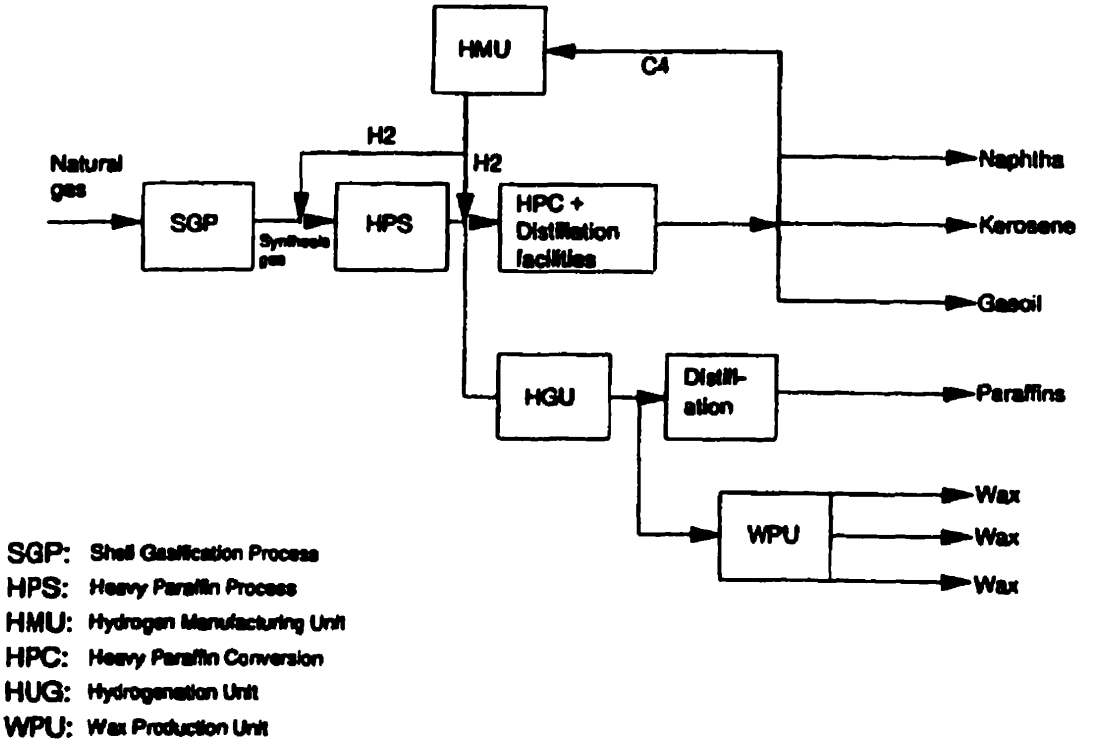

Figure 3.9. Schematic of the Shell Middle Distillate Synthesis (SMDS) process (Senden *et al.*, 1992)

The paraffinic hydrocarbons produced via the FTS in the second stage are highly linear, thus the distillation products (mainly kerosene, gas-oil and some naphtha) obtained from the HPC stage are high quality products.

It should be mentioned that the syngas manufacture (SGP), the first stage of the SMDS process, uses a non-catalytic autothermal partial oxidation of methane operating at 1300 to 1500 °C and pressures up to 7.0 MPa; with a carbon efficiency of over 95%. One of the advantages of SGP over steam reforming of methane (SMR) is that a H_2/CO ratio of about two can be produced.

As the H_2/CO usage ratio of the FT reaction amounts to about 2.1 mol/mol. Thus, only a little adjustment of the desired 2:1 H_2/CO is required (Senden et al., 1992).

In the last step, the heavy paraffin synthesis (HPS), converts syngas (hydrogen and carbon monoxide) into heavy paraffins by the FTS. The reaction is catalyzed by cobalt plus a noble metal in a highly energy efficient fixed bed tubular reactor. The ASF polymerization kinetics determines the products distribution, which is characterized by the probability of chain growth and chain termination (van Burgt *et al.*, 1988).

In the HPC, the waxy product of the HPS is hydro-isomerized and hydro-cracked to give a high yield of middle distillates. The HPC is a mild trickle flow hydrocracking process using a Shell catalyst operating a typically 3.0-5.0 MPa total pressure and at a temperature of about 300-350 °C (van Burgt *et al.*, 1988).

3.7. Fixed-bed Catalytic Reactors for Exothermic Reactions

The fixed-bed reactor has been for many years one of the most important and useful units in the chemical industry. For that reason many solid catalyzed gas-phase reactions are carried out in them. Fixed-bed reactors are generally classified in three categories: isothermal, adiabatic and non-isothermal/non-adiabatic (Tarhan, 1983). For the case of highly exothermic reactions, a very important design consideration is the control of the temperature rise.

A typical packed bed reactor design is the adiabatic reactor (Figure 3.10). The main consideration in this design is the minimization of the heat transferred

through the reactor towards the outside the wall. Thus, the heat evolved in the chemical reaction (released or absorbed by the catalytic bed) is much bigger than the heat transferred. The fluid moves through the unit in a nearly plug flow pattern, and the temperature rise is close to proportional to the percentage of reactant conversion (Froment and Bischoff, 1979; Rase, 1990).

Adiabatic reactors are adequate for slow and moderately exothermic reactions given they are relatively inexpensive and designs are well known. However, when an exothermic reaction takes place in an adiabatic reactor some operational strategies have to be considered to ensure a small temperature change through the reactor (Doraiswamy and Sharma, 1984). Among others, the following can be mentioned:

- A partial recycle of the product and mixed with fresh feed.
- One reactant may be used in excess.
- An inert gas may be added to dilute the feed.

In all these cases, the reactor is used only partially and there are important drawbacks.

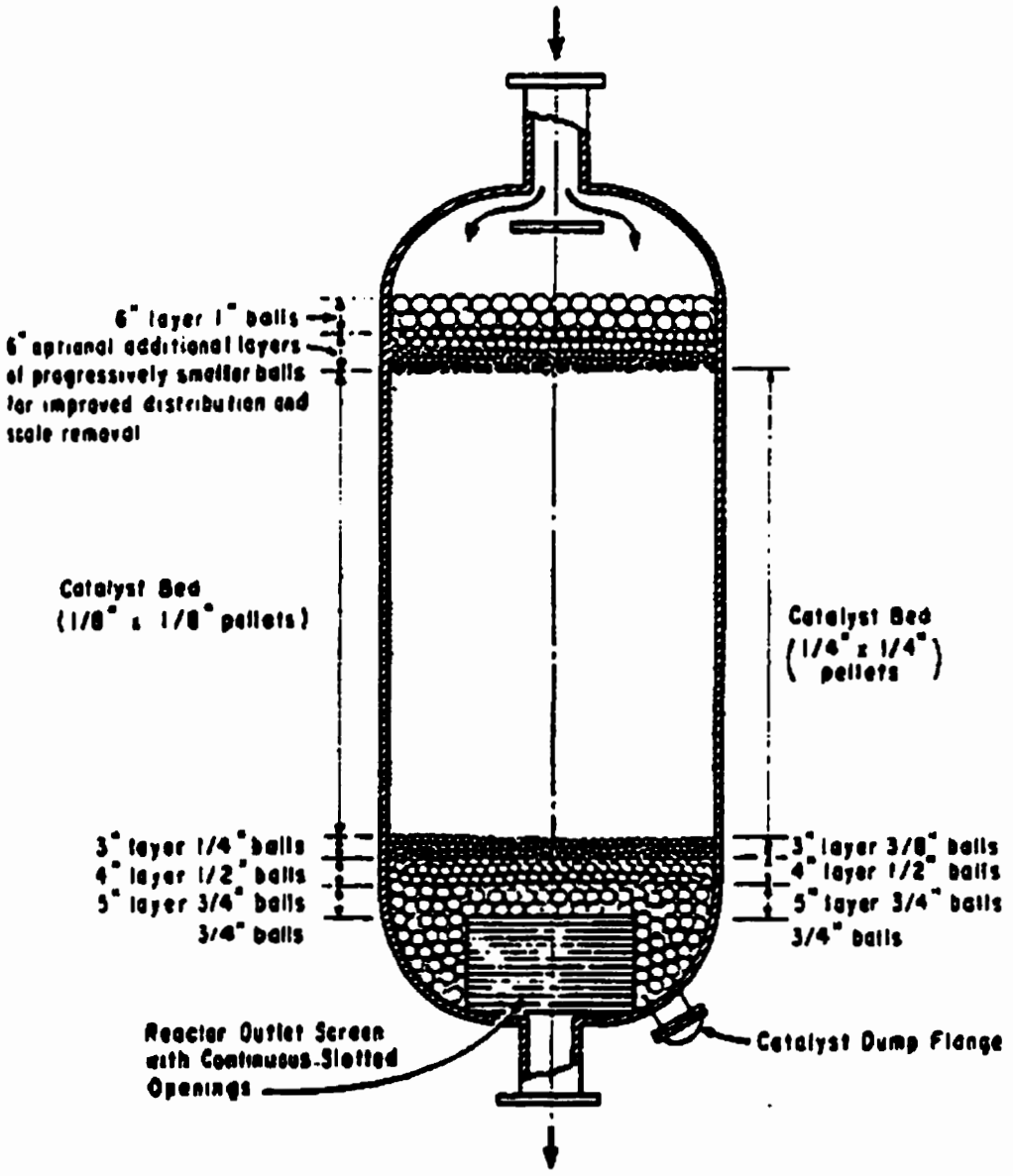

Figure 3.10. Typical design of an adiabatic fixed-bed reactor (Rase, 1990).

For all the reasons already cited, for rapid and highly exothermic reactions, the adiabatic unit is not recommended (Froment and Hoffman, 1987). An excessive increment of temperature may negatively influence catalyst performance (e.g. selectivity). Besides, catalyst deactivation can be the result of temperature runaway.

An alternative reactor for highly exothermic processes is the so-called non-isothermal, non-adiabatic fixed-bed reactor also known as the heat exchanger or multibular fixed-bed reactor (Tarhan, 1983).

Different configurations have been considered in the design of multibular fixed-bed reactor. However, the most usual one (Figure 3.11) consists of a unit mounted vertically with down-flow reactant circulation: reactants are fed from the top of the reactor. This kind of arrangement facilitates catalyst handling and prevents potential problems with fluidization and instabilities of the catalyst bed. These reactors consists usually of large capacity units with tens of thousands of tubes operating in parallel.

In these units the heat of reaction, or a certain fraction of it, is transferred from the reacting stream to a cooling fluid through the walls of a packed bed. With this end, different kinds of cooling fluids can be considered: the reacting mixture, water, or a heat transfer fluid.

Note that the specific option chosen depends of the specific type of process under consideration. For very exothermic reactions, the use of a

heat transfer fluid is highly recommended, given water-cooled heat-exchanger reactor present several problems of operation, safe design and cost (Nelson, 1987).

Furthermore, special attention has been devoted to study the circulation of coolant fluids in a multitubular fixed-reactor. Coolant fluids can be circulated with different flow patterns (Figure 3.12): fully countercurrent, fully concurrent and cross flow. Note that the cooling flow pattern has an important influence on the coolant temperature, which is in turn a design parameter of special importance.

Because of the nature of the process good dynamic control of the reactor temperature is obtained when the temperature difference between reactor and coolant is small (Ravella, 1987). In the ideal case, the conditions of heat removal could be close to identical for all catalytic tubes, which creates conditions of so called "thermal-symmetry", (Simard, 1991). In this particular condition, various tubes of the bundles will have very similar temperature profile.

Most multitubular units present a temperature profile characterized by a hot spot (Froment and Hoffman, 1987). When the hot-spot regime, in a multibular fixed-reactor, is reached the system become very unstable and extremely sensitive to small changes in the process variables. Additionally, the axial position of the hot spot inside the tubes can vary significantly, resulting in changes of activity of the catalyst. This phenomenon is called parametric

sensitivity and has been discussed by a number of authors (Froment and Hoffman, 1987; Froment, 1984; Soria Lopez et. al., 1981).

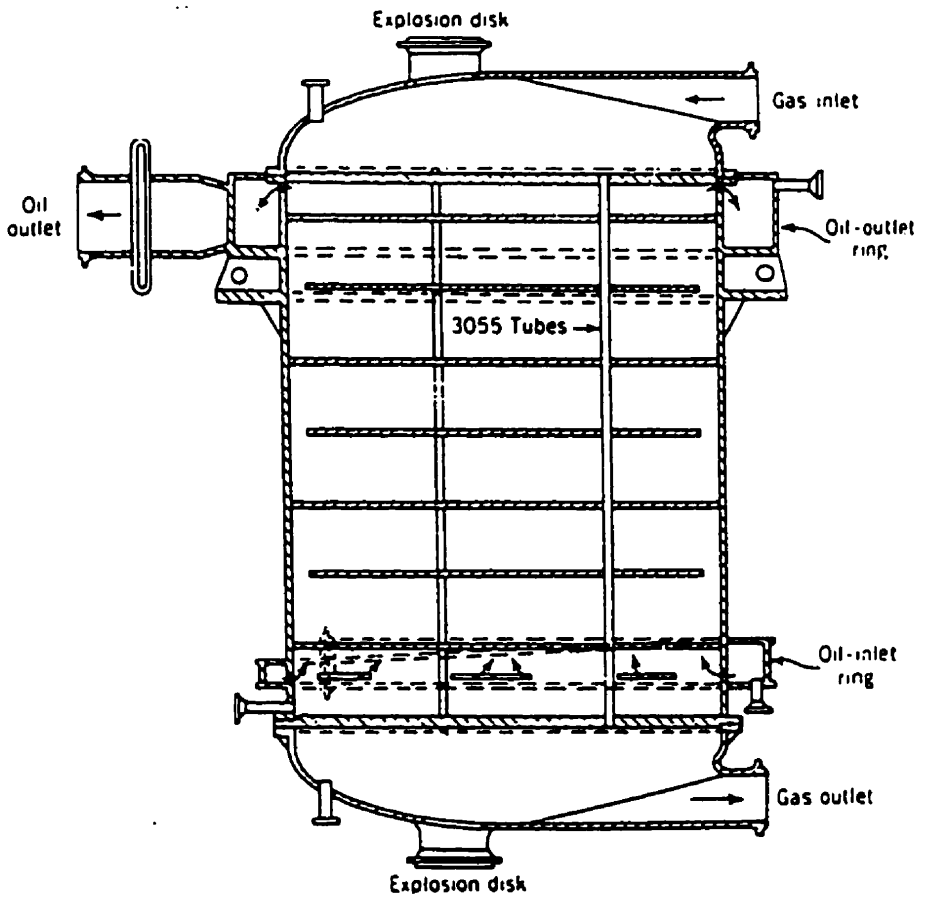

Figure 3.11. Typical design of a multitubular fixed-bed reactor (Rase, 1990).

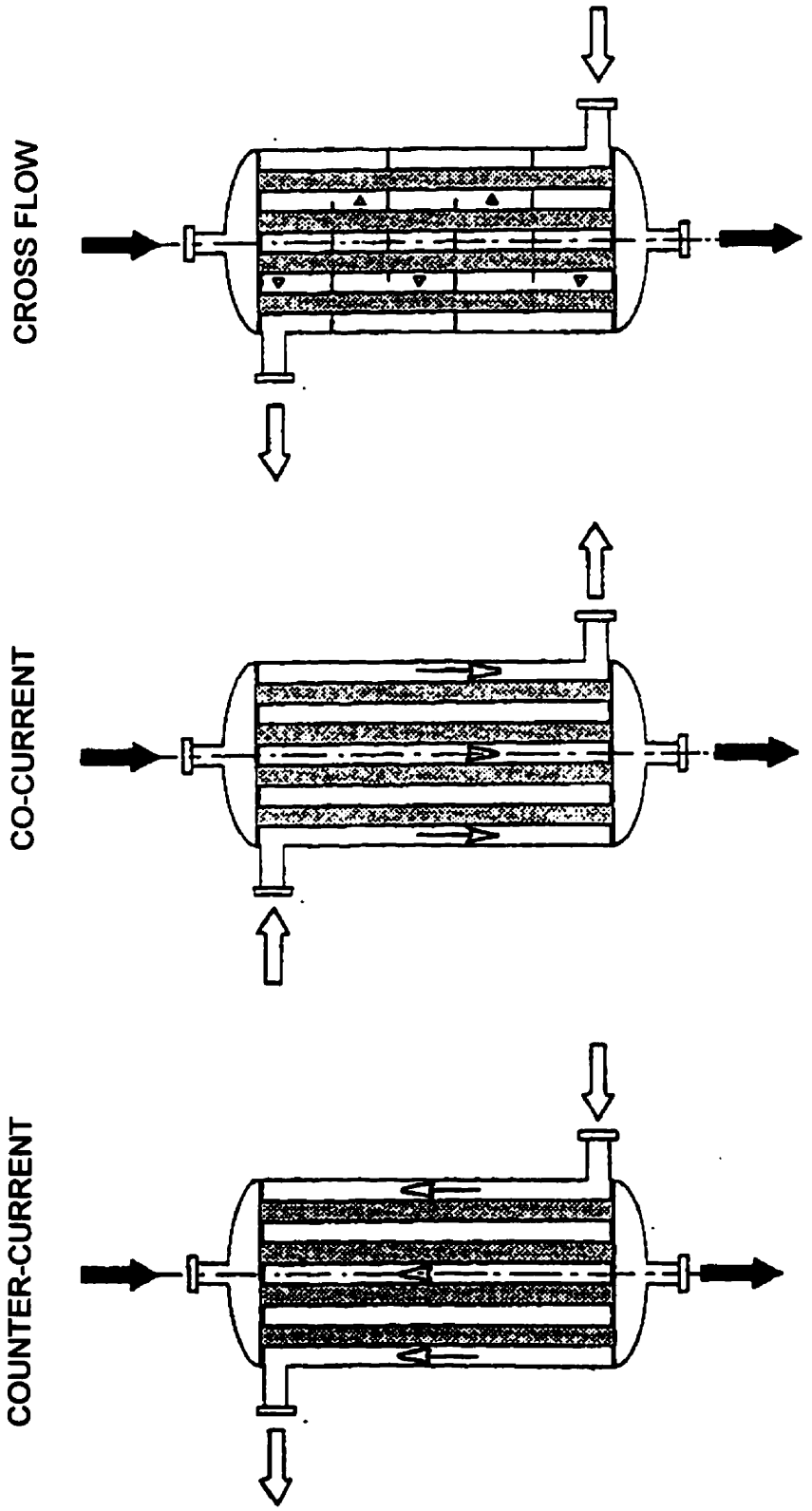

Figure 3.12. Cooling flow patterns in a multitubular fixed-bed reactor (Simard, 1991).

3.8. Pseudoadiabatic operation of a fixed-bed reactor

As mentioned earlier, the flow and temperature of the coolant have an important influence in the design and operation of multitubular fixed bed catalytic reactors. Borio *et al.* (1989a and 1989b) have demonstrated that, for equivalent production rates, the fully concurrent operation is the one which leads to the lowest values for the maximum temperature and parametric sensitivity. Under the fully concurrent scheme and adequate operating conditions in a fixed-bed reactor seven different thermal regimes can be found with the Pseudoadiabatic operation (PO) being one of these regimes (Arandes and de Lasa, 1995; de Lasa et. al., 1981; de Lasa, 1982, 1983; Soria Lopez et al., 1981). The PO regime is reached by changing the inlet temperatures of the gas and coolant streams, as well as the coolant flowrate in a fully concurrent regime. Adequate changes of these operating parameters lead to axial thermal profiles very different from the hot-spot profiles usually found in these units.

The PO regime of a catalytic fixed bed reactor for exothermic reactions is by definition a regime where the axial temperature increases steadily with the bed length so that the highest temperature in the unit is reached at the reactor outlet. The PO regime takes place when a non-boiling fluid is co-currently circulated with respect to the reactants and when at the same time the operating parameters are such that the heat generated is always greater that the heat removed by the coolant (de Lasa, 1982 and 1987).

The PO concept modifies substantially the design and the operation of exothermic multitubular reactors (de Lasa, 1982, 1983, and de Lasa *et al.*, 1985). The simplicity of the PO contrasts with the more complex instrumentation and control strategies required to sense and control conventional "hot-spots" (temperature maxima in the axial direction) that develop under non-PO regime.

In fact, the prediction of the magnitude and of the exact position of the "hot spot" in non-PO reactors is quite uncertain, making the design of highly exothermic fixed bed reactors susceptible to important errors. These important errors can influence both the selectivity prediction and the assessment of reactor runaway conditions. The problem of sensing "hot-spots" becomes a critical issue in multitubular reactors when a non-boiling coolant is circulated under cross flow conditions (de Lasa *et al.*, 1981). All these problems are eliminated under the PO regime because all the tubes in the reactor have the same temperature profile (thermal symmetry) and besides all "hot-spots" are located at the exit of the reactor.

Computer simulations using: a) one- and two-dimensional pseudohomogeneous and heterogeneous models, and b) experimental runs in a pilot plant facility at the University of Western Ontario were performed to confirm these observations. Two different processes were simulated, the first one, a reactor to convert methanol into gasoline (de Lasa, et. al., 1984; 1985, and 1986; Ravella, 1987) and the second one a reactor to convert synthesis gas into hydrocarbon (gasoline range) (Simard, 1991; Simard et al. 1991). These studies

confirmed the application of the novel Pseudoadiabatic operation for both processes.

3.9. Modeling of fixed-bed reactors

Although the PO concept brings forth a substantially novel approach to the design of fixed-bed catalytic reactors, most of the fundamentals used in its development were based on conventional methods of reactor simulation.

A widely accepted classification of the available models is the one introduced by Froment 1972a, 1972b, 1974, and 1984. This classification can be used for pseudo-homogeneous or heterogeneous models. The most important characteristics of these models are presented in Table 3.1.

The one-dimensional model considers only the changes that occur in the longitudinal direction of the reactor, and the two-dimensional model provides information on the conditions at every physical point of the reactor, as opposed to the one-dimensional model that describes only "slices" of the bed.

Table 3.1. Classification for modeling of fixed-bed reactors.

	Pseudo-homogeneous	Heterogeneous
One-dimensional model	AI = Basic model, ideal AII = AI + axial mixing	BI = AI + interfacial gradient BII = BI + intraparticle gradient
Two-dimensional model	AII = AI + radial mixing	BIII = BI + radial mixing

While pseudo-homogeneous models consider the reactor as a continuum by using average transfer parameters, heterogeneous models distinguish between solid and gas phases. Note that, as will be discussed later, only the basic pseudo-homogeneous model (AI) has been used in the context of the present work.

3.9.1. Pseudo-homogeneous one-dimensional model

The basic pseudo-homogeneous model (AI) is generally used for the majority of reactor simulations (Froment, 1984) because it is easy to solve and manipulate. Since concentration (or partial pressure) are considered to occur in the axial direction only, it is hypothesized mass transport takes place as a result of the overall flow motion (Froment 1972a). Thus, this model simulates a "plug flow" reactor. Mass and energy conservation equations for this model may be written as follows:

$$\frac{-dx}{dz} = A\,P\exp\left(\frac{-a}{T+b}\right) \tag{3.22}$$

$$\frac{dT}{dZ} = B\,P\exp\left(\frac{-a}{T+b}\right) + C\,(T - T_c) \tag{3.23}$$

$$\frac{dT_c}{dZ} = D\,(T - T_c) \tag{3.24}$$

The four parameters appearing in Eqs. 3.22 to 3.24 are defined as follows:

$$A = (P\ M\ \rho_B) / (u_S\ \rho g) \tag{3.25}$$

$$B = (-\Delta H)\ \rho_B / (u_s\ \rho_g\ Cp_g) \quad (3.26)$$

$$C = 2\ U / (u_s\ \rho_g\ Cp_g\ R) \quad (3.27)$$

$$D = (2\ \Pi\ R\ t_n\ U) / (W_c\ Cp_c) \quad (3.28)$$

The most important assumptions while using a one-dimensional model are the following:

- Temperature is constant across the section of reactor with the only exception of the region close to the wall.
- Mass and thermal axial dispersion effects may be neglected. This assumption is consistent with the finding of several researchers for the range of conditions usually encountered in industrial applications of fixed-bed reactors (Froment, 1972a, 1979b; Froment and Bischoff, 1979).
- The concentration and the temperature differences between the solid catalysts and the gas phase may be considered negligible.
- The axial pressure drop in the bed is comparatively small with respect to the total pressure, so this change can be neglected.
- The kinetic rate equation used in this model should be obtained at the same conditions and using the same catalyst pellets than the process being simulated.

In addition, a pseudo-homogeneous one-dimensional representation requires the evaluation of the overall heat transfer coefficient, U. The importance of the heat transfer parameter in the simulation has been thoroughly reviewed in the open technical literature (Stankiewick, 1989, Feyo de Azevedo *et al.*, 1990).

The overall heat transfer coefficient was first evaluated with the following equation derived from data summarized by Froment and Bischoff (1979)

$$\frac{1}{U} = \frac{1}{h_{out}} + \frac{1}{\alpha_W} + \frac{R}{4k_{er}} \tag{3.29}$$

Various parameters involved in eq (3.29) were calculated with the following correlations, as recommended by Froment and Bischoff (1979a):

$$\alpha_W = \frac{k_g}{d_p} \exp^{(0.077+0.523 \ln Re_p)} \tag{3.30}$$

$$k_{er} = k_g \left(8.33 + \frac{Pr Re_p}{Pe_{mr}} \right) \tag{3.31}$$

with: $$Pe_{mr} = u_s \times \frac{d_p}{D_{er}} \tag{3.32}$$

$$h_{out} = k_c \times \frac{(0.203 \times Re^{0.333} \times Pr^{0.333} + 0.22 \times Re^{0.8} \times Pr^{0.4})}{0.0015} \tag{3.33}$$

Eq (3.29) provides good modeling of U in an ample range of conditions (flow rates, particle and tube diameters, type of packing).

It has to be mentioned that the pseudo-homogeneous one-dimensional model, as such, generates a predicted temperature profile representing the average temperature in the cross- section.

In order to estimate the temperature at the reactor centerline, r=0, eq (3.34) can be adopted:

$$T^* = T + \frac{\frac{B_i}{4}}{1+\frac{B_i}{4}}(T - T_c) \qquad (3.34)$$

Eq. (3.34) (Beek and Singer, 1951) relates the average temperature and the centerline temperature by means of the Biot number. The basic assumptions of eq (3.34) are that the temperature is a quadratic function of the radial position and that the average rate of the reaction is equal to the reaction rate corresponding to the average temperature. Eq 3.34 normally apply for mild radial temperature changes.

3.10. Conclusions

The present chapter reviews the technical literature concerning Fischer-Tropsch and particularly synthesis of hydrocarbons using cobalt supported catalysts. Various relevant aspects regarding reactor modeling such as probability growth, chain parameter, reaction stoichiometry and kinetic rates are reviewed.

This review expands on the various possible available kinetic models and the interrelation of these models with various mechanistic steps.

The literature review is completed with a description of the FT reactors and the modeling aspects of fixed bed reactors operating. Also the pseudoadiabatic regime, a desired operating condition to be studied in the context of the present study, is reviewed in significant detail.

CHAPTER 4

EXPERIMENTAL APPARATUS

4.1. Catalyst testing apparatus.

Figure 4.1 reports a schematic diagram of the experimental set-up used to evaluate the catalyst for the production of paraffins by the Fischer-Tropsch synthesis. This set-up includes a pressurized cylinder containing the reactants mixture (H_2/CO ratio of 1, 2, and 3), hydrogen gas (Hydrogen 99.99%), and inert gas (nitrogen). The inert gas was used to purge the system and to test the system for any leaks. Traps of molecular sieves were used to remove O_2, H_2O, and any metal carbonyl (Ni, Fe) impurities present in the reactant gas.

The flow-rates were measured and controlled using a Brooks 5850 series mass flow controller. A detailed explanation about the calibration procedure of the mass flow controller is given in Appendix A.

A check valve is placed immediately after the mass controller to prevent back flow. A relief valve is also included for safety measures in order to prevent any undesirable increment of the system total pressure. A three-way valve is used to direct the flow of gas either to the reactor or to bypass the reactor.

During a typical experiment the reactants mixture was circulated through the reactor, a 7.62 cm (3") I.D. Berty recirculation reactor manufactured by Autoclave Engineers. Products and unreacted synthesis gas exited the reactor via two condensers. The first of these two condensers was operated at 60°C, to

collect most of the liquid products. The second condenser was operated at 3 °C (ice trap) to trap the remaining fraction of any remaining condensable hydrocarbons.

The reactor pressure was controlled by a Tescom back-pressure regulator series 26-3200 provided with a high temperature polyamide seat. An additional valve was installed just before the back-pressure regulator to prevent the flow of feed returning into the reactor through the bypass loop. These two valves were set inside a heated box.

A three-way valve was installed after the backpressure regulator to direct the product gas flow (unreacted gas and uncondensed products) either to the wet test meter or to the gas chromatograph. A wet test meter (Precision Scientific Co.) was used to meter the gas flow. Periodic calibration of the wet test meter was performed using a bubble flow meter located at the outlet of the apparatus.

On-line gas chromatograph injection was performed in a Hewlett-Packard 5890 Series gas chromatograph. A heated six-port valve with a 1 ml loop with an additional one-way valve and a manometer at the outlet of the loop were used to keep constant both the volume and the pressure of the injection.

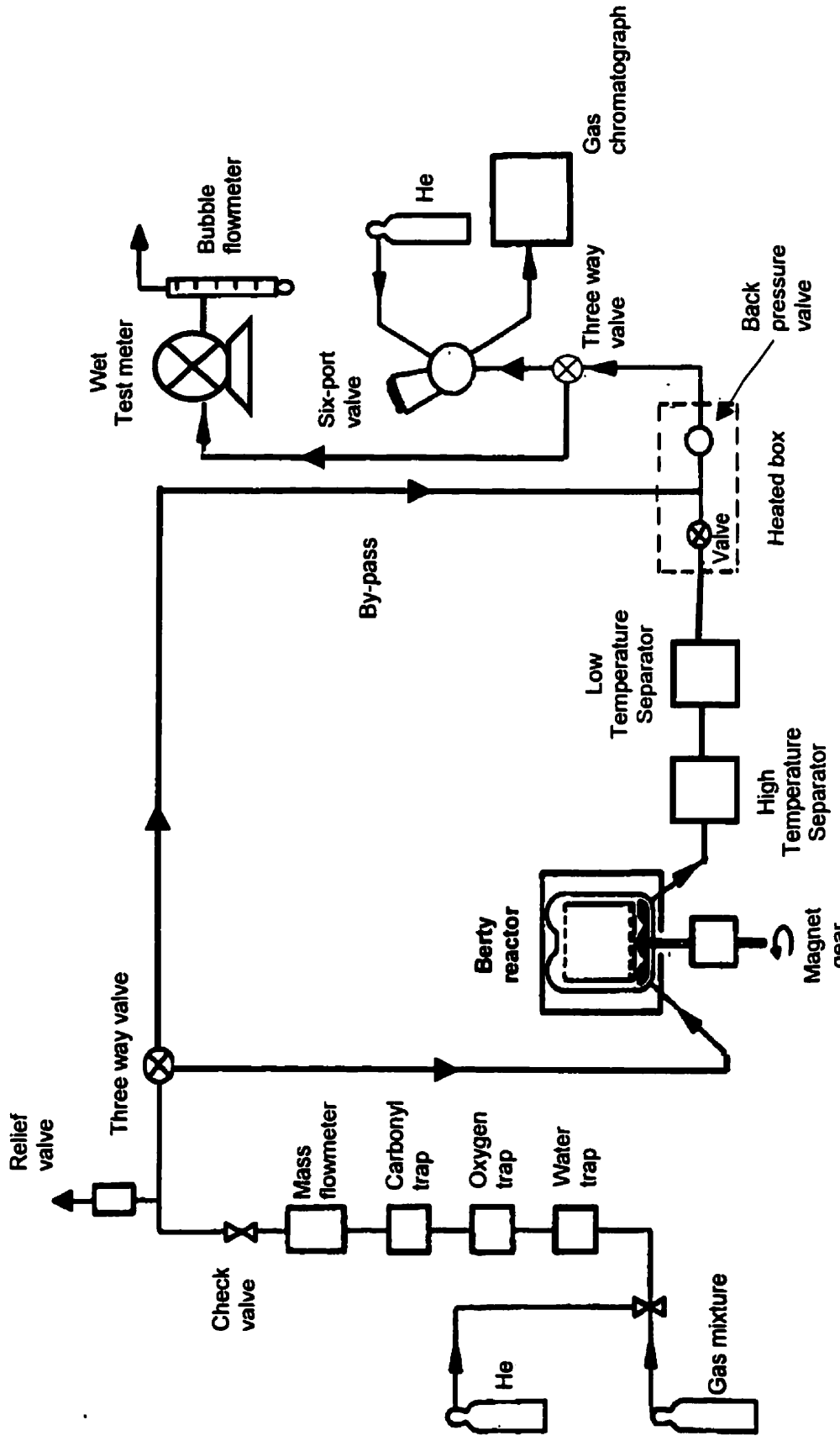

Figure 4.1. Catalyst testing apparatus

All lines from the outlet of the Berty reactor until the six-port valve were wrapped with heating tapes to keep temperatures around 75 °C. This was done to prevent any possible gas condensation or solidification of higher hydrocarbons (waxes).

Finally, the reactor outlet stream, after it circulated through the wet test meter, was sent outside the building through a ventilated exhaust.

4.2. Berty Reactor

All experimental runs were performed in a Berty reactor with internal recirculation manufactured by Autoclave Engineers. Details about the reactor and its configuration are shown in Figure 4.2. The Berty reactor used includes a 7.64 cm (3") inner diameter stainless steel body with an original basket volume of 2.54 cm (1") diameter and 5.08 cm (2") height. The basket volume was reduced by means of an aluminum insert. This was done to facilitate the testing of smaller samples.

Three heated zones (two at 1.1 kW and one at 0.8 kW) constitute the reactor heating system. The reactor temperature was controlled within ± 1°C by a proportional temperature controller. The temperature of the system was monitored by two thermocouples, the first one located in the upper reactor section and the second one inside the catalytic bed. The thermocouples were connected to an electrical circuitry, which enables the measurement of temperature gradients in the gas film surrounding the basket and the temperature gradients inside the catalysts.

A magnetically driven impeller induces internal gas recirculation: upflow in the circumferential area around the basket and downflow in the catalyst bed (located in the basket). Bub and Baerns., (1980) reported that a gradientless operation is achieved with this unit at the speed of 1450 rpm of the impeller.

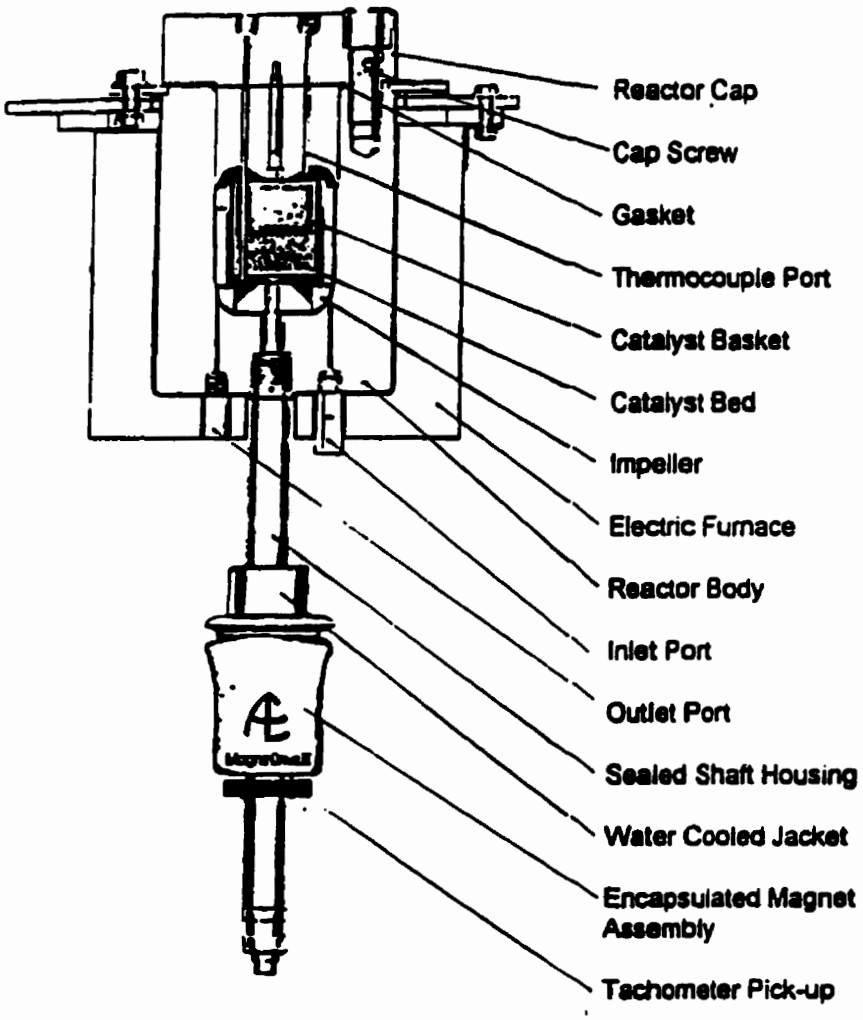

Figure 4.2. Berty fixed bed reactor, manufactured by Autoclave Engineers.

The Berty reactor reproduces reaction rates and mass velocities occurring in commercial fixed bed reactors. This unit operates, in fact, under

a kinetic regime and heat and mass transfer conditions between the catalyst and the reactant close to industrial catalytic units (Berty, 1974).

It is interesting to mention that the Berty reactor has already been employed by several researchers to get kinetic measurements for the Fischer-Tropsch reaction. Bub and Baerns (1980) used a Berty reactor with a iron-manganese catalyst to get a kinetic expression to predict the performance of catalytic fixed bed reactors for the FTS. Dixit and Tavlarides (1983) proposed several kinetics models for the FTS having as a starting point experimental runs performed in an internally recycled Berty reactor.

4.3. Startup procedure

A standard catalyst activation pretreatment was used in all experiments. The catalyst (10cc) was reduced in a Berty reactor at 1.6 MPa on a stream of pure hydrogen (40 cc/min). The reduction process was carried out in three steps using three different heating ramps and dwelling times. Details about the conditions employed during the reduction process are summarized in Figure 4.2.

After the reduction was completed, the reactor was cooled down under hydrogen flow. When the reactor temperature reached about 180 °C the hydrogen flow was cut off, and synthesis gas (H_2/CO = 2:1) was circulated at a gas space velocity of about 500 h^{-1}, with the space velocity being defined in STP cm^3/cm^3 catalyst • h. Moreover, the reactor temperature was gradually increased to 220 °C over a period of 24 h (conditioning period). This

conditioning is required not only to prevent the formation of hot spots but also to achieve nearly isothermal conditions.

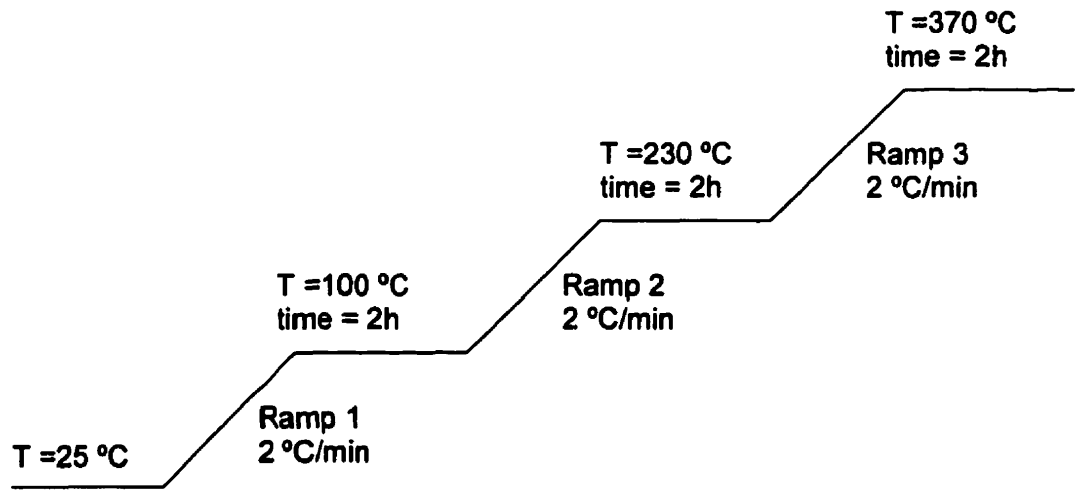

Figure 4.3. Operating conditions for activation process.

During the first 36 hours of operation an initial unsteady-state behavior (catalyst initial deactivation) was observed. Thus, the first mass balance was effected after having the catalyst 48 hours on stream. This ensured that steady state had been reached. Also after any change of process conditions, the reactor was allowed to operate undisturbed for 24 hours and this in order to achieve steady conditions and before the next mass balance was performed.

Both total mass and atomic material balances were performed with the special consideration that to accept a run for further analysis the oxygen material balance has to be closed between 97 to 103 %. Otherwise the run was rejected. This consideration was adopted since compounds containing carbon and hydrogen may accumulate in the reactor in the form of high

molecular weight hydrocarbons. This accumulation of heavy hydrocarbons may negatively affect the overall mass balance.

4.4. Gas Chromatograph Analysis.

The quantification of the mixture composition was performed by using the External Standard (ESTD) method of calibration. The ESTD procedure reports the amounts of components according to the formula:

$$\text{Amount of } i = Ap_{(i)} \times ARF_{(i)} \qquad (4.1)$$

where $Ap_{(i)}$ is the area of the GC peak for sample component (i) and $ARF_{(i)}$ is the absolute response factor for the sample component (i).

4.4.1. H_2/CO calibrations

Three reactant mixtures, with different hydrogen to carbon monoxide ratios, were used during the catalyst evaluation. Thus, H_2/CO of 1:1, 2:1 and, 3:1 ratios were considered. These mixtures were prepared using gases certified by BOC Gases. A typical report of the gas certification is included in Appendix B. TCD calibrations for this mixture were carried out and the results of these calibrations are presented in Table 4.1.

Table 4.1. Calibration of TCD for the different H_2/CO ratios

Component	BOC Gases analysis	UWO Lab. Analysis	Response factor ARF(i)
H_2/CO ratio	1		
H_2	51.1	50.9	2.512e-3
CO	48.9	49.1	1.0344e-4
H_2/CO ratio	2		
H_2	33.7	32.9	2.1805e-3
CO	66.3	65.1	9.8348e-5
H_2/CO ratio	3		
H_2	75.3	75.7	1.6874e-3
CO	24.7	24.3	8.4414e-5

4.4.2. Gas Product Analyses

The stream leaving the reactor (unreacted gas and non-condensable products) was analyzed on-line into a Hewlett Packard gas chromatograph (GC) model 5890 equipped with a cryogenic unit. The equipment also included a 1.83 m long, 0.318 cm diameter (6 ft-1/8") Porapak Q column and a Thermal Conductivity Detector (TCD).

A temperature program was set in the GC to improve separation of the product mixture. After the injection, the column was maintained at -30 °C for 1 minute, after that the temperature was ramped at 40 °C/min to a maximum temperature of 240 °C where it was held for 4 minutes. Because helium was used as a carrier gas and as a reference gas a change of the polarity of the TCD was implemented, after the hydrogen peak was detected.

4.4.2.1. Calibration with Gas Mixtures

A gas calibration mixture prepared and certified for BOC Gases, which simulates the composition of the gaseous products, was used to calibrate the TCD. The reported composition provided by BOC Gases for this mixture is included in Appendix C.

Table 4.2 presents the results of the calibration of the TCD using a gas mixture supplied by BOC Gases. It can be appreciated, from Table 4.2, that both compositions BOC Gases and UWO-Laboratory are similar. Also, the absolute response factor for each component was calculated and reported in Table 4.2. Note that periodic calibrations of TCD were also performed in order to secure reproducibility of the analytical technique.

Table 4.2 Calibration of the TCD for gaseous product.

Component	Composition BOC Gases (%vol/vol)	Composition UWO-Lab (%vol/vol)	Absolute response factor $ARF_{(i)}$
n-Hexane	0.106	0.111	4.8747E-5
n-Pentane	0.204	0.211	5.1132E-5
n-Butane	0.499	0.509	4.1411E-5
Propane	0.501	0.505	5.9785E-5
Ethylene	0.782	0.80	8.9480E-5
Ethane	0.292	0.29	2.8616E-5
Methane	3.0	3.01	7.1188E-5
Carbon dioxide	4.99	5.04	1.4415E-4
Nitrogen	2.89	2.86	4.2676E-5
Carbon monoxide	28.0	27.91	9.8348E-5
Hydrogen	58.7	58.13	2.180E-3

4.4.3. Liquid Product Analyses

During the mass balance period the liquid products (hydrocarbons + water) were allowed to accumulate in the two separators (HTS and LTS; Figure 4.1). After that, the liquid product was collected and physically separated into aqueous fraction and hydrocarbon fraction. Note that in the present study the aqueous fraction is considered only water given that oxygenates compounds are rarely produced when a cobalt catalyst is used (Adesina, 1996).

The hydrocarbon fraction was analyzed by using a 25m - 0.33μm HP-1 crossed linked methyl-silicone capillary column and a flame ionization detector (FID). The temperature program adopted was as follows: a) the temperature of the column was initially maintained at -20 C for 1 min, b) the column was heated up to 300 C at the rate of 25 C/min., where it was held for 60 minutes.

4.4.3.1. Calibration with Liquid Mixture

The identification of the hydrocarbon fraction was performed using a flame ionization detector (FID). For the calibration of the FID a Boiling Point Calibration Sample # 1, from Hewlett Packard, was used. This calibration sample, a mixture of hydrocarbons from C_5 to C_{40}, is described in detail in Appendix B.

CHAPTER 5

CATALYST PREPARATION AND CHARACTERIZATION

5.1. Introduction

This chapter presents details about the apparatus and methodology used for the preparation and characterization of the catalysts evaluated in the present study. Two types of catalysts were prepared using the following components: a) cobalt as active phase, b) zirconium as promoter, and c) silica gel as a support. One of the catalysts was uniformly impregnated (standard) while the other was the so-called eggshell catalyst, in which the active metals were deposited on the external surface of the support.

This chapter has been divided into two sections. The first section describes the materials used for the preparation of the catalysts and the techniques employed for their characterization. The second section reports a discussion about catalyst characterization results.

5.2. Experimental

5.2.1. Materials

Spherical silica gel from UOP, DAR-240, was used as a support for the catalysts investigated in the present study. The main properties of this material are reported in Table 5.1.

The impregnation of the support was effected with an aqueous solution of cobalt nitrate prepared with $Co(NO_3)_3 \bullet 6H_2O$ from Aldrich, 99% purity. This solution contained about 1 wt % of an aqueous solution of 20 wt % zirconia added to promote the FTS.

Table 5.1. Physical properties of the silica DAR-240.

Property		Reference
Surface area (m^2/g)	372	This work
Pore volume (cm^3/g)	1.0342	This work
Apparent particle density (g/m^3)	0.368 – 0.364	Supplier
True particle density (g/cm^3)	0.589 – 0.582	Supplier
Average particle size (mm)	1.81 ± 0.01	This work
Porosity (dimensionless)	0.6401	This work
Pore radius (Å)	55	This work
Particle radius (mm)	0.905	This work

5.2.2. Preparation of standard catalysts

In the context of this work a "standard" catalyst is defined as a uniformly impregnated catalyst, where the metal loaded has a nearly homogeneous metal distribution across the radius of the support.

The experimental set-up used in the preparation of the standard catalyst is shown in Figure 5.1. The incipient wetness technique was used to prepare this type of catalyst. This technique is based on the quantitative

addition of an impregnating solution: the amount of solution added depends on the available pore volume in the catalytic support with no excess of supernatant liquid allowed on top of the particles.

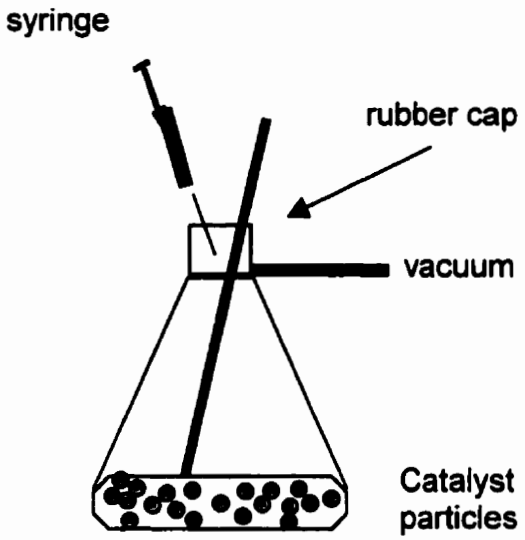

Figure 5.1. Experimental set-up for the preparation of standard catalysts.

Following this procedure 20 g of silica gel were placed in the glass container (Figure 5.1) and evacuated during 20 min. After this period, the calculated amount of solution (cobalt nitrate + zirconium solution) was incorporated into the container using a syringe. In order to insure the uniform distribution of the solution into the support, the liquid from the syringe was injected in several steps. After each step, the wet support was thoroughly mixed with a glass rod until even distribution was visually observed.

After impregnation, the catalysts were dried at ambient conditions over night. Following this, the catalyst was dried at 100 °C, during 2h. Finally, the sample was calcined during 4 hours in air at 400 °C with a heating rate of 5 °C/min.

5.2.3. Preparation of eggshell catalyst.

This section includes a detailed description of the methodology used to prepare a non-uniform impregnated cobalt-zirconium eggshell catalyst. Basically most of the active metal is preferentially located near the outlet support surface. Figure 5.2 shows a schematic representation of the assembly used to prepare the eggshell catalyst.

For the preparation of the eggshell catalyst the support (20 g) was pre-wet with water. The objective of this was to fill the pore network before impregnation with the metal. However, no excess water was allowed on top of the particles (or interparticle). After that the prewetted support was placed in the container for impregnation. Then, an impregnating solution in a solution/support volume ratio of 5 was poured on the support. After 4 seconds, the vacuum line was opened and the excess of solution removed from the container. In order to stop the advance of the impregnating solution a "quench-in-hot" process was employed. With this end, the impregnated sample was placed in a sand fluidized bath which was equipped with a metal basket to recover the catalyst. The sand (particles of 60 μm average size) acted as heat transfer media to enhance fast drying of the catalyst particles

with drying being carried out at about 90°C to prevent the collapse of the porous structure.

After this quick drying process, the catalyst was heated at 5 °C/min up to 400 °C and calcined at that temperature during 4 hours.

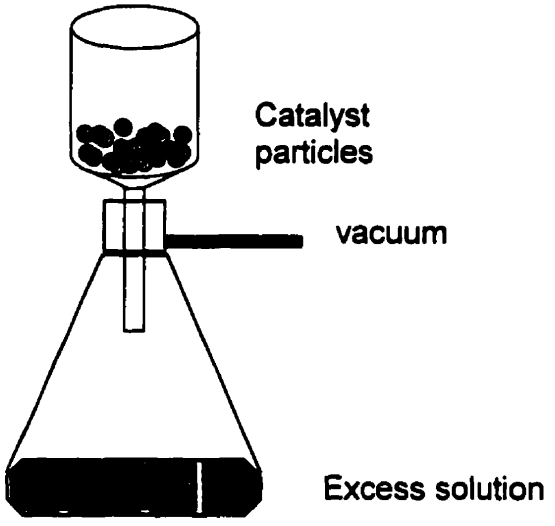

Figure 5.2. Experimental apparatus used to impregnate eggshell catalysts.

An alternative technique for preparing eggshell catalysts was also attempted by CREC researchers pouring the impregnating solution in a dry support. More details about this type of "eggshell" catalyst can be found in Galarraga (1998).

5.2.4. Catalyst characterization techniques

The catalysts considered in this study were evaluated using the following surface characterization techniques: a) atomic absorption (AA), b) BET surface area, c) temperature programmed reduction (TPR), and d) optical microscopy,

5.2.4.1. Metal content

The atomic absorption analyses were developed using the equipment of the Analytical Evaluation laboratories of PDVSA-INTEVEP in Venezuela. This technique was applied mainly to corroborate the amount of metal loaded on the support. The analyses were performed by dissolving the mineral species present on the catalysts samples.

5.2.4.2. Surface Area Analysis (BET)

The surface area of the catalysts was determined using a TPD/TPR 2900 Analyzer instrument, manufactured by Micromeritics. The type of analysis performed by this instrument is known as the single point BET since only one equilibrium pressure is obtained for the adsorption of nitrogen.

For the BET surface area analysis the sample was weighed and then outgassed under flow of helium at 120 °C during 2 hours. After outgassing, a mixture of 30% nitrogen and 70% helium (vol.) was circulated through the catalyst. The sample container was immersed in a liquid nitrogen bath to refrigerate the catalyst to 77 K at which temperature nitrogen was absorbed

onto the catalyst surface. Immersing the sample in water at room temperature desorbed the nitrogen.

Nitrogen desorption was measured by a Thermal Conductivity Detector (TCD). Four consecutive adsorption-desorption cycles were performed to assure reproducibility of the system and to determine the total amount of nitrogen desorbed.

In order to determine unknown amount of nitrogen a calibration of the TCD is required. Thus pulses of known volumes of nitrogen were injected directly to the TCD. The calibration curve obtained using this method is reported in Appendix D. The total amount of nitrogen desorbed was correlated with the total surface area by employing the BET model. A sample calculation is also presented in Appendix D.

5.2.4.3. Temperature programmed reduction (TPR).

The temperature programmed reduction (TPR) was also carried out on the TPD/TPR 2900 Analyser instrument. During the development of this analysis the sample is exposed to a mixture of hydrogen (10% vol.) in argon (carrier gas) with a flowrate of approximately 45 cc/min. In the meantime, the temperature of the sample was increased at a rate of 10 °C/min. As the catalyst was heated up, changes in the composition of the gaseous mixture were detected using a Thermal Conductivity Detector (TCD). Mainly, these changes were due to the hydrogen consumption by effect of the reducibility and reaction of the cobalt species on the catalyst.

5.2.4.4. Optical microscopy

This technique was used to confirm the formation of the so-called "eggshell" catalyst. The apparatus consists of: a) and stereomicroscope WILD model M3Z, b) a colour camera 3CCD from Hitachi, model HV-C20, and c) a colour video printer Mavigraph model UP-3000 from Sony. Direct micrographies were collected at the laboratories of Surface Science Western, by taking pictures of cross sections of eggshell catalysts. Pellet cross sections were prepared with the aid of he Department of Earth Sciences, The University of Western Ontario.

5.3. Results and Discussion

5.3.1. Metal content

Table 5.3 summarizes the results from the analytical evaluation of "standard" and "eggshell" catalysts. The table includes the elemental percentage for cobalt and zirconium. It can be appreciated that the "eggshell" catalyst has only 35% of cobalt and 25% of zirconium of the total amount loaded in the standard catalyst.

5.3.2. BET surface area.

Regarding the surface area for the "standard' and the "eggshell" catalysts (Table 5.3) it was found that the impregnation methodology has an important effect on the final surface area of the catalysts when compared with the surface area of the support (372 m^2/g). It was observed that the "standard'

catalyst displays a lower surface area (295 m^2/g) than the "eggshell" catalyst (352 m^2/g). These different surface areas for these catalysts may be explained given some plugging of pores occurs as metal is dispersed in the structure by impregnation. Note that the degree of plugging depends on metal loading. Because more metal was added to the standard catalyst then the reduction of the surface area was more significant than the one observed in the "eggshell" catalyst.

Table 5.2. Properties of the standard and eggshell catalysts.

Catalyst	Surface Area	Metal Content (wt %)	
	(m^2/g)	Co	Zr
Standard	295	11.92	0.89
Eggshell	352	4.18	0.223

5.3.3. Temperature programmed reduction

Figures 5.3 and 5.4 show the TPR profiles observed for the standard and eggshell catalysts, respectively. For both cases two very well defined peaks were observed. The first one close to 300 °C (low temperature) was assigned to the transition of Co^{3+} to Co^{2+}. The second peak about to 320°C (high temperature) is very likely due to the transition from Co^{2+} to Co^0. It has to be mentioned that Ming and Baker (1995) and Lapidus *et al* (1991) reported similar results when studying the reducibility of Co based catalysts supported either on silica or on alumina.

However, it is interesting to mention that some differences between the two spectra were observed. The first difference is that for the eggshell catalyst the transitions occurred at lower temperatures than those observed for the standard one. The second aspect involves the existence of a broader profile found in the eggshell catalysts at temperatures around 400 °C (Figure 5.3 zone marked as "a"). This behavior was not detected for the standard catalyst. It has been claimed that the sharpness on a TPR profile depends on both crystallite size and particle size uniformity (Micromeritics, 1992). Since the silica support employed exhibits a high uniformity between particle sizes, it can be concluded that the eggshell catalysts exhibits a broader crystallite size distribution than that of the standard catalyst.

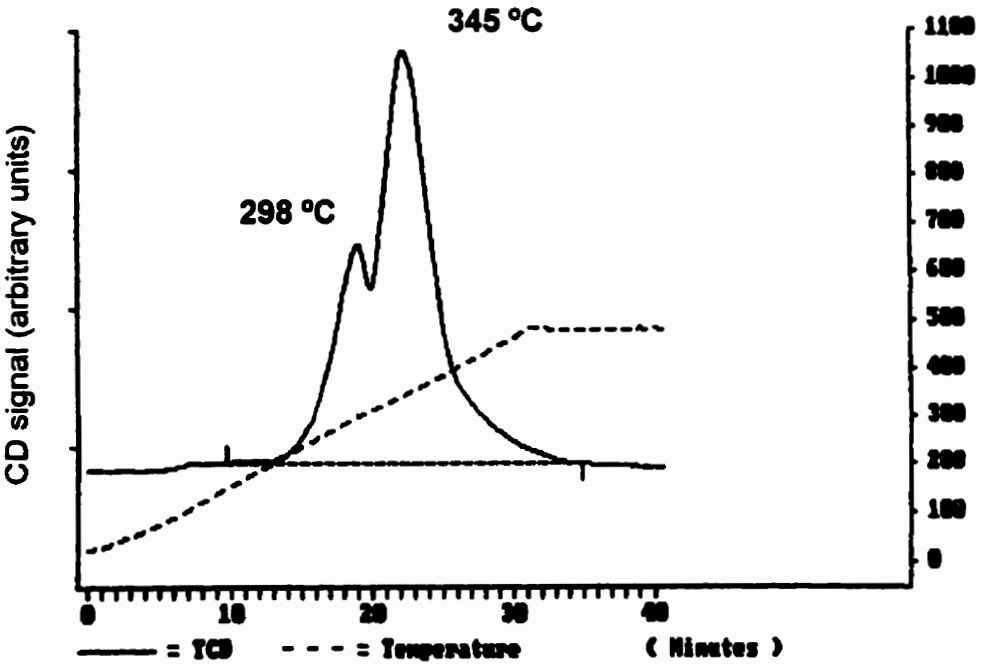

Figure 5.3. TPR profile for standard catalyst.

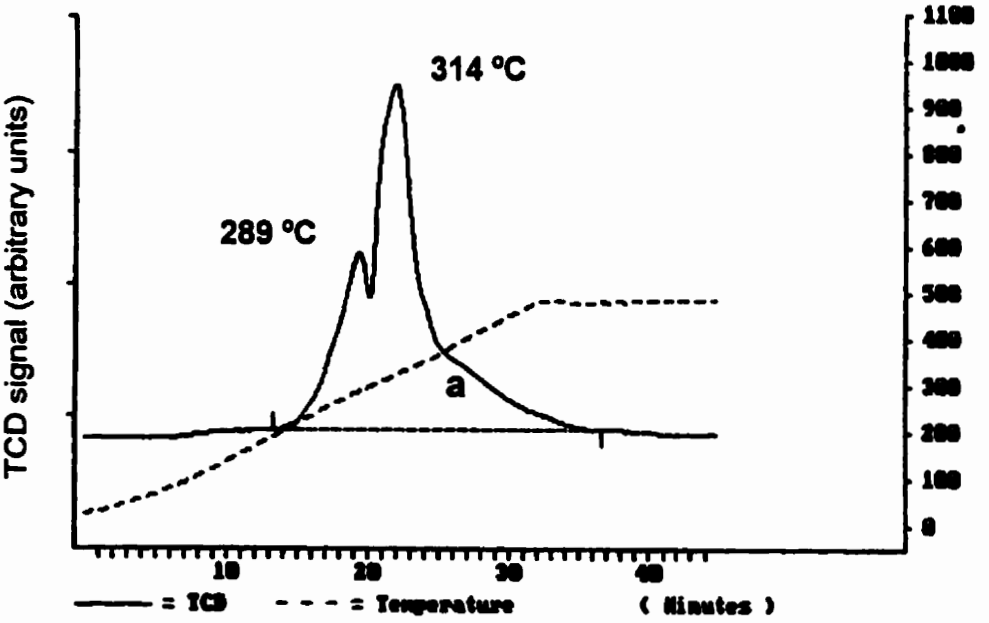

Figure 5.4. TPR profile for the eggshell catalyst.

5.3.4. Optical microscopy

The visual observation of the eggshell thickness was performed using the optical microscopy technique. Figure 5.5 shows micrographies of cross-sections for both the standard and the eggshell catalysts. The micrography for the standard catalyst (Fig. 5.5.a) shows, as it was expected, a homogeneous distribution of the metal in the silica gel support.

On the other hand, the eggshell catalyst (Fig. 5.5.b) exhibits a non-uniform distribution of metal in the support with most of the metal preferentially located near the outer region of the support surface. A very homogeneous external annulus was observed (black circumference) which indicates a high concentration of metal in this zone. On the other hand, the inner core represented by a grey and white colour zone, shows a very low concentration of metal.

From Fig. 5.5.b it can be inferred that the preparation of eggshell catalyst, where most of the active metal is placed in the outer surface of the support, was successfully achieved.

Finally, it is worth to mention that additional characterization work on these eggshell catalysts has been reported elsewhere (Galarraga, 1998). This work also included: a) the determination of metal distribution profiles by means of scanning electron microscopy, b) the evaluation of metal crystallite sizes and metal dispersion by using hydrogen pulse chemisorption.

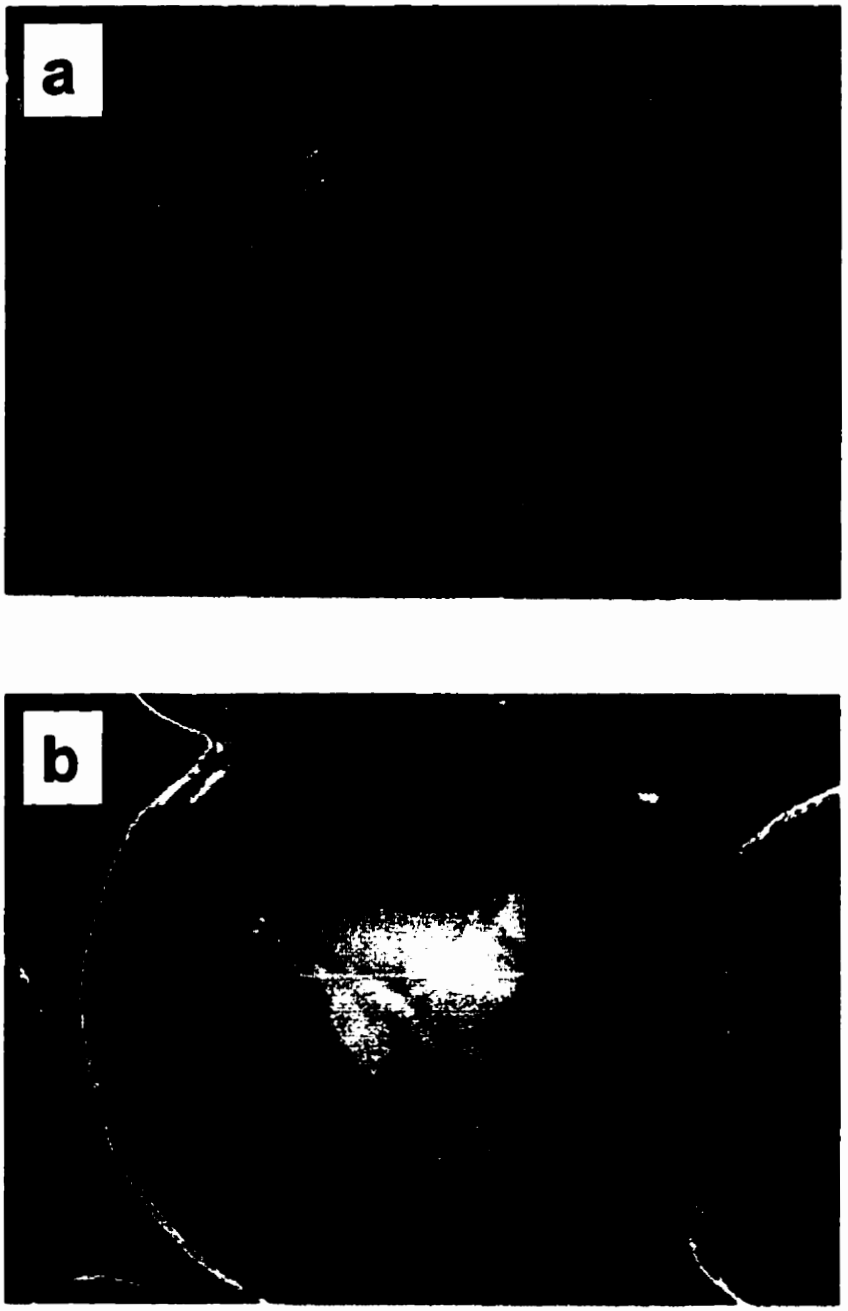

Figure 5.5. Micrographies as obtained from optical microscopy: a) standard catalyst (27 x), b) eggshell catalyst (42 x).

5.4. Conclusion

The characterization techniques used in this work allow to establish the difference between the standard and the eggshell catalyst. The TPR for both catalysts shows two peaks as indication of the chemical evolution of the species present in these catalysts. It was also found, that 350 °C is the minimum temperature required to produce the desired active species.

Various characterization techniques provided useful information about metal content, surface area and distribution of the metal in the support. Thus, it was demonstrated that the methodology used for the preparation of the eggshell catalysts was adequate.

CHAPTER 6

RESULTS AND DISCUSSION

6.1. General overview

This chapter reports experimental results obtained during the course of this research. The first section of Chapter 6, provides a comparison between two Co-Zr-Si catalysts: a) a standard (uniformly impregnated) catalyst, b) an eggshell catalyst. Following this, the effect of various operating conditions such as temperature, pressure, gas hourly space velocity and inlet H_2/CO ratio on the performance of the eggshell Co-Zr-Si catalyst is examined.

More specifically, to provide a comprehensive evaluation of catalyst performance the overall CO conversion, the product selectivity and the hydrocarbon distribution are considered. Finally, this data is employed to find a suitable kinetic model representing properly the experimental results.

6.2. Preliminary study

6.2.1. Introduction

In this section a comparison of the performance of two different types of catalysts, a) Standard (uniformly impregnated) Co-Zr-Si catalyst, and b) Eggshell Co-Zr-Si catalyst, is analyzed on the basis of the CO conversion, the product selectivity and the hydrocarbon distribution. Details about the

procedures for preparing and characterizing these catalytic systems are described in section 4.4.4.

For the reaction testing, the apparatus already described in Chapter 4 was employed. In terms of general experimental procedure, the one already presented in detail in Chapter 4, was adopted. Care was taken in order that the runs were developed under conditions close to steady state: catalyst time-on-stream > 48 h.

Regarding the overall mass balances, mass balances were carried out for these experiments every 24 hours with complete runs exceeding 120 hours.

Note that two digits were employed to identify each experimental run. The first digit represents the number of a complete experiment while the second one identifies the run number inside a complete experiment. To provide a complete description of the runs performed a detail listing of experiments is included in Appendix E.

6.2.2. Comparison between Standard (uniformly impregnated) and Eggshell catalysts.

In order to compare the performance of the two catalysts the standard (uniformly impregnated) catalyst was evaluated at two different temperatures, 230 and 220 °C while the eggshell catalysts was tested at 220 °C only. The rest of the other operating conditions were kept constant, as presented in Table 6.1. Details about the experimental conditions are included in Appendix E.

6.2.2.1. Carbon monoxide conversion

Given that the total amount of cobalt loaded in the standard (uniformly impregnated) catalyst is much higher than the cobalt content in the eggshell catalyst, a performance comparison was developed with reaction rates defined on the basis of the unit weight of cobalt.

Thus, Table 6.1 reports reaction rates for these two catalysts, with rates in millimoles of carbon monoxide converted per unit time and per unit mass of cobalt available. Comparison of these reaction rates shows that the eggshell catalyst is more active than the standard catalyst at the same operating conditions. For example, at 220°C the eggshell catalysts displayed a CO consumption rate of -0.01435-mmole/(min gCo) while the standard catalyst showed a CO consumption rate of -0.00813-mmole/(min gCo). Even more, increasing the temperature from 220 to 230 °C, the rates increased, with the standard catalyst, displaying a CO consumption reaction rate up to -0.01268-mmole/ (min gCo). This rate was still lower than the CO consumption rate found at 220 °C with the eggshell catalyst.

Concerning product selectivity it was found (Table 6.1) that CO_2 formation increases from 2.58% to 8.47% when temperature was increased from 220 to 230 °C. In both cases, however, the selectivity towards CO_2 was significantly higher than the one observed in the eggshell catalysts where it remained at 0.5%.

Table 6.1. Summary of operating conditions used for testing standard and eggshell catalysts.

Catalysts	Standard		Eggshell
Experiment number	13-6	14-6	15-6
Operating conditions			
Temperature (°C)	230	220	220
Pressure (MPa)	1.52	1.52	1.52
GHSV (h^{-1})	342	342	342
H_2/CO ratio inlet	2:1	2:1	2:1
Analytical results			
CO conversion, %	70.44	50.62	25.7
H_2 conversion, %	72.41	49.09	25.93
$-r_{CO}$,(mmol CO conv. /min/gCo)	0.01268	0.00813	0.01435
Mass balance, % (global)	95.5	99.9	97.5
Mass balance, % (oxygen)	98.3	99.9	98.6
Product selectivity (%)			
Carbon dioxide	8.47	2.58	0.5
Water	49.12	54.35	56.90
Hydrocarbons	42.41	43.07	42.6

6.2.2.2. Hydrocarbon product distribution

Hydrocarbon distribution is another important parameter while using the catalysts of the present study. Fig. 6.1 reports the various weight fractions within the hydrocarbon fraction. It can be observed that, in this respect, the standard (uniformly impregnated) Co-Zr-Si catalyst displayed a similar behaviour than the one reported in the literature for other similar catalysts

(Dry, 1990 and Dalai et al. 1992). First, it can be noticed, that an increment of temperature led to shifts in hydrocarbon production towards lower molecular products: selectivity to methane, C_2-C_4 and C_5-C_9 hydrocarbon fractions was increased while the C_{10}-C_{20}, and C_{21}^+ fractions were reduced.

Moreover, hydrocarbon distributions for the standard (uniformly impregnated) catalyst and for the eggshell catalyst are presented in Fig. 6.1. It can be observed that the eggshell catalyst has an important impact on hydrocarbon distribution. The eggshell catalyst has a lower selectivity towards methane as well as toward C_{21}^+ hydrocarbons. However, the eggshell catalyst favours the formation of hydrocarbons in the C_{10}-C_{20} range (refer to Fig 6.1), a very interesting fraction for refining processes. This is even more relevant given the prevalent paraffinic character of this fraction (van Burgt *et al.*, 1988).

6.2.2.3. Anderson Schultz Flory distribution

It is interesting to further analyze the hydrocarbon distribution using the Anderson-Schultz-Flory (ASF) distribution. Fig. 6.2 presents the changes in W_n/n as a function of the carbon number "n" for the standard catalyst at 220 °C and 230 °C and for the eggshell catalyst at 220 °C. Therefore, one can analyze the effect on the chain growth probability for two different cases: a) effect of temperature for the uniformly impregnated catalyst, and b) effect of impregnation methodology (by comparing both standard and eggshell catalysts tested at 220 °C).

For all the cases considered (standard and eggshell catalysts), it was found that there is some deviation of the ASF distribution between carbon

numbers 2 and 3 with a break point of the ASF at carbon number 8 (Fig. 6.2). This deviation has been reported previously by several authors (Dalai et al. 1997, Soled et al. 1995, Fox and Tam 1995, Satterfield and Stenger 1984). A possible explanation of this deviation is the existence of at least two different α values with this parameter expressing the probability of chain hydrocarbon growth: one α represents the synthesis of the low carbon number molecules while the other the synthesis of high carbon number molecules.

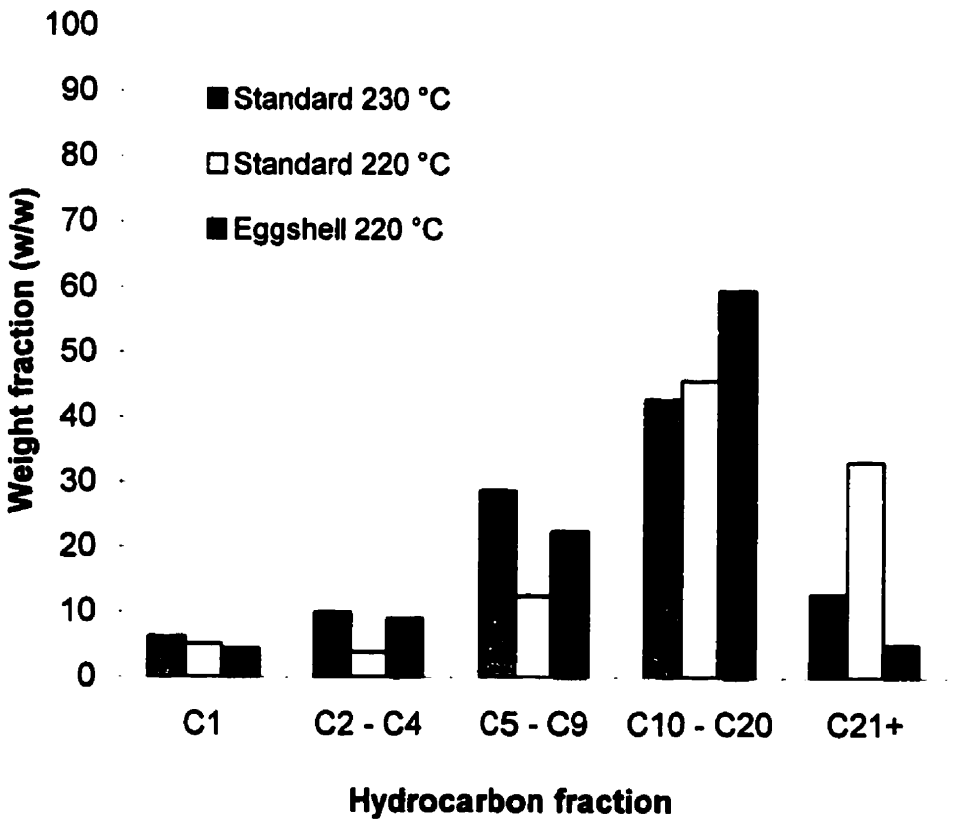

Figure 6.1. **Hydrocarbon product distribution for Standard (uniformly impregnated) and Eggshell catalysts. Tests performed at: pressure = 1.52 MPa, GHSV = 342 h^{-1}, and inlet H_2/CO ratio = 2.**

In spite of this and to be able to compare in a quantitative basis the effect of temperature on α, the slope of the best straight line in Fig.6.2 for the range of C_{12}^{+} was calculated. It can be observed (Fig. 6.2) that in the case of the standard (uniformly impregnated) catalyst a decrease in the value of α, from 0.9 to 0.85, arises when temperature is increased from 220 to 230 °C. Thus, higher temperatures tend to favour formation of lower carbon number molecules. Note that a similar temperature effect over α was reported by several authors (Singleton and Regier 1983; Stenger and Askonas, 1986; Dry, 1990 and Dalai et. al. 1992).

Fig. 6.2 also presents the Anderson-Schultz-Flory distribution for the eggshell catalyst. Similar anomalies were observed for molecules with 2 and 3 carbon numbers with a break point of the ASF distribution at carbon 8. Further, it is interesting to mention that the eggshell catalyst displayed a similar α parameter with respect to the standard (uniformly impregnated) catalyst between carbon 9 to 15. However, the eggshell catalyst yielded a hydrocarbon product distribution for the C_{10}-C_{20} fraction that deviated significantly from the one of the standard (uniformly impregnated) catalyst. As a result, a lower α parameter ($\alpha \approx 0.8$) showing a narrower hydrocarbon product distribution was obtained with the eggshell catalyst.

For standard cobalt catalysts it has been reported that the diffusional problems during the FT synthesis produce consecutive reinsertions of the α-olefins, which are a product of the β-hydrogenation reaction (Kuipers *et al.*,

1996). A consequence of this reinsertion is that the α-olefins grow bigger and since the active metal exhibits a high hydrogenating activity the α-olefins end up as high molecular weight paraffins. On the other hand, the hydrogenolyzing activity of cobalt (cleavage of C-C bonds as a result of hydrogen presence) favours the production of the C_{11}-C_{16} range.

Thus, it can be argued that the eggshell catalyst exhibits such a balance, between hydrogenation and hydrogenolysis, that it produces a narrower product distribution than the standard catalyst. Furthermore, it appears there is reduced probability of α-olefin reinsertion in the eggshell catalyst versus the one observed for standard catalysts.

6.2.3. Conclusion

This section reports a comparison between Co-Zr-Si catalyst based on a standard (uniformly impregnated) and eggshell formulations. Comparisons are mainly developed assessing the influence of catalyst formulation on carbon monoxide conversion (carbon monoxide disappearance rates), product selectivity and hydrocarbon distribution.

It is observed that the standard catalyst displays an increase of the carbon monoxide disappearance rates with reaction temperature. This increment of temperature also produces an important increment of carbon dioxide yields with a concurrent shift towards the production of lower molecular weight hydrocarbons.

Moreover the prepared eggshell catalyst shows the following: a) a higher carbon monoxide disappearance rate, and b) a richer hydrocarbon product fraction in the C_{10}-C_{20} range.

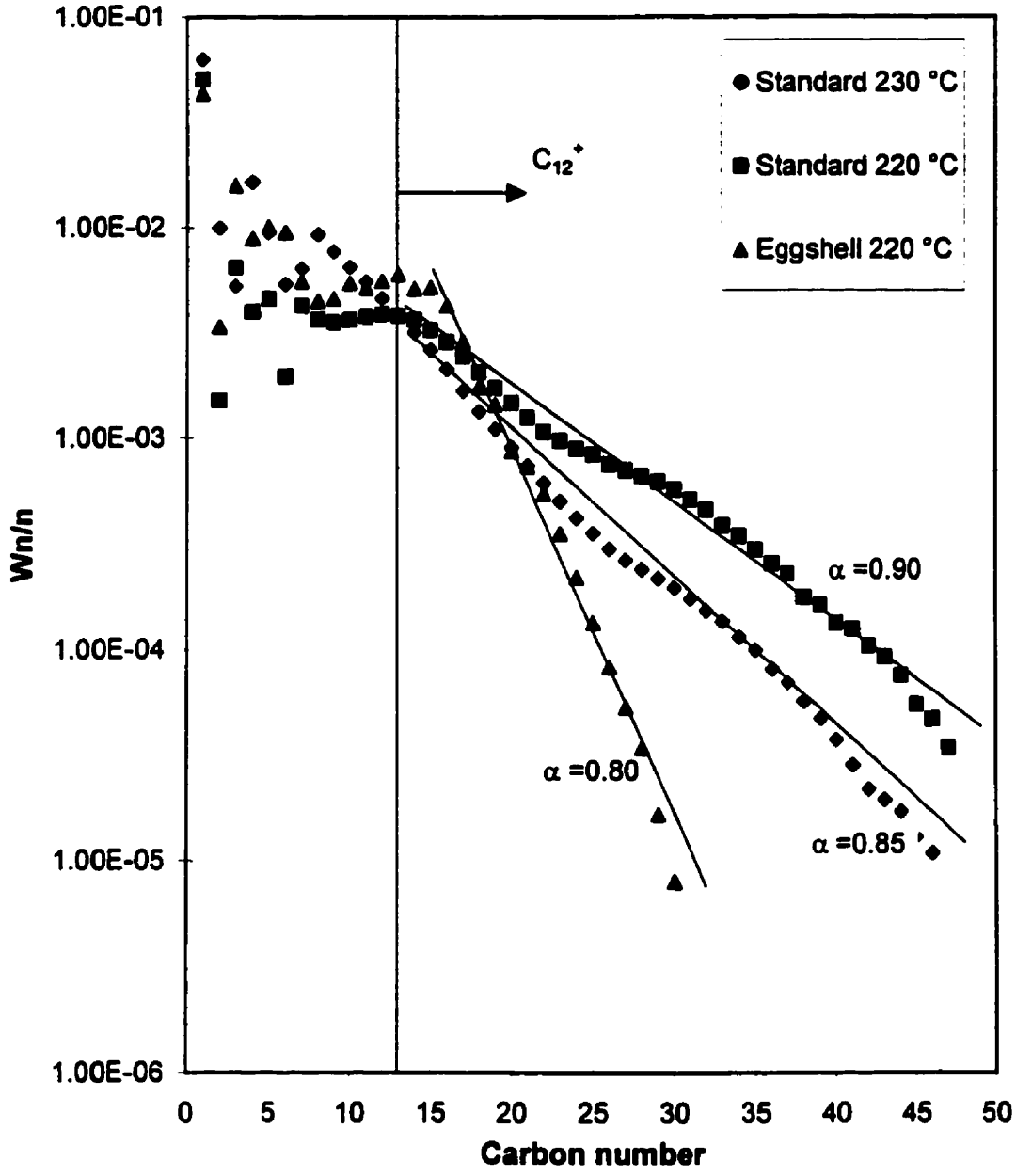

Figure 6.2. Anderson-Schultz-Flory distributions and alfa parameters for Standard and Eggshell catalysts. Tests performed at P = 1.52 MPa, GHSV = 342 h^{-1} and inlet H_2/CO ratio =2.

6.3. Effect of the operating conditions

6.3.1. Introduction

Given the encouraging results obtained while comparing the performance of both the standard (uniformly impregnated) and the eggshell catalysts it was decided to proceed to a systematic evaluation of the eggshell catalyst.

In this respect, this section describes the effect of changing various operating conditions such as temperature, pressure, gas hourly space velocity and inlet H_2/CO ratio on carbon monoxide conversion, product selectivity, and hydrocarbon product distribution.

The following range of operating conditions were selected for the studies:

a) Temperature : 209 - 229°C,

b) Pressure: 0.35 – 1.52 MPa,

c) Gas hourly space velocity, GHSV: 200-505 h^{-1},

d) H_2/CO ratio: 1 to 3.

6.3.2. Experimental Procedure

The experimental set-up, as well as the experimental procedure for these runs, has been already described in Chapter 4 of this thesis. The catalyst used was an eggshell Co-Zr supported on silica. Details about the preparation and the characterization of this catalyst are reported in Chapter 5.

During the development of these experiments, a single batch of catalyst (10 cm^3) was employed. After reduction (refer to Section 4.3.) the synthesis gas was fed to the reactor unit with the catalyst being kept under the same operating conditions for 120 hours.

After completing this preparatory phase, the first experimental test was developed (Run 17-1). This experimental condition to be repeated frequently during the experimental program was, in the context of the present study, identified as the "reference condition". In addition to this, runs were extended in between operating conditions having the catalyst on stream, for periods long enough as to ensure that the steady-state behavior was reached. It was judged that the time for reaching steady state was than 24 h given the fact that the outlet gas compositions remained unchanged before that period of time.

Overall mass balances were carried out for these experiments based on 24 hours runs with various experiments being carried out over a total of 3200 hours of reactor continuous operation. A detailed listing of experimental conditions considered is included in Appendix E.

Three additional experiments (Runs 17-40, 17-79, and 17-121) were developed at the so-called "reference condition" to assess periodically the catalyst activity, the catalyst deactivation and the reproducibility of the system results. Table 6.2 describes operating conditions, conversions, product distributions, and mass balances for these four reference runs.

From Table 6.2, it can be observed that the carbon monoxide conversion, for the repeat experiments called "reference condition", were very close. Since all the experimental data for the kinetics studies were carried out over a period of five months of continuous operation, all evidence indicates that the catalyst was quite stable and did not deactivate significantly during these extended runs.

Reproducibility of experimental data was determined using carbon monoxide conversion as a basis. With this end in view, the standard deviation and the 95% confidence interval level were calculated for various repeats.

The carbon monoxide conversion was found to range from 15.67% to 18.58%, which gives an average of about 17.28% with a standard deviation of ± 1.4%. This represents an error close to 8% value which is commonly found for this type of experiments. Figure 6.3 presents the carbon monoxide conversion versus the time-on-stream. The dotted lines in Figure 6.3 report the 95% confidence interval level confirming the trends already observed from the standard deviation.

Table 6.2. Summary of operating conditions and results for the "Reference Condition"

Experiment number	17-1	17-40	17-79	17-121
Operating conditions				
Temperature (°C)	220	220	220	220
Pressure (Mpa)	1.52	1.52	1.52	1.52
GHSV (h^{-1})	390	390	390	390
H_2/CO ratio inlet	2:1	2:1	2:1	2:1
Hours on stream (h)	144	1065	2020	3012
Analytical results				
CO conversion, %	18.58	16.56	15.67	18.32
H2 conversion, %	19.64	19.64	13.15	13.31
Mass balance, % (global)	98.18	97.15	96.39	98.65
Mass balance, % (oxygen)	99.10	98.23	98.76	98.76
Product selectivity (%)				
Carbon dioxide	2.81	3.01	4.04	2.33
Water	53.55	53.18	54.10	56.33
Hydrocarbons	43.63	43.81	41.86	41.34

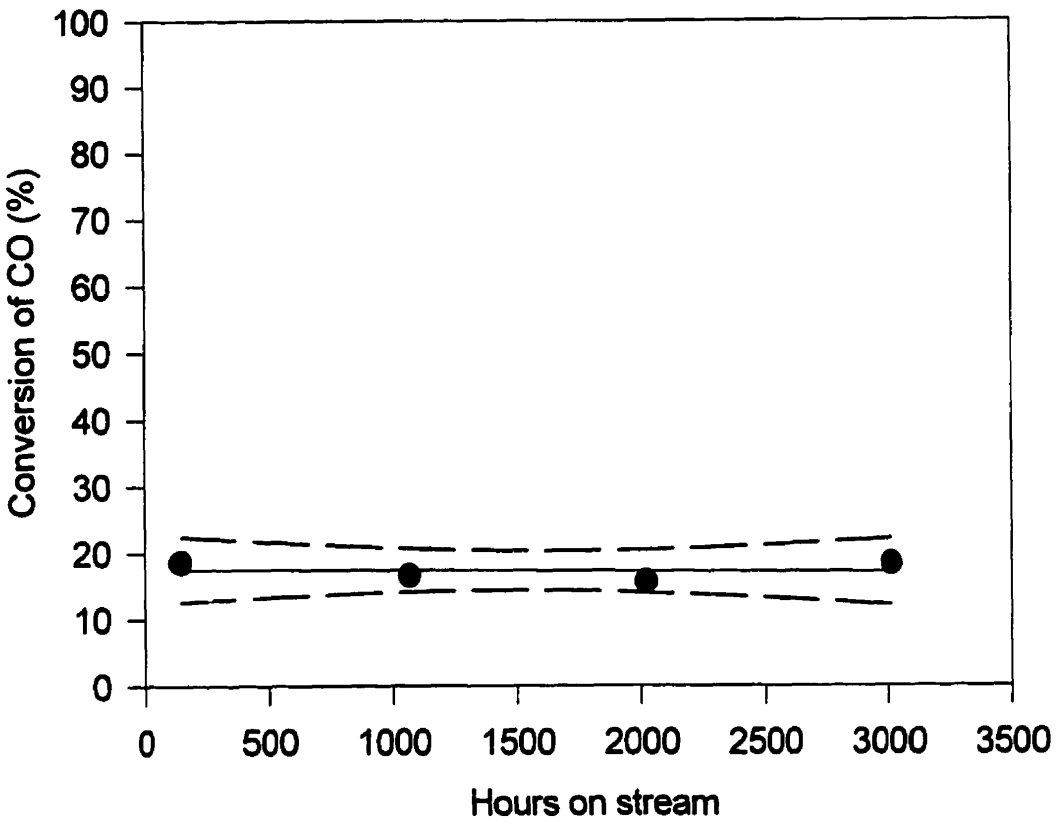

Figure 6.3. **Change of carbon monoxide conversion with time-on-stream. Runs 17-1, 17-40, 17-79 and 17-121. Tests performed at T = 220 °C, P = 1.52 MPa, GHSV = 390 h^{-1} and inlet H2/CO = 2.**

6.3.3. Effect of temperature

Several experiments were performed in order to study the influence of the temperature over the CO conversion, selectivity, and hydrocarbon product distribution. Two sets of experiments were selected (refer to Table 6.3) covering a wide range of the typical operating conditions for FTS.

The first set of experiments was performed with an initial $H_2/CO=2$ ratio, 1.52 MPa pressure and 348 h^{-1} GHSV. The second set of operating conditions was at $H_2/CO= 1$, 0.73 MPa pressure and 234 h^{-1} GHSV.

Table 6.3. Summary of Operating Conditions: Effect of the Temperature.

SET	1				2		
Experiment number	17-4	17-7	17-10	17-13	17-70	17-67	17-64
Operating conditions							
Temperature (°C)	209	215	220	226	209	215	222
Pressure (MPa)	1.52	1.52	1.52	1.52	0.73	0.73	0.73
GHSV (h^{-1})	348	348	348	348	234	234	234
H_2/CO ratio inlet	2:1	2:1	2:1	2:1	1:1	1:1	1:1
Analytical results							
CO conversion, %	10.16	16.3	20.51	23.42	2.89	6.78	10.8
H_2 conversion, %	9.68	15.5	21.27	24.13	9.94	17.33	21.78
Mass balance, % (global)	97.21	100.6	98.2	98.2	98.7	98.02	98.1
Mass balance, % (oxygen)	98.75	99.35	99.2	99.0	98.9	98.32	98.9
Product selectivity (%)							
Carbon dioxide	0.00	1.04	1.17	1.6	0.89	0.48	4.29
Water	56.83	54.95	54.93	54.79	55.13	55.93	52.65
Hydrocarbons	43.17	44.01	43.89	43.61	43.98	43.59	43.06

6.3.3.1. Carbon monoxide conversion

Figure 6.4 reports the effect of temperature on the CO conversion. It was found that the CO conversion increased steadily with temperature and this for both sets of operating conditions studied. Note that these results are in agreement with those published before by Vannice (1975), and Everson and Mulder (1993).

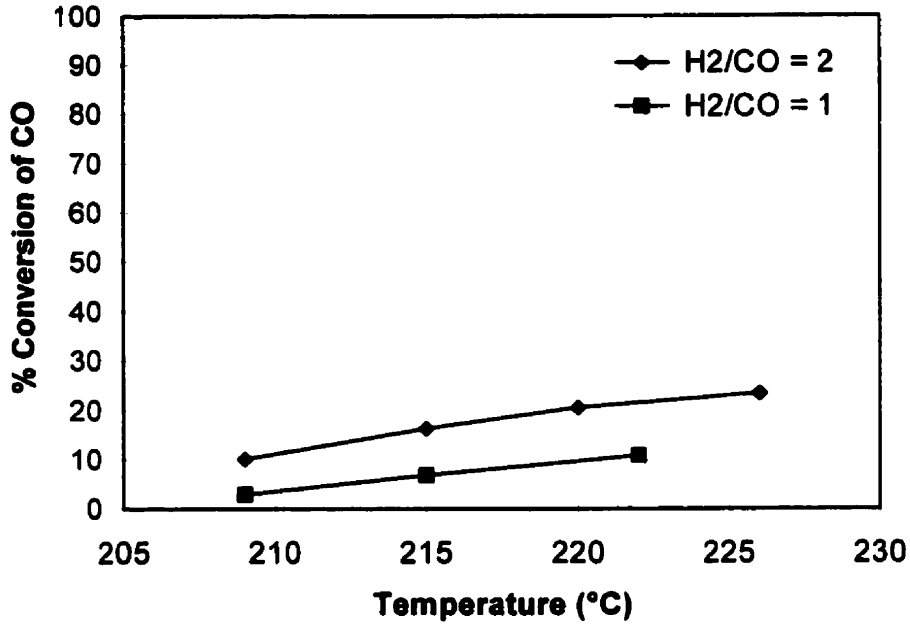

Figure 6.4. Effect of the temperature on the CO conversion. Runs as listed in Table 6.3. Tests performed at: gas pressure = 1.52 MPa, GHSV = 348 h^{-1}

6.3.3.2. Hydrocarbon product distribution

Regarding products formed, the product distribution is given for set #1 of the operating conditions. Fig. 6.5 reports product distribution for an inlet H_2/CO ratio of 2. In this case, as temperature increases, the product distribution shifts towards higher molecular weight hydrocarbons and this does not agree with trends reported by other investigators. A possible justification for this is that

temperatures were changed in a lower range than previous work. Dalai *et al.* (1992) employed, for instance, temperatures from 250 to 275 °C while in the development of this research temperatures were kept in the 200-220 °C range and as close as possible to the ones found in industrial units. Similar results to the ones of the present study were reported by Everson and Mulder (1993) using supported ruthenium catalysts at 230 °C. It is also interesting to note (Fig. 6.5) the low selectivity towards methane and high selectivity to C_{10}-C_{20} fraction exhibited by the eggshell catalyst within the range of temperatures considered in this work.

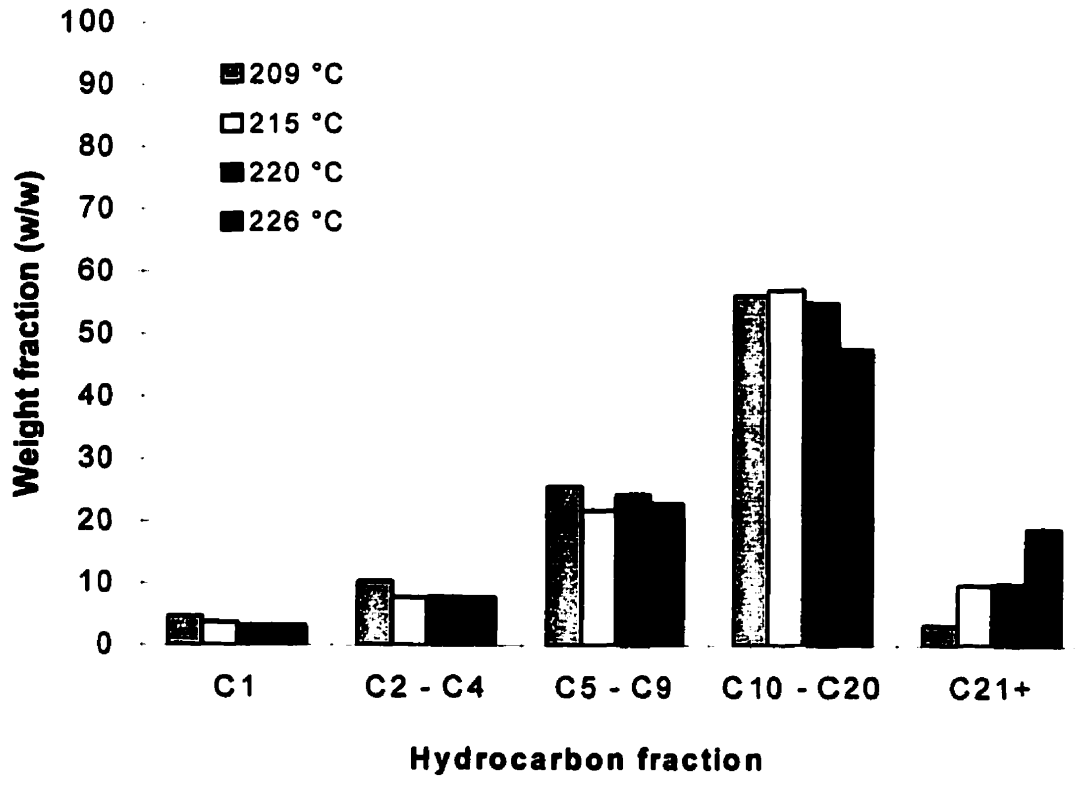

Figure 6.5. Effect of temperature on the hydrocarbon product distribution. Runs as summarized in Table 6.3. Tests performed at: gas pressure = 1.52 MPa, GHSV = 348 h^{-1}, and inlet H_2/CO ratio = 2.

6.3.3.3. Anderson-Schultz-Flory distribution

The Anderson-Schultz-Flory (ASF) distribution (W_n/n versus the hydrocarbon carbon number) at four different temperatures, as used in set #1, are displayed in Fig. 6.6. It was found that in all cases there is some deviation from the ASF distribution. Most FT product distributions reported in the technical literature, present appreciable deviations from ASF polymerization kinetics. Practically all these deviations are caused either by secondary reactions or by the need of involving at least two different values of α.

ASF distributions in Fig 6.6 are characterized by a sudden decline in the C_2-C_3 range. This can be attributed to a decrease of the desorption rate constant with increasing carbon numbers (Schulz *et.al.*, 1995). The ASF distributions also present a sudden drop at C_8 carbon number and this indicates that no single value of the chain growth probability, α, can be used to describe the complete spectrum of hydrocarbons products. This sudden drop in ASF plots was observed by Dalai *et al.* (1997), and by Satterfield and Stenger (1984). Moreover, the slight increase in α in the range C_9-C_{15} can be explained by an increased re-adsorbability of product molecules (Schulz, *et al.* 1995).

The α parameter was estimated by the slope of the best straight line for the C_{15}^+ range. It can be observed (Fig 6.6) that α augmented from 0.79 to 0.86 when the temperature increased from 209 to 226 °C. Thus, the increment of temperature, in the range studied leads to a product distribution with a higher average molecular weight and consequently, hydrocarbons of longer carbon chain lengths. This is certainly an undesired effect if one would like to maximize the hydrocarbon fraction in the C_{10}-C_{20} range and this calls for a close temperature control in industrial scale units using the eggshell catalyst.

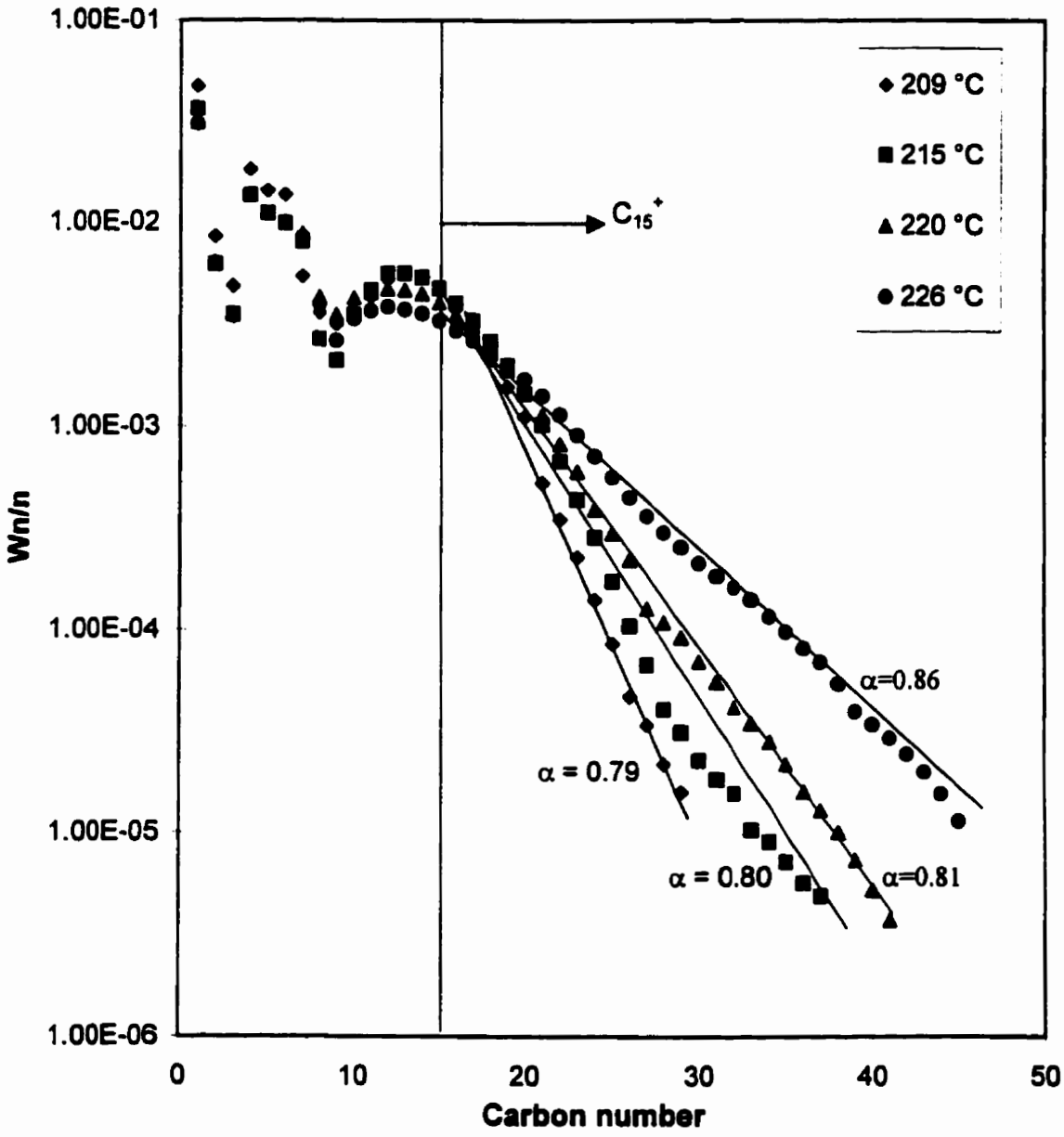

Figure 6.6. **Anderson-Schultz-Flory distribution as a function of the temperature. Runs as listed in Table 6.3. Tests performed at: P = 1.52 MPa, GHSV = 348 h^{-1} and inlet H_2/CO ratio = 2.**

6.3.4. Effect of the Pressure

While using the eggshell catalyst, several experiments were performed to study the influence of the pressure on CO conversion, selectivity, and product distribution. The pressure was increased from 1.1 to 1.52 MPa, while other operating conditions were, as described in Table 6.4, kept constant.

Table 6.4. Summary of Operating Conditions: Effect of the Pressure

Experiment number	17-22	17-25	17-79
Operating conditions			
Temperature (°C)	221	221	221
Pressure (MPa)	1.10	1.33	1.52
GHSV (h^{-1})	390	390	390
H_2/CO ratio inlet	2:1	2:1	2:1
Analytical results			
CO conversion, %	10.82	14.13	15.67
H_2 conversion, %	13.96	14.44	13.15
Mass balance (overall), %	97.88	97.03	96.39
Mass balance, % (oxygen)	98.12	98.32	98.76
Product selectivity (%)			
Carbon dioxide	3.43	2.98	4.04
Water	51.48	53.66	54.10
Hydrocarbons	45.09	43.36	41.86

6.3.4.1. Carbon monoxide conversion

Carbon monoxide conversion, and its change with total pressure, is reported in Fig 6.7 for the 1.1-1.52 MPa total pressure range. In this respect, catalyst activity in terms of CO conversion showed a slight increase with total pressure. These results were expected, given the corresponding increment of partial pressures of both CO and H_2, which lead overall to an increment of the FT synthesis rate and consequently of the CO conversion. Regarding pressure effects, it can be stated that they compare well with those obtained previously by Dalai (1997).

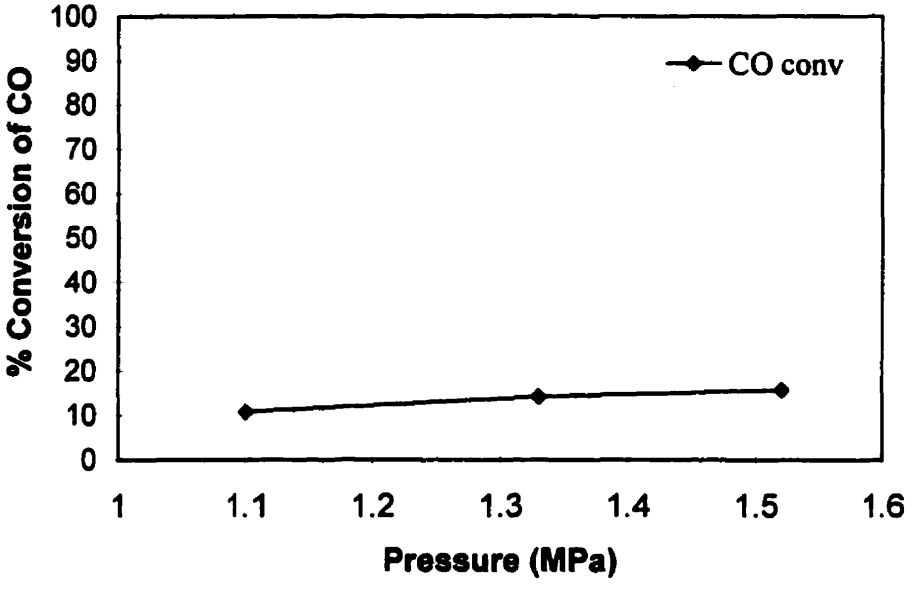

Figure 6.7. Pressure effect on Carbon Monoxide Conversion. (Runs reported in Table 6.4). Tests performed at: Temperature = 221 °C, GHSV = 390 h^{-1}, and inlet H_2/CO ratio =2.

6.3.4.2. Hydrocarbon product distribution

The influence of total pressure on product distribution is reported in Fig 6.8 with the hydrocarbon product distribution moving towards heavier products at higher total pressures. This figure also shows that consistent with this selectivity to methane, C_2-C_4, and C_5-C_9 hydrocarbon fractions decrease with total pressure. It is speculated that observed changes in the product selectivity are probably due to the changes in the relative rates of elementary reactions involved in the hydrocarbon synthesis (Dalai *et al.*, 1992).

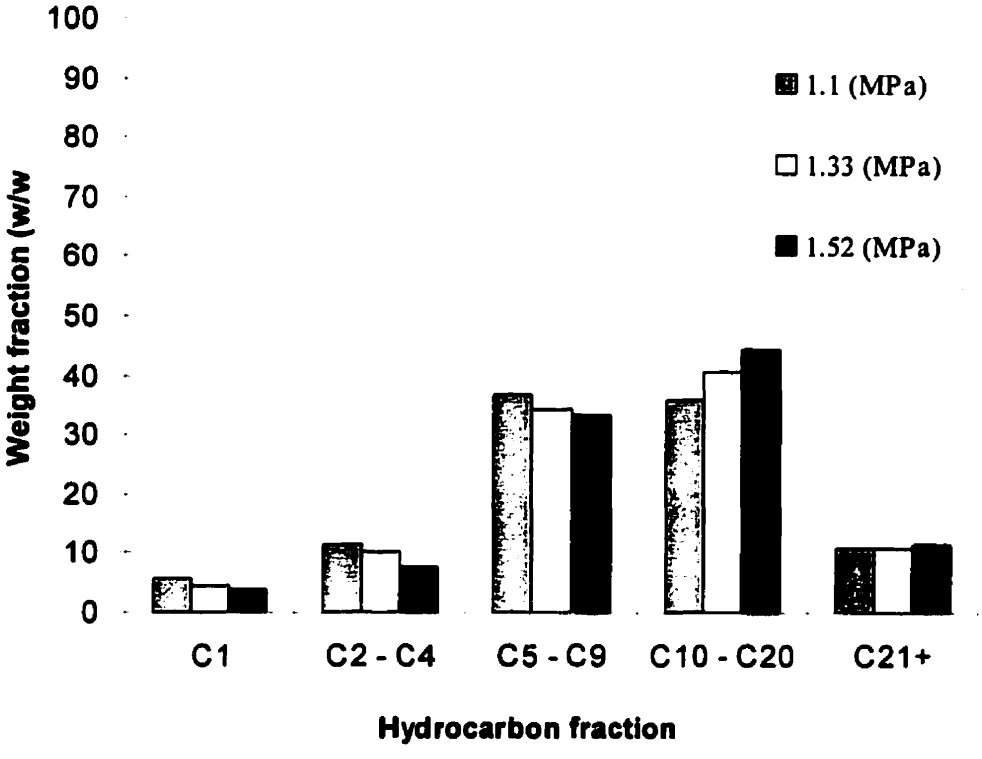

Figure 6.8. Effect of the pressure on the hydrocarbon product distribution. (Runs listed in Table 6.4). Tests performed at: Temperature = 221 °C, GHSV = 390 h^{-1}, and inlet H_2/CO ratio = 2.

6.3.4.3. Anderson-Schultz-Flory Distribution

The ASF distributions and the effect of total pressure are reported in Fig. 6.9. Important deviations of the classical ASF distribution with single α values were noticed. Furthermore for α defined for C_{15}^{+} it was observed that there is a consistent increment of α from 0.83 to 0.87 when the total pressure is increased from 1.1 MPa to 1.52 MPa.

In this respect, Stenger and Askonas (1986) found similar results while using a iron-based catalyst measuring increasing α parameters from 0.56 at 0.37 MPa to 0.68 at 1.48 MPa.

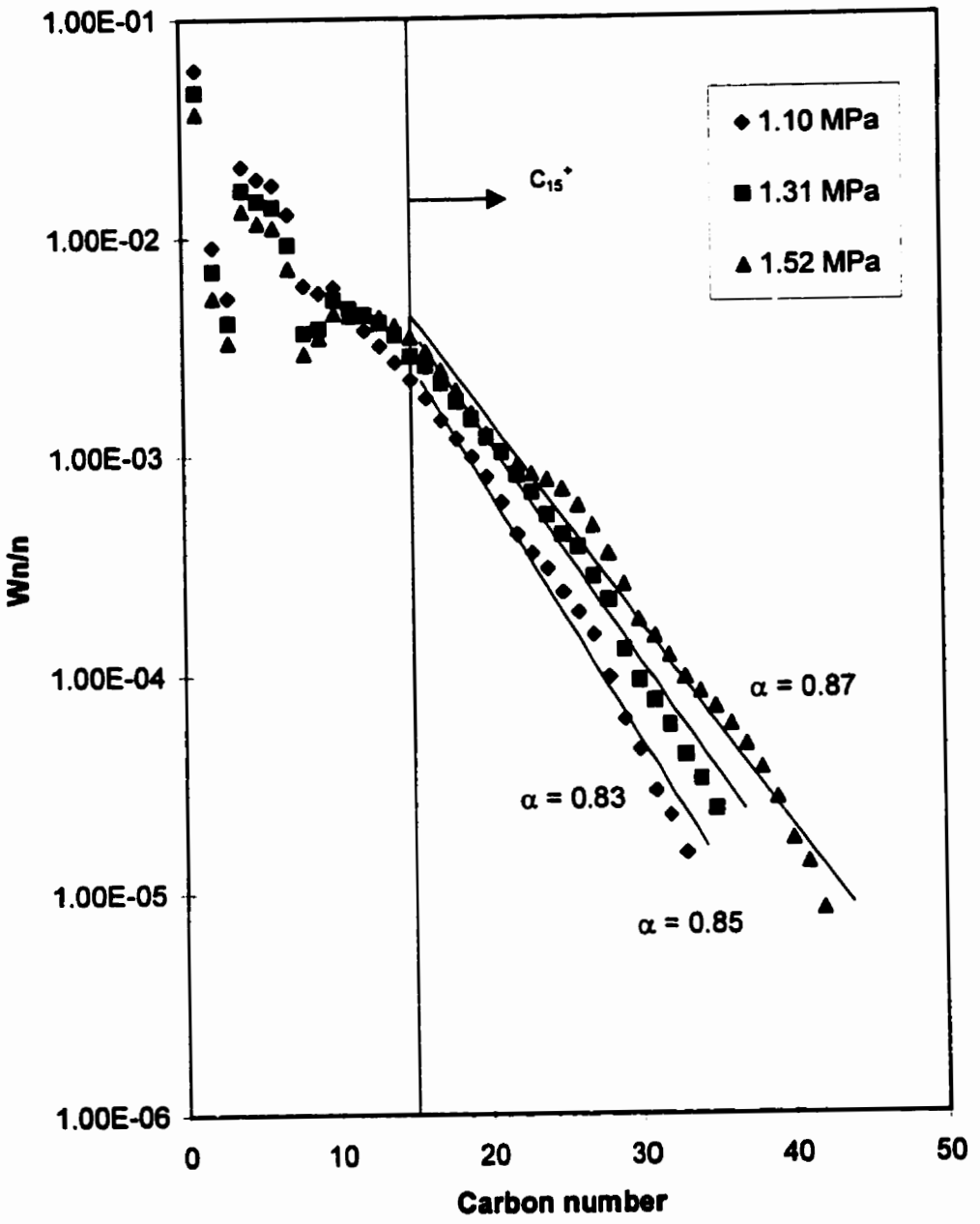

Figure 6.9. **Anderson-Schultz-Flory distribution as a function of the pressure. (Runs listed in Table 6.4). Tests performed at : T = 221 °C, GHSV = 390 h^{-1} and inlet H_2/CO ratio = 2**

6.3.5. Effect of GHSV.

In order to study the influence of the gas hourly space velocity, GHSV, over CO conversion, product selectivity, and hydrocarbon distribution four experiments were carried out. The operating conditions used are reported in Table 6.5.

In these experiments the GHSV was varied from 432 to 210 h^{-1}, while the rest of the operating conditions were kept at constant values. The temperature selected (230 °C) for this experiment was higher than other temperatures used in previous experiments. This was done to obtain a reasonable CO conversion when the GHSV was increased from 210 to 432 h^{-1}.

Table 6.5. Summary of Operating Conditions: Effect of the GHSV.

Experiment number	17-88	17-91	17-94	17-97
Operating conditions				
Temperature (°C)	230	230	230	230
Pressure (MPa)	1.52	1.52	1.52	1.52
GHSV (h^{-1})	432	360	276	210
H_2/CO ratio inlet	2:1	2:1	2:1	2:1
Analytical results				
CO conversion, %	18.2	24.36	31.37	39.67
H_2 conversion, %	17.79	22.32	29.98	40.16
Mass balance, % (global)	98.8	98.4	98.2	97.2
Mass balance, % (oxygen)	98.9	98.4	98.5	98.5
Product selectivity (%)				
Carbon dioxide	4.47	4.49	4.34	4.35
Water	53.53	53.17	53.47	52.60
Hydrocarbons	41.99	42.34	42.19	43.04

Table 6.5 also summarizes overall mass balances closing in the 97% range and oxygen balances closing in the 98 % range.

6.3.5.1. Carbon monoxide conversion

The effect of the gas hourly space velocity, GHSV, over the carbon monoxide conversion is reported in Fig 6.10. As expected the highest CO conversion was obtained when the GHSV was 210 h^{-1} and the lowest CO conversion for a GHSV of 432 h^{-1} and this agrees with the results of Everson and Mulder (1993).

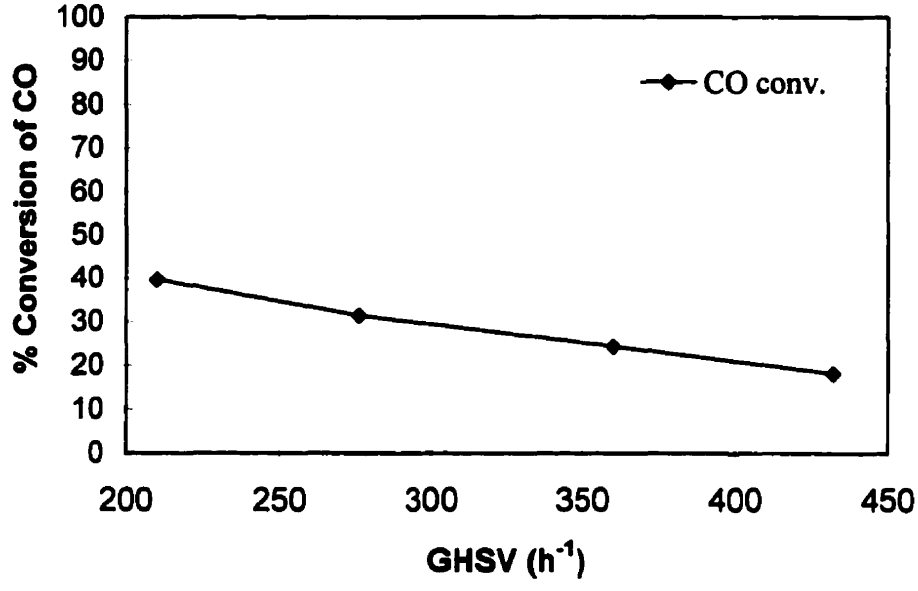

Figure 6.10. Effect of the GHSV on the conversion of Carbon Monoxide. Runs numbers listed in Table 6.5. Tests performed at: T = 230 °C, P = 1.52 MPa, and inlet H_2/CO ratio = 2.

6.3.5.2. Hydrocarbon product distribution

The hydrocarbon product distribution as a function of the GHSV is reported in Fig. 6.11. It is shown that the distribution of lighter products (methane, C_2-C_4 and C_5-C_9) is favoured with increased GHSV. On the other

hand, the C_{10}-C_{20} and C_{21}^{+} hydrocarbon fractions show an increment with smaller GHSV. This result confirms that for conditions leading to longer contact times, lower GHSV, chain growth takes place in a more significant extent and there is, as a result, an increase in the formation of higher molecular weight hydrocarbons.

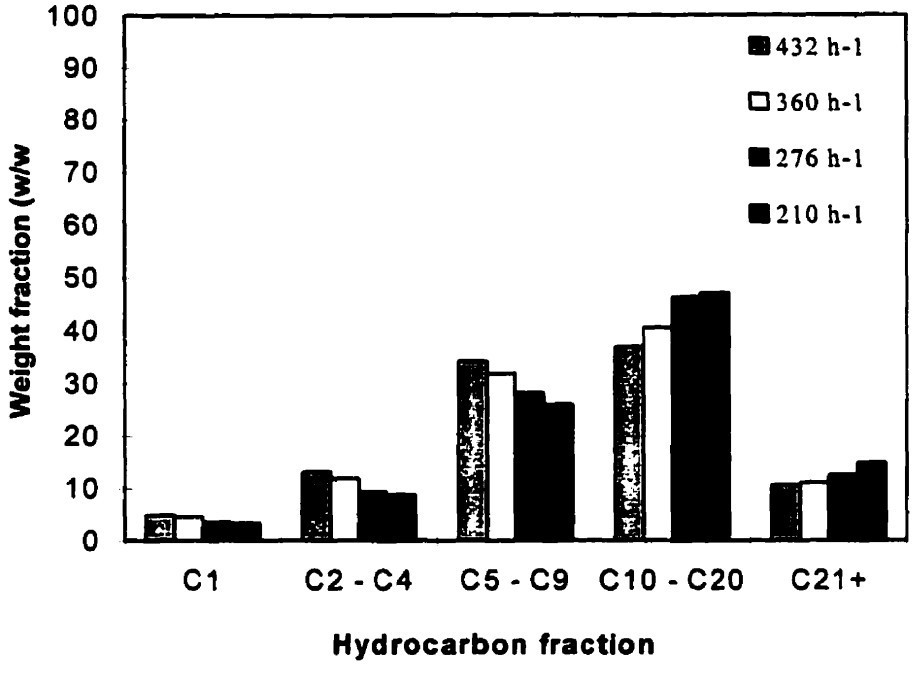

Figure 6.11. Effect of the GHSV on the hydrocarbon products distribution. Runs numbers reported in Table 6.5. Tests performed at: T = 230 °C, P = 1.52 MPa, and inlet H_2/CO ratio = 2.

6.3.5.3. Anderson-Schultz-Flory distribution.

The effect of the GHSV on the Anderson-Schultz-Flory, ASF, distribution is reported in Fig. 6.12. Deviations previously reported in the ASF

distributions were also present here. However for the higher GHSV, these deviations were less important than in prior cases. Another finding was the similarity of the various distributions in the C_{11}-C_{20} sections of the plot. In fact, from carbon 11 to carbon 26 ASF distributions have almost the same α values, indicating a small effect of GHSV on chain growth probability. Outside this region, however, an important difference was observed between ASF distributions and this suggests the important influence of GHSV on chain growth probability after carbon number 26.

This phenomenon can be explained by the different contact times provided to reactants and products. Higher GHSV lead to lower contact-times, and as a result to a decreased probability of secondary reactions due to a decreased opportunity for α-olefin reinsertion. Furthermore, a lower GHSV or higher contact time, gives more opportunity for α-olefin reinsertion and as a result higher chain growth probability.

In this respect, it is important to point out that reinsertion rates augment exponentially with carbon number and this due to the preferential physisorption of longer hydrocarbons on catalyst surface [Kuipers *et al.* (1996) and Iglesia *et al.* (1991)].

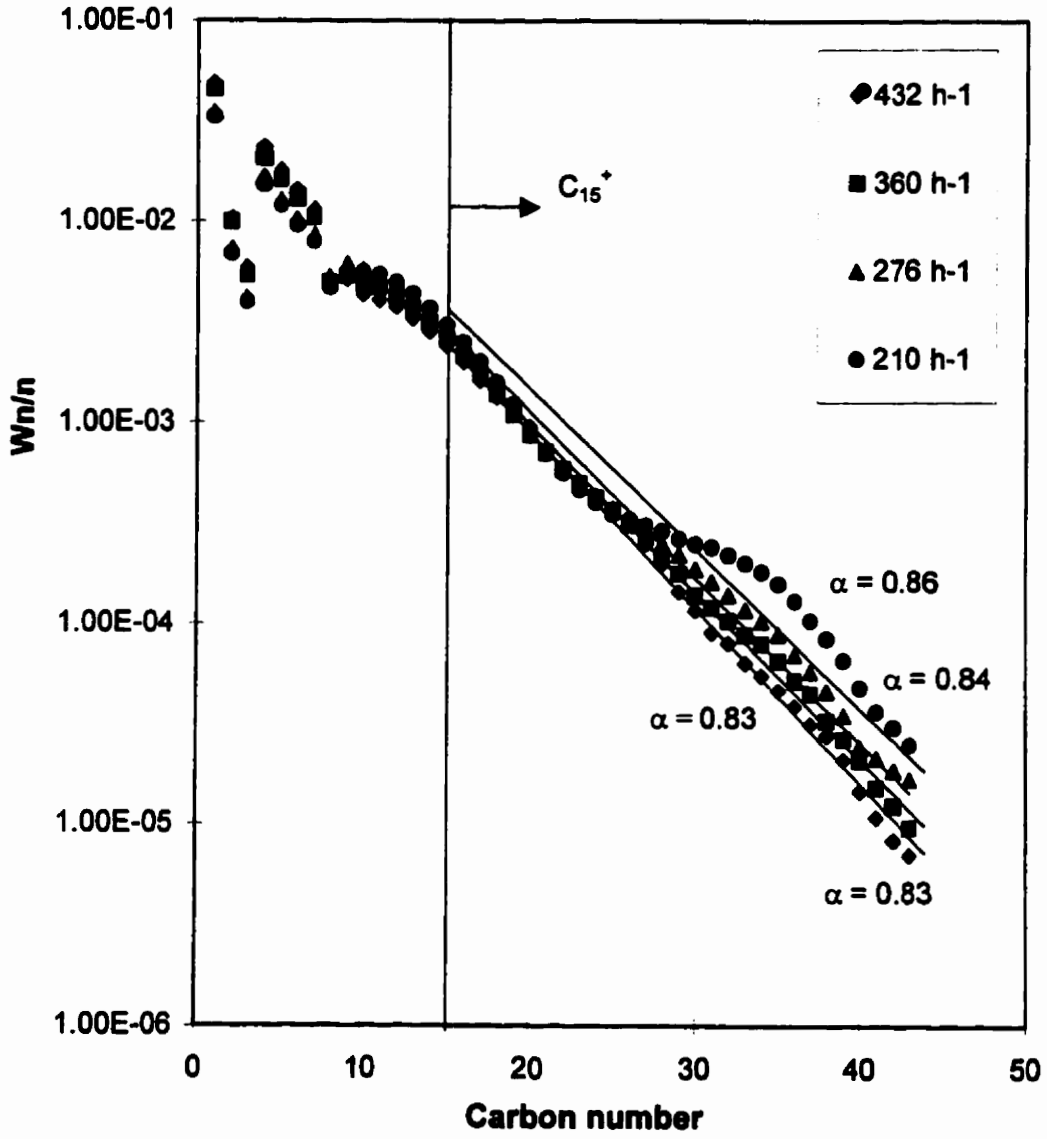

Figure 6.12. Anderson-Schultz-Flory distribution as a function of the GHSV. Runs numbers listed in Table 6.5. Tests performed at: P = 1.52 MPa, T = 230 °C and inlet H_2/CO ratio = 2.

6.3.6. Effect of H_2/CO ratio.

A number of experiments were carried out at different H_2/CO ratios with the temperature, pressure and GHSV kept constant. Three H_2/CO ratios were tested: 1:1, 2:1 and 3:1. This was done to understand the influence of this parameter on carbon monoxide conversion, selectivity and product distribution. The operating conditions used are described in Table 6.6.

Table 6.6. Summary of Operating Conditions: Effect of the H_2/CO ratio

Experiment number	17-106	17-91	17-127
Operating conditions			
Temperature (°C)	230	230	230
Pressure (MPa)	1.52	1.52	1.52
GHSV (h^{-1})	360	360	360
H_2/CO ratio inlet	1:1	2:1	3:1
Analytical results			
CO conversion, %	7.87	24.36	56.86
H_2 conversion, %	22.5	22.32	42.33
Mass balance, % (global)	97.37	98.4	97.2
Mass balance, % (oxygen)	98.45	98.4	97.6
Product selectivity (%)			
Carbon dioxide	5.81	4.49	5.57
Water	48.61	53.17	50.24
Hydrocarbons	45.58	42.34	44.19

6.3.6.1. Carbon Monoxide Conversion

As reported in Fig 6.13 the CO conversion increased from 8 to 57 % while the H_2/CO ratio was changed from 1:1 to 3:1. This demonstrates that the ratio of hydrogen to carbon monoxide in the feed stream had a marked effect on the catalytic activity and this is consistent with published results (Singleton and Reigier, 1983; and Everson and Mulder, 1993). These changes were also consistent with the strong influence of hydrogen partial pressures in the reaction kinetics.

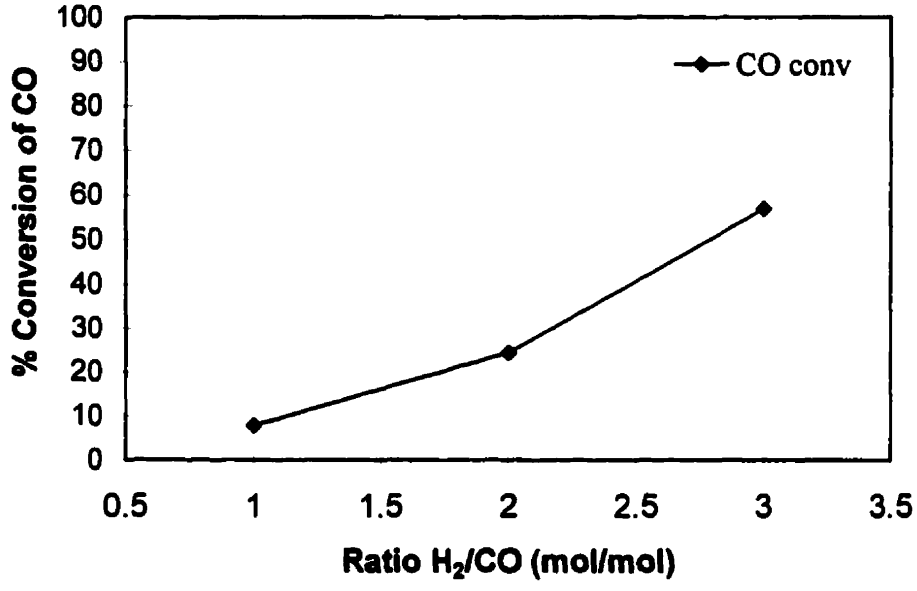

Figure 6.13. Effect of the H_2/CO ratio on the conversion of carbon monoxide. Runs numbers listed in Table 6.6. Tests performed at: T = 230 °C, P = 1.52 MPa and GHSV = 360 h^{-1}.

6.3.6.2. Hydrocarbon product distribution

The effect of the H_2/CO ratio on the overall product distribution is reported in Fig. 6.14. It is observed that there is a marked effect of H_2/CO ratio on hydrocarbon distribution. For example, selectivity to methane, C_2-C_4 and C_5-C_9 hydrocarbon fractions increased with H_2/CO ratio, while selectivity to C_{10}-C_{20} and C_{21}^+ hydrocarbon fractions decreased with the same ratio.

This shift of hydrocarbon selectivity towards lighter molecular weight hydrocarbons with H_2/CO ratio was reported by Everson and Mulder (1993) and also by Singleton and Reigier (1983). It is argued that higher partial pressures of hydrogen, favour secondary reactions such as hydrogenation and hydrogenolysis. Thus for example, hydrogenolysis of paraffins and olefins reverse or moderate the process of chain growth leading to a decrease in the α values (Kuipers *et al.* 1996).

6.3.6.3. Anderson-Schultz-Flory distribution.

Figure 6.15 reports the Anderson-Schultz-Flory distribution for experiments where the H_2/CO was changed. Deviations from the classical ASF distribution are observed. The level of these deviations was however quite different for various cases studied. When the $H_2/CO=3$ ratio was used, deviations from the classical ASF were relatively small. For the $H_2/CO=2$ ratio deviations were, yet more important. Even more, significant deviations from the classical ASF distribution were found when the $H_2/CO=1$ ratio was employed.

Regarding the α parameter it was estimated using the slope of the best linear fitting for carbon number over C_{15}. The α parameter showed a consistent increase from 0.76 to 0.87 while the H_2/CO ratio varied from 3 to 1. This effect on the α parameter was expected given the reduction of the hydrogen partial pressure and the correspondingly higher carbon monoxide partial pressure.

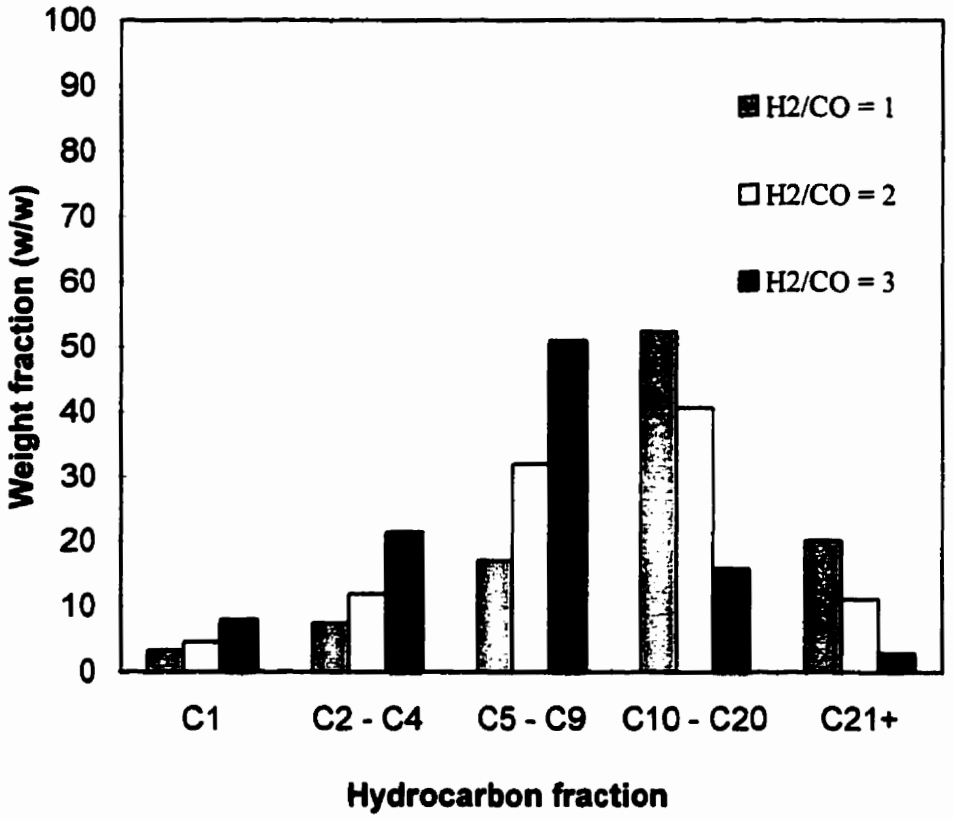

Figure 6.14. Effect of the H_2/CO ratio on the hydrocarbon products distribution. Runs numbers reported in Table 6.6. Tests performed at: T = 230 °C, P = 1.52 MPa and GHSV = 360 h^{-1}.

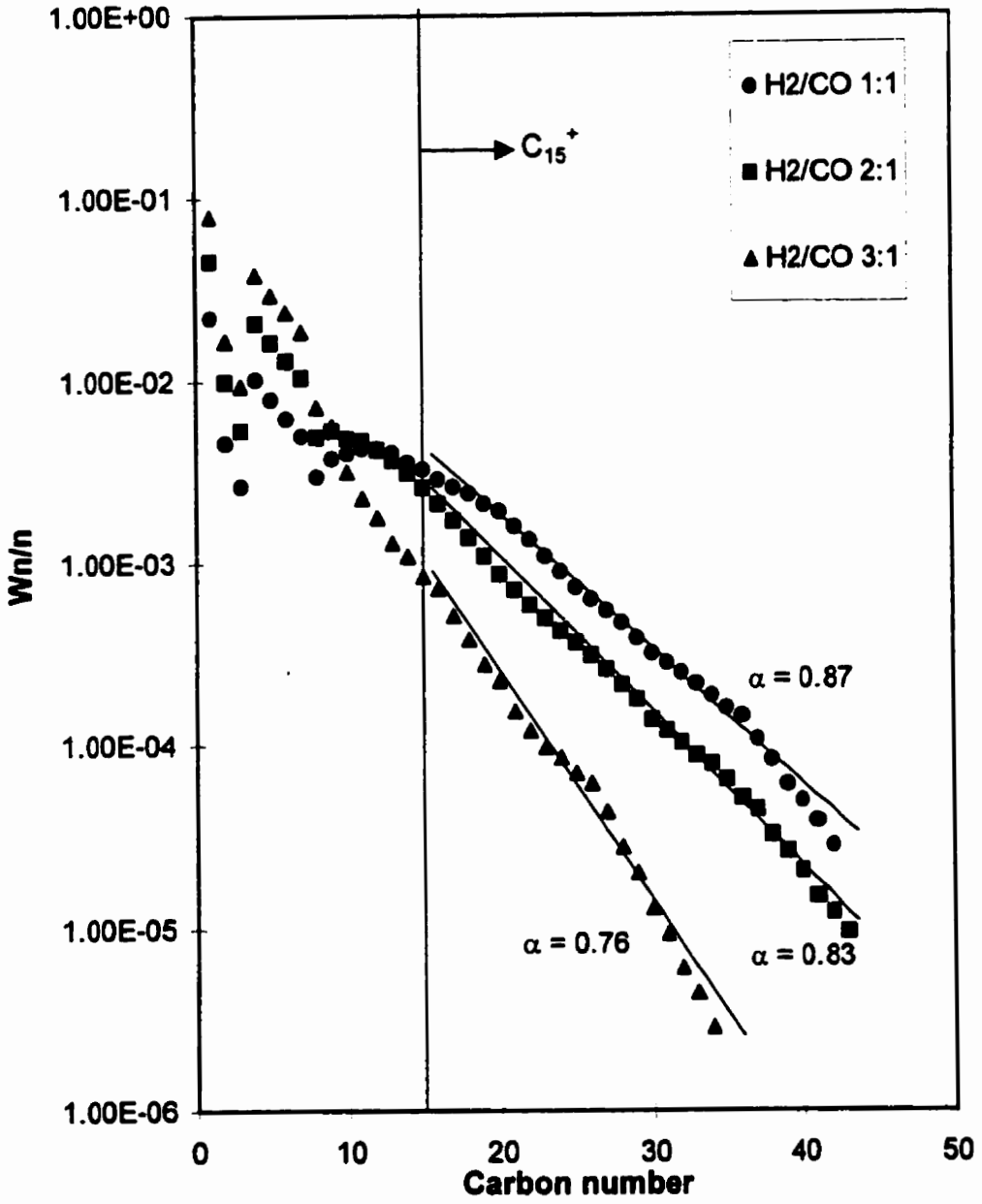

Figure 6.15. Anderson-Schultz-Flory distribution as a function of the H_2/CO ratio. Runs numbers summarized in Table 6.6. Tests performed at: T = 230 °C, P = 1.52 MPa and GHSV = 360 h^{-1}.

6.3.7. Conclusion

For the eggshell catalyst of this study, a series of experiments were carried out to study the influence of the operating conditions on carbon monoxide conversion, product selectivity, and hydrocarbon product distribution. The results obtained led to the following conclusions:

- Carbon monoxide conversion increased with temperature. In addition, within the range covered in these experiments, an increment of temperature shifted the hydrocarbon distribution towards higher molecular weight hydrocarbons.
- The total pressure had a mild effect on carbon monoxide conversion with the total pressure increasing the chain length of the hydrocarbons formed.
- The effect of gas hourly space velocity (GHSV) on carbon monoxide conversion and hydrocarbon products distribution was also important. Increasing GHSV decreased the CO conversion shifting the hydrocarbons distribution towards lighter molecular weight hydrocarbons.
- Carbon monoxide conversion increased with H_2/CO ratio with lower H_2/CO ratios favouring the production of higher molecular weight hydrocarbons.
- The Anderson-Schultz-Flory, ASF distribution, for all the experiments developed, presented systematic deviations of the classical ASF distribution. It appears that more than one α parameter is needed for this type of distribution. While this phenomenon may be attributed to either secondary reactions or the presence of different sites on the catalyst it

appears that for the eggshell catalyst, of this study, secondary reactions are the most likely chemical events explaining these deviations.

6.4. Kinetic modeling

This section describes the kinetic models considered for FTS on cobalt-catalysts. The main goal was to discriminate between possible kinetic models for the conversion of synthesis gas into higher hydrocarbons. These kinetic models are required to provide satisfactory simulation of the pseudoadiabatic reactor using an eggshell cobalt catalyst.

6.4.1. Kinetic Experiments

Overall the Fischer-Tropsch synthesis is a complex network of parallel and series reactions with these reactions involving different extents and determining catalyst performance. These reactions can be classified into primary and secondary reactions with different dependence with respect to pressure, temperature and composition.

Given the above mentioned facts a kinetic study with a FTS catalyst should be made over a wide range of process conditions and this to evaluate more precisely the catalyst performance.

The data used in this section is based on the experimental runs reported in Section 6.3 (Appendix E). Table 6.7 reports run number, operating conditions as well as the reaction rates found for each run. It can be appreciated that operating conditions were varied as follows: temperature from

209 to 230 °C, pressure from 0.34 to 1.52 MPa, GHSV from 210 to 504 h^{-1}, and H_2/CO ratio from 1 to 3.

The rate of reaction for the FTS was defined based on the assumption that the CSTR model applies for the internally circulated Berty reactor operated at 1900 RPM.

$$r_{H_2} = -\frac{F\left(C^{o}_{H_2} - C_{H_2}\right)}{W_{cat}} \tag{6.1}$$

and

$$r_{CO} = -\frac{F\left(C^{o}_{CO} - C_{CO}\right)}{W_{cat}} \tag{6.2}$$

Adding eqs (6.1) and (6.2), r_{H_2+CO}, the combined moles of hydrogen plus carbon monoxide converted per unit time and mass of catalyst were calculated from:

$$r_{H_2+CO} = -\frac{F}{W_{cat}}\left[\left(C^{o}_{H_2} - C_{H_2}\right) - \left(C^{o}_{CO} - C_{CO}\right)\right] \tag{6.3}$$

It can in this way be shown that the r_{H_2+CO} increases from -0.0326 to -0.3018 mmol/min/g of catalyst.

Table 6.7. Experimental Reaction Rates

Run #	Temp. (°C)	Pressure (MPa)	GHSV (h^{-1})	H_2/CO ratio (mol/mol)	r_{H2+CO} (mmol/min/g of catalyst)
17-16	209	1.10	390	2	0.0326
17-31	209	1.33	372	2	0.0384
17-34	209	1.52	360	2	0.0425
17-49	209	1.52	210	2	0.0447
17-52	209	1.52	258	2	0.0441
17-61	209	0.73	210	2	0.0245
17-70	209	0.73	234	2	0.0231
17-19	215	1.10	390	2	0.0621
17-28	215	1.33	272	2	0.0751
17-37	215	1.52	360	2	0.0879
17-46	215	1.52	210	2	0.0905
17-55	215	1.52	264	2	0.0815
17-58	215	0.73	222	2	0.0426
17-67	215	0.73	234	2	0.0463
17-22	221	1.1	390	2	0.0878
17-25	221	1.33	390	2	0.1096
17-40	220	1.52	390	2	0.1212
17-43	221	1.52	210	2	0.1088
17-64	222	0.73	234	1	0.0675
17-73	221	0.73	210	2	0.0678
17-76	222	0.73	300	2	0.0676
17-79	222	1.52	390	2	0.0965
17-82	222	1.52	504	2	0.0771
17-85	222	1.52	432	2	0.0816
17-109	222	1.52	372	1	0.0853
17-112	222	1.07	402	1	0.0736
17-121	222	1.52	390	2	0.0993
17-123	221	1.52	378	3	0.1561
17-124	221	1.52	378	3	0.1576
17-88	230	1.52	432	2	0.1262
17-91	230	1.52	360	2	0.1460
17-94	230	1.52	276	2	0.1528
17-97	230	1.52	210	2	0.1677
17-100	229	1.52	240	1	0.1155
17-103	229	1.52	306	1	0.1113
17-106	229	1.52	372	1	0.1077
17-115	229	1.07	402	1	0.1125
17-118	230	0.59	402	1	0.0647
17-127	229	1.52	378	3	0.3018
17-130	229	0.34	402	3	0.1078

6.4.2. Kinetic models

There is a significant volume of technical literature dealing with kinetic modeling for FTS (Storch *et al.*, 1951; Anderson, 1956; Yang *et al.*, 1979; Bub and Baerns, 1980, Pannell *et al.*, 1980; Rautavuoma and van der Baan 1981; Dixit and Tavlarides 1982; Wojciechowski, 1988; Sarup and Wojciechowski, 1989; Post *et al.*, 1989; Yates and Satterfield 1991; Iglesia *et al.*, 1993). While there are important differences in between equations there are a number of common factors that should be the basis of the kinetic models postulated: a) FTS occurs far from the reaction equilibrium. Thus, there is no reverse reaction term involved in the numerator of the rate equation, b) there is minimum influence of water gas shift reaction and consequently there is no external condition (other reaction equilibrium condition) interelating partial pressures, c) FTS rate is constantly inhibited by carbon monoxide, thus there should be a CO partial pressure term included in the denominator of the rate equation.

In 1991, Yates and Satterfield published a study summarizing most common and accepted kinetic equations for the Fischer-Tropsch synthesis on cobalt catalysts. On this basis five different kinetics models were considered:

Model 1 (Power law model)

$$r_{H_2+CO} = -k_o e^{\left(\frac{-E}{R_1}\left(\frac{1}{T}-\frac{1}{Tav}\right)\right)} p_{CO}^{n} p_{H_2}^{m} \qquad (6.4)$$

Model 2 (Iglesia *et.al.*,1993)

$$r_{H_2+CO} = -\frac{k_o e^{\left(\frac{-E}{R_1}\left(\frac{1}{T}-\frac{1}{Tav}\right)\right)} p_{CO}^{n} p_{H_2}^{m}}{\left(1+bp_{CO}\right)} \qquad (6.5)$$

Model 3 (Sarup and Wojciechowski, 1989)

$$r_{H_2+CO} = - \frac{k_o e^{\left(\frac{-E}{R_1}\left(\frac{1}{T}-\frac{1}{Tav}\right)\right)} p_{CO}^{n} \; p_{H_2}^{m}}{\left(1 + bp_{CO}^{n}\right)^2} \qquad (6.6)$$

Model 4 (Rautavuoma and van der Baan,1981)

$$r_{H_2+CO} = - \frac{k_o e^{\left(\frac{-E}{R_1}\left(\frac{1}{T}-\frac{1}{Tav}\right)\right)} p_{CO}^{n} \; p_{H_2}^{m}}{\left(1 + bp_{CO}^{n}\right)^3} \qquad (6.7)$$

Model 5 (Anderson, 1956)

$$r_{H_2+CO} = - \frac{k_o e^{\left(\frac{-E}{R_1}\left(\frac{1}{T}-\frac{1}{Tav}\right)\right)} p_{CO}^{n} \; p_{H_2}^{m}}{\left(1 + b\, p_{CO}^{n} \; p_{H_2}^{m}\right)} \qquad (6.8)$$

Regarding eq (6.4) this is a straight forward empirical power law equation frequently used by many authors in the technical literature (Pannel *et. al.*, 1980; Yang *et al.*, 1979; Wang *et al.*, 1987). In these power law expressions the constants are empirical parameters used to adjust the data and having very limited physicochemical meaning. In eq (6.4) the *m* coefficient for the p_{H2} term is positive while the power *n* for p_{CO} is negative and this confirms the inhibition effect by adsorbed CO.

Eqs 6.5-6.8, however were derived using a Langmuir-Hinshelwood-Hoogen expression. These expressions highlight different key reaction steps. For instance, some kinetic models postulate a role for the dissociated CO while others claim that the CO is adsorbed but not dissociated (Sarup and Wojciechowski, 1989). Moreover, there is also the possibility of assuming that

hydrogen adsorbed onto catalyst surface dissociatively (Rautavuoma and van der Baan, 1981).

While there are, as already described, important differences the Arrhenius' equation for correlating the dependence of reaction coefficients with temperature have been used consistently in kinetic models reported:

$$k = k_o \, e^{\left[-\frac{E_a}{R_1 T}\right]} \tag{6.9}$$

with k being the rate coefficient, k_o the pre-exponential term, E_A the activation energy, R_1 the ideal gas law constant of 8.3144 joules/g.-moles.K and T the absolute temperature in degrees Kelvin.

Regarding eq (6.9), it involves parameters, such as the pre-exponential factor and the activation energy. These parameters may sometimes display strong cross-correlation. To overcome cross-correlation, since the range of the observed temperatures is relatively much smaller than the mean temperature the following form of the equation is frequently preferred (Bates and Watts, 1988; and Kittrell, 1970):

$$k = k_o e^{\left(-\frac{E}{R_1}\left(\frac{1}{T}-\frac{1}{T_{av}}\right)\right)} \tag{6.10}$$

where T_{av} is the average absolute temperature corresponding to the experimental range where experiments were developed.

With this end in view, and to use eq (6.10) data was analyzed using the value of 493 K, average temperature for experiments performed.

6.4.3. Modeling Results

The kinetic parameters for the five kinetic models were estimated by a non-linear least square method. A FORTRAN program UWHAUS, which operates using the Marquardt algorithm (Marquardt, 1963). This program was used to calculate the best estimates of these parameters. A so-called MAIN program was used to read the experimental data and the subroutine MODEL was employed to compute the function values required to access UWHAUS. A detailed listing of the program MAIN and MODEL, is included in Appendix E.

The fitting for the estimation of the parameters was based on the minimization of the summation of the squares of the differences between experimental and predicted reaction rates. Discrimination between the different kinetic expressions was based on the following criteria:

- The quality of the fitting which was indicated by the value of the variance,
- The 95% confidence interval levels of the parameters,
- The randomness of the distribution of the residuals,
- The correlation matrix obtained to identify cross-correlation between the parameters.

Results of the parameter estimation obtained for the Models 1, 2, 3, 4,and 5 are presented in Tables 6.8, 6.9, 6.10, 6.11, and 6.12. It has to be mentioned that the quality of fitting for the models was satisfactory. The variance of normalized residuals calculated from the summation of the squares of the residuals were in the range of 3.171×10^{-4} – 3.629×10^{-4}

m.mol/(min.g.cat) which, compared to the average experimental rate of 9.175 $x10^{-2}$ m.mol/(min.g.cat), corresponded to an approximate deviation of 0.44%.

Also in Tables 6.8 through 6.12, it can be observed that reasonable confidence intervals on parameters were obtained: For example, for the pre-exponential factors (k_0) confidence intervals were in the 0.5 – 12%. Moreover, the confidence interval for the energies of activation, E_A, were in the range 0.8 – 23%, with values of the energies of activation between 113 to 129 KJ/mole.

It is important to notice that, as reported in Table 6.13, these values of the activation energies are in the range of those reported in the technical literature (Storch *et al.*, 1951; Anderson, 1956; Yang *et al.* 1979 and Post *et al.* 1989). This confirms the validity of the experimental methods and parameter estimation techniques applied. It can also be argued that the magnitude of energies of activation is a good indication of no or very limited mass and heat transport controls. In fact, smaller energies of activation for FTS are normally indicators of potential mass and heat transport limitations.

Finally, for the exponent of the various concentration terms the confidence intervals were in the range of 15 – 52%. For Model 1 the reaction order in CO is negative suggesting that adsorbed CO and derived CH_x species are the most abundant reactive intermediates. In this respect, Iglesia *et al.*, (1993) suggested that positive reaction order for CO while using a kinetic expression as the empirical one advanced in Model 1, is an indication of the

catalyst surface not being saturated with CO and CH_x species. Saturation of the surface leads to negative CO reaction orders in eq (6.4), an expected condition in eggshell catalysts having a surface rich on adsorbed CO and CH_x species.

Models 2, 3, 4, and 5 led to positive reaction orders for CO and this demonstrated the dominant influence of "b" parameters. These "b" parameters representing adsorption coefficients in Models 2, 3, and 4 were in the range of 55 -82 % with values between 5 - 39 (units varied for each case). Thus , given the magnitude of "b" (e.g. $bp_{CO} >> 1$ for Model 2) this leads, once the proper algebra considered, to effective negative orders for CO and this allows to reconcile the trends of Model 1 with all the other models. Note that the only exception was Model 5 which led to a smaller b value and to a situation where $b\, p_{CO}^{n}\, p_{H_2}^{m} \cong 1$.

Regarding parameter mutual dependence, this can be examined in the cross-correlation matrix (Tables 6.8 to 6.12). From these tables it can be noticed that the five models considered have independent kinetic parameters with little cross-correlation: all cross-correlation coefficients smaller than 1. Consequently, it can be concluded that there is, in the present work, little cross-correlation between the kinetics constants considered and the numerical methods used to asses the kinetic constants are correct.

Table 6.8. Results of the parameter estimation obtained for the kinetic model 1 (Equation 6.4 Power law model)

Parameters Values

Parameter	Guess	Final	Lower	Upper	± %
K_0	2.0E+12	2.19E+12	2.18E+12	2.19E+12	0.457
E	90	127	126	128	0.787
n	1	-0.428	-0.568	-0.287	32.71
m	1	0.886	0.706	1.07	20.32

Correlation Matrix

	k_0	E	N	m
k_0	1.0000			
E	0.0012	1.0000		
n	0.0000	-.08827	1.0000	
m	0.0000	0.0568	-0.3226	1.0000

Sum of squares after regression = 0.0130644

Variance of residuals = 0.0003629 36 degrees of freedom

$$-r_{H_2+CO} = k_0 e^{\left(\frac{-E}{R_1}\left(\frac{1}{T}-\frac{1}{Tav}\right)\right)} p_{CO}^{n} p_{H_2}^{m} \qquad (6.4)$$

Table 6.9. Results of the parameter estimation obtained for the kinetic model 2 (Equation 6.5 Iglesia *et al.*, 1993).

Parameters Values

Parameter	Guess	Final	Lower	Upper	± %
k_0	2.0E+18	1.43E+14	1.43E+14	1.43E+14	10.79
b	1000	38.53	10.25	66.81	73.40
E	90	129	101	157	21.70
n	1	0.547	0.415	0.679	24.13
m	1	0.945	0.707	1.16	25.19

Correlation Matrix

	k_0	b	E	n	m
k_0	1.0000				
b	-0.0028	1.0000			
E	0.0094	-0.1345	1.0000		
n	-0.0399	0.6815	-0.1154	1.0000	
m	-0.0238	-0.0367	0.0380	-0.2993	1.0000

Sum of squares after regression = 0.01110077

Variance of residuals = 0.0003172 35 degrees of freedom

$$-r_{H_2+CO} = \frac{k_0 e^{\left(\frac{-E}{R_1}\left(\frac{1}{T}-\frac{1}{Tav}\right)\right)} p_{CO}^{n} p_{H_2}^{m}}{\left(1 + bp_{CO}\right)} \qquad (6.5)$$

Table 6.10. **Results of the parameter estimation obtained for the Kinetic model 3 (Equation 6.6 Sarup and Wojciechowski model).**

Parameters Values

Parameter	Guess	Final	Lower	Upper	± %
k_0	2.0e+18	1.01E+14	1.01E+14	1.01E+14	7.05
b	1000	19.32	5.01	33.63	74.06
E	90	129	100.7	157.2	21.94
n	1	0.453	0.323	0.583	28.70
m	1	0.945	0.777	1.11	17.78

Correlation Matrix

	k_o	b	E	n	m
k_0	1.0000				
b	0.0027	1.0000			
E	-0.0076	-0.1766	1.0000		
n	-0.0638	-0.6597	-0.1066	1.0000	
m	0.0030	-0.0348	0.0360	0.3025	1.0000

Sum of squares after regression = 0.0111058

Variance of residuals = 0.0003172 35 degrees of freedom

$$-r_{H_2+CO} = \frac{k_o e^{\left(\frac{-E}{R_1}\left(\frac{1}{T}-\frac{1}{Tav}\right)\right)} p_{CO}^{n} p_{H_2}^{m}}{\left(1 + bp_{CO}^{n}\right)^2} \qquad (6.6)$$

Table 6.11. Results of the parameter estimation obtained for the Kinetic model 4 (Equation 6.7 Rautavuoma and van der Baan model).

Parameters Values

Parameter	Guess	Final	Lower	Upper	± %
k_0	2.0E+18	7.00E+13	7.00E+13	7.00E+13	11.35
b	1000	12.22	2.20	22.24	82.0
E	90	129	100	157	22.48
n	1	0.229	0.1629	0.2942	28.47
m	1	0.9434	0.777	1.112	17.63

Correlation Matrix

	k_0	b	E	n	m
k_0	1.0000				
b	0.0003	1.0000			
E	-0.1765	0.0758	1.0000		
n	-0.0929	0.6758	-0.0553	1.0000	
m	0.0071	0.0321	0.0330	0.3051	1.0000

Sum of squares after regression = 0.01110005

Variance of residuals = 0.0003171 35 degrees of freedom

$$-r_{H_2+CO} = \frac{k_o e^{\left(\frac{-E}{R_1}\left(\frac{1}{T}-\frac{1}{Tav}\right)\right)} p_{CO}^{n} p_{H_2}^{m}}{\left(1+bp_{CO}^{n}\right)^{3}} \qquad (6.7)$$

Table 6.12. Results of the parameter estimation obtained for the Kinetic model 5 (equation 6.8 Anderson et al. model)

Parameters Values

Parameter	Guess	Final	Lower	Upper	± %
k_0	2.0E+18	2.80E+13	2.80E+13	2.80E+13	0.71
b	1000	4.6	2.07	7.15	55
E	90	113	111.7	114	1.15
n	1	0.21	0.1	0.32	52.3
m	1	1.27	1.08	1.46	14.96

Correlation Matrix

	k_0	b	E	n	m
k_0	1.0000				
b	0.0002	1.0000			
E	0.002	-0.4532	1.0000		
n	0.0052	0.0407	-0.5874	1.0000	
m	-0.0000	0.816	-0.3870	-0.49	1.0000

Sum of squares after regression = 0.0480579

Variance of residuals = 0.0003156 37 degrees of freedom

$$-r_{H_2+CO} = \frac{k_0 e^{\left(\frac{-E}{R_1}\left(\frac{1}{T}-\frac{1}{Tav}\right)\right)} p_{CO}^{n} p_{H_2}^{m}}{\left(1+b p_{CO}^{n} p_{H_2}^{m}\right)} \qquad (6.8)$$

Table 6.13. Comparison between parameters as obtained from this work and the ones reported in the technical literature.

Model	Reference	Parameter		
		n	m	E_A (Kj/mole)
1	Yang *et al.* (1979)	-0.5	1	120
	Wang (1987)	-0.33	0.55	-
	Pannell et al. (1980)	-0.5	0.68	-
	This work	-0.43	0.89	127
2	Iglesia et al. (1993)	0.65	0.60	-
	This work	0.547	0.945	129
3	Sarup and Wojciechowski (1989)	0.5	1	-
	This work	0.453	0.945	129
4	Rautavuoma and van der Baan (1981)	0.5	1	-
	This work	0.23	0.94	129
5	Anderson (1956)	1	2	102
	This work	0.21	1.27	113

The adequacy of the five kinetic models is also shown comparing the predicted and experimental rates of synthesis gas conversion. Figs. 6.16 to 6.20 report predicted rates and experimental rates for Models 1, 2, 3, 4, and 5 respectively. These figures (6.16 to 6.20) also include a linear regression and the 95% prediction interval for these models. Note that all models considered provide good fitting for all the range of reaction rates studied.

Moreover, comparison between normalized residuals, experimental and predicted rates of synthesis gas conversion for the Models 1, 2, 3, 4, and 5 are presented in Figs. 6.21, 6.22, 6.23, 6.24 and 6.25. A visual check of these plots demonstrate that residuals fluctuate around a constant mean with, however Models 2 and 3 (Figs. 6.22 and 6.23) providing a residual distribution quite symmetrical over the entire range of observations.

Adequacy of postulated kinetic models can also be considered based on the values of the constants "n" and "m". For example, Model 2 yields a value of n = 0.547 and m = 0.945 and these two values are consistent with mechanistic explanations. Model 3 yields a value of n = 0.453 and a value of m = 0.945 also consistent with expectations. Model 4, however, gives a n = 0.229 and m = 0.9434 with the n value being too small for a proper mechanistic justification.

Regarding Model 5, n and m values were 0.21 and 1.27 respectively with "b" yielding the group $b\, p_{CO}^{n}\, p_{H_2}^{m}$ a value close to one. Similarly to Model

4, Model 5 displayed an "n" to small to be valid. In summary, considering these facts Models 2 and 3 are the more likely ones to be valid.

Moreover while comparing Models 2 and 3, Model 2 shows a denominator with a power of one while Model 3 a denominator with a power of 2. Given the expected two sites mechanism leading to a denominator with a power of 2, Model 3 is overall favoured as the expression for further calculations. Thus, while reviewing the five kinetic models considered even if in terms of data adjustment there are small differences, one can argue about the advantage of considering Model 3 for further analysis given its higher probability of being phenomenologically consistent.

6.4.4. Conclusion

Five kinetic rate expressions were considered in the context of the present study. This was done on the basis of comparing experimental and predicted rates and the following can be concluded:

- The kinetic parameter estimated for the five kinetics models presented a reasonable confidence interval, which indicates the adequacy of the 40 kinetic runs and the numerical technique adopted.
- Plots of the residuals as a function of the predicted rates for the models presented a symmetrical (normal) distribution of residuals and this was particularly true for the Models 2 and 3.

- Models 2, 3 and 4 presented a positive reaction order for CO in the range of 0.23-0.55 and for H_2 consistently close to 0.95.
- The empirical Model 1 presented a negative reaction order for CO and a positive one for H_2 suggesting that adsorbed CO and derived CH_x species are the most abundant reactive intermediates. While the order for CO was compared with the one of Models 2, 3, and 4 it was realized that given these models display a high adsorption parameter (b) the effective CO order for the models is negative as well and there is as a result consistency between Models 1, 2, 3 and 4.
- Regarding the Model 5, it displayed an adsorption parameter "b" leading to a $b\, p_{CO}^{n}\, p_{H_2}^{m}$ of about 1.
- The apparent activation energy for the various kinetics expression was in the range of 113-129 KJ/mole range suggesting no intraparticle mass transfer controls.
- Overall Model 3 was the one preferred for further simulation, given it was the one more consistent with various mechanistic steps.

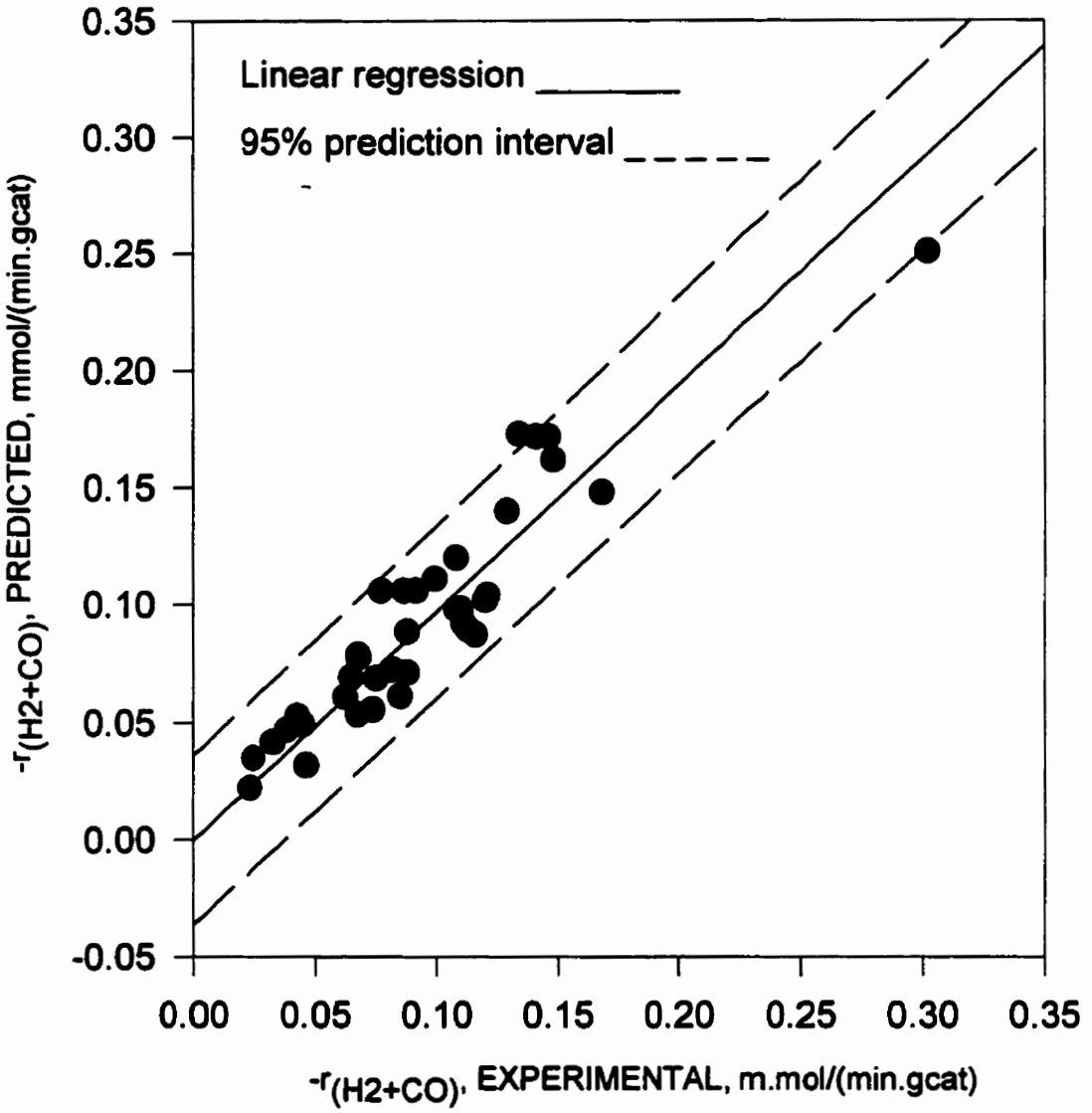

Figure 6.16. Predicted versus experimental reaction rate for Model 1.

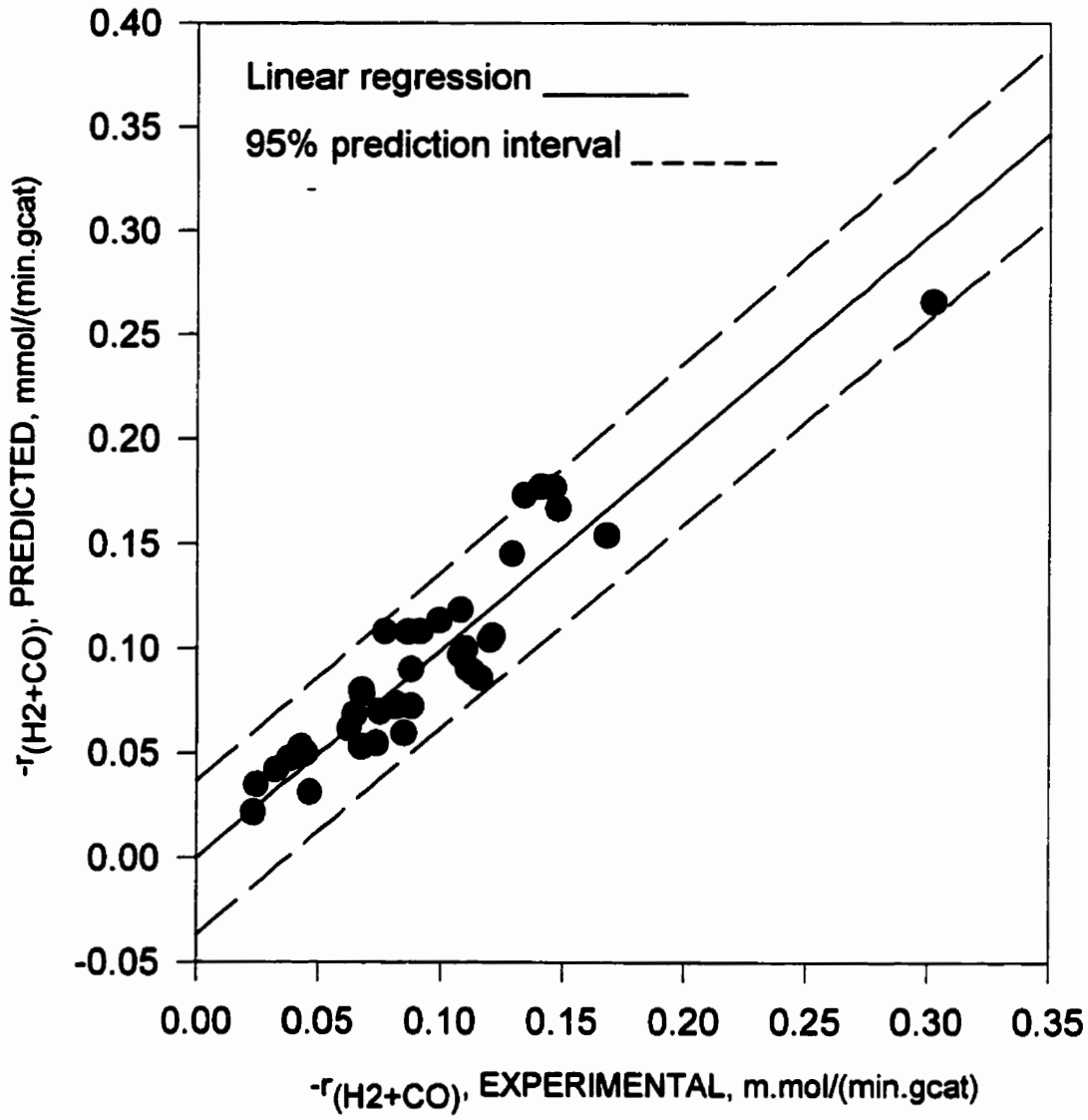

Figure 6.17. Predicted versus experimental reaction rate for Model 2.

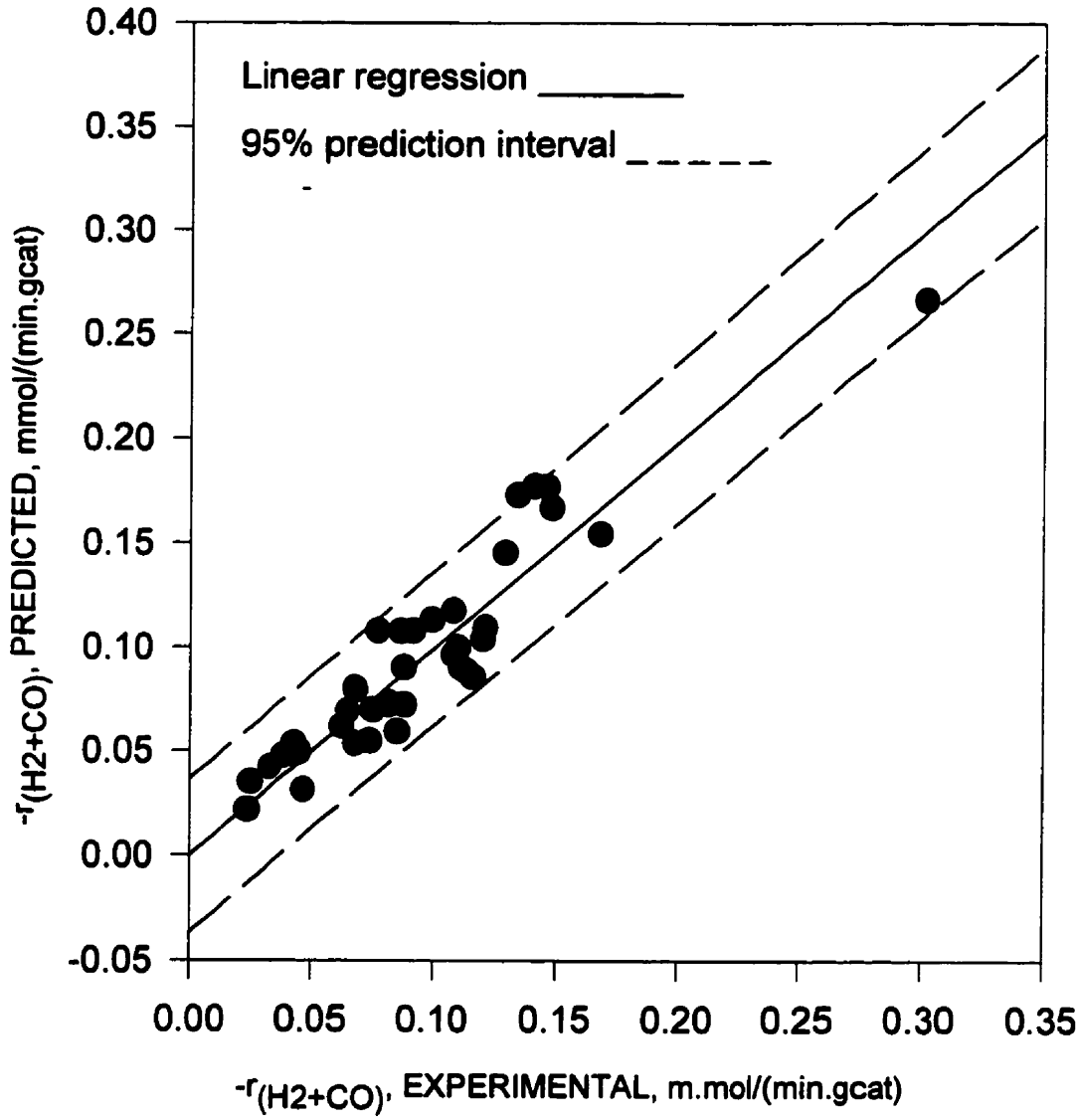

Figure 6.18. Predicted versus experimental reaction rate for Model 3.

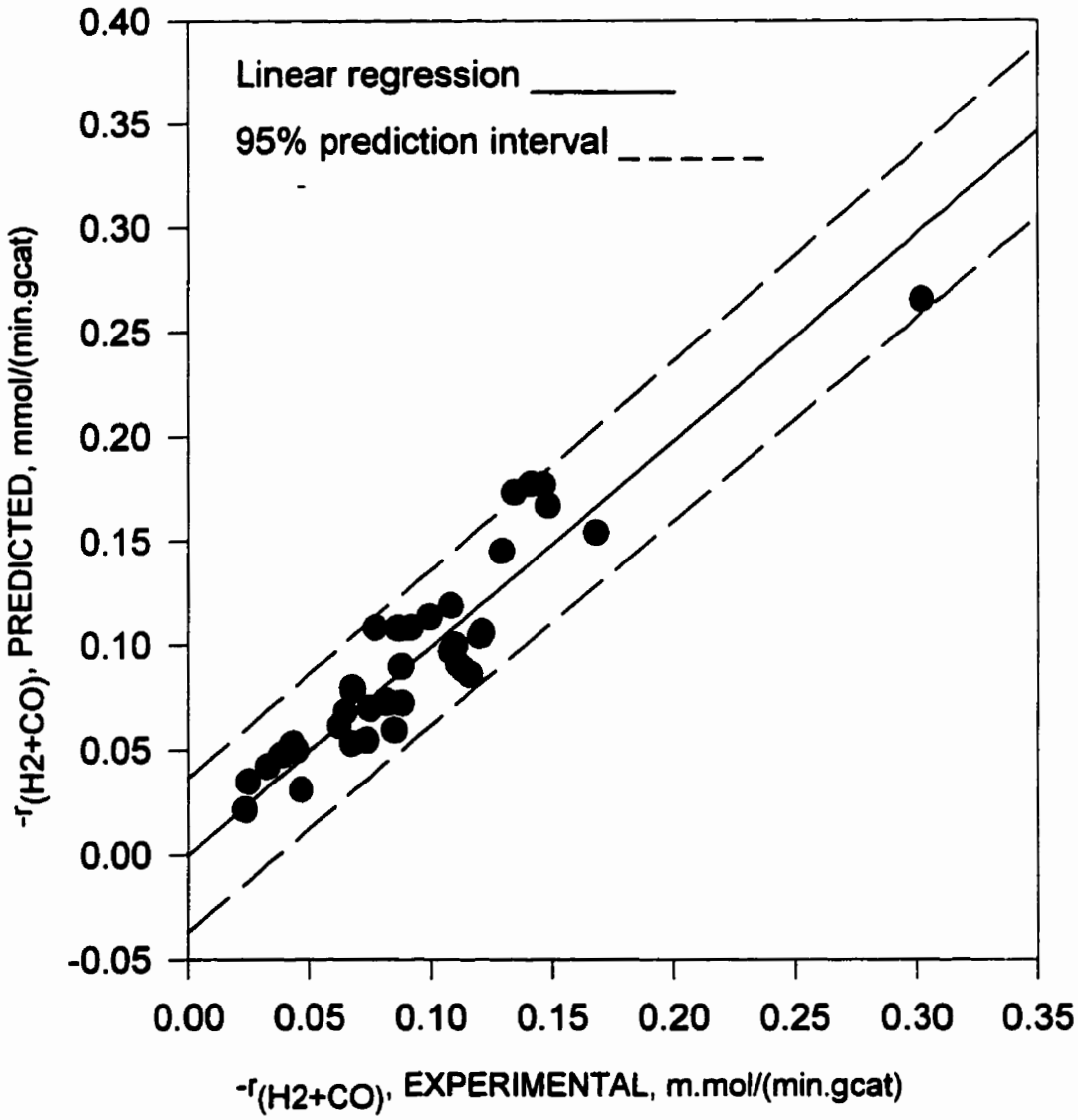

Figure 6.19. Predicted versus experimental reaction rate for Model 4.

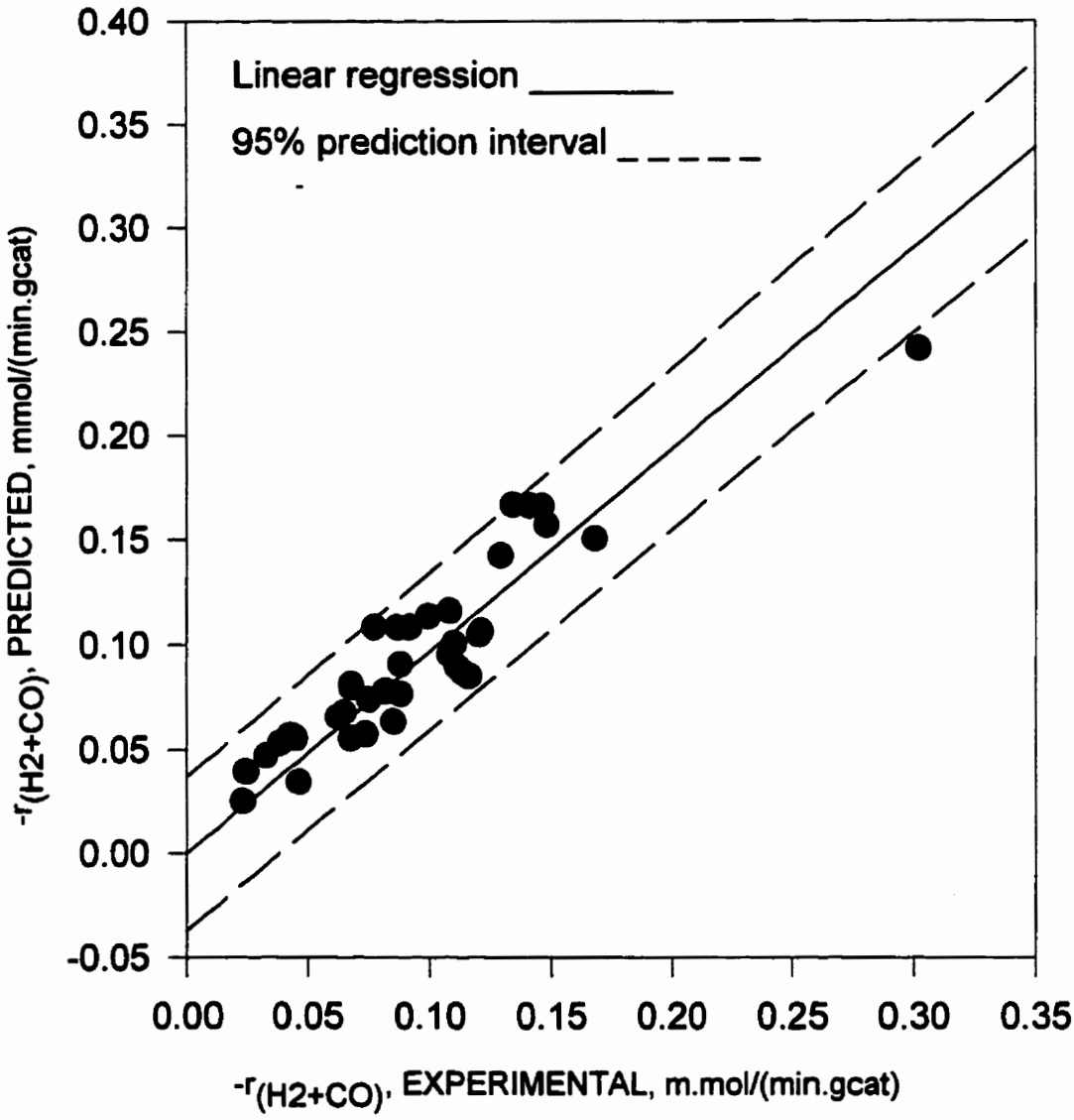

Figure 6.20. Predicted versus experimental reaction rate for Model 5.

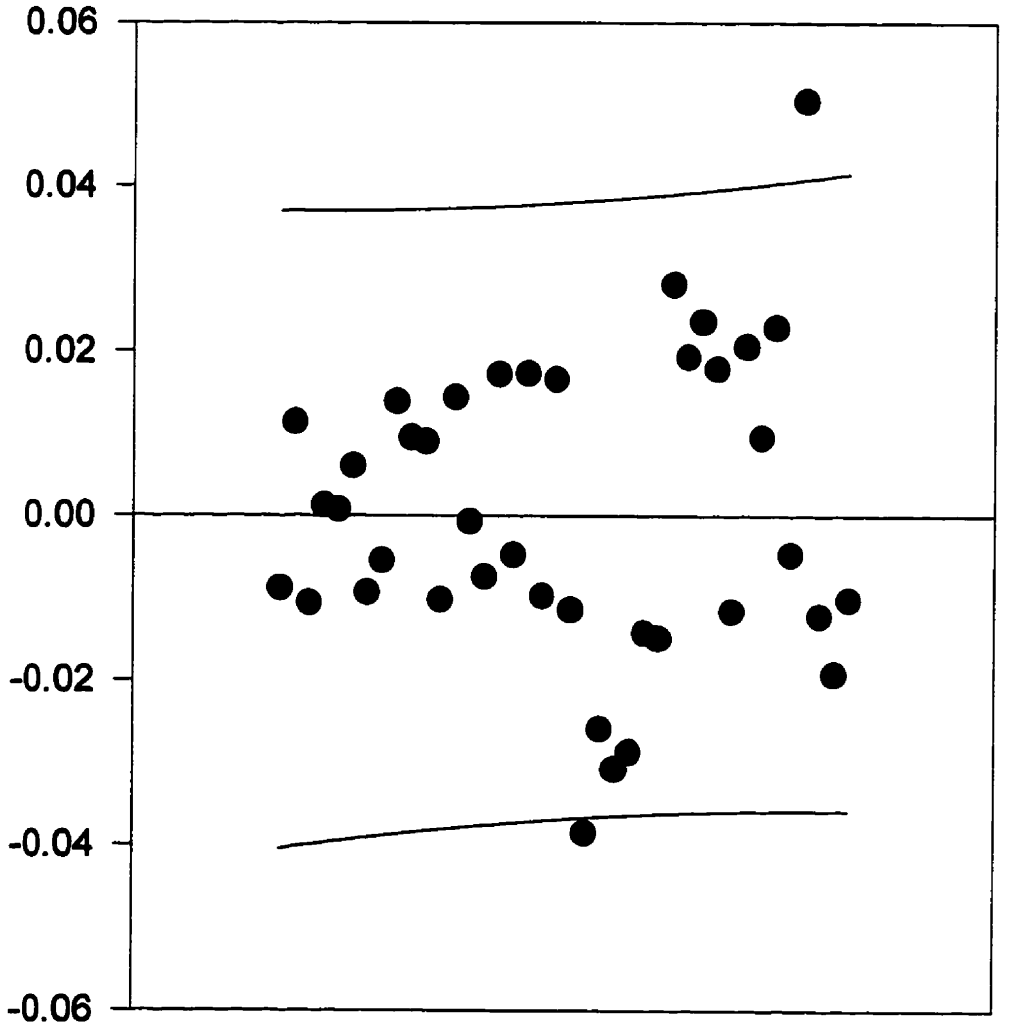

Figure 6.21. Comparison between the predicted and the experimental residuals for Model 1 .

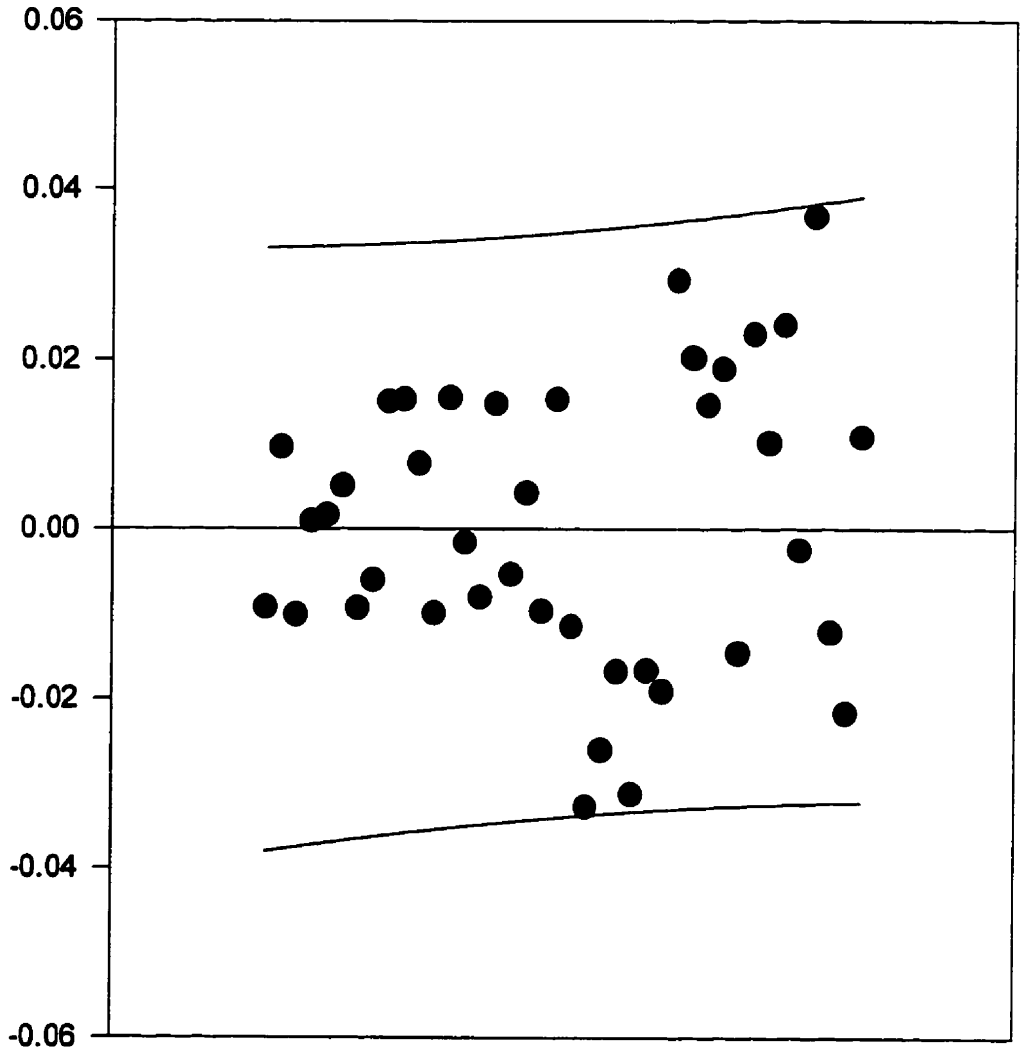

Figure 6.22. Comparison between the predicted and the experimental residuals for Model 2 .

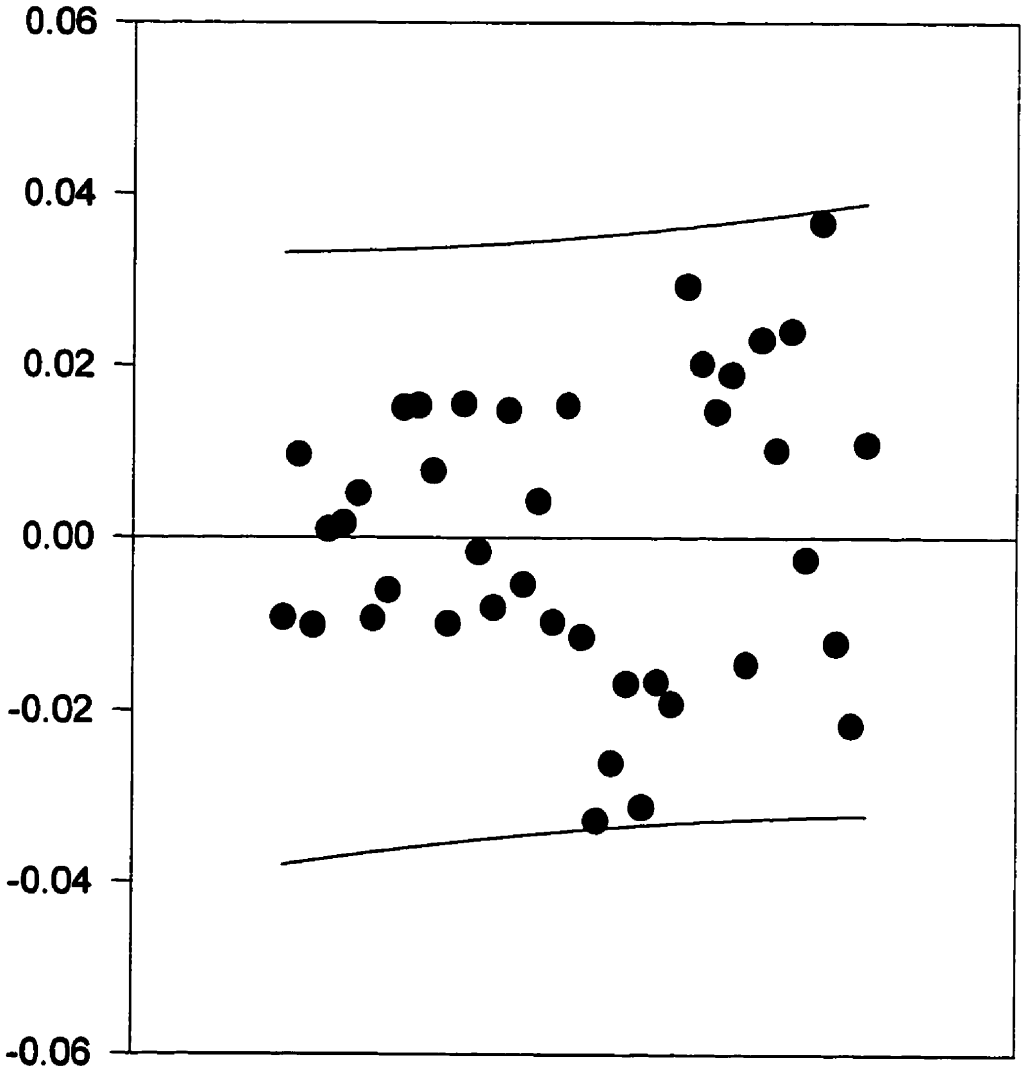

Figure 6.23. Comparison between the predicted and the experimental residuals for Model 3 .

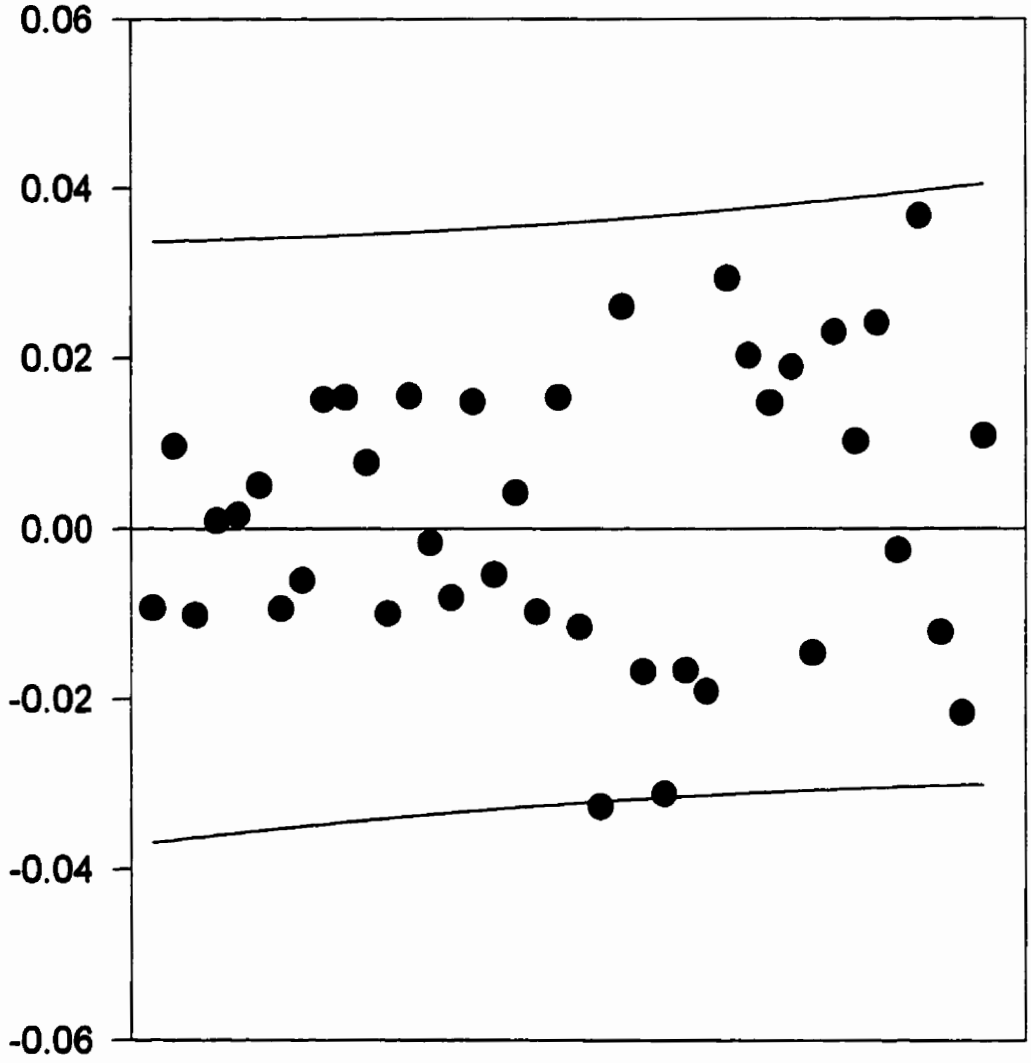

Figure 6.24. Comparison between the predicted and the experimental residuals for Model 4 .

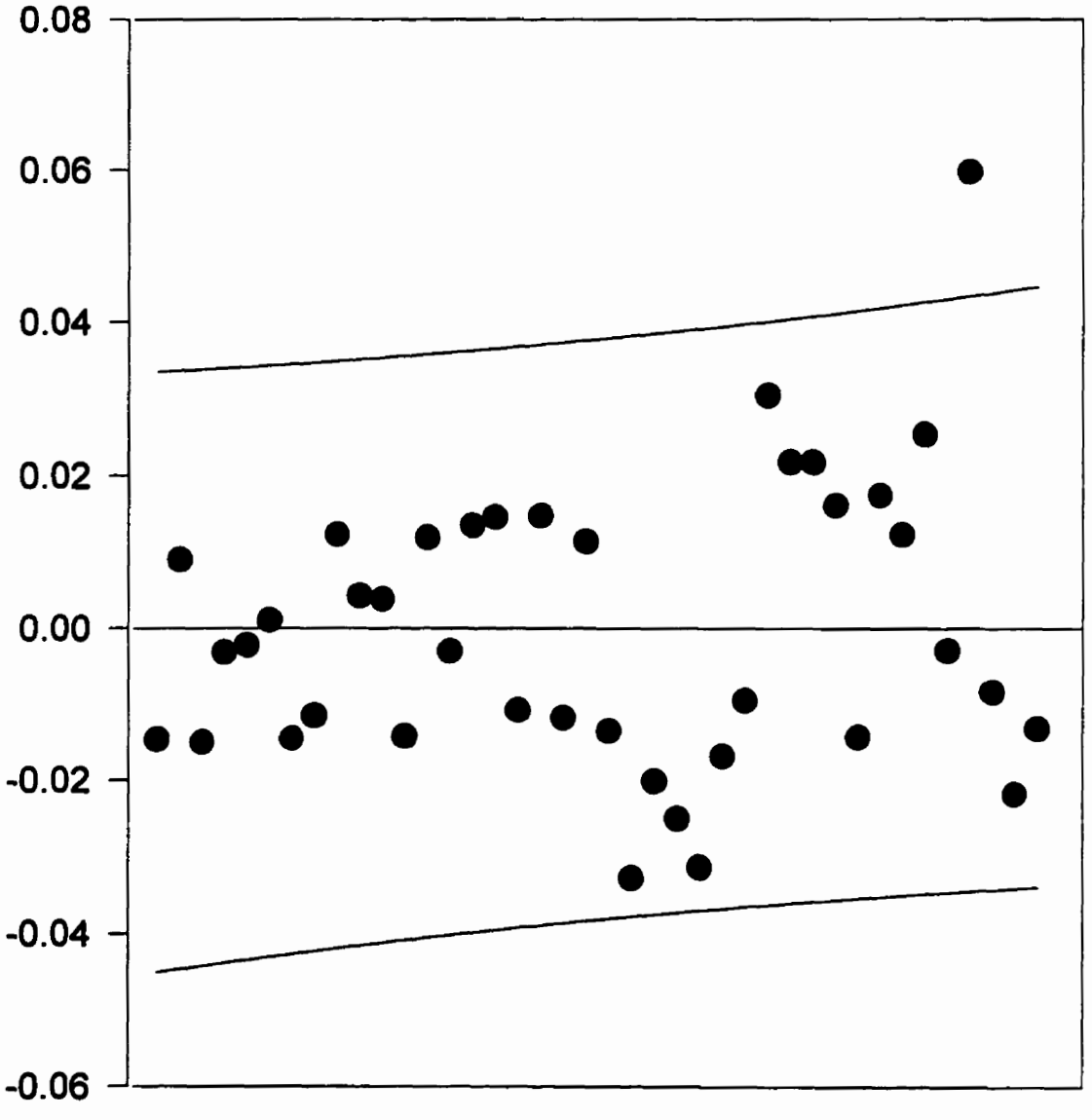

Figure 6.25. Comparison between the predicted and the experimental residuals for Model 5 .

CHAPTER 7

PSEUDOADIABATIC REACTOR SIMULATION

7.1. Introduction

This chapter describes results of the numerical simulation of a pseudo-adiabatic (PO) fixed bed reactor using a Co-Zr/SiO_2 catalyst. This type of catalytic reactor is considered of particular value for the conversion of synthesis gas into hydrocarbons in the C_{10}-C_{20} range.

As mentioned earlier, (refer to the Literature Review Section) a pseudo-homogeneous one-dimensional model is considered for the numerical simulation of the PO reactor. Note that there are other models available in the technical literature, pseudo-homogeneous and heterogeneous two-dimensional models. These models were considered in previous contributions by UWO researchers (de Lasa et al., 1985; Ravella and de Lasa , 1987a; Ravella, 1987; Simard, 1991). It was found that for the PO regime simulations from these models do not significantly differ from the one-dimensional pseudo-homogeneous representation. Consequently this representation can provide satisfactory reactor simulation.

A specific objective of the reactor simulation, in a pseudo-adiabatic mode of operation, is the study of the influence of several operational parameters, such as inlet CO partial pressure, inlet gas and coolant temperature, and flow of coolant over the CO conversion and temperature. In any case, results of this

study are very useful to assess the range of operation for the pseudo-adiabatic regime (PO) or alternatively for the development of control strategies for further scale-up of the PO unit.

A summary of the simulated experiments and of the various operating conditions selected is presented in Table 7.1. These operational ranges were chosen given they represent the normal range of operating conditions in a FT reactor.

7.2. Pseudo-homogeneous One-dimensional Model

A number of important assumptions have to be made while using a pseudo-homogeneous one-dimensional model (Soria Lopez et al., 1981; Ravella, 1987, Simard, 1991). These assumptions can be summarised as follows:

- Mass and thermal axial dispersion effects may be neglected. This assumption is consistent with the findings of several researchers (Froment, 1972a; Froment and Bischoff, 1979) and is applicable for the range of operating conditions usually encountered in industrial fixed-bed reactors. In the case of the PO reactor, simulated in this research, this assumption is valid since the L/d_t ratio was approximately 100 (Froment 1972b).

- Concentration and temperature gradients between the solid catalysts and the gas phase may be considered negligible. This hypothesis was justified given the small Prater number and the effectiveness factor very close to unity (Post *et al.*, 1989).

Table 7.1. Simulated Operating Conditions

Run #	Inlet Gas Temp (°C)	Inlet Coolant Temp (°C)	Flow of gas (Liter/min)	Flow of coolant (kg/h)	Pressure (MPa)
1	210	210	10	15	0.3
2	210	210	10	15	0.8
3	210	210	10	15	1.0
4	210	210	10	15	1.5
5	210	210	10	15	2.0
6	210	210	10	15	3.0
7	210	210	10	15	5.0
8	200	200	10	15	1.5
9	210	210	10	15	1.5
10	220	220	10	15	1.5
11	230	230	10	15	1.5
12	240	240	10	15	1.5
13	210	195	10	15	1.5
14	210	200	10	15	1.5
15	210	205	10	15	1.5
16	210	220	10	15	1.5
17	210	230	10	15	1.5
18	210	210	10	5	1.5
19	210	210	10	7.5	1.5
20	210	210	10	10	1.5
21	210	210	10	15	1.5
22	210	210	10	20	1.5

- The axial pressure drop in the bed is comparatively small with respect to the total system pressure, so pressure drop changes can be neglected. This assumption was confirmed given that the pressure drop, calculated using the Ergun equation (Mccabe and Smith, 1976) was 0.9 KPa/m. Thus, the pressure drop influence on the total pressure was safely neglected.

- The overall heat transfer coefficient U, is considered to be constant. This means that both the physical properties of the fluids (represented by the Prandtl number) and the fluid dynamics of the system (represented by a Reynolds number) can be taken as constants in the reactor. This was verified while performing the reactor simulation re-evaluating at every step of the calculation the different physical properties of the reaction gas mixture and of the liquid coolant: density, viscosity, heat capacity, and thermal conductivity. It was observed that variation of these physical properties was less than 3%, which confirmed the adequacy of the postulated assumption.

- In the one-dimensional model it was considered that the temperature and the partial pressure were essentially constant across the reactor cross-section. Temperature changes were only accounted in the vicinity of the wall using a modified heat transfer coefficient. While many authors agree that there could be important gradients in the radial direction for conditions leading to hot spots, in the pseudo-adiabatic regime with no hot spots or very small hot spots neglecting temperature and partial pressure radial variations is fully adequate.

Regarding the simulation of FT synthesis under PO conditions, there are a number of specific problems to be addressed. First, the reactor operates with some fraction of liquid products. While for typical conditions selected for the simulation (200-230 °C, 1-3 MPa) water remains in the vapour phase (Chaumette et al., 1995), heavier hydrocarbons can condense forming liquid inside the reactor tubes. This condensed phase can fill potentially the pore of the catalyst and can generate intra-particle mass transfer limitations (Post et al., 1989). Note that it is expected these effects are very likely minimized in an eggshell catalyst.

Another effect of hydrocarbon condensation is their contribution to the overall exothermicity of the reaction. Note that the heat released during condensation generates an extra 2% of the heat being produced (Chaummette et al., 1995).

Furthermore, the presence of a liquid fraction enhances heat transfer and leads to a better distribution of heat inside the reactor tubes, thus helping to get more uniform temperatures. This may eventually contribute to the development of the pseudo-adiabatic regime.

Unfortunately, fully accounting for the effect of condensed liquid in the reactor simulation is not an easy task. Consequently, as a first approximation it was decided to develop a PO simulation assuming no liquid products was present and thus, having all reaction products in the gas phase. In order to justify this assumption, a simulation was performed using a HYSIM package having a stream with an hypothetical conversion of carbon monoxide of 65 %.

This simulation demonstrated that under the conditions of the present study with hydrocarbon products rich in the C_{10}-C_{20} fraction the liquid fraction is only 3.3 wt % of the total outlet stream (Galarraga and Peluso, 1995). Thus, to neglect the liquid fraction in terms of potential effects on transport phenomena is a sound approximation.

More specifically numerical simulation of the pseudo-adiabatic reactor was achieved solving a set of three differential equations. These equations represent the mass and heat balances of the reactor model.

$$\frac{-dx}{dz} = A\,P\,\exp\left(\frac{-a}{T+b}\right) \tag{7.1}$$

$$\frac{dT}{dZ} = B\,P\,\exp\left(\frac{-a}{T+b}\right) + C\,(T - T_c) \tag{7.2}$$

$$\frac{dT_c}{dZ} = D\,(T - T_c) \tag{7.3}$$

In the present project the simulation was implemented by means of a computer program written in the FORTRAN 77 language. The three model equations were solved simultaneously along the longitudinal direction of the reactor, Z. In order to integrate this set of three equations the program used a fourth-order Runge-Kutta routine. A listing of the program used for the calculations called "PBREACT" is presented in Appendix G.

As a brief outline of the "PBREACT" program, it can be stated that this program employs data to calculate heat-transfer parameters for each point in the

reactor. Then, these results were used to generate a U value, "U calculated from correlation". Finally, the program used the values of U, ΔH_R, and the kinetic information to calculate the group of constants called A, B, C and D (refer to equations 3.24, 3.25, 3.26 and 3.27 in Chapter 3 section 3.9.1). Note that these parameters are needed to solve the set of three ordinary differential equations getting the average reactor temperature (T), coolant temperature (T_c), the centreline temperature (T*), partial pressure of CO and CO conversion for every point in the reactor.

Table 7.2 presents a typical output from the numerical simulation of the one-dimensional model. In the first section of Table 7.2 the input values for the simulation are listed. In the second section of this table the calculated parameters required to estimate the overall heat transfer coefficient, U, are reported. Finally, a second page of the program output summarises the following results: a) reactor temperature profile (T), b) coolant temperature profile (T_c), c) centreline temperature profile (T*), d) partial pressure of CO (p_{CO}), and e) the CO conversion (X_{CO}) as function of the reactor axial distance (Z).

Concerning the rate equation, the kinetic model called "Kinetic Model 3", described in Chapter 6, was used in the reactor simulation. It has to be mentioned that this model was developed in a Berty reactor using an eggshell catalyst of 1.8 mm particle size. Kinetic parameters in this model are apparent kinetic constants including eventually intra-particle diffusional phenomena.

Regarding the heat of reaction, it was evaluated based on CO converted. Note that to evaluate this heat of reaction is of major importance in the range

temperatures of interest. This is essential for an adequate reactor simulation. Classical thermodynamics methods, involving heats of formation of the various reactants and products, were employed. A listing of the program "HEAT" used to perform these calculations is presented in Appendix G.

For CO conversion ranging between 60 to 90 %, the ΔH_R values were found to oscillate in a relatively narrow range with an average enthalpy of -162.83 KJ/mole of CO converted with standard deviations equal to ± 0.076 kJ/mole of CO converted. This deviation only represents 0.04 % of the mean values and this result shows that it is possible to use an average enthalpy of reaction for all calculations. Note that this average value of ΔH_R is very close to those reported in the literature (refer eq 3.3 in Chapter 3) and therefore, the ΔH_R for this reaction was kept constant at -162.83kJ/mole of CO converted (-38889.34 Kcal/ Kmole of CO converted).

Regarding the reactor to be simulated, in this study, it is similar to the unit already installed in the Chemical Reactor Engineering Centre laboratories of the University of Western Ontario. This reactor was successfully used for the following: a) methanol conversion into hydrocarbons (Ravella, 1987) and b) synthesis of gas into hydrocarbons (Simard, 1991). This reactor is a single-tube, 2 m long and 0.0209 m diameter (3/4 inch Schedule 40S) jacketed unit. The jacket of the reactor consists of a concentric pipe (1-1/4 inch Schedule 40S). The gap between the central pipe and the jacket, where the coolant will circulate, is to be filled with steel shots of 1.5 mm in diameter to improve heat transfer in the coolant side. For additional details about the design and operation of this reactor unit refer to Ravella (1987) and Simard (1991).

Table 7.2. Output program-PO Reactor Simulation (PBREACT)

```
**************************************
  SIMULATION ONE-DIMENSIONAL MODEL
**************************************

EXPERIMENT NUMBER    1

**************************************
  INPUT VALUES FOR THE SIMULATION
**************************************

INITIAL TEMPERATURE OF GAS                    205.00     C
INITIAL GAS FLOW                               10.00    liter/min
H2/CO RATIO                                     2.00
TOTAL PRESSURE                                  1.5      MPa
INITIAL TEMPERATURE OF COOLANT                205.0      C
COOLANT FLOW                                   15.0    Kg/h
INLET MOLES TOTAL                               .026786  Kmol/hour
INITIAL MOLES OF H2                             .018389  Kmol/hour
INITIAL MOLES OF CO                             .008397  Kmol/hour
ENTHALPY OF REACTION                       -38889.00 Kcal/kmol CO converted
KO OF THE REACTION                              .219E+11  m3/m3 cat/s


*****************************************
  CALCULATED VALUES DURING THE SIMULATION
*****************************************

MOLAR FLOW                                      .022     Kmol/hour
GAS DENSITY                                    4.087     Kg/m3
GAS SUPERFICIAL VELOCITY                     169.70830   m/h
GAS HEAT CAPACITY                               .7351    Kcal/ C/Kg
GAS VISCOSITY OUT                               .070     Kg/m/h
GAS THERMAL CONDUCTIVITY OUT                    .103     Kcal/ C/ m/h
REYNOLDS GAS                                  27.8533
PRANDTL NUMBER GAS                              .4975
PECLET GAS                                    13.45
BIOT GAS                                       2.99
COOLANT DENSITY                              943.4     Kg/m3
COOLANT VISCOSITY                              1.888 Kg/m/h
COOLANT THERMAL CONDUCTIVITY                    .103 Kcal/ C/ m/h
REYNOLDS COOLANT                              28.9
PRANDTL COOLANT                                9.49
EFFECTIVE RADIAL THERMAL CONDUCTIVITY           .796 Kcal/H/m/ C
JACKET HEAT TRANSFER COEFFICIENT             637.086 Kcal/h/m2/ C
WALL HEAT TRANSFER PARAMETER                 226.399 Kcal/h/m2/  C
U FROM CORRELATIONS                          107.73  Kcal/h/m2/  C
```

Table 7.2. Output Program –PO Reactor simulation (PBREACT) (Cont....)

```
************************************
SIMULATED TEMPERATURE PROFILE
************************************
```

RUN NUMBER 1

Z	T	T*	Tc	Pco	Xco
.010	205.35	205.50	205.00	.46995	.13
.060	205.98	206.40	205.04	.46877	.80
.110	206.12	206.57	205.09	.46756	1.48
.160	206.19	206.65	205.15	.46634	2.16
.210	206.25	206.71	205.20	.46510	2.85
.260	206.31	206.77	205.25	.46384	3.53
.310	206.37	206.83	205.31	.46257	4.22
.360	206.43	206.89	205.36	.46129	4.91
.410	206.49	206.96	205.42	.45999	5.60
.460	206.55	207.02	205.47	.45868	6.30
.510	206.61	207.08	205.53	.45735	6.99
.560	206.67	207.14	205.58	.45601	7.69
.610	206.73	207.21	205.64	.45465	8.39
.660	206.79	207.27	205.69	.45328	9.09
.710	206.85	207.33	205.75	.45189	9.79
.760	206.91	207.39	205.80	.45048	10.49
.810	206.97	207.46	205.86	.44906	11.19
.860	207.03	207.52	205.91	.44762	11.90
.910	207.09	207.58	205.97	.44616	12.61
.960	207.16	207.65	206.02	.44469	13.32
1.010	207.22	207.71	206.08	.44320	14.03
1.060	207.28	207.78	206.14	.44169	14.74
1.110	207.34	207.84	206.19	.44016	15.45
1.160	207.41	207.91	206.25	.43861	16.17
1.210	207.47	207.97	206.31	.43705	16.89
1.260	207.53	208.04	206.36	.43546	17.61
1.310	207.60	208.10	206.42	.43386	18.33
1.360	207.66	208.17	206.48	.43223	19.05
1.410	207.72	208.23	206.53	.43059	19.77
1.460	207.78	208.30	206.59	.42893	20.49
1.510	207.85	208.37	206.65	.42724	21.22
1.560	207.91	208.43	206.70	.42553	21.95
1.610	207.98	208.50	206.76	.42381	22.68
1.660	208.04	208.57	206.82	.42206	23.41
1.710	208.11	208.63	206.88	.42028	24.14
1.760	208.17	208.70	206.94	.41849	24.87
1.810	208.24	208.77	206.99	.41667	25.61
1.860	208.30	208.84	207.05	.41483	26.34
1.910	208.37	208.91	207.11	.41296	27.08
1.960	208.43	208.97	207.17 .	.41107	27.82

7.3. Effect of the CO Inlet Partial Pressure on Reactor Temperature Profile.

Regarding the simulation of the PO reactor, a first aspect was to evaluate the effect of the inlet CO partial pressures on the PO regime. This was done considering a plot like the one of Fig.7.1 relating the CO partial pressure and the temperatures found at different axial positions. It was observed that the variation of the inlet partial pressure generates different CO conversions and consequently produces different temperature profiles in the reactor.

As mentioned previously, the PO regime is the regime where the axial reactor temperature increases steadily with the bed length in such a way the highest temperature in the unit is reached at the reactor outlet (Soria Lopez, 1981). When the reactor operates outside the PO regime, "hot-spots" develop at a finite axial reactor position. This condition is known as "maximum in a finite axial reactor position" (MFARP) (de Lasa, 1983).

From Fig.7.1, it can be observed that the reactor temperature profiles change significantly as the initial CO partial pressure increases. Note that for instance at an initial total pressure of 0.3 MPa, which corresponds to an inlet CO partial pressure of 0.09 MPa, a progressive temperature increment was noticed. This represents an ideal PO condition with temperature always increasing along reactor axis.

Moreover, for a total pressure of 0.8, 1.0, 1.5 and 2.0 MPa, conditions equivalent to an inlet CO partial pressure of 0.25, 0.31, 0.47, and 0.63 MPa the

reactor temperature shows a trend similar to the one at 0.3 MPa. Reactor operating conditions practically remain in the PO regime with the axial temperature always increasing and with the outlet temperature being the highest. Note that in these cases, using higher initial p_{CO} leads to higher CO conversions. It has to be mentioned that towards the end of the temperature profiles, p_{CO} of 0.003 MPa, 0.006 MPa, 0.009 MPa, and 0.017 MPa at the axial positions of 12, 9.5, 7.5 and 6 m respectively, there is a minor hot spot : 0.1°C, above the thermal level reached at the infinite reactor position ($z \rightarrow \infty$). This hot spot was considered small enough and outside the actual reactor length of 2m to practically change the trend of the overall curve. Thereby, it was judged that the PO regime still dominates the operation of the unit for p^{o}_{CO} of 0.25 MPa, 0.31 MPa, 0.47 MPa, and 0.63 MPa. Note that for the operating conditions of Table 7.1 (inlet total pressure of 3.0 MPa) the overall CO conversion is about 55% and this represents a typical performance of a FTS reactor.

On the other hand operating conditions at a total pressure of 5.0 MPa (inlet CO partial pressure of 1.56 MPa) a well-defined hot spot appears inside the 2m length reactor. Significant changes in the dp/dT slope are observed with important hot spots developing inside the unit. In this case, the MFARP operation dominates and consequently hot spots ($dp/dT \rightarrow \infty$) are encountered inside the 2m-reactor length.

It was thus concluded that for this particular set of operating conditions the limit of the domain for PO operation was found to be close to 2.0 MPa of total pressure, which is equivalent to 0.63 MPa of CO inlet partial pressure.

In summary, this demonstrates that there are two characteristic regimes associated with changes in the inlet reactor pressure:

a) the MFRAP, with the hot-spots placed inside the reactor : $dp/dT \rightarrow \infty$ for $Z < 2m$,

b) the PO regime with temperature always increases along the reactor length: $dT/dz > 0$ for $z < 2m$.

Since the normal ranges of operating pressures in FT with Co-Zr catalysts are expected to be between 1.0 to 3.0 MPa, these results demonstrate that the PO concept can be applied with advantage to the FT process.

Another interesting observation concerns the differences between the centerline temperature and the average cross-sectional temperature. It was observed that this difference is typically for a PO condition of not more than 0.5 °C (refer to Table 7.2). Thus, for all practical purposes the average temperature at a given axial position is a good estimate of the reactor temperature.

7.4. Coolant Inlet Temperature Effect on the Reactor Temperature Profile.

The coolant temperature is another important parameter to be investigated keeping constant all the other operating parameters. With this end in view, changes of CO partial pressures with reactor temperature were calculated at different coolant inlet temperatures: 195, 200, 205, 210, 220 and 230 °C having a gas inlet temperature set at 210 °C and a total gas pressure of 1.5 MPa. Fig. 7.2 summarises simulation results.

As it can be noticed, all the T-p_{CO} profiles showed the characteristic behaviour of the PO regime. Special trends were found, however, close to the reactor entry and this was the result of the differences of inlet temperatures between the coolant and the reactant. For example, when the coolant was fed at 195, 200 and 205 °C it produced a cooling effect in the gas stream. Consequently the temperature and the conversion in the top reactor section showed a slight overall reduction. This change on the shape of the curves can be explained given in the first few centimetres of the reactor the coolant removes a significant fraction of the heat of the reaction and a fraction of the enthalpy of the incoming gas stream.

However, when the inlet coolant temperature was set at 210 °C, the same temperature used for the inlet gas, no phenomenon of temperature equilibration was observed between the coolant and the gas. This yielded, as expected a PO profile.

Furthermore, for 220 °C and 230 °C of coolant inlet temperature, the PO regime was still developed. An interesting characteristic is that the reactant temperature rises in the first section of the reactor until surpassing the coolant temperature. Nevertheless, due to the temperature differences between the coolant and the gas at inlet conditions, higher overall carbon monoxide conversions were reached.

It has to be mentioned, as shown by Arandes and de Lasa (1995), that higher differences of coolant and reactor temperatures with the coolant having

the highest temperature can lead to hot-spots in the first section of the reactor. Therefore it is recommended to avoid excessive differences between these two operating variables to prevent the presence of hot spots.

7.5. Effect of the inlet temperature on the reactor temperature profile.

To study the effects of different inlet temperatures over the reactor performance both coolant and gas inlet temperatures where varied from 200 °C to 240 °C. The combined inlet gas pressure was set at 1.5 MPa.

T-P_{co} plots (Fig. 7.3) shows that increasing the inlet temperature change significantly the T-P_{co} profiles. While for inlet temperature of 200 °C, 205 °C, 210 °C, and 220 °C the behaviour is pseudoadiabatic, for 230 °C, however the PO condition applies up to the last reactor section. At this point there is a hot spot present. This effect was even more pronounced at 240 °C inlet temperature. In this case the hot spot developed close to the reactor entry yielding a characteristic MFRAP operation.

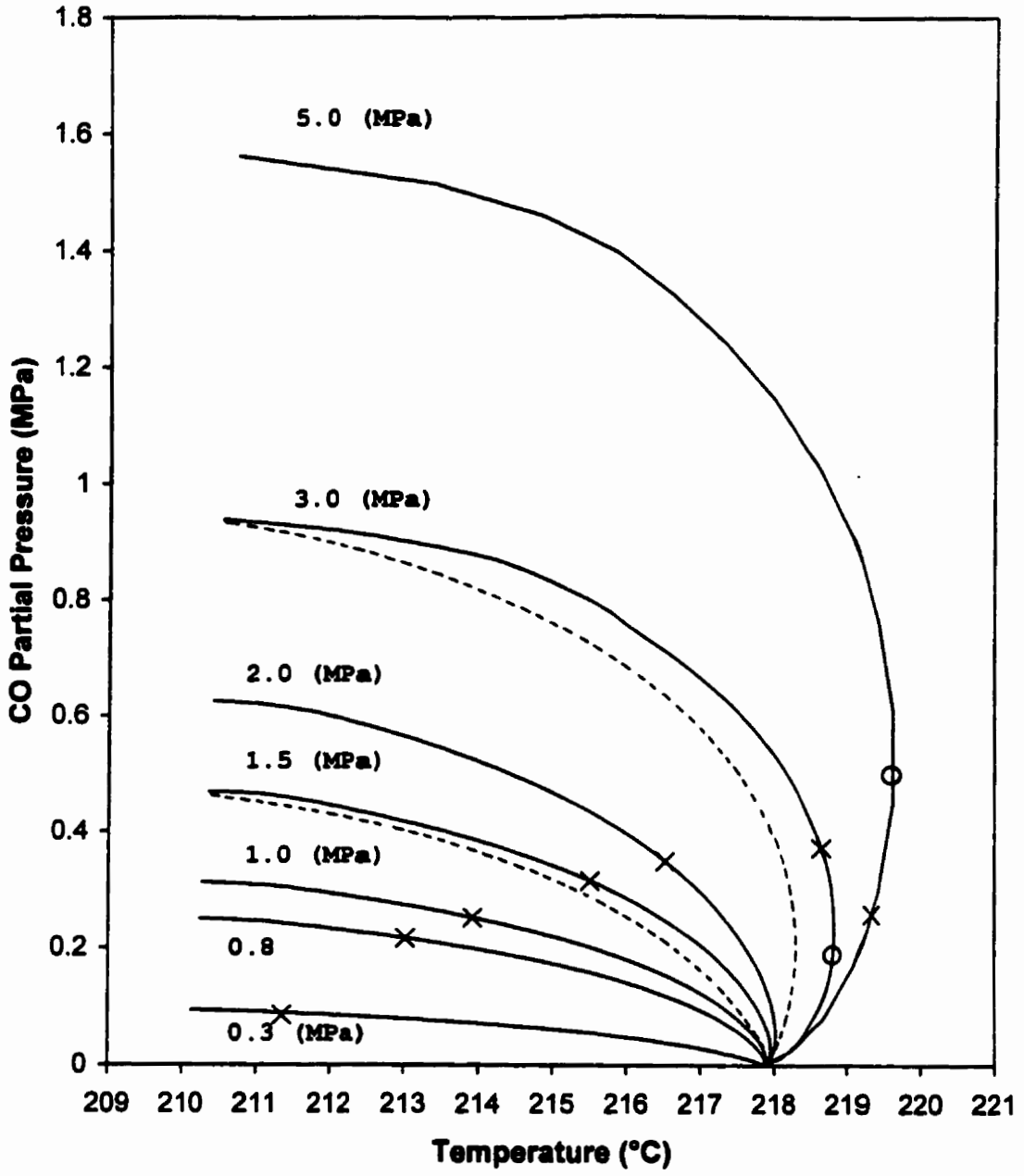

Figure 7.1. **Effect of inlet total gas pressure on the reactor temperature profile. (Run 1 to 7 from Table 7.1). Inlet gas temperature and coolant temperature: 210 °C, inlet flow of gas 10 l/min and inlet flow of coolant 15 Kg/h. Full lines represent condition inside the reactor. Broken lines represent conditions in the coolant side. Crosses in the curves indicate the outlet conditions for a 2m reactor. Open circles indicate the position of the hot spot with dp/dT→∞.**

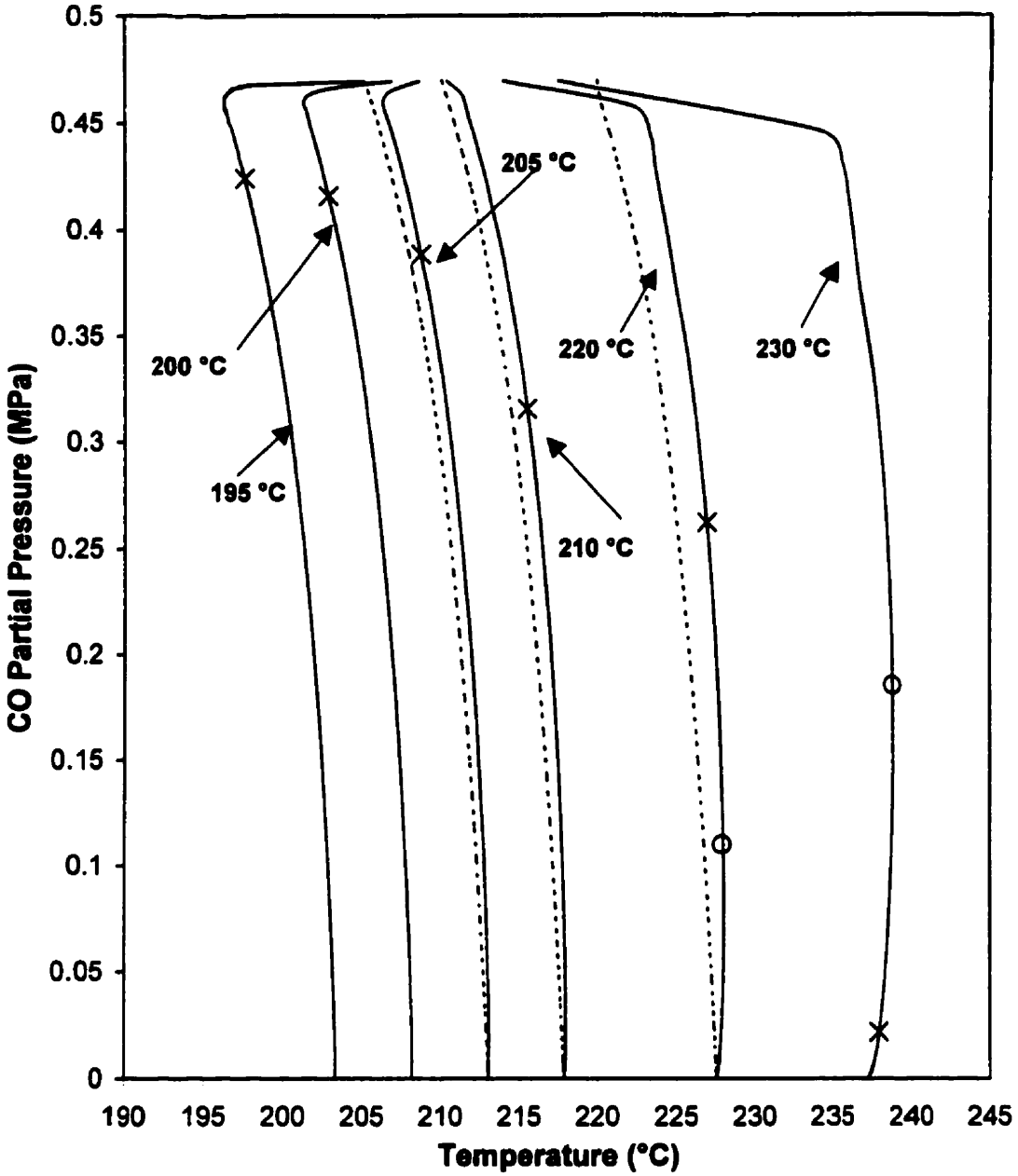

Figure 7.2. **Effect of inlet coolant temperatures on the reactor temperature profile. (Run 13 to 17 and 9 from Table 7.1). Inlet gas temperatures: 210 °C, inlet gas pressure 1.5 MPa, inlet flow of gas 10 l/min, and inlet flow gas of coolant: 15 Kg/h. Full lines represent condition inside the reactor. Broken lines represent conditions in the coolant side. Crosses in the curves indicate the outlet conditions for a 2m reactor. Open circles indicate the position of the hot spot with $dp/dT \rightarrow \infty$.**

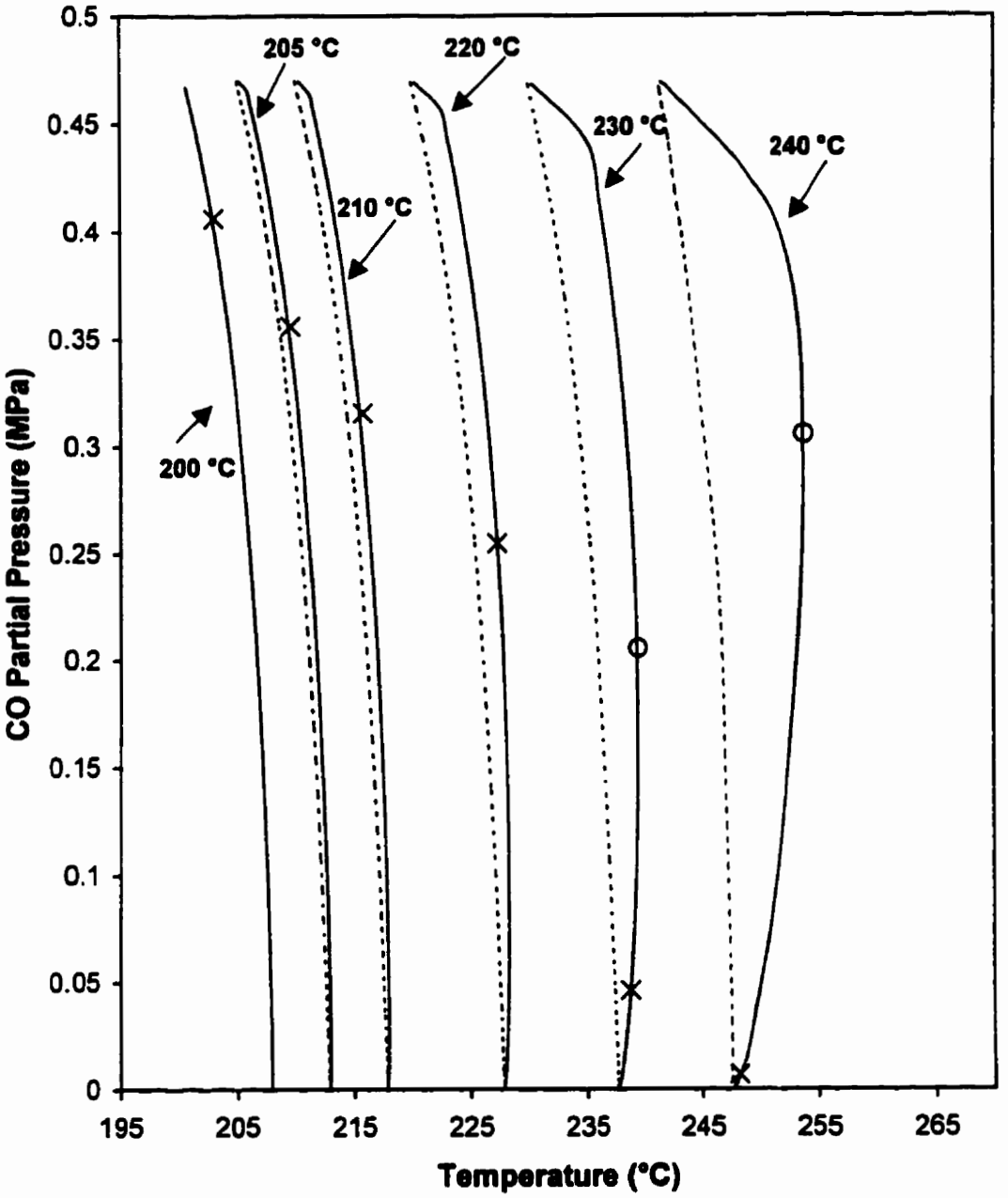

Figure 7.3. **Effect of inlet temperature on the reactor temperature profile. (Run 8 to 12 from Table 7.1). Inlet gas pressure: 1.5 MPa, inlet flow of gas 10 l/min, and inlet flow of coolant: 15 Kg/h.) Full lines represent condition inside the reactor. Broken lines represent conditions in the coolant side. Crosses in the curves indicate the outlet conditions for a 2m reactor. Open circles indicate the position of the hot spot with $dp/dT \rightarrow \infty$.**

7.6. Effect of the flow of coolant on the reactor temperature profile.

The physicochemical properties of coolant and the coolant flow play a very important role in multi-tubular reactors with heat exchange. The flow of coolant, in particular, influences heat transfer and affects the operating regime. To clarify this matter the coolant flow effect was investigated simulating the variation of this parameter between 5 and 20 Kg/h, while the other parameters were kept constant.

Fig.7.4 displays T-p_{CO} profiles for different coolant flows. It can be appreciated that T-p_{CO} plots show consistently PO regimes with small difference between them. Thus, T-p_{CO} profiles for 15 and 20 kg/h coolant flows display PO conditions with temperature differences of 6 and 8 °C, between the reactor entry and reactor outlet. Note that these temperature differences are quite acceptable and this given the exothermic reaction involved in this simulation.

When flows of coolant were decreased to 10, 7.5 and 5 kg/h the operation was still practically PO, with small hot spots calculated outside the reactor (z> 2m). It was also observed that as expected the ΔT between the top and bottom of the reactor increased as the flow of coolant decreased. For example when the simulation was performed with a flow of the coolant of 5.0 kg/h the ΔT increase was up to 22 °C. Lower flows of coolant removed less heat and consequently yielded higher reactor temperatures with significantly increased reaction rates.

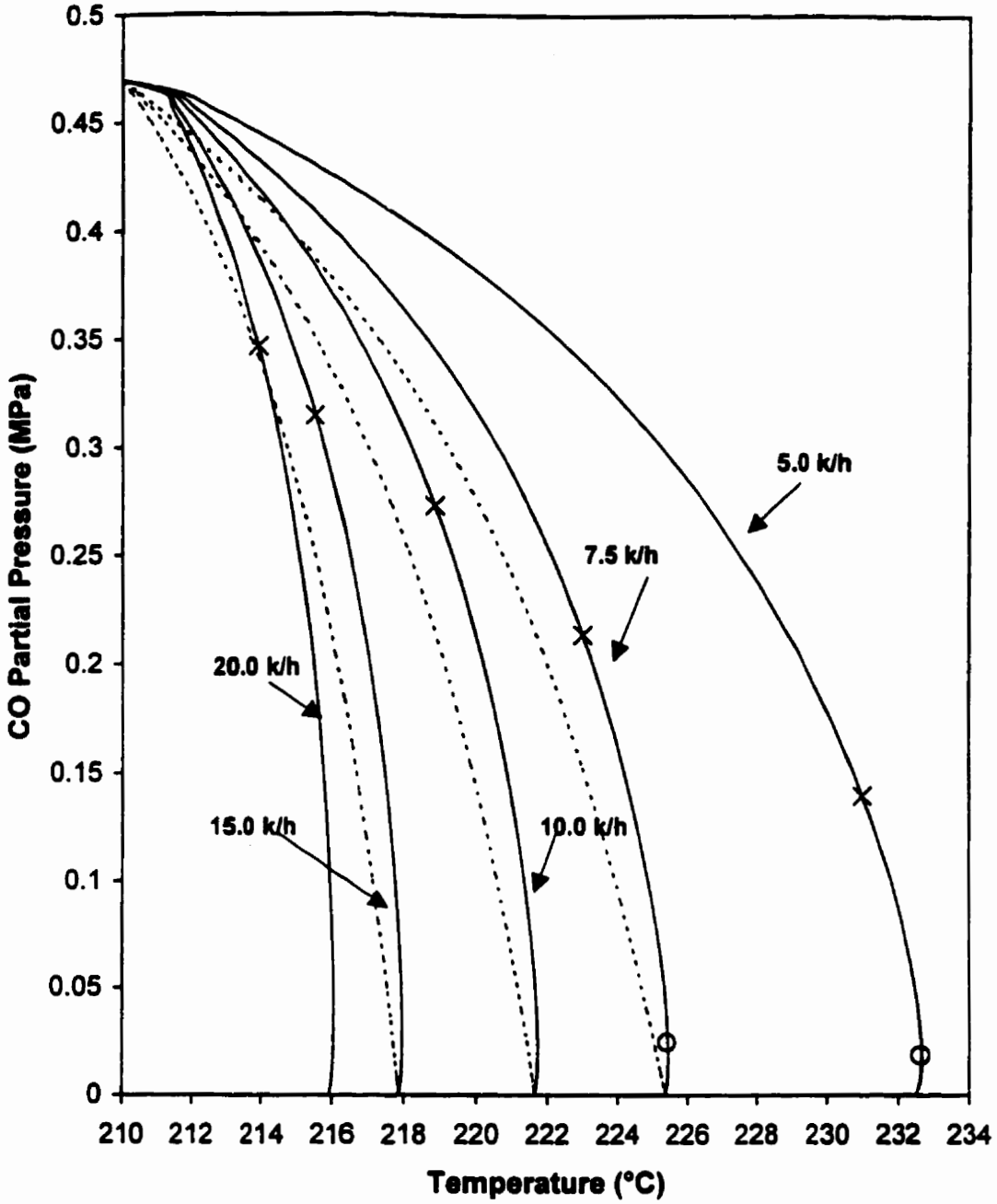

Figure 7.4. **Effect of flow of coolant on the reactor temperature profile. (Run 18 to 21 from Table 7.1). Inlet gas and coolant temperature: 210 °C, inlet gas pressure of 1.5 MPa, and inlet flow of gas of 10 l/min. Full lines represent condition inside the reactor. Broken lines represent conditions in the coolant side. Crosses in the curves indicate the outlet conditions for a 2m reactor. Open circles indicate the position of the hot spot with $dp/dT \rightarrow \infty$.**

7.7. Effect of the kinetics expression on the reactor temperature profile.

As mentioned before five kinetics models, described in Chapter 6, were evaluated during the development of this work. Model 3 was selected, as the more adequate kinetic expression, to perform the reactor simulation. However and to evaluate the possible effects of a different kinetic models on the temperature profile developed, the five kinetics models were evaluated using a standard operating condition such as:

- Inlet gas and coolant temperature at 210 °C,
- Total pressure of the system at 1.5 MPa,
- Flow of coolant as 15 kg/h, and
- Flow of gas at 10 l/min.

The results of this simulation are presented in Fig. 7.6. The T-p_{CO} profiles for all the cases display in general similar profiles with however small differences between models.

Note that for the conditions selected Models 3 and 4 display PO profiles. As well, Model 2 provides close temperature profile still in the PO regime. Models 1 and 5 show the highest reaction rates and as result a PO condition inside the reactor with an expected hot spot at $z > 2m$.

Thus, it was concluded that the PO regime under the conditions tested is too not sensitive to the kinetic model selected.

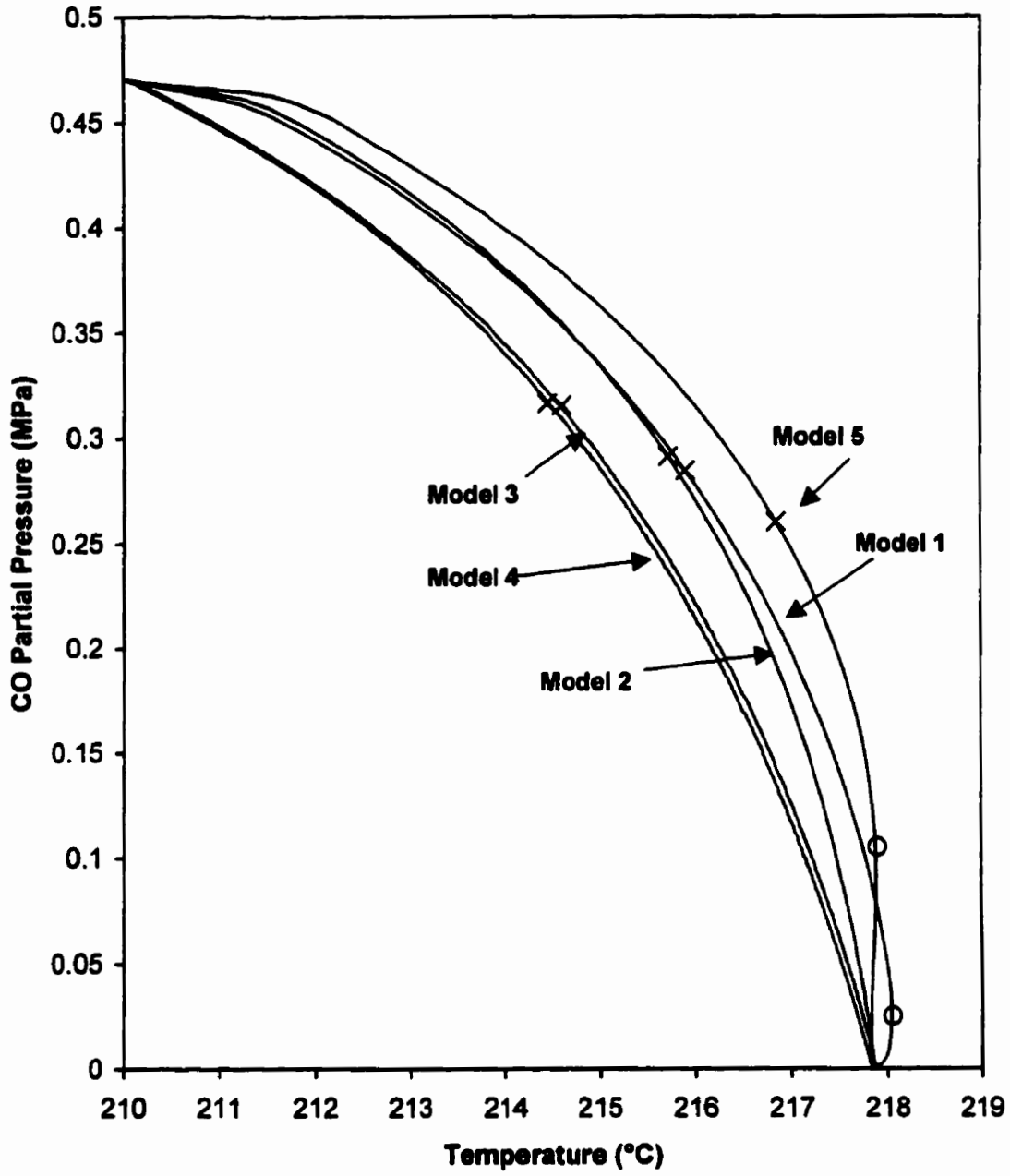

Figure 7.5. **Effect of the Kinetics models in the reactor temperature profile. Inlet gas and coolant temperature: 210 °C, inlet gas pressure of 1.5 MPa, inlet flow of coolant: 15 Kg/h, and inlet flow of gas of 10 l/min. Full lines represent condition inside the reactor. Crosses in the curves indicate the outlet conditions for a 2m reactor. Open circles indicate the position of the hot spot with $dp/dT \rightarrow \infty$.**

7.8. Conclusions

A one-dimensional pseudo-homogeneous model was considered to simulate a pseudo-adiabatic reactor for the conversion of synthesis gas into hydrocarbons in the diesel range via FTS. The pseudo-adiabatic regime was consistently observed in several of these runs.

Moreover, the predicted CO conversions obtained from this simulation demonstrate that the PO regime is a very useful regime in such a reaction system, and justifies further research and experimental studies.

Results of this study are very relevant for the definition of the domain of operating conditions leading to the pseudoadiabatic operation (PO regime).

It is also demonstrated here that various kinetics models with the kinetics constants obtained for an eggshell catalyst yield similar CO conversion and reactor performance results. Thus, the PO regime is not too sensitive to the specific kinetic model selected for the reactor simulation.

CHAPTER 8

CONCLUSIONS AND RECOMMENDATIONS

8.1. Conclusions

The results and the achievements of the present study can be summarized as follows:

8.1.1. Catalyst development

Two catalysts were successfully developed for the conversion of syngas into heavy paraffinic oils via the Fischer-Tropsch reaction. One of the catalysts was a uniformly impregnated (standard) catalyst while the other was the so-called eggshell catalyst, in which the active metals were deposited on the external surface of the support. The catalysts were prepared using the following components: a) cobalt as active phase, b) zirconium as promoter, and c) silica gel as a support. Catalysts were characterized using several characterization techniques and this provided useful information about metal content, surface area and distribution of the metal in the support. It was demonstrated that the methodology used for the catalyst preparation of the eggshell catalysts was adequate.

An evaluation of standard and eggshell catalyst in an internally recycled Berty reactor was performed. The objective was to assess the effect of catalyst design on the CO conversion (carbon monoxide disappearance rates), the product selectivity and the hydrocarbon distribution. It was found that the

eggshell catalyst yielded higher carbon monoxide disappearance rates than the standard one. It was also demonstrated that the standard catalyst has an undesirable higher selectivity towards carbon dioxide than the eggshell catalysts. Finally it was noticed that the hydrocarbon distribution yielded by the eggshell catalyst present a favorable hydrocarbon distribution in the range of C_{10}-C_{20}.

8.1.2. Effect of the Operating Conditions

Once it was established that the eggshell catalyst was an interesting choice for FTS, systematic runs were developed in a Berty reactor to test the effect of operating conditions on CO conversion, product selectivity, and hydrocarbon distribution. This led to the following conclusions:

- Carbon monoxide conversion increases with temperature. Also while temperature is increased there is a shift towards the hydrocarbons of higher molecular weight.
- The total pressure has a minor effect on carbon monoxide conversion and hydrocarbon distribution.
- The carbon monoxide conversion decreases with GHSV and at smaller GHSV the hydrocarbon distribution is shifted towards lighter molecular weight hydrocarbons.
- The H_2/CO ratio (defined at inlet reactor conditions) has an important impact on hydrocarbon distribution. For instance, for lower H_2/CO ratio, the production of higher molecular weight hydrocarbon is favored.

- Important deviations from the classical ASF distribution were observed and this was attributed to secondary reactions present during the FTS.

8.1.3. Kinetic modeling

Using the experimental results obtained five kinetic models reported in the literature were considered. The model discrimination process was based on the mathematical expression which best represent the experimental data. Proper fitting of the experimental data was carried out using a non-linear regression algorithm. From this the following can be concluded:

- The kinetic parameters estimated for the five kinetics models presented reasonable confidence intervals, which indicates the adequacy of the experimental design and the numerical technique adopted.
- Models 2, 3, and 4 presented a positive reaction order for CO in the range of 0.23-0.55 and for H_2 consistently close to 0.95.
- Models 2 and 3 presented the best fitting to the experimental data. Between these two models, Model 3 was considered to be the one more phenomenologically viable.
- Model 1 displayed a negative reaction order for CO and a positive for H_2. This suggests that adsorbed CO and derived CH_x species are the most abundant reactive intermediates present in the catalyst surface. This was further confirmed observing the high CO adsorption constant for Models 2, 3, and 4.
- Apparent activation energy for all the kinetic expression fell within the range of 104-127 KJ/mol. These values are very close to those reported in the

technical literature. This was an important indication that mass transport restrictions were not a major factor affecting catalyst performance.

8.1.4. Pseudoadiabatic simulation

A one-dimensional model was employed to simulate the Pseudoadibatic reactor (PO) for the conversion of syngas in the C_{10}-C_{20} range via FTS. The influence of several operational parameters such as inlet CO partial pressure, inlet gas and coolant temperature, and coolant flow over the reactor performance was studied.

Results of the reactor simulation, show a pseudoadiabatic regime for most of the conditions explored and this for operating conditions within the normal range for FTS. Thus, the PO regime is a very attractive alternative to explore and justifies further research and experimental studies in this area.

It was also demonstrated that various kinetics models with the kinetic constants obtained in the context of the conversion of CO on a "eggshell" catalyst provide close results and could be thus, used with confidence for the simulation of the reactor performance and the PO regime.

8.2. Recommendations.

The previously stated conclusions lead to some recommendations for future research:

- Further testing of eggshell catalysts are needed to establish its performance (stability) during extended periods of operation.

- Additional consideration of the FTS kinetics while using eggshell catalysts is necessary to better understand deviations of the ASF distribution. In this respect, determination of the olefin/paraffin ratio for the outlet reactor stream is highly advisable.
- Evaluation of the eggshell catalyst in the Pseudoadiabatic reactor pilot plant unit, available at CREC, will be most valuable to compare experimental and simulated temperature and CO conversion profiles. This evaluation is a must for scaling up this unit for FTS process in the near future.
- Economic analysis of a process converting syngas into middle distillate hydrocarbons range, involving an eggshell catalyst and a multitubular Pseudo-adiabatic reactor is a very critical step. This evaluation, including a fair comparison with existing technologies, will demonstrate the commercial feasibility of the proposed approach.

REFERENCES

Adesina, A. A., "Hydrocarbon synthesis via Fischer-Tropsch reaction: travails and triumphs", *Applied Catalysis A: General* , 138, 345-367 (1996).

Ali, S., Chen, B., and Goodwin, Jr. J. G., "Zr promotion of Co/SiO_2 for Fischer-Tropsch synthesis", *J. Catal.*,157, 35-41 (1995).

Anderson, R. B., *In Catalysis*; Emmett, P.H., Ed. Reinhold: New York, Vol. IV, 257-371, (1956)

Anderson, R. B., *The Fischer-Tropsch Synthesis*, Academic press, Orlando, FL.,(1984)

Araki, M., and Ponec, V., "Methanation of carbon monoxide on nickel and nickel-copper alloys", *J. Catal.*, 44, 439-448. (1976)

Arandes, J., and de Lasa, H. I., "Pseudoadiabatic operation for fixed-bed catalytic reactors: methods for finding the limits of the regime", *Chem. Eng. J.*, 58, 34-44 (1995).

Beek, J., and Singer, E., "A procedure for scaling-up a catalytic reactor", *Chem. Eng. Prog.*, 47 (10), 534-540 (1951).

Berty, J. M., "Reactor for vapor-phase catalytic studies", *Chem. Eng. Progr.*, 70 (5), 78-84, (1974).

Bessel, S., "Investigation of bifunctional zeolite supported on cobalt Fischer-Tropsch catalysts", *Appl. Catal. A.: General*, 126, 235-244 (1995).

Biloen, P., Helle, J. N., and Sachtler, W. M. H., "Incorporation of surface carbon into hydrocarbons during Fischer-Tropsch synthesis: mechanistic implications" *J. Catal.*, 58, 95-107 (1979).

Borio, D. O., Bucala, V., Orejas, J. A., and Porras, J. A., "Cocurrently-cooled fixed-bed reactors: A simple approach to optimal cooling design", *AIChE J.*, 35 (11), 1899-1902 (1989a).

Borio, D. O., Gatica, J. E.,and Porras J. A., "Wall-cooled fixed-bed reactor: parametric sensitivity as a design criterion", *AIChE J.*, 35 (2), 287-295 (1989b).

Bruce, L. A., Hoang, M., Hughes, A. E., and Turney, T. W., "Ruthenium promotion of Fischer-Tropsch synthesis over coprecipitated cobalt/ceria catalysts.", *Appl. Catal. A: General,* 100, 51-67 (1993).

Bub, G. and Baerns, M., "Prediction of the performance of catalytic fixed bed reactors for Fischer-Tropsch synthesis", *Chem. Eng. Science*, 35, 348-355 (1980).

Chaumette, P., Verdon, C., and Boucot, P., "Influence of the hydrocarbons distribution on the heat produced during Fischer-Tropsch synthesis", *Topics in Catalysis*, 2 , 301-311 (1995).

Dalai, A. K., Bakhski, N. N., and Esmail M. N., "Conversion of syngas to hydrocarbons in a tube-wall reactor using Co-Fe plasma-sprayed catalysts: experimental and modeling studies", *Fuel Processing Technology*, 51, 219-238 (1997).

Dalai, A. K., Esmail, M. N., and Bakhski, N. N., "Carbon monoxide hydrogenation over cobalt catalyst in a tube-wall reactor: Part II. Modelling studies", *Can. J. Chem. Eng.*, 70, 278-285, (1992).

de Lasa, H. I, Ravella, A.,and Rost, E., "Converting methanol into gasoline in a novel pseudoadiabatic catalytic fixed bed reactor", *Proc. CSChE Meeting*, Calgary (1985).

de Lasa, H. I., Ravella, A.,and Rost E., "Pseudoadibatic operation of fixed bed catalytic reactor for the conversion of methanol into gasoline", *Proc. XVI ICHMT Symp. on Heat and Mass Transfer in Fixed and Fluidized Beds*, Yugoslavia (1984).

de Lasa, H. I., "Pseudoadiabatic reactor for exothermic catalytic conversions", Canadian Patent No. 1223895 (1987).

de Lasa, H. I., "The pseudoadiabatic operation. A useful tool for eliminating the hot spots of catalytic fixed bed reactors", *Proc. of the 32nd Canadian Chem. Eng. Conference*, Vancouver, British Columbia , CSChE, 954-964, (1982).

de Lasa, H. I., "Pseudoadiabatic reactor for exothermal catalytic conversions", U.S. Patent, 4,929,798 (1989).

de Lasa, H. I., Mok, L. K., and Soria Lopez, A., "Oxidation of orthoxylene in a catalytic packed bed reactor. The cross flow operation. The critical row of tubes", *Proc. CSChE Meeting,* Montreal, 297-300 (1981).

de Lasa, H. I., Ravella, A., Rost, E., and Mahay, A., "Operation of co-axially cooled fixed-bed catalytic reactor: Conditions of existence of the pseudoadiabatic regime", *Che. Eng. Sci.*, 44 (5), 1221-1226 (1989).

de Lasa, H. I., Ravella, A.,and Rost, E., "Pseudoadiabatic operation of a fixed-bed catalytic reactor for the conversion of methanol into gasoline", *Heat*

and Mass Transfer in Fixed and Fluidized Beds, Eds. Van Swaaij and Agfan, Washington, D.C., 645 (1986).

de Lasa, H. I.,"Application of the pseudoadiabatic operation to the catalytic fixed bed reactors. Case of orthoxylene oxidation", *Can. J. Chem. Eng.*, 61, 710-718 (1983).

Dixit, R. S., and Tavlarides, L. L., "Kinetics of the Fischer-Tropsch synthesis", *Ind. Eng. Chem. Process Des. Dev.*, 22, 1-9 (1983).

Doraiswamy, L. K., and Sharma, M. M. *Heterogeneous Reactions: Analysis, Examples and Reactor Design*. Vol. 1 Gas-Solid and Solid-Solid Reactions, J. Wiley & Sons, (1984).

Dry, E. M., "Practical and theoretical aspects of the catalytic Fischer-Tropsch process.", *Applied Catalysis A: General*, 138, 319-344 (1996).

Dry, M. E. and Hoogendoorn, J. C., "Technology of the Fischer-Tropsch process", *Catal. Rev.-Sci. Eng.*, 23(1&2), 265-278 (1981).

Dry, M. E., "The Fischer-Tropsch – Commercial aspects", *Catal. Today*, 6, 183-206 (1990)

Dry, M. E., "*The Fischer-Tropsch Synthesis*", Catalysis: Science and Technology, Eds. Anderson and Boudart, vol. 1, Chap. 4, 159-255 (1981).

Dwyer, D.J.; and Somorjai, G. A., "The role of readsorption in determing the product distribution during CO hydrogenation over Fe single crystals" *J. Catal.*, 56, 249-257 (1979)

Everson, R. C, and Mulder, H., "Fischer-Tropsch reaction studies with supported ruthenium catalysts", *J. Catal.*, 143 ,166-174 (1993).

Feyo de Azevedo, S., Romero-Ogawa, M.A.,and Wardle, A.P., "Modelling of tubular fixed-bed catalytic reactors: A brief review", *Trans. IChemE* 68, 483-502 (1990).

Fox III, J. M., and Tam S. S., "Correlation of slurry reactor Fischer-Tropsch yield data", *Topics in Catalysis*, 2 ,285-300 (1995).

Froment, G. F., "Analysis and design of fixed bed catalytic reactors", *ACS Adv. Chem. Ser.* 109, 1-35, Washington DC (1972a).

Froment, G. F., "Fixed Bed catalytic reactors. technological and fundamental design aspects", *Chemie. Ing. Techn.* 46, 374-386 (1974).

Froment, G. F., "Progress in the fundamental design of fixed-bed reactors", *Frontieres in Chemical Reaction Engineering* 1, Eds. Doraiswamy and Mashelkar, J. Wiley and Sons, N. Y. 12-38 (1984).

Froment, G. F., "Fixed-Bed reactors. steady state conditions", *Chemical Reaction Engineering*, Proc. 5th European/2nd International Symposium on Chemical Reaction Engineering, Amsterdam, Elsevier Pub., a5.1-A5.20, (1972b).

Froment, G. F., and Bischoff, K. B., *"Chemical Reactor Analysis and Design"*, John Wiley & Sons, (1979).

Froment, G. F., and Hofmann, H. P. K., "Design of fixed-bed gas-solid catalytic reactors", *Chemical Reaction and Reactor Engineering*, 26, Eds. Carberry and Varma, 373-441, (1987).

Galarraga, C. E., and Peluso, E., *Production of waxes from conversion of synthesis gas by Fischer-Tropsch process*. Course ES 497 (Final Report), University of Western Ontario, Canada, (1996).

Galarraga, C. E., Heterogeneous catalyst for the synthesis of middle distillate hydrocarbon., Thesis (M. E. Sc.), University of Western Ontario, Canada, (1998).

Huff, A. G., and Satterfield C. N., "Evidence for two chain growth probabilities on iron catalysts in the Fischer-Tropsch synthesis." *J. Cat.*, 85, 370-379 (1984).

Iglesia, E., Reyes, S. C, Madon, R. J., and Soled, S. L., "Selectivity control and catalysts design in the Fischer-Tropsch synthesis: sites, pellets, and reactors", *Advances in Catalysis*, 39, 221-302, (1993)

Iglesia, E., Reyes, S. C., and Madon, R. J., "Transport-enhanced α-olefin readsorption pathways in Ru-catalyzed hydrocarbon synthesis", *J. Catal.*, 129, 238-256 (1991).

Iglesia, E., Soled, S. L., Baumgartner, J. E., and Reyes, S. C., "Synthesis and catalytic properties of eggshell cobalt catalysts for the Fischer-Tropsch synthesis", *Topics in Catalysis*, 2, 17-27 (1995).

Iglesia, I., Soled, S. L., and Fiato, R. A., "Fischer-Tropsch synthesis on cobalt and ruthenium. Metal dispersion and support. Effects on reaction rate and selectivity.", *J. Catal.*, 137, 212-224 (1992).

Jager, B., Espinoza, R., " Advances in low temperature Fischer-Tropsch synthesis", *Catalysis Today*, 23, 17-28 (1995).

Kirk-Othmer, Encyclopedia of Chemical Technology, Fourth edition, Volume 12, John Wiley & sons editor, (1986).

Kuipers, E. W., Scheper, C., Wilson, J. H., Vinkenburg, I. H., and Oosterbeek, H., "Non-ASF product distributions due to secondary reactions during Fischer-Tropsch synthesis", *J. Catal.*, 158, 288-300, (1996).

Kuipers, E. W., Vinkenburg, I. H., and Oosterbeek, H., "Chain length dependence of α-olefin readsorption in Fischer-Tropsch synthesis", *J. Catal*, 152, 137-146, (1995).

Lee, S. Y., and Aris, R., "The distribution of active ingredients in supported catalysts prepared by impregnation", *Catal. Rev. –Sci. Eng.*, 27, 207-340 (1985).

Lapidus, A., Krylova, A., Kasankio, V., Borovkov, V., Zaitsev, A., Rathaousky, J., Kuzal, A., and Jancalkova, M., "Hydrocarbon synthesis from carbon monoxide and hydrogen on impregnated cobalt catalysts. Part I. Physico-chemical properties of 10% cobalt/alumina and 10% cobalt/silica", *Appl. Catal.*, 73, 65-82 (1991).

Marquardt, D. W., "An algorithm for least-squares estimation of non-linear parameters", J. Soc. Ind. Appl. Math., 11(2), 431-441 (1963).

Maxwell, I. E. and Naber, J. E., "New and improved processes for clean fuels", *Catalysis Letters* ,12 ,109-116, (1992)

McCabe W. L., Smith J. C., *Unit Operation of Chemical Engineering* , Eds. McGraw-Hill Book Company, third edition, (1976)

Micromeritics, *TPD/TPR 2900 Analyzer-Operator's Manual*, 1992.

Ming, H., and Baker, B. G., "Characterization of cobalt Fischer-Tropsch catalysts. I. Unpromoted cobalt-silica gel catalysts", *Appl. Catal., A: General*, 123, 23-36 (1995).

Nelson, J. R., "Impact of coolant side on performance of plug-flow reactor containing an exothermic reaction", *Frontiers for Reaction Engineering*, Second Conference on Chemical Reaction Engineering, Engineering Foundation, Santa Barbara, CA, March 8-13 (1987).

Pannell, R. B., Kibby, C. L.;and Kobylinski, T. P., "A steady-state study of Fischer-Tropsch product distributions over cobalt, iron and ruthenium", *Proc 7th Int. Congr. Catal.*, Tokyo, 447-459 (1980)

Ponec. V., "Some aspects of the mechanism of methanation of Fischer-Tropsch synthesis", *Cat. Rev. Sci. Eng.*, 18, 151-171 (1978).

Post, M. F. M., Hoog, A. C. , Minderhoud, J. K.,and Sie S.T. , "Diffusion limitations in Fischer-Tropsch catalysts", *AIChE J.*, 35 (7) , 1107-1114 (1989).

Rase, H. F., *Fixed-Bed Reactor Design and Diagnostics. Gas-Phase Reactions*, Butterworth Pub., Stoneham, MA, (1990).

Rautavuoma, A. O. I., and van der Baan, H. S.,"Kinetics and mechanism of the Fischer-Tropsch hydrocarbon synthesis on a cobalt on alumina catalyst.", *Appl. Catal.*, 1, 247-272 (1981).

Ravella, A., "A pseudoadiabatic catalytic reactor for the conversion of methanol to hydrocarbons", *Ph.D. Dissertation*, The University of Western Ontario, Canada, (1987).

Ravella, A., and de Lasa, H. I., "Cooling exothermic catalytic fixed bed reactors: co-current versus countercurrent operation in a methanol conversion reactor", *Can. J. Chem. Eng.*, 65, 1021-1026 (1987b).

Ravella, A., and de Lasa, H. I., "The pseudoadiabatic regime for catalytic fixed-bed reactors: The limiting operating conditions ", *Chem. Eng. J.*, 34, 47-53 (1987a).

Ravella, A., de Lasa, H. I.,and Mahay, A., "Pseudoadiabatic axial thermal profiles in a catalytic fixed-bed reactor: Measurement and modeling", *Chem. Eng. J.*, 42 , 7-15 (1989).

Reid, R. C., Prausnitz, J. M., and Sherwood, T. K., *The properties of gases and liquids*, 3rd ed., McGraw-Hill, New York ,(1977).

Reuel, C. R., and Bartholomew, C. H., "The stoichiometries of H_2 and CO adsorption on cobalt: Effects on support and preparation", *J. Catal*,. 85, 63-77 (1984).

Röper, M., "Fischer-Tropsch synthesis", *Catalysis in C1 Chemistry*. W. Keim (ed)., Reidek Publishing Co, 41-88. (1983)

Sarup, B., and Wojciechowski, B. W., "Studies of the Fischer-Tropsch synthesis on a cobalt catalyst II. Kinetics of carbon monoxide conversion to methane and to higher hydrocarbons", *Can. J. Chem. Eng.*, 67, 62-74 (1989).

Satterfield, C. N., and Stenger, H. G., "Fischer-Tropsch synthesis on a precipitated Mn/Fe catalyst in a well-mixed slurry reactor", *Ind. Eng. Chem. Proc. Des. Dev.*, 23, 26-29, (1984).

Schulz, H., van Steen, E., and Claeys, M., " Specific inhibition as the kinetics principle of the Fischer-Tropsch synthesis", *Topics in Catalysis*, 2, 223-234 (1995).

Senden, M. M. G., Sie, S. T., Post, M. E. M., and Ansorge, J., "Engineering aspects of the conversion of natural gas into middle distillates", *Chemical Reactor Technology for Environmentally Safe Reactors and Products*, H.I. de Lasa. (eds.), 227-247 (1992).

Sie, S. T., Senden, M.M.G., and Van Wechem, H.M.H., " Conversion of natural gas to tranportation fuels via the Shell Middle Distillate Synthesis Process (SMDS)", *Catalysis Today*, 8 , 371-394 (1991).

Simard, F., "A pseudoadiabatic catalytic reactor for the direct conversion of synthesis gas into hydrocarbons", *Ph.D. Dissertation*, The University of Western Ontario, Canada, (1991).

Simard, F., Mahay, A., Ravella, A., Jean, G., and de Lasa, H. I., "Pseudoadiabatic catalytic reactor for the conversion of synthesis gas into hydrocarbons (Gasoline range)", *Ind. Eng. Chem. Res.*, 30, 1448-1455 (1991).

Singleton, A. H, and Regier, S., "Produce diesel from gas", *Hydrocarbon Processing*, May, 71-74. (1983)

Siri, G. J., Guerrero-Ruiz, A., Rodriquez-Ramos, I., Terreros, P,. and Fierro, J. L. G., "Hydrocarbons from synthesis gas: Selectivity changes induced by the zeolite matrix on the metallic function in Rh/Y catalysts", *Applied Catalysis A: General* , 107, 59-71 (1993).

Snel, R., "Olefins from Syngas." *Catal. Rev.-Sci. Eng.*, 29(4), 361-445 (1987).

Soled, S. L., Iglesia, E., Miseo, S., DeRites, B., and Fiato, R. A., "Selective synthesis of α-olefins on Fe-Zn Ficher-Tropsch catalysts", *Topics in Catalysis*,2, 193-205 (1995).

Soria Lopez, A. , de Lasa, H. I., and Porras, J. A. ,"Parametric sensitivity of a fixed-bed catalytic reactor. cooling fluid flow influence", *Chem. Eng. Sci.* 36, 285-291 (1981).

Stankiewicz, A., "Advances in modelling and design of multitubular fixed-bed reactors", *Chem. Eng. Technol.*, 12, 113-130 (1989).

Stenger, H. G.,and Askonas C. F., "Thermodynamic product distributins for the Fischer-Tropsch synthesis", *Ind. Eng. Chem. Fundam.*, 25, 410-413, (1986).

Storch, H. H., Golumbic,. N., and Anderson, R. B. *The Fischer-Tropsch and Related Synthesis*, Weley: New York, 1951.

Tarhan, M. O., *Catalytic Reactor Design*, Ed. McGraw-Hill, New York (1983).

van Barneveld, W. A. A.; Ponec, V., "Influence of alloying on the selectivity in Fischer-Tropsch synthesis by nickel-copper alloys", *J. Catal.*, 51, 426-430 (1978).

van Burgt, M. J., van Leeuwen, C. J., del'Amico, J. J. and Sie S. T.,"The Shell Middle Distillate Synthesis Process", *Methane Conversion*, D.M. Bibby, Chang, R. F., Howe R. F. and Yurchak S. (editors), Elsevier Science Publishers B. V., Amsterdam (1988).

Vannice, M. A., "The catalytic synthesis of hydrocarbons from H_2/CO mixtures over the group VIII metals", *J. Catal*, 37, 449-462 (1975).

Wang, J., "Physical, chemical and catalytic properties of borided cobalt Fischer-Tropsch catalysts", *Ph.D. Dissertation*, Brigham Young University, Provo, UT, 1987.

Wender, I., "Reactions of synthesis gas", *Fuel Processing Technology*, 48, 189-297 (1996).

Wojciechowski, B. W., "The kinetics of the Fischer-Tropsch synthesis", *Catal. Rev.-Sci. Eng*, 30 (4), 629-707 (1988).

Yang, C. H., Massoth, F. E., Oblad, A. G., "Kinetics of CO + H_2 reaction over Co-Cu-Al_2O_3 catalyst", *Adv. Chem. Ser.*, 178, 35-46 (1979).

Yates, I. C., and Satterfield, C. N., "Intrinsic kinetics of the Fischer-Tropsch synthesis on a cobalt catalyst", *Energy & Fuels*, 5, 168-173 (1991)

Zagli, A. E., Falconer, J. L., Keenan, C. A., "Methanation on supported nickel catalysts using temperature programmed heating", *J. Catal.*, 56, 453-467 (1979).

Zowtiak, J., and Bartholomew, C. H., "The kinetics of H_2 adsorption on and desorption from cobalt and the effects of support thereon", *J. Catal.*, 83, 107-120 (1983).

APPENDICES

APPENDIX A. Equipment calibration

A.1. Mass Flow Controller Calibration

This appendix describes the calibration of the mass flow controller. This calibration was performed at room temperature and at the pressure selected for the experimental test. It is important to mention that no effect of pressure in the reactor was expected over the mass flow since a ΔP from 5 to 50 psig was kept between the inlet and the outlet of the mass flow controller.

The procedure used for the calibration of the mass flow controller was as follows:

- After the catalyst was loaded into the reactor, and the reactor was sealed a test for leaks was carried out. The calibration was performed for different mass flow controller positions, which represent various opening of the valve.
- A valve position was selected in the controller display. After 30 minutes the first flow reading was taken.
- A bubble flowmeter installed in the outlet of the experimental set-up was used in order to estimate the gas flow leaving the reactor.
- Every 15 minute a new lecture was taken until the difference between the successive values was no more than 10 %. After that a new valve position was selected and the procedure was repeated again.

Table A.1 summarizes the results for the calibration of the mass flow controller at the different valve positions evaluated. It can be appreciated that all the reading are very close to the average value for each valve position. A small Standard deviations were found to be smaller than 1.1 with an error 1.0%. The

average values from Table A.1 are plotted in Fig. A.1 with all the average value falling into the 95% confidence interval.

Table A.1. Example of calibration reading for the mass flow controller at various positions of the valve

Valve position	Reading # 1	Reading # 2	Reading # 3	Reading # 4	Average	STD	Error
0.0	0.0	0.0	0.0	0.0	0.0	0.0	0.0
1.0	28.5	28.2	27.7	28.0	28.10	0.29	1.04
1.1	31.7	32.2	31.8	32.1	31.95	0.21	0.65
1.5	43.1	42.7	42.4	42.2	42.60	0.34	0.8
2.0	60.1	58.7	59.2	59.3	9.33	0.50	0.85
3.1	85.0	88.0	87.0	87.0	86.75	1.09	1.26

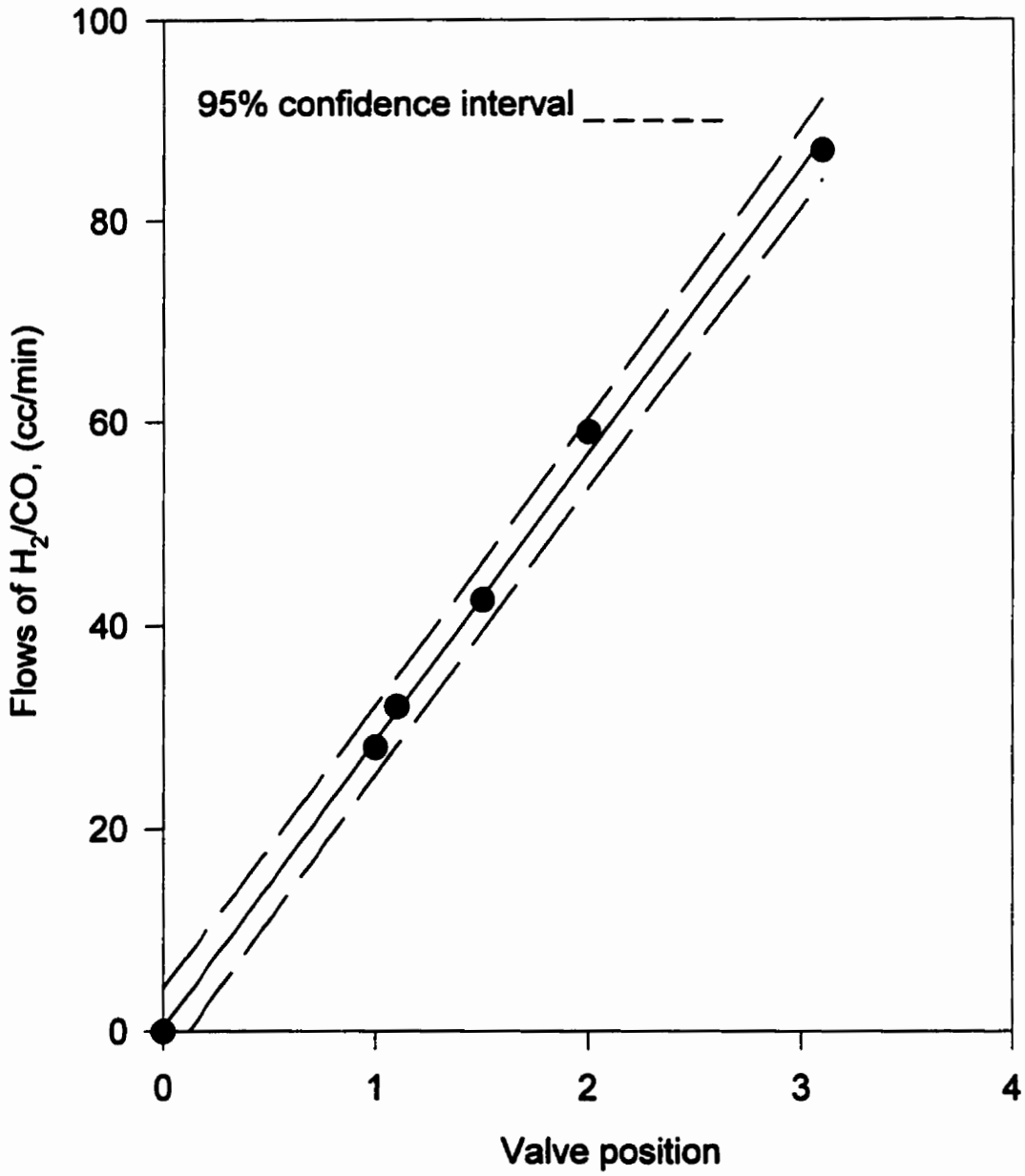

Figure A.1. Calibration curve for the mass controller valve.

A-2. Calibration of the wet test meter

Simultaneously to the calibration of the mass flow controller the wet test meter, located in the experimental setup previously described in Chapter 4, was also calibrated. The gas stream leaving the experimental set-up goes through the wet test meter before it is sent to the bubble flowmeter. The procedure used for the calibration of the wet test meter is as follows:

a) Once the valve position for the flow meter controller was selected in the controller display, 10 minutes were allowed in order the flow to stabilize inside the system.

b) After 10 minutes, the wet test meter indicators were set in zero and 20 minutes later (30 minutes on stream), the first wet test meter reading (volume accumulated in 20 minutes) was taken. This was done at the same time a reading in the bubble flowmeter was effected.

c) After 15 minutes two new reading were performed: a) in the wet test meter (volume accumulate in 35 minutes), and b) in the bubble flowmeter.

d) This procedure is repeated two more times with an interval of 15 minutes.

The results of this calibration are reported in Table A-2. It can be observed that values obtained for the flow reported from the readings in the bubble flow meter were very close to that those obtained with the wet test meter "single point reading". These values, wet test meter "single point reading", were calculated using equation A.1.

$$WET_{(punctual)} = \frac{V_{accumulated}}{HOS} \qquad \text{(A-1)}$$

where $WET_{(punctual)}$ is the wet test meter "single point reading", $V_{accumulated}$ is the volume accumulated in the wet test meter during the time of the experiment, and HOS is the time elapsed from the moment of the wet test meter was set in zero unil the end of the experiment.

Average reported values in Table A-2 were estimated between the values obtained for the bubble flowmeter and the wet test meter "single point reading"). Values are very close to 28.1 cc/min with a standard deviation between 0.1 to 0.3 cc/min, which is very aceptable value for this type of calibration. Thus, the error associated with the measurement of the flow is smaller than 1.5 %,

Table A.2 Calibration of the wet test meter

HOS (min.)	Lecture, Bubble flow meter (cc/min)	Wet test meter, $V_{accumulated}$ (cc)	Wet test meter, Single point reading (cc/min)	Average	STD	Error (%)
20	28.5	556	27.8	28.15	0.35	1.24
35	28.2	987	28.2	28.2	-	-
50	27.7	1415	28.3	28.0	0.3	1.07
65	28.0	1833	28.2	28.1	0.1	0.36

APPENDIX B. Calibration of TCD for CG

This appendix include 4 sections as follows:

- Appendix B.1: Certificate of analysis for H_2/CO mixture.
- Appendix B.2: Calibration of TCD for different H2/CO ratios (raw data).
- Appendix B.3: Certificate of analysis for hydrocarbon gas mixture
- Appendix B.4 :Calibration of TCD for hydrocarbon gas mixture (raw data).

B.1. Certificate of analysis for H_2/CO mixture

Certificate of Analysis

To: BOC Gases London **Date:** October 6. 1997

For: **PO#:**

Material Submitted: 33% Carbon Monoxide Balance Hydrogen **Specification:** BOC Standard

Analytical Method: Gas Chromatograph

Batch Number	Cylinder #	CO	H2
971565	142214	33.5 %	Balance

B.2. Calibration of TCD for different H_2/CO ratios (raw data).

As mentioned before, section 4.4.1, a TCD calibration for the GC was carried out. This calibration was performed for different H_2/CO ratios. Results are reported in Table B1. This table also lists the average concentration value, the Standard deviation, and the percentage error.

Table B.1. Calibration of the TCD for different H_2/CO ratio (raw data)

Component	Injection 1	Injection 2	Injection 3	Average comp. (vol/vol)	STD	Error in Injection (%)
H_2/CO ratio	**1**					
H_2	50.8	51.9	49.6	50.75	0.96	1.89
CO	49.2	48.1	50.5	49.25	0.96	1.94
H_2/CO ratio	**2**					
H_2	66.81	65.78	67.07	66.55	0.56	0.84
CO	33.19	34.22	32.93	33.45	0.56	1.67
H_2/CO ratio	**3**					
H_2	76.45	74.6	75.1	75.38	0.78	1.04
CO	23.55	25.4	24.9	24.62	0.78	3.17

B.3. Certificate of analysis for hydrocarbon gas mixture

Certificate of Analysis

To: BOC Gases .London **Date:** 16 July, 1996

For: University of Western Ontario **PO#:**

Material Submitted: Hydrocarbon Mixture **Specification:** BOC Standard

Analytical Method: Gas chromatography

Cylinder #	Component	Requested	Analytical
960744 286017	n-Hexane	0.1%	0.106%
	n-Pentane	0.2%	0.2.04%
	n-Butane	0.5%	0.499%
	Propane	0.5%	0.501%
	Ethylene	0.3%	0.782%
	Ethane	0.5%	0.292%
	Methane	5.0%	3.00%
	Carbon Dioxide	3.0%	4.99%
	Nitrogen	2.9%	2.89%
	Carbon Monoxide	28%	28.0%
	Hydrogen	Balance	Balance

B.4 Calibration of TCD for hydrocarbon gas mixture (raw data).

This calibration was performed for the gaseous product and the results are reported in Table B.2. This table also lists the average concentration value, the Standard deviation, and the percentage error. Figure B.1 shows a typical chromatogram for gaseous product.

Table B.2. Calibration of the TCD for gaseous product (raw data).

Component	Injection 1	Injection 2	Injection 3	Average comp. (vol/vol)	STD	Error in Injection (%)
n-Hexane	0.111	0.11	0.111	0.111	0.001	0.52
n-Pentane	0.215	0.207	0.211	0.211	0.004	1.90
n-Butane	0.517	0.5	0.509	0.509	0.01	1.67
Propane	0.50	0.498	0.504	0.505	0.006	1.16
Ethylene	0.796	0.805	0.8	0.8	0.005	0.56
Ethane	0.289	0.292	0.29	0.29	0.002	0.6
Methane	2.98	3.04	3.01	3.01	0.031	1.10
Carbon dioxide	5.1	5.05	5.06	5.04	0.06	1.2
Nitrogen	2.87	2.89	2.87	2.857	0.042	1.46
Carbon monoxide	28.01	27.8	27.91	27.91	0.106	0.38
Hydrogen	58.17	58.15	58.18	58.13	0.019	0.03

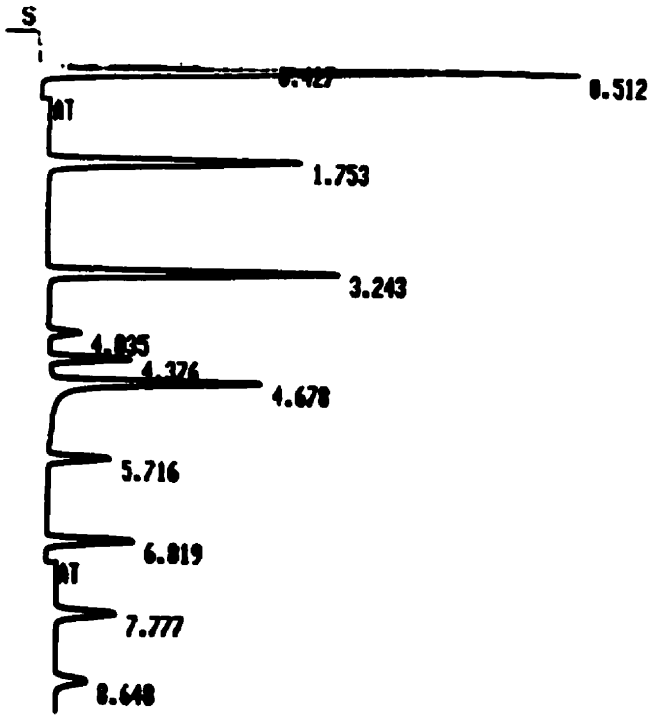

STOP

RUN# 10 AUG 28, 1996 10:50:52

ESTD

RT	CAL#	AMOUNT	NAME
.283	1R	58.133	H2
.427	2	2.859	N2
.512	3	27.910	C0
1.753	4R	3.887	CH4
3.243	5	5.040	C02
4.635	6	.000	ETHYLEN
4.376	7	.298	C2
4.678		.000	
5.716	8	.505	C3
6.819	9	.509	C4
7.777	10	.211	C5
8.648	11	.111	C6

TOTAL AREA= 518506
MUL FACTOR=1.0000E+00

Figure B.1. A typical chromatogram for gaseous product.

APPENDIX C: Identification of the components in the liquid hydrocarbon fraction.

The boiling point calibration Sample #1 from Hewlett Packard, was used for the identification of the hydrocarbon components contained in the liquid hydrocarbon product. Table C.1 shows in detail the composition of this calibration sample. Moreover a typical chromatogram of the expected synthesized hydrocarbons is presented in Fig C.1

Table C.1. Boiling point calibration sample #1

Table C.1 Boiling point calibration sample #1

Catalog Number: 5080-8716 **Lot Number:** K1253
Page: 1

This analytical standard was gravimetrically prepared, and the analyte concentrations were verified using high resolution gas chromatography and/or high performance liquid chromatography. The solution was prepared at the nominal concentration stated on the box label. The true value for each analyte, determined gravimetrically, is listed below.

Component	% by Weight
n-pentane	8.32
n-hexane	4.38
n-heptane	4.55
n-octane	4.67
n-nonane	4.77
n-decane	9.71
n-undecane	4.92
n-dodecane	19.91
n-tetradecane	10.14
n-pentadecane	5.11
n-hexadecane	10.28
n-heptadecane	5.17
n-octadecane	2.21
n-eicosane	1.30
n-tetracosane	0.90
n-octacosane	0.90
n-hexatriacontane	0.91
n-tetracontane	0.92
n-dotriacontane	0.90

Solvent: none

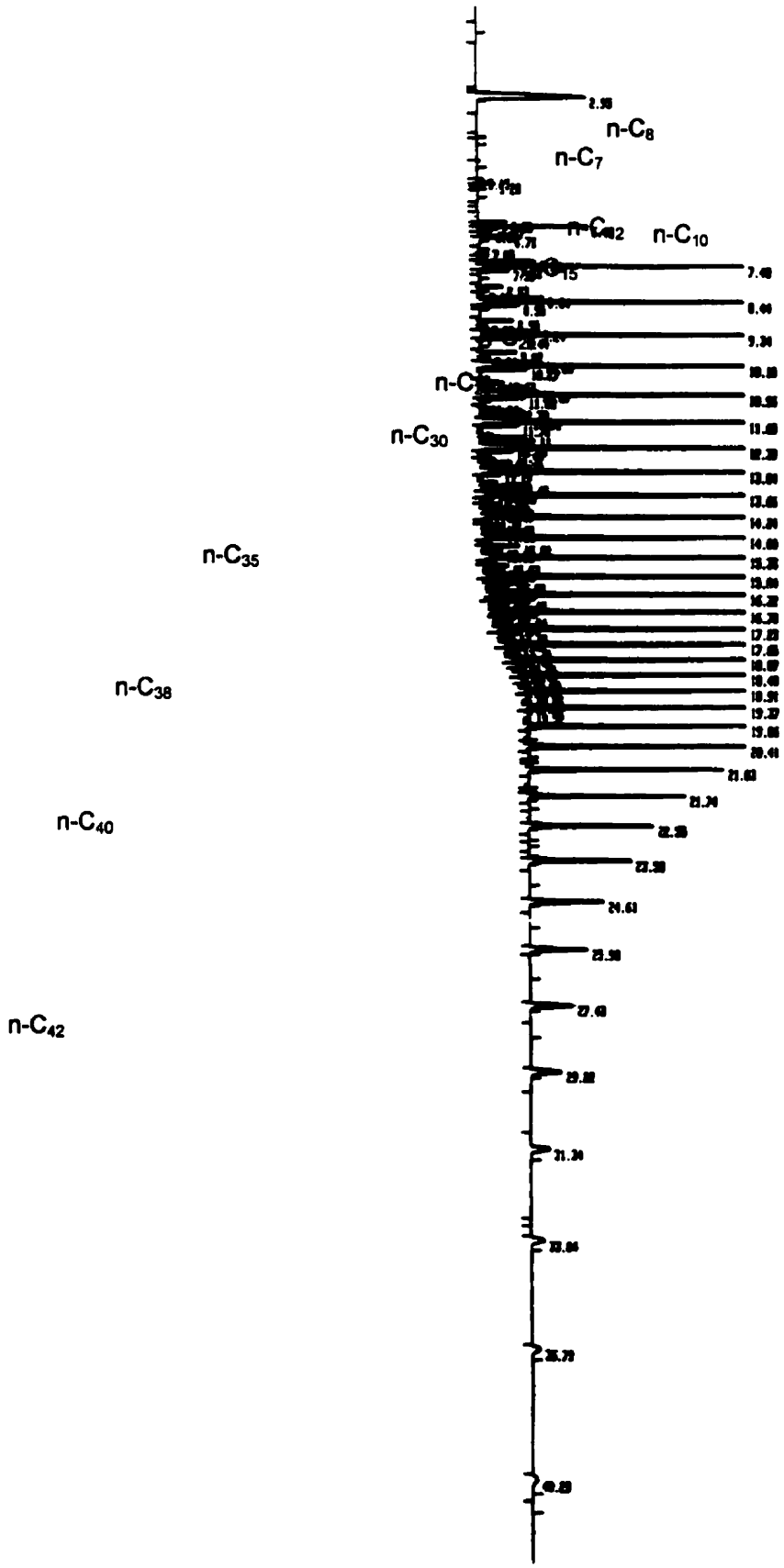

Figure C.1. Typical chromatogram for liquid hydrocarbon product.

APPENDIX D: BET Analysis.

D.1. Calibration of the thermal conductivity detector (TCD)

As mentioned before, in Chapter 5, a calibration of the thermal conductivity detector (TCD) of the TPD/TPR 2900 is required in order to perform the specific surface area measurements.

This calibration was carried out by injecting known volumes of pure nitrogen directly into the detector using a precision syringe. The change of the TCD signal, by effect of the nitrogen injected, is sent to a computer and integrated to give an area proportional to the volume injected.

In order to prepare a calibration curve different volumes of nitrogen were injected. Each volume was injected three times to insure reproducibility. Table D.1 summarizes the data collected during a typical calibration. This table includes the amount of nitrogen injected with the precision syringe (ml), the area detected by the analyzer for the three repeats. The table also lists the average of the detector response, the standard deviation for each injection, as well as the percental error.

The data from Table D.1. was used to prepare the calibration curve as presented in Fig. D.1. This figure shows a plot of the different areas detected as a function of the volume of nitrogen injected. Dots in this figure represents the average of repeats. Average data was fitted with a second order polynomial with a correlation index, R^2, higher than 0.99.

Table D.1. Data obtained during a typical calibration for BET analysis.

Volume	Area detected by the analyzer (AU)					
Injected (ml)	Response 1	Response 2	Response 3	Average area	STD	Error in injection
1	3.447e+6	3.426e+6	3.294E+6	3.39E+06	8.29E+04	2.45
2	7.009e+6	7.061E+6	7.032E+6	7.03E+06	2.61E+04	0.37
3	1.119E+7	1.126E+7	1.120E+7	1.12E+07	3.79E+04	0.34
4	1.557E+7	1.558E+7	1.557E+7	1.56E+07	5.77E+03	0.04
5	2.056E+7	2.034E+7	2.048E+7	2.05E+07	1.11E+05	0.54
6	2.521E+7	2.535E+7	2.534E+7	2.53E+07	7.81E+04	0.31
8	3.465E+7	3.475E+7	3.472E+7	3.47E+07	5.13E+04	0.15
9	3.978E+7	3.974E+7	3.974E+7	3.98E+07	2.31E+04	0.06
10	4.518E+7	4.529E+7	4.616E+7	4.55E+07	5.37E+05	1.18

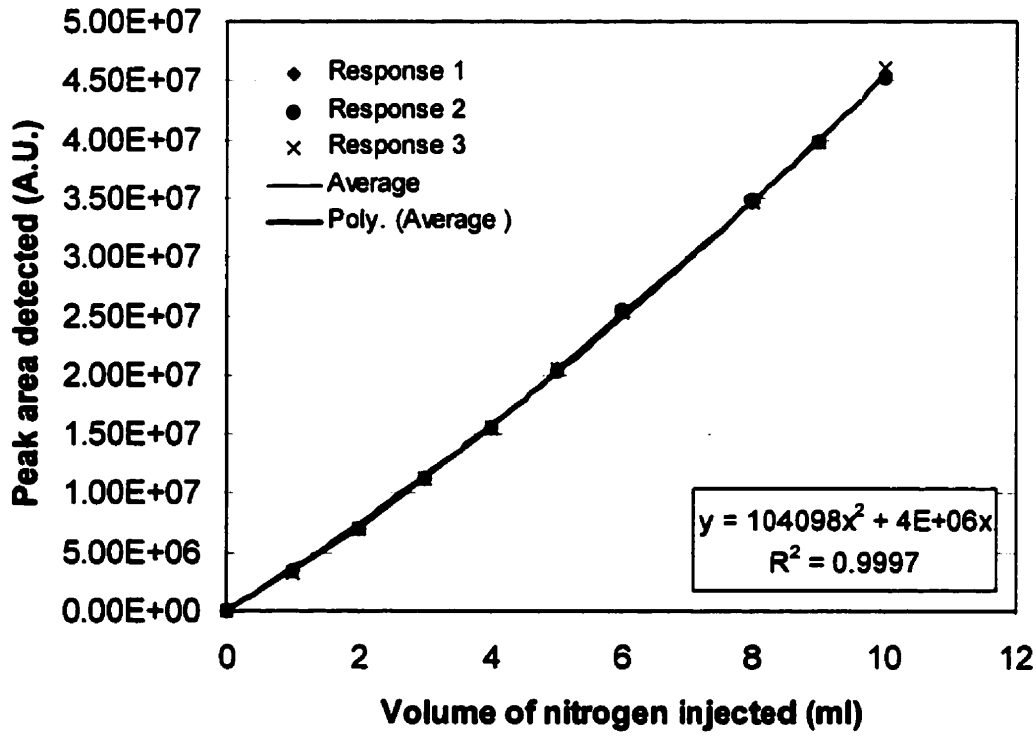

Figure D.1. Calibration curve for BET analysis

D.2. Measurement

The complete methodology to determine the surface area of a solid sample consisted of the following steps (Micromeritics, 1992):

a) Sample tube is weighed before analysis (w_1),

b) Sample (amount is between 50 to 80 mg) is placed into the sample tube and weighed to know the exact amount of sample (w_2),

c) Sample tube is located in the equipment sample port,

d) The sample surface is cleaned by degassing at 150 °C during 30 min under inert atmosphere (He),

e) A dewar containing liquid nitrogen is placed around the sample, then the gas mixture (containing 30 % of nitrogen) is flowed over the sample to adsorb nitrogen at liquid nitrogen temperatures,

f) After equilibration, the baseline of the recorder must return to zero, the dewar is withdrawn and instead of it a beaker containing tap water is now placed around the sample in order to facilitate the nitrogen desorption as the sample reaches room temperature,

g) Following this, three pulses of nitrogen are injected directly to the detector (through the injection port) in order to verify the calibration curve,

h) Sample tube is withdrawn and weighed to determine the weight of the sample after the analysis.

D.3. Surface Area Calculation.

Typical information< as obtained from the BET analysis, is included in Figure D.2.

Peak#	RTime	Area	Height	RTemp	Identifier	Total Qty
1	00:02:22	3.357E+05	9.753E+03	-22		
2	00:03:00	4.100E+07	8.257E+05	-22		
3	00:09:11	5.884E+07	2.585E+06	18		
4	00:14:03	2.171E+07	2.471E+06	23		
5	00:18:34	2.162E+07	2.443E+06	23		
6	00:22:20	2.137E+07	2.403E+06	24		

Data File: @SA-UOP
Remarks: BET analysis of SAB-2 sample (UOP)

Method: CG-BET
Detector Type: TCD

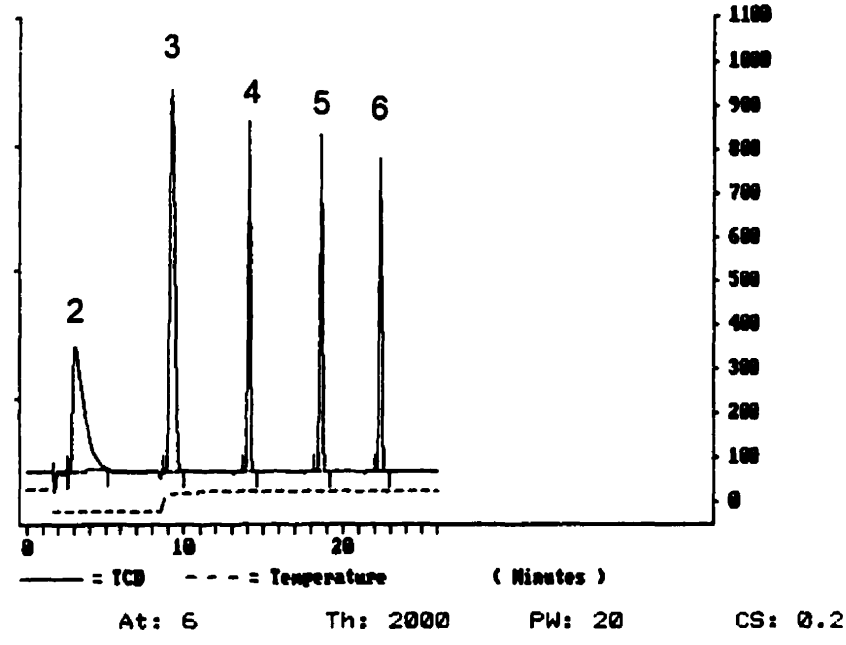

At: 6 Th: 2000 PW: 20 CS: 0.2

Figure D.2. Print-out from a BET analysis on a support sample

Figure D.2 shows 5 peaks and their corresponding areas as reported in the print-out. Peak number 2 and number 3 correspond to the adsorption and desorption process, respectively. Meanwhile peaks, 4,5 and 6 were known

amounts of nitrogen injected directly to the detector in order to check the detector response.

The BET method specifies that the volume required to calculate the surface area is that of the desorption peak. Thus, the unknown volume of nitrogen, V_{N2}, was calculated using the calibration curve. The next step involved the calculation of the volume of nitrogen at Standard Temperature and Pressure conditions, V_{STP} using equation D.1.

$$V_{STP} = V_{N2}\frac{273K}{273.2 + T_{room}} x \frac{P_{ATM}}{760} \qquad (D.1)$$

where T_{room} = 22 °C and P_{ATM} = 766 mmHg. After that, the volume of the nitrogen monolayer was calculated employing equation D.2

$$V_m = V_{STP}\left[1 - \frac{P_N}{P_{NO}}\right] \qquad (D.2)$$

where P_N is the partial pressure of nitrogen and P_{NO} is the saturation pressure of nitrogen, with P_{NO} being equal to P_{ATM} + 15 mmHg.

Finally, the volume of the nitrogen monolayer was related with the surface area using equation D.3

$$S_A = \frac{V_m\left(cm^3\right) * 6.023x10^{23}\left(\frac{molecule}{mol}\right) * 16.21x10^{-20}\left(\frac{m^2}{molecule}\right)}{22414\left(\frac{cm^3}{mole}\right) x W_{cat}(g)} \qquad (D.3)$$

Table D.2 presents the data obtained from the BET analyses performed on samples of the present study, namely: the silica support, standard catalyst

and eggshell catalyst. The table also includes data obtained for BET analyses carried out on a reference sample. The reference sample was an alumina support supplied by UOP with a surface area of 180 m^2/g.

Table D.2. Data obtained from the BET analyses.

				Reference	
Sample	**Support**	**Standard**	**Eggshell**	**Test 1**	**Test 2**
Tube weight	14.2532	13.5584	14.3621	15.9440	13.3154
+ sample before analysis	14.2982	13.6023	14.3925	16.1460	13.4855
+ sample after analysis	14.2918	13.5987	14.3912	16.1407	13.4800
Sample weight (g)	0.0386	0.0403	0.0291	0.1967	0.1646
Analysis conditions					
Temperature (°C)	25	22	22	23	22
Pressure (mmHg)	764	766	764	762	760
Gas composition (N_2)	0.3	0.3	0.3	0.3	0.3
Partial pressure of nitrogen (P_{N2})	229.2	229.8	229.2	228.6	228.0
Saturation pressure (P_{NO})	779	781	779	777	775
P_{N2}/P_{NO}	0.2942	0.2942	0.2942	0.2942	0.2942
Desorption data					
Desorption peak area	2.08e+7	1.72E+7	1.48E+7	5.02E+7	4.45E+7
Desorption volume (ml)	5.0648	4.1995	3.6142	12.2331	10.8441
Vx STP (ml)	4.6680	3.8705	3.3311	11.2774	9.9945
Vmonolayer (ml)	3.2948	2.7319	2.3511	7.9579	7.0543
Surface (m^2)	14.35	11.8997	10.2412	34.6638	30.7279
BET surface area (m^2/g)	372	295	352	176	187

APPENDIX E: Summary of Operating Conditions, Conversions, Selectivity and Hydrocarbon distribution

This appendix include 4 tables as follow:

Table E.1 : Summary for Exp. 13 (Standard catalyst)

Table E.2 Summary for Exp. 14 (Standard catalyst)

Table E.3 Summary for Exp. 15 (Eggshell Catalyst)

Table E.4 Summary for Exp. 17 (Eggshell Catalyst)

The % of CO conversion was calculated as:

$$\frac{CO_{in} - CO_{out}}{CO_{in}} * 100\% \qquad (E.1)$$

as well, the H_2 conversion was estimated with the same procedure.

The product selectivity was determined using Equation E.2

$$Selectivity\ of\ product\ X_i = (mass\ product\ X_i / \Sigma X_i) x 100\% \qquad (E.2)$$

Mass balance data based on oxygen balance, of 100 ± 3% was accepted as adequate.

Finally all product selectivity were reported as a function of % mass by mass of the total product spectrum.

Table E.1. Summary of Operating Conditions, Conversions, Selectivity and Hydrocarbon Distribution.

Run #	13-1	13-2	13-3	13-4	13-5	13-6
Operating conditions						
Temperature, °C	230	230	230	230	230	230
Pressure, MPa	1.52	1.52	1.52	1.52	1.52	1.52
GHSV,h^{-1}	348	348	348	348	348	348
Ratio H_2/CO, mol/mol	2	2	2	2	2	2
Operation time, h.	20.0	25.2	25.1	21.0	23.0	23.3
Operation on stream, h.	20	45.2	70.3	91.3	114.3	137.6
Experimental Results						
% CO conversion	99.14	93.88	70.69	69.71	68.96	70.44
% H_2 conversion	57.41	65.29	74.80	74.79	72.92	72.41
R_{CO},(mmol CO conv./min/gCo)	0.01641	0.01690	0.01377	0.01248	0.01245	0.01268
Mass (H_2+CO) in, g	30.38	38.28	38.28	31.90	34.95	35.39
Mass (gases) out, g	2.99	8.19	13.76	12.04	15.23	13.38
Mass (H_2O_{liquid}) out, g	2.72	17.51	11.20	12.59	13.10	12.94
Mass (HC_{liquid}) out, g	0.40	4.42	7.80	5.72	6.49	6.78
Overall mass balance %	20.1	78.7	85.6	95.1	99.6	93.5
Oxygen mass balance %	18.94	89.23	86.8	101.7	101.6	98.33
Products Distribution						
CO_2 selectivity, %w/w	1.88	6.11	9.43	8.33	9.03	8.47
H_2O selectivity, %w/w	57.83	53.48	48.12	48.93	48.46	49.12
HC selectivity, %w/w	40.28	40.41	42.44	42.74	42.51	42.41
Hydrocarbon Distribution						
Fraccion C_1				6.75	6.04	6.11
Fraccion C_2 - C_4				8.32	9.75	9.9
Fraccion C_5 - C_9				31.23	29.34	28.59
Fraccion C_{10} - C_{20}				41.12	43.13	42.67
Fraccion C_{21}^+				12.58	11.74	12.73

Table E.2. Summary of Operating Conditions, Conversions, Selectivity and Hydrocarbon Distribution.

Run #	14-1	14-2	14-3	14-4	14-5	14-6
Operating conditions						
Temperature, °C	220	220	220	220	220	220
Pressure, MPa	1.52	1.52	1.52	1.52	1.52	1.52
GHSV,h^{-1}	342	342	342	342	342	342
Ratio H_2/CO, mol/mol	2	2	2	2	2	2
Operation time, h.	23.0	23.0	25.3	24.0	23.8	23.8
Operation on stream, h.	23	46	71.3	95.3	119.3	143.1
Experimental Results						
% CO conversion	85.00	71.28	63.73	51.75	51.20	50.62
% H_2 conversion	81.23	62.43	61.43	58.60	50.60	49.09
R_{CO},(mmol CO conv./min/gCo)		0.01175	0.01056	0.00957	0.00832	0.00813
Mass (H_2+CO) *in*, *g*	34.94	34.94	38.36	36.46	36.46	36.08
Mass (gases) out, g	8.56	11.96	15.69	16.90	17.89	19.56
Mass (H_2O_{liquid}) out, g	3.45	10.10	10.45	10.69	10.70	10.48
Mass (HC_{liquid}) out, g	1.75	2.30	6.23	6.93	6.35	6.02
Overall mass balance %	39.4	69.7	84.4	94.7	98.1	99.9
Oxygen mass balance %	41.23	82.56	86.7	95.6	98.5	100.0
Products Distribution						
CO_2 selectivity, %w/w	3.15	2.03	1.97	1.63	2.62	2.58
H_2O selectivity, %w/w	55,62	55.48	54.89	54.82	54.67	54.35
HC selectivity, %w/w	41.23	42.49	43.14	43.56	42.71	43.07
Hydrocarbon Distribution						
Fraccion C_1			6.24	5.49	5.35	5.04
Fraccion C_2 - C_4			4.53	3.98	3.75	3.82
Fraccion C_5 - C_9			12.67	12.3	12.27	12.45
Fraccion C_{10} - C_{20}			48.24	45.47	45.9	45.59
Fraccion C_{21}^+			28.31	32.76	32.73	33.11

Table E.3. Summary of Operating Conditions, Conversions, Selectivity and Hydrocarbon Distribution.

Run #	15-1	15-2	15-3	15-4	15-5	15-6
Operating conditions						
Temperature, °C	220	220	220	220	220	220
Pressure, MPa	1.52	1.52	1.52	1.52	1.52	1.52
GHSV,h^{-1}	342	342	342	342	342	342
Ratio H_2/CO, mol/mol	2	2	2	2	2	2
Operation time, h.	25.0	23.5	24.0	23.0	24.0	20.3
Operation on stream, h.	25	48.5	72.5	95.5	119.5	139.8
Experimental Results						
% CO conversion	67.52	45.07	24.35	27.45	25.30	25.74
% H_2 conversion	54.16	44.00	23.45	30.93	24.90	25.93
R_{CO},(mmol CO conv./min/gCo)		0.02310	0.01423	0.01459	0.01427	0.01435
Mass (H_2+CO) in, g	37.31	35.08	35.82	34.33	35.82	30.23
Mass (gases) out, g	12.30	17.21	26.43	25.81	25.70	22.05
Mass (H_2O_{liquid}) out, g	3.75	8.74	5.91	6.32	6.03	5.41
Mass (HC_{liquid}) out, g	1.23	4.42	2.35	2.82	2.72	2.03
Overall mass balance %	46.3	86.6	96.8	101.8	97.9	97.5
Oxygen mass balance %	54.30	87.94	95.6	99.1	98.5	98.6
Products Distribution						
CO_2 selectivity, %w/w	1.33	1.13	1.19	0.97	0.45	0.50
H_2O selectivity, %w/w	61.04	5.49	54.92	55.58	55.4	56.9
HC selectivity, %w/w	37.63	43.38	43.89	43.46	44.15	42.6
Hydrocarbon Distribution						
Fraccion C_1			4.91	4.28	4.29	4.32
Fraccion C_2 - C_4			6.89	9.95	8.75	8.98
Fraccion C_5 - C_9			14.35	23.65	23.10	22.28
Fraccion C_{10} - C_{20}			65.77	56.12	58.45	59.45
Fraccion C_{21}^+			8.08	6.00	5.41	4.97

Table E.4. Summary of Operating Conditions, Conversions, Selectivity and Hydrocarbon Distribution .... cont'd....

Run #	17-1	17-2	17-3	17-4	17-5	17-6	17-7	17-8	17-9	17-10	17-11	17-12	17-13	17-14	17-15
Operating conditions															
Temperature, °C	220	209	209	209	215	215	215	220	220	220	226	226	226	209	209
Pressure, MPa	1.52	1.52	1.52	1.52	1.52	1.52	1.52	1.52	1.52	1.52	1.52	1.52	1.52	1.1	1.1
GHSV,h^{-1}	390	348	348	348	348	348	348	348	348	348	348	348	348	390	390
Ratio H_2/CO, mol/mol	2	2	2	2	2	2	2	2	2	2	2	2	2	2	2
Operation time, h.	24	23.5	23.5	24.5	24.5	23.0	23.5	23	24	24.0	25.5	25.5	23.5	24	24.0
Operation on stream, h.	144	167.5	191	215.5	240	263	286.5	309.5	333.5	357.5	383	408.5	432	456	480
Experimental Results															
% CO conversion	18.58	12.10	10.89	10.16	18.20	15.60	16.3	18.87	19.29	20.51	23.60	22.52	23.42	7.87	5.52
% H_2 conversion	19.64	11.69	9.39	9.68	15.68	17.30	15.5	20.93	21.27	21.27	24.85	22.30	24.13	7.95	6.72
Mass (H_2+CO) in, g	40.17	35.10	35.10	36.60	36.60	34.35	35.1	34.35	35.85	35.85	38.09	38.08	35.1	40.17	40.17
Mass (gases) out, g	33.10	30.58	30.98	31.80	29.96	29.10	29.9	27.10	28.03	28.31	28.87	28.30	26.85	36.60	37.40
Mass (H_2O_{liquid}) out, g	3.78	2.55	2.12	2.21	3.63	3.34	3.48	4.34	4.57	4.56	5.65	5.82	5.01	1.75	1.71
Mass (HC_{liquid}) out, g	2.56	1.62	1.45	1.57	2.01	1.78	1.94	2.04	2.57	2.32	3.32	3.10	2.62	1.23	1.30
Overall mass balance %	98.18	99.00	98.43	97.21	97.27	99.62	100.63	97.47	98.10	98.16	99.34	97.74	98.234	98.53	100.60
Oxygen mass balance %	99.10	98.13	101.1	98.75	98.65	99.35	99.35	98.13	98.8	99.16	99.40	97.86	99.01	98.8	99.34
Products Distribution															
CO_2 selectivity, %w/w	2.81	0.00	0.00	0.00	0.95	1.05	1.04	1.26	1.33	1.17	1.41	1.49	1.6	0.00	0.00
H_2O selectivity, %w/w	53.55	57.2	56.46	56.83	54.89	54.95	54.95	54.73	54.62	54.93	54.58	54.31	54.79	56.12	56.17
HC selectivity, %w/w	43.63	42.8	43.54	43.17	44.16	44.01	44.01	4.02	44.05	43.89	44.01	44.19	43.61	43.88	43.83
Hydrocarbon Distribution															
Fraccion C_1	4.54		4.59	4.66		3.78	3.64		3.1	3.11		3.06	3.08		4.94
Fraccion C_2 - C_4	13.32		11.02	10.34		6.79	7.73		8.04	7.81		7.76	7.69		12.56
Fraccion C_5 - C_9	31.05		24.67	25.62		21.98	21.82		23.56	24.35		21.54	22.89		28.64
Fraccion C_{10} - C20	42.45		57.04	56.18		57.56	57.06		55.47	54.91		48.01	47.52		50.12
Fraccion C_{21}^+	8.64		2.68	3.2		9.89	9.75		9.83	9.82		19.63	18.82		3.74

Table E.4. Summary of Operating Conditions, Conversions, Selectivity and Hydrocarbon Distribution .... cont'd....

Run #	17-16	17-17	17-18	17-19	17-20	17-21	17-22	17-23	17-24	17-25	17-26	17-27	17-28	17-29	17-30
Operating conditions															
Temperature, °C	209	215	215	215	221	221	221	221	221	221	215	215	215	209	209
Pressure, MPa	1.1	1.1	1.1	1.1	1.1	1.1	1.1	1.33	1.33	1.33	1.33	1.33	1.33	1.33	1.33
GHSV,h^{-1}	390	390	390	390	390	390	390	390	390	390	372	372	372	372	372
Ratio H_2/CO, mol/mol	2	2	2	2	2	2	2	2	2	2	2	2	2	2	2
Operation time, h.	24	24.0	24.0	24.0	24.5	24	24	24.0	16.5	23.5	23.5	23.5	20	24.0	24.0
Operation on stream, h.	504	528.0	552.0	576.0	600.5	624.5	648.5	672.5	689.0	712.5	736	759.5	779.5	803.5	827.5
Experimental Results															
% CO conversion	4.77	7.87	7.42	7.57	11.51	12.48	10.82	13.5	14.56	14.13	13.28	12.33	11.73	9.5	7.7
% H_2 conversion	4.86	7.95	7.32	8.51	15.4	15.56	13.96	14.5	17.81	14.44	12.62	10.45	11.5	10.2	88
Mass (H_2+CO) in, g	40.17	40.17	40.17	40.17	41	40.17	40.17	40.17	27.62	39.33	37.51	37.51	31.93	38.31	38.31
Mass (gases) out, g	36.9	35.02	36.6	35.49	36.96	35.3	35.52	32.4	23.899	33.45	32.21	32.37	27.8	34.00	34.4
Mass (H_2O_{liquid}) out, g	1.65	2.24	2.53	2.45	2.4	2.53	2.46	3.41	1.87	2.69	2.54	2.57	2.09	1.91	1.76
Mass (HC_{liquid}) out, g	1.21	1.75	1.61	1.75	1.31	1.45	1.34	2.67	1.34	2.02	1.91	1.81	1.5	1.32	1.03
Overall mass balance %	98.979	97.112	101.42	98.805	99.195	97.784	97.884	95.793	98.15	97.025	97.734	97.974	98.309	97.181	97.076
Oxygen mass balance %	99.01	98.21	99.54	98.99	99.1	98.67	98.12	97.12	98.56	98.32	98.65	98.01	99.12	98.12	98.44
Products Distribution															
CO_2 selectivity, %w/w	0	1.07	1.27	1.48	3.23	3.52	3.43	3.51	3.01	2.98	1.94	1.51	1	0.00	0.00
H_2O selectivity, %w/w	56.04	45.19	53.12	52.95	52.73	51.69	51.48	51.85	52.98	53.66	55.76	44.03	56.39	56.4	56.31
HC selectivity, %w/w	43.96	44.12	45.61	45.57	44.04	44.79	45.09	44.64	44.01	43.36	42.3	42.52	42.61	44.6	44.69
Hydrocarbon Distribution															
Fraccion C_1	4.94			7.23			5.6			4.56			5.34		
Fraccion C_2 - C_4	12.86			9.33			11.27			10.06			6.11		
Fraccion C_5 - C_9	28.64			25.10			36.63			34.02			19.92		
Fraccion C_{10} - C20	50.62			51.21			35.86			40.46			59.45		
Fraccion C_{21}^+	2.94			7.13			10.64			10.90			9.18		

Table E.4. Summary of Operating Conditions, Conversions, Selectivity and Hydrocarbon distribution... cont'd...

Run #	17-31	17-32	17-33	17-34	17-35	17-36	17-37	17-38	17-39	17-40	17-41	17-42	17-43	17-44	17-45
Operating conditions															
Temperature, °C	209	209	209	209	215	215	215	220	220	220	221	221	221	215	215
Pressure, MPa	1.33	1.52	1.52	1.52	1.52	1.52	1.52	1.52	1.52	1.52	1.52	1.52	1.52	1.52	1.52
GHSV,h^{-1}	372	360	360	360	360	360	360	390	390	390	210	210	210	210	210
Ratio H_2/CO, mol/mol	2	2	2	2	2	2	2	2	2	2	2	2	2	2	2
Operation time, h.	24	24	24	26	23.0	23.0	23.0	23.5	23.5	23.5	24.0	24.0	24.0	24	24
Operation on stream, h.	851.5	875.5	899.5	925.5	948.5	971.5	994.5	1018	1041.5	1065	1089	1113	1137	1161	1185
Experimental Results															
% CO conversion	7.30	7.8	8.1	8.2	12.1	11.61	13.25	17.08	18.58	16.56	26.55	28.19	28.02	17.13	14.79
% H_2 conversion	6.30	8.1	7.9	6.24	13.5	12.63	14.25	19.34	19.64	19.64	27.69	30.59	30.63	18.82	16.12
Mass (H_2+CO) in, g	38.31	37.07	37.07	40.16	35.53	35.53	35.53	39.33	39.33	39.33	21.62	21.62	21.62	21.62	21.62
Mass (gases) out, g	34.72	33.1	33.5	35.98	31.1	31.58	30.93	32.78	32.5	33.1	15.91	15.8	16.19	18.3	18.41
Mass (H_2O_{liquid}) out, g	1.61	1.64	1.71	1.89	2.45	2.26	2.49	3.46	3.752	3.24	2.968	3.36	3.23	1.91	1.95
Mass (HC_{liquid}) out, g	1.05	1.06	1.03	1.24	1.52	1.21	1.51	1.87	2.23	1.87	1.81	2.07	2.05	1.02	0.9
Overall mass balance %	97.572	96.574	97.761	97.385	98.705	98.649	98.311	96.898	97.844	97.152	95.689	98.196	99.306	98.196	98.335
Oxygen mass balance %	98.56	97.8	97.98	98.15	98.92	99.01	98.87	97.34	98.01	98.23	97.56	98.92	99.35	98.67	99.05
Products Distribution															
CO_2 selectivity, %w/w	0.00	0	0.1	0.19	2.03	1.96	1.44	3.74	2.81	3.01	1.06	3.19	3.02	2.35	0.35
H_2O selectivity, %w/w	58.24	57.79	58.1	57.83	54.16	54.25	54.73	52.27	53.55	53.18	55.08	53.05	53.13	54	55.34
HC selectivity, %w/w	41.76	42.21	41.8	41.99	43.81	43.79	43.83	43.98	43.64	43.81	43.86	43.76	43.85	43.65	44.31
Hydrocarbon Distribution															
Fraccion C_1	4.82			4.69			3.77			4.6			4.72		
Fraccion C_2 - C_4	12.86			10.9			9.87			12.11			12.25		
Fraccion C_5 - C_9	28.64			26.09			26.01			24.05			20.72		
Fraccion C_{10} - C20	50.62			55.31			49.64			47.15			5.58		
Fraccion C_{21}^+	2.94			3.01			10.71			12.09			16.73		

Table E.4. Summary of Operating Conditions, Conversions, Selectivity and Hydrocarbon distribution... cont'd...

Run #	17-46	17-47	17-48	17-49	17-50	17-51	17-52	17-53	17-54	17-55	17-56	17-57	17-58	17-59	17-60
Operating conditions															
Temperature, °C	215	209	209	209	209	209	209	215	215	215	215	215	215	215	215
Pressure, MPa	1.52	1.52	1.52	1.52	1.52	1.52	1.52	1.52	1.52	1.52	0.73	0.73	0.73	0.73	0.73
GHSV,h^{-1}	210	210	210	210	264	264	264	264	264	264	222	222	222	210	210
Ratio H_2/CO, mol/mol	2	2	2	2	2	2	2	2	2	2	2	2	2	2	2
Operation time, h.	24	23.5	23.5	24.0	24.0	24.0	24.0	24.0	23.5	23.5	24.0	24.0	24.0	24.0	24.0
Operation on stream, h.	1209	1232.5	1256	1280	1304	1328	1352	1376	1399.5	1423	1447	1471	1495	1519	1543
Experimental Results															
% CO conversion	17.33	12.63	15.13	12.29	9.06	9.5	9.9	17.37	17.41	16.91	13.9	12.1	11.2	10.2	9.07
% H_2 conversion	18.82	11.79	14.49	11.64	9.78	9.35	9.37	16.77	17.68	18.32	14.5	13.2	10.96	8.2	7.81
Mass (H_2+CO) in, g	21.62	21.17	21.17	21.62	27.18	27.18	27.18	27.18	26.61	26.61	22.86	22.86	22.86	21.62	21.62
Mass (gases) out, g	18.23	18.48	17.83	19.02	24.4	24.1	23.97	22.76	21.65	21.81	20.1	20.37	20.06	19.4	19.62
Mass (H_2O_{liquid}) out, g	1.89	1.45	1.76	1.31	1.27	1.36	1.46	2.56	2.56	2.45	1.45	1.43	1.46	1.23	1.12
Mass (HC_{liquid}) out, g	1.04	0.78	1.22	1.02	0.97	0.99	1.02	1.66	1.71	1.61	0.75	0.62	0.67	0.76	0.56
Overall mass balance %	97.872	97.827	98.299	98.751	98.013	97.314	97.314	99.264	97.407	97.219	97.55	98.075	97.069	98.936	98.52
Oxygen mass balance %	98.45	98.15	99.05	99.1	98.9	98.56	98.75	99.3	99.01	98.55	97.65	99.52	98.6	99.15	99.03
Products Distribution															
CO_2 selectivity, %w/w	1.72	0.88	0.91	0.43	0.25	0.32	0.15	2.2	2.28	2.39	4.81	3.54	4.85	3.21	3.45
H_2O selectivity, %w/w	55.02	55.64	56.7	56.23	56.12	55.7	56.63	54.69	54.28	53.25	52.56	52.27	52.43	53.58	46.41
HC selectivity, %w/w	43.26	43.48	42.39	43.34	43.63	43.98	43.22	43.11	43.44	44.36	42.63	44.19	42.72	43.21	50.14
Hydrocarbon Distribution															
Fraccion C_1	3.43			3.10			3.71			3.52			11.3		
Fraccion C_2 - C_4	6.59			12.72			9.87			7.02			8.33		
Fraccion C_5 - C_9	16.52			27.55			28.1			19.85			17.74		
Fraccion C_{10} - C20	48.06			47.21			49.5			53.65			47.44		
Fraccion C_{21}^+	25.4			9.42			7.43			15.96			15.19		

Table E.4. Summary of Operating Conditions, Conversions, Selectivity and Hydrocarbon Distribution .... cont'd....

Run #	17-61	17-62	17-63	17-64	17-65	17-66	17-67	17-68	17-69	17-70	17-71	17-72	17-73	17-74	17-75
Operating conditions															
Temperature, °C	215	222	222	222	215	215	215	209	209	209	222	221	221	222	222
Pressure, MPa	1.1	0.73	0.73	0.73	0.73	0.73	0.73	0.73	0.73	0.73	0.73	0.73	0.73	0.73	0.73
GHSV,h^{-1}	210	234	234	234	234	234	234	234	234	234	210	210	210	300	300
Ratio H_2/CO, mol/mol	2	1	1	1	1	1	1	1	1	1	2	2	2	2	2
Operation time, h.	24.0	27.0	23.0	20.0	24.0	26.0	24.0	25.0	17.0	26.0	48.0	23.0	24.0	27.0	24
Operation on stream, h.	1567	1594	1617	1637	1661	1687	1711	1736	1753	1779	1827	1850	1874	1901	1925
Experimental Results															
% CO conversion	8.79	12.69	11.66	10.8	3.96	7.22	6.78	3.18	3.48	2.89	19.2	18.82	18.7	13.91	15.43
% H_2 conversion	8.45	18.92	20.89	21.78	15.84	14.93	17.33	11.06	8.93	9.94	18.78	17.29	17.63	13.23	11.56
Mass (H_2+CO), g	21.62	38.71	32.98	28.68	34.41	37.28	34.41	35.85	24.37	37.28	43.34	21.17	21.62	34.75	31.37
Mass (gases) out, g	19.56	33.58	29.06	25.19	31.5	34.02	31.59	33.34	22.56	35.08	35.67	17.37	16.94	30.42	26.93
Mass (H_2O_{liquid}) out, g	1.13	2.53	2.07	1.69	0.75	1.35	1.13	0.91	0.79	0.94	4.47	2.06	2.75	2.58	2.52
Mass (HC_{liquid}) out, g	0.65	2.02	1.31	1.26	0.69	1.12	1.01	0.82	0.7	0.79	2.35	1.01	1.53	1.39	1.28
Overall mass balance %	98.705	98.502	98.363	98.117	95.728	97.881	98.024	97.824	98.687	98.739	98.039	96.552	98.15	98.964	97.96
Oxygen mass balance %	99.12	98.91	98.76	98.91	97.65	98.01	98.32	98.75	98.7	98.93	99.23	97.85	98.45	99.08	99.32
Products Distribution															
CO_2 selectivity, %w/w	3.34	3.98	3.79	4.29	0.74	0.49	0.48	0.99	0.98	0.89	4.97	5.96	5.12	5.32	4.63
H_2O selectivity, %w/w	52.45	54.82	53.86	52.65	49.35	55.59	55.93	54.91	55.31	55.13	52.77	51.78	51.76	52.24	54.28
HC selectivity, %w/w	44.21	41.2	42.34	43.06	49.91	43.93	43.59	44.1	43.71	43.98	42.77	42.26	43.12	42.44	41.09
Hydrocarbon Distribution															
Fraccion C_1	10.5			1.47			2.81			3.41			13.9		
Fraccion C_2 - C_4	9.37			3.66			4.51			8.49			8.88		
Fraccion C_5 - C_9	15.15			5.29			7.98			12.18			17.06		
Fraccion C_{10} - C20	47.51			51.49			50.67			46.86			40.59		
Fraccion C_{21}^+	17.47			38.10			34.03			29.07			19.57		

Table E.4. Summary of Operating Conditions, Conversions, Selectivity and Hydrocarbon Distribution .... cont;d....

Run #	17-76	17-77	17-78	17-79	17-80	17-81	17-82	17-83	17-84	17-85	17-86	17-87	17-88	17-89	17-90
Operating conditions															
Temperature, °C	222	222	222	222	222	222	222	220	220	220	230	230	230	230	230
Pressure, MPa	0.73	1.52	1.52	1.52	1.52	1.52	1.52	1.52	1.52	1.52	1.52	1.52	1.52	1.52	1.52
GHSV,h^{-1}	300	390	390	390	504	504	504	432	432	432	432	432	432	360	360
Ratio H_2/CO, mol/mol	2	2	2	2	2	2	2	2	2	2	2	2	2	2	2
Operation time, h.	23.0	24.0	24.0	24.0	24.0	29.0	19.0	27.0	22.0	22.0	24.0	24.0	24.0	21.0	23
Operation on stream, h.	1948	1972	1996	2020	2044	2073	2092	2119	2141	2163	2187	2211	2235	2256	2279
Experimental Results															
% CO conversion	15.41	15.45	16.67	15.67	9.34	10.5	10.79	13.31	13.96	12.73	18.1	17.13	18.2	24.26	25.02
% H_2 conversion	11.81	12.91	13.87	13.15	7.02	9.83	9.72	11.29	11.23	12.94	19.2	18.03	17.79	22.46	23.05
Mass (H_2+CO) in, g	29.6	40.17	40.17	40.17	51.91	62.73	41.1	50.06	40.79	40.79	44.5	44.5	44.5	32.44	36.15
Mass (gases) out, g	26.08	32.94	31.94	33.02	47.24	56.289	37.31	43.40	35.11	35.72	36.67	37.97	37.87	25.42	28.82
Mass (H_2O_{liquid}) out, g	2.21	3.47	3.9	3.68	2.445	3.27	2.08	3.41	2.98	2.85	3.97	4.04	4.12	3.99	4.01
Mass (HC_{liquid}) out, g	0.95	2.31	2.45	2.02	1.25	2.14	1.19	2.4	1.62	1.51	2.01	1.89	1.97	1.78	1.82
Overall mass balance %	98.784	96.39	95.32	96.39	98.122	98.356	98.735	98.302	97.352	98.259	95.843	98.652	98.787	96.147	95.851
Oxygen mass balance %	98.90	97.8	98.01	98.76	98.56	99.01	99.19	98.9	98.32	98.80	97.45	98.9	98.91	97.4	97.82
Products Distribution															
CO_2 selectivity, %w/w	5.45	4.19	4.1	4.04	5.15	4.5	4.37	4.33	3.86	3.87	4.76	4.52	4.47	4.74	4.81
H_2O selectivity, %w/w	53.49	54	53.9	54.1	57.19	54.41	54.75	53.8	54.51	54.66	51.99	52.64	53.53	52.86	52.334
HC selectivity, %w/w	41.07	41.81	42	41.86	37.66	41.08	40.88	41.88	41.64	41.46	43.25	42.84	41.99	42.35	42.86
Hydrocarbon Distribution															
Fraccion C_1	6.46			3.76			5.93			5.26			4.88		
Fraccion C_2 - C_4	14.41			7.45			12.32			11.11			13.18		
Fraccion C_5 - C_8	34.3			33.24			29.96			28.77			34.22		
Fraccion C_{10} - C20	32.33			44.28			45.01			45.28			37.01		
Fraccion C_{21}^{+}	12.50			11.27			6.78			9.58			10.61		

Table E.4. Summary of Operating Conditions, Conversions, Selectivity and Hydrocarbon Distribution .... cont,d....

Run #	17-91	17-92	17-93	17-94	17-95	17-96	17-97	17-98	17-99	17-100	17-101	17-102	17-103	17-104	17-105
Operating conditions															
Temperature, °C	230	230	230	230	230	230	230	229	229	229	229	229	229	229	229
Pressure, MPa	1.52	1.52	1.52	1.52	1.52	1.52	1.52	1.52	1.52	1.52	1.52	1.52	1.52	1.52	1.52
GHSV,h^{-1}	360	276	276	276	210	210	210	240	240	240	306	306	306	372	372
Ratio H_2/CO, mol/mol	2	2	2	2	2	2	2	1	1	1	1	1	1	1	1
Operation time, h.	25.0	25	22	22.0	22.0	22.0	26.0	23.0	21.0	26.0	22.0	24.0	23.0	24.0	24
Operation on stream, h.	2304	2329	2351	2373	2395	2417	2443	2466	2487	2513	2535	2559	2582	2606	2630
Experimental Results															
% CO conversion	24.36	34.19	32.15	31.37	39.39	39.21	39.67	29.2	16.64	13.83	10.59	12.09	11.58	9.57	8.23
% H_2 conversion	22.32	30.77	31.3	29.78	40.73	39.01	40.16	28.3	38.15	37.95	31.91	32.17	30.74	23.5	21.9
Mass (H_2+CO), g	38.61	29.61	26.06	26.06	19.86	19.86	23.48	33.82	30.88	38.23	41.25	45	43.12	54.7	54.7
Mass (gases) out, g	31.055	20.92	18.54	18.73	13.04	13.28	15.19	26.91	25.72	32.61	36.53	38.99	38	48.82	48.78
Mass (H_2O_{liquid}) out, g	4.76	5.1	4.37	4.12	4.13	4.05	4.86	3.78	2.23	2.61	2.39	2.19	2.39	2.78	2.91
Mass (HC_{liquid}) out, g	2.16	3.02	2.55	2.73	2.13	2.07	2.76	1.87	1.98	1.98	1.78	1.67	1.86	1.99	2.01
Overall mass balance %	98.355	98.075	97.698	98.158	97.18	97.684	97.147	96.274	96.924	97.306	98.667	95.222	97.982	97.971	98.172
Oxygen mass balance %	98.40	98.67	98.10	98.45	98.50	98.30	98.45	97.75	97.48	98.01	98.75	97.1	98.01	98.3	98.2
Products Distribution															
CO_2 selectivity, %w/w	4.49	4.03	4.18	4.34	4.47	4.29	4.35	3.88	5.84	6.87	6.65	5.30	5.70	5.81	5.43
H_2O selectivity, %w/w	53.17	53.66	53.82	53.47	52.35	52.92	52.60	56.95	50.46	48.13	47.46	49.68	49.38	48.61	50.45
HC selectivity, %w/w	42.34	42.30	42.00	42.19	43.18	42.79	43.04	39.17	43.70	45.00	45.89	45.02	44.92	45.59	44.12
Hydrocarbon Distribution															
Fraccion C_1	4.55			3.49			3.34			2.58			2.73		
Fraccion C_2 - C_4	11.87			9.38			8.71			6.97			7.23		
Fraccion C_5 - C_9	31.9			28.25			26.03			16.05			16.87		
Fraccion C_{10} - C20	40.59			46.32			47.06			50.66			51.65		
Fraccion C_{21}^{+}	11.09			12.56			14.86			23.74			21.53		

Table E.4. Summary of Operating Conditions, Conversions, Selectivity and Hydrocarbon Distribution .... cont,d....

Run #	17-106	17-107	17-108	17-109	17-110	17-111	17-112	17-113	17-114	17-115	17-116	17-117	17-118	17-119	17-120
Operating conditions															
Temperature, °C	230	222	222	222	222	222	222	229	229	229	230	230	230	220	220
Pressure, MPa	1.52	1.52	1.52	1.52	1.07	1.07	1.07	1.07	1.07	1.07	0.59	0.59	0.59	1.52	1.52
GHSV,h^{-1}	372	372	372	372	402	402	402	402	402	402	402	402	402	390	390
Ratio H_2/CO, mol/mol	1	1	1	1	1	1	1	1	1	1	1	1	1	2	2
Operation time, h.	24.0	23	24	26.0	23.0	24.0	24.0	22.0	24.0	24.0	24.0	24.0	24.0	24.0	24.0
Operation on stream, h.	2654	2677	2701	2727	2750	2774	2798	2820	2844	2868	2892	2916	2940	2964	2988
Experimental Results															
% CO conversion	7.87	5.45	6.45	7.1	5.74	6.25	6.03	7.9	10.25	10.7	5.6	6.02	5.81	18.93	17.76
% H_2 conversion	22.55	17.31	17.98	18.81	15.61	16.1	15.37	25.68	22.2	22.43	13.16	13.23	12.95	10.06	14.45
Mass (H_2+CO) in, g	54.7	52.42	54.7	59.26	56.65	59.15	59.15	54.19	59.15	59.15	59.15	59.15	59.15	40.17	40.17
Mass (gases) out, g	49.36	48.11	48.12	54.59	52.01	53.96	54.41	49.06	53.19	53.47	54.9	54.7	54.8	31.79	33.67
Mass (H_2O_{liquid}) out, g	2.31	1.34	1.54	2.12	1.77	1.75	1.87	2.12	3.12	3.01	1.74	1.71	1.66	3.89	3.52
Mass (HC_{liquid}) out, g	1.59	1.4	1.36	1.67	1.53	1.51	1.45	1.91	1.98	2.14	1.35	1.27	1.11	2.03	2.02
Overall mass balance %	97.367	97.00	93.272	98.515	97.635	96.737	97.60	97.97	98.546	99.10	98.039	97.515	97.329	93.876	97.61
Oxygen mass balance %	98.45	97.35	97.44	98.95	98.35	97.65	97.73	98.32	98.59	98.91	98.45	97.32	97.45	97.98	98.01
Products Distribution															
CO_2 selectivity, %w/w	5.81	5.26	3.72	3.95	4.48	4.65	4.79	6.42	4.56	4.27	7.11	5.98	6.52	2.28	2.43
H_2O selectivity, %w/w	48.61	48.09	48.7	50.82	50.16	50.92	50.47	46.91	51.94	52.43	49.23	50.21	50.13	57.88	55.47
HC selectivity, %w/w	45.58	46.65	44.98	45.23	45.36	44.43	44.74	46.66	43.49	43.31	43.66	43.81	43.36	39.83	42.1
Hydrocarbon Distribution															
Fraccion C_1	3.25			5.93			2.72			1.85			3.32		
Fraccion C_2 - C_4	7.38			4.8			6.07			4.81			6.83		
Fraccion C_5 - C_9	17.01			8.42			14.42			15.98			18.46		
Fraccion C_{10} - C20	52.28			51.37			46.59			52.09			42.75		
Fraccion C_{21}^+	20.09			29.49			30.2			25.26			28.63		

Table E.4. Summary of Operating Conditions, Conversions, Selectivity and Hydrocarbon Distribution .... cont'd....

Run #	17-121	17-122	17-123	17-124	17-125	17-126	17-127	17-128	17-129	17-130	
Operating conditions											
Temperature, °C	220	221	221	221	229	229	229	229	229	229	
Pressure, MPa	1.52	1.52	1.52	1.52	1.52	1.52	1.52	0.34	0.34	0.34	
GHSV,h^{-1}	390	378	378	378	378	378	378	402	402	402	
Ratio H_2/CO, mol/mol	2	3	3	3	3	3	3	3	3	3	
Operation time, h.	24.0	23	26	23.0	24.0	24.0	24.0	24	24	24.0	
Operation on stream, h.	3012	3035	3061	3084	3108	3132	3156	3180	3204	3228	
Experimental Results											
% CO conversion	18.32	25.59	31.96	32.64	55.22	56.1	56.86	18.83	19.19	20.54	
% H_2 conversion	13.31	23.04	21.35	23.29	44.1	43.65	42.33	13.81	15.82	13.6	
Mass (H_2+CO) in, g	40.15	27.97	31.62	27.97	29.18	29.18	29.18	31.03	31.03	31.03	
Mass (gases) out, g	33.63	22.32	24.17	21.06	17.5	17.72	17.11	27.71	26.79	26.37	
Mass (H_2O_{liquid}) out, g	3.85	3.61	4.88	4.53	7.64	8.01	8.58	2.28	3.07	3.19	
Mass (HC_{liquid}) out, g	2.127	1.67	2.07	1.87	3.38	2.59	2.67	0.68	0.68	0.78	
Overall mass balance %	98.648	98.677	98.419	98.177	97.738	97.053	97.19	98.84	98.421	97.776	
Oxygen mass balance %	98.76	98.75	98.9	98.35	98.47	98.01	97.57	98.9	98.56	98.1	
Products Distribution											
CO_2 selectivity, %w/w	2.33	2.78	2.55	2.61	4.46	5.23	5.57	1.56	3.09	3.35	
H_2O selectivity, %w/w	56.33	50.89	53.56	52.87	50.57	50.71	50.24	53.64	51.42	52.97	
HC selectivity, %w/w	41.34	46.34	43.89	44.52	44.97	44.06	44.19	44.8	45.49	43.68	
Hydrocarbon Distribution											
Fraccion C_1	3.76			17.87			7.95			13.54	
Fraccion C_2 - C_4	9.84			12.91			21.4			15.35	
Fraccion C_5 - C_9	36.17			31.65			50.88			34.35	
Fraccion C_{10} - C20	41.16			34.31			15.78			34.75	
Fraccion C_{21}^{+}	9.07			3.26			2.79			2.01	

APPENDIX F: Program for the estimation of the kinetics parameters

Appendix F.1. Main Program used to call UWHAUS and Model subroutines

```
*       Main prog example for uwhaus

      program uwmain
       parameter(nobmax=100,npmax=15)
       parameter(nscrat=5*npmax+npmax**2 +2*nobmax +npmax*nobmax)
       parameter (nprob=1)
c
       dimension scrat(nscrat)
c
      dimension signs(npmax),diff(npmax)
      dimension th(npmax)

c     X1=PH2  X2=PCO (MPa), r=(RH2+CO), t= Temp (K)
      dimension  X1(nobmax), X2(nobmax),r(nobmax), t(nobmax)
c
       character*3 filein*30, fileout*30
      real tav, tsum
c
      common X1,X2,tav, t
      external model
c
      write(*,*) 'enter name of input data file'
      write(*,*) 'enter name of output data file'
      read(*,'(A30)')fileout
c
      open(5,file=filein)
      open(6,file=fileout)
c
      write(*,*) 'enter the number of parameters and observations'
      read (*,*) np,nob
      write(6,*) 'Number of parameters and observations are:'
c
      do 10 i=1, nob
        read(5,*) X1(i),X2(i),r(i), t(i)
        write(6,*) X1(i),X2(i), r(i), t(i)
   10 continue
c
      do i=1,np
       signs(i)=0.
       diff(i)=.01
       enddo
c
c     set pre-exponential parameter to retain the given sign
      signs(1)=1.
c     set activation energy to retain the given sign
      signs(2)=1.
      signs(3)=1.
c     set variables used in UWHAUS
```

```
      eps1=.0000001
      eps2=.0000001
      mit=999
      flam=.1
      fnu=10.
C
      write(6,100)
  100 format ('the initial guesses are:')
      do i=1,np
       read(5,*)th(i)
       write(6,*) th(i)
      enddo
C
      tsum=0.0
      do i=1, nob
      tsum= tsum+t(i)

      enddo
      tav=tsum/nob
      write (6,*) tav

C
      call uwhs(nprob,model,nob,r,np,th,diff,signs,eps1,eps2,
     1 mit,flam,fnu,scrat)
      close(5)
      close(6)
      stop
      end
```

Appendix F.2: Subroutine model

```
subroutine model(nprob,th,f,nob,np)

      dimension th(*), f(*), X1(100),X2(100), t(100)

      common X1,X2, tav, t

      real tav

      do  i=1,nob

c     Model 1   Power law

      f(i)=th(1)*exp((-1.*th(2)/8.314)*(1/t(i)-1/tav))*X2(i)**th(3)
     1     *X1(i)**th(4)

c      Model Iglesia
c     f(i)=th(1)*exp((-1.*th(3)/8.314)*(1/t(i)-1/tav))
c          *X1(i)**th(4)*X2(i)**th(5)/(1+th(2)*X2(i)**1)

c     Model Sarup and Wojciechowski
c     f(i)=th(1)*exp((-1.*th(3)/8.314)*(1/t(i)-1/tav))*X2(i)**th(4)
c     1 *X1(i)**th(5)/(1+th(2)*X2(i)**th(4))**2

c     Model Rautavuoma and van der Baan model
c     f(i)=th(1)*exp((-1.*th(3)/8.314)*(1/t(i)-1/tav))*X2(i)**th(4)
c     1 *X1(i)**th(5)/(1+th(2)*X2(i)**th(4))**3

c     Model Anderson
c     f(i)=th(1)*exp((-1.*th(3)/8.314)*(1/t(i)-1/tav))*X2(i)**th(4)
c     1 *X1(i)**th(5)/(1+th(2)*X2(i)**th(4)*X1(i)**th(5))


      enddo
      return
      end
```

APPENDIX G: Program for the PO reactor simulation.

Appendix G.1 PO REACTOR SIMULATION

```
C    PROGRAM REACTOR "PBREACT PROGRAM"
C**********************************************************************
C
C       PSEUDOHOMOGENEUS ONE DIMENSIONAL MODEL
C
C    FOR THE SIMULATION OF THE SINGLE-TUBE P.O REACTOR
C
C            UPDATE 12th June 1998
C
C**********************************************************************
C
      DOUBLE PRECISION DT1, DZ, COf
      DIMENSION NC(40), FM(40), NWMEZ(40)
      REAL NC, NHCT, NCPA, NCP,NWMEZT,NWMEZ
      REAL NC2H2i,NH2Oi,NTi,NT,NH2i,NCOi,NCO,NH2,NC2H2,NH2O
      REAL KCO,KH2,C2H2KG,KH2O,KG,KC
      REAL REC,PRC,REG,PRG,PEMR,KER,PT
      REAL VCT(50000),VCTC(50000),   VZ(50000),VTCTR(50000)
      REAL COS(50000), H2S(50000),C2H2S(50000), H2OS(50000)
      REAL  XT(50000),CONVCO(50000),Pco(50000), ntf(50000)
      REAL MOL(6), TMOL(6)
C**********************************************************************
C                INPUT DATA
C**********************************************************************
      WRITE (6,*) 'Experiment number'
      read (6,*) num
      write (6,*) 'Temperature gas in ( C )'
      read (6,*) tgin
      write (6,*) 'Inlet total pressure (MPa)'
      read (6,*) P
      write (6,*) 'Inlet gas flow rate (Liters/minute)'
      read  (6,*) flow
      write (6,*) 'Coolant flow rate (kg/hr)'
      read (6,*) wc
      write (6,*) 'Inlet Coolant temperature ( C )'
      read (6,*) tcin

C**********************************************************************
C     INITIAL VALUES
      TGIN=TGIN+273
      TIN=TGIN-273
      TCIN=TCIN+273
      TCOLI=TCIN-273
      T=TGIN
      TC=TCIN
```

```
      PT=P/0.10133
      r=0.0105
      d1=0.0266
      d2=0.0351
      DZ = 0.01
      ZZ=0.0
c
      ZT=12.0
      TN=1.0
      X1=0.0
      AK1=0.0
      AK3=0.0
      AK4=0.0
 c    E =Activation energy = 129 KJ/mol = 29119 cal/mol
c     R = 1.987 cal/mol*K
c     EA =E/R
c
      EA=14654.0
c     CORR1=Ko
c      Kinetic model 1
      CORR1=2.19E+12

c     Kinetic model 2
c      corr1=1.43E+14

c      Kinetic model 3
c     CORR1=1.01E+14

c      Kinetic model 4
c     CORR1=7.00E+13

c      Kinetic model 5
c     CORR1=2.80E+13

C     AHr = -163 Kj/mol = -38889 Kcal/Kmol CO conv.
      AHR=-38889
      NNN=0
C*************************************************************************
C     OPEN FILE DATA2.TXT ( MOLES OF HIDROCARBONS FROM C1 TO C30 )
      OPEN (5, FILE = 'DATA6.TXT')
      REWIND (5)
      I=0
      NT=0
      DO 5 I=1,30
         READ (5,10) NC(I)
   10    FORMAT(16x,F9.7)
      NHCT=NHCT+NC(I)
    5 CONTINUE
C     LOOP FOR CALCULATION OF MOLAR FRACTION OF HIDROCARBONS FM(J)
      FMT=0
      REWIND (5)
```

```
      DO 300 J=1,30
           READ (5,10) NC(J)
           FM(J)=NC(J)/NHCT
           FML=FML+FM(J)
  300 CONTINUE
C       CALCULATION OF THE MOLECULAR WEIGHT OF HIDROCARBONS
(NWMEZT)
      M=0
      REWIND (5)
      MM=16
      DO 400 M=1,30
           NWMEZ(M)=FM(M)*MM
           NWMEZT=NWMEZT+NWMEZ(M)
           MM=MM+14
  400 CONTINUE
C     AVERAGE CARBON NUMBER OF THE HIDROCARBON FRACTION
      NCP = 0
      DO 500 K=1,30
         NCPA=FM(K)*K
         NCP=NCP+NCPA
  500 CONTINUE
C*********************************************************************
C            CALCULATION OF MOLAR FLOW
C
C          FLOW = GAS OF SINTESIS FLOW RATE LTS/MIN
C          NTi= FLUJO DE MOLES INICIALES KGMOL/HR
C          NCOi= INLET MOLAR FLOW OF CO
C          NH2i= INLET MOLAR FLOW OF H2
C          NH2Oi= INLET MOLAR FLOW OF H2O
C          NC2H2i= INLET MOLAR FLOW OF HIDROCARBONS
C          ALPHA= M OF THE ESTEQUIOMETRICA REACTION
C          OMEGA = N OF THE ESTEQUIOMETRICA REACTION
C          BETA = H2/CO RATIO
C          NT = MOLAR FLOW
C          NT= NTi (At z=0)
C
      NC2H2i=0.0
      NH2Oi=0.0
      ALPHA=(NCP*2)+1
      OMEGA = NCP
      BETA=2.19
C       INLET MOLES
      NTi=FLOW*60.0/(22.4*1000)
      NT=NTi
C       INLET MOLES OF CO E H2
      NCOi=NTi/(1+BETA)
      NCO=NCOi
      NH2i=NCOi*BETA
      NH2=NH2i
C     Open file
      open (1, file = 'Xmol1.txt')
```

```
      rewind (1)
      DO 13 N = 1,5
            READ (1,1000) MOL (N)
1000          FORMAT (16X,F9.7)
            SMOL = SMOL + MOL(N)
   13 CONTINUE
      REWIND (1)
      DO 15 NN = 1,5
            READ (1,10) MOL (NN)
            TMOL(NN) = MOL(NN)/SMOL
   15 CONTINUE
      WTO = TMOL(1)*28 + TMOL(2)*2 + TMOL(3)*44 + TMOL(4)*18 +
     1    TMOL(5)*NWMEZT
      WT=(28*NCOi+2*NH2i)/(NCOi+NH2i)
C       CALCULATION OF MOLAR FLOW
 9500 NT=NTi + (1-ALPHA)*X1
      WT =(NCO*28 + NH2*2 + NH2O*18 + NC2H2*NCP)/NT
      NNN=NNN+1
C*************************************************************************
C     CALCULATION OF INLET GAS DENSITY GAS (H2 AND CO)
C
C            NCOi = INLET MOLAR FLOW OF CO (KGMOL/HR)
C            NH2i = INLET MOLAR FLOW OF H2 (KGMOL/HR)
C            WTi =  MOLECULAR WEIGHT OF GAS IN (KG/KMOL)
C            R = 0.08200 (ATM*LTS)/(KMOL* K)
C            PT = INLET PRESSURE TOTAL (ATM)
C            GASD = GAS DENSITY IN (KG/M3)
      GASD=(PT/0.08200/T)*WT
C*************************************************************************
C       CALCULATION GAS SUPERFICIAL VELOCITY
C
C             V= GAS SUPERFICIAL VELOCITY ( M / H )
      V= NT/(3.14159*R**2*PT)*0.08208*T
C*************************************************************************
C      CALCULATION OF HEAT CAPACITY
C
C     CALCULATION OF HEAT CAPACITY OF THE HIDROCARBONS (OULET)
C          WHERE FM(I) = MOLAR HIDROCARBON FRACTION

c              HYDROCARBON GAS PHASE
C        CALCULATION CP MEAN FOR THE GAS FRACTION
      cpc1=(25.36+168.678E-04*t+713.121E-07*t**2-408.371E-10*t**3)*FM(1)
      cpc2=(8.181+161.465e-03*t-400.710e-07*t**2-694.209e-11*t**3)*FM(2)
      cpc3=(-5.338+310.239e-03*t-164.64e-06*t**2+346.908e-10*t**3)*FM(3)
      cpc4=(-1.78+386.961e-03*t-193.255e-06*t**2+348.326e-10*t**3)*FM(4)
      cpc5=(-3.411+485.009e-03*t-251.94e-06*t**2+486.767e-10*t**3)*FM(5)
      cpc6=(-4.738+582.41e-03*t-310.64e-065*t**2+629.232e-10*t**3)*FM(6)
      cpc7=(-5.619+676.93e-03*t-363.95e-06*t**2+740.735e-10*t**3)*FM(7)
      cpc8=(-7.477+777.47e-03*t-428.442e-06*t**2+917.635e-10*t**3)*FM(8)
      cpc9=(-8.386+872.155e-03*t-482.164e-06*t**2+103.11e-09*t**3)*FM(9)
      cpc10=(-9.30+966.713e-03*t-535.09e-06*t**2+113.89e-09*t**3)*FM(10)
```

```
      cpc11=(-11.24+106.784e-02*t-600.95e-06*t**2+132.4e-09*t**3)*FM(11)
      cpc12=(-12.18+116.265e-02*t-654.55e-06*t**2+143.6e-09*t**3)*FM(12)
      cpc13=(-13.15+125.77e-02*t-708.69e-06*t**2+155.1e-091*t**3)*FM(13)
      cpc14=(-14.95+135.79e-02*t-772.74e-06*t**2+172.59e-09*t**3)*FM(14)
      cpc15=(-15.97+145.32e-02*t-826.97e-06*t**2+184.07e-09*t**3)*FM(15)
      cpc16=(-17.07+154.83e-02*t-880.61e-06*t**2+195.15e-09*t**3)*FM(16)
      cpc17=(-18.72+164.83e-02*t-945.0e-06*t**2+213.020e-09*t**3)*FM(17)
      cpc18=(-19.57+174.25e-02*t-997.55e-06*t**2+223.64e-09*t**3)*FM(18)
      cpc19=(-20.5+183.732e-02*t-105.14e-05*t**2+235.09e-09*t**3)*FM(19)
      cpc20=(-22.42+193.82e-02*t-111.63e-05*t**2+252.93e-09*t**3)*FM(20)
      cpc21=(-16.201+1.9984*t-0.001186*t**2+2.391e-07*t**3)*FM(21)
      cpc22=(-17.11+2.09384*t-0.001173*t**2+2.51e-07*t**3)*FM(22)
      cpc23=(-18.019+2.18884*t-0.0012274*t**2+2.63e-07*t**3)*FM(23)
      cpc24=(-18.928+2.28384*t-0.0012818*t**2+2.75e-07*t**3)*FM(24)
      cpc25=(-19.837+2.37884*t-0.0013362*t**2+2.87E-07*t**3)*FM(25)
      cpc26=(-20.746+2.47384*t-0.0013906*t**2+2.986e-07*t**3)*FM(26)
      cpc27=(-21.655+2.56884*t-0.001445*t**2+3.105e-07*t**3)*FM(27)
      cpc28=(-22.564+2.66384*t-0.0014994*t**2+3.23e-07*t**3)*FM(28)
      cpc29=(-23.473+2.75884*t-0.0015538*t**2+3.34e-07*t**3)*FM(29)
      cpc30=(-24.382+2.85384*t-0.0016082*t**2+3.462e-07*t**3)*FM(30)
C       CALCULATION OF THE AVERAGE HEAT CAPACITY OF THE
C        HIDROCARBONS (OULET)
      cpC2H2=cpc1+cpc2+cpc3+cpc4+cpc5+cpc6+cpc7+cpc8+cpc9+cpc10+
     1    cpc11+cpc12+cpc13+cpc14+cpc15+cpc16+cpc17+cpc18+cpc19+cpc20
     1   +cpc21+cpc22+cpc23+cpc24+cpc25+cpc26+cpc27+cpc28+cpc29+cpc30
C     CALCULATIONS OF HEAT CAPACITY OF THE GAS SINTESIS (UNREACTED)
AND
C      THE H2O
      CPCO=(2.90063e+01+2.49235e-03*t-1.86440e-05*t**2+4.79889e-08
     1     *t**3-2.87266e-11*t**4)
      CPH2=(1.76386e+01+6.70055e-02*t-1.31485e-04*t**2+1.05883e-07
     1     *t**3-2.91803e-11*t**4)
      CPH2O=(3.40471e+01-9.65064e-03*t+3.29983e-05*t**2-2.04467e-08
     1     *t**3+4.30228e-12*t**4)
      CPCO2=19.87+7.344E-2*T-5.602E-5*T**2+1.715E-8*T**3
C      CALCULATIONS OF THE AVERAGE HEAT CAPACITY (CPGAS OUT) CPGAS
C        AND HEAT CAPACITY TOTAL CPGAST
C        CP     KCAL/(KG HR)
C        T = K
cf       CPGAS = (CPCO*TMOL(1) + CPH2*TMOL(2) + CPCO2*TMOL(3) +
cf     1          CPH2O*TMOL(4) + CPC2H2*TMOL(5))
      cpgas = (cpco*nco/nt) +  (cph2*nh2/nt) + (cph2o*nh2o/nt) +
     1        (cpc2h2*nc2h2/nt)
      CPGAS = (cpgas/WT)*0.2389
C*********************************************************************
C             CALCULATION OF GAS VISCOSITY
C                 UG = KG/ (H M)
c                HYDROCARBON GAS PHASE
C        CALCULATION uG MEAN FOR THE GAS FRACTION
      UGC1=(3.8435 +4.0112E-01*t -1.4303E-04*t**2)*FM(1)*3.6e-04
      UGC2=(0.5142 +3.3449e-01*t -7.1071e-05*t**2)*FM(2)*3.6e-04
```

```
      UGC3=(-5.4615 +3.272e-01*t -1.0672e-04*t**2)*FM(3)*3.6e-04
      UGC4=(-4.9462 +2.900e-01*t -6.9665e-05*t**2)*FM(4)*3.6e-04
      UGC5=(-3.2016 +2.675e-01*t -6.6178e-05*t**2)*FM(5)*3.6e-04
      UGC6=(-8.2223 +2.623e-01*t -5.7366e-05*t**2)*FM(6)*3.6e-04
      UGC7=(-10.378 +2.441e-01*t -5.4003e-05*t**2)*FM(7)*3.6e-04
      UGC8=(3.9404  +1.664e-01*t +1.4470e-05*t**2)*FM(8)*3.6e-04
      UGC9=(-6.8021 +1.869e-01*t +3.4929e-07*t**2)*FM(9)*3.6e-04
      UGC10=(-7.2970 +1.8506e-01*t -4.8008e-06*t**2)*FM(10)*3.6e-04
      UGC11=(-10.044 +1.8311e-01*t -6.9885e-06*t**2)*FM(11)*3.6e-04
      UGC12=(-12.217 +1.8099e-01*t -8.9955e-06*t**2)*FM(12)*3.6e-04
      UGC13=(-10.691 +1.6482e-01*t -1.8752e-06*t**2)*FM(13)*3.6e-04
      UGC14=(-10.397 +1.5709e-01*t +1.0229e-06*t**2)*FM(14)*3.6e-04
      UGC15=(-11.516 +1.5643e-01*t -6.6776e-07*t**2)*FM(15)*3.6e-04
      UGC16=(-13.585 +1.6007e-01*t -5.5846e-06*t**2)*FM(16)*3.6e-04
      UGC17=(-6.1661 +1.2965e-01*t +1.9105e-05*t**2)*FM(17)*3.6e-04
      UGC18=(-6.9467 +1.2597e-01*t +2.2320e-05*t**2)*FM(18)*3.6e-04
      UGC19=(-7.6815 +1.2181e-01*t +2.5813e-05*t**2)*FM(19)*3.6e-04
      UGC20=(-7.9886 +1.1866e-01*t +2.7167e-05*t**2)*FM(20)*3.6e-04
C
      UGC21=((2.8375e-7*t**6.2562e-1)/(1+(7.0216e+2/t)))*FM(21)*3600
      UGC22=((2.7626e-7*t**6.2625e-1)/(1+(7.0084e+2/t)))*FM(22)*3600
      UGC23=((2.7013e-7*t**6.2634e-1)/(1+(6.9950e+2/t)))*FM(23)*3600
      UGC24=((2.6670e-7*t**6.2528e-1)/(1+(6.9999e+2/t)))*FM(24)*3600
      UGC25=((2.6350e-7*t**6.2421e-1)/(1+(6.9965e+2/t)))*FM(25)*3600
      UGC26=((2.6118e-7*t**6.2258e-1)/(1+(6.9931e+2/t)))*FM(26)*3600
      UGC27=((2.5989e-7*t**6.2059e-1)/(1+(6.9898e+2/t)))*FM(27)*3600
      UGC28=((2.5860e-7*t**6.1860e-1)/(1+(6.9864e+2/t)))*FM(28)*3600
      UGC29=((2.5833e-7*t**6.2211e-1)/(1+(6.9823e+2/t)))*FM(29)*3600
      UGC30=((2.5806e-7*t**6.2562e-1)/(1+(6.9843e+2/t)))*FM(30)*3600

C     CALCULATION OF THE AVERAGE UG OF THE
C      HIDROCARBONS (OULET)
      UGC2H2=UGc1+UGc2+UGc3+UGc4+UGc5+UGc6+UGc7+UGc8+UGc9+UGc10+
     1
UGC11+UGC12+UGC13+UGC14+UGC15+UGc16+UGc17+UGc18+UGc19+UGc20
     1
+UGc21+UGc22+UGc23+UGc24+UGc25+UGc26+UGC27+UGc28+UGc29+UGc30
c
C    CALCULATIONS OF VISCOSITY OF THE GAS SINTESIS (UNREACTED) AND
C     THE H2O
      UCO=(23.8114 + 5.3944e-01*t -1.5441e-04*t**2)*3.6e-04
      UH2=(21.87 + 22.2e-02*T - 37.51e-06*T**2)*3.6e-04
      UCO2=(11.8109 +4.9838e-01*t -1.0851e-04*t**2)*3.6e-04
      UH2O=(-31.89 + 41.45e-02*T - 8.272e-06*T**2)*3.6e-04
C
      UG=(UCO*NCO*28**0.5 + UH2*NH2*2**0.5 + UGC2H2*NC2H2*NCP**0.5
     1  + UH2O*NH2O*18**0.5)/(NCO*28**0.5 + NH2*2**0.5 +NC2H2*NCP**0.5
     1  + NH2O*18**0.5)
C*************************** ******************************************
C          THERMAL CONDUCTIVITY OF THE PRODUCTS
C               KG = KCAL / (H M K)
```

```
c              HYDROCARBON GAS PHASE +
C       CALCULATION k MEAN FOR THE GAS FRACTION
      GKC1=(-0.00935 +1.4028E-04*t +3.3180E-08*t**2)*FM(1)
      GKC2=(-0.01936 +1.2547e-04*t +3.8298e-08*t**2)*FM(2)
      GKC3=(-0.00869 +6.6409e-05*t +7.8762e-08*t**2)*FM(3)
      GKC4=(-0.00182 +1.9396e-05*t +1.3818e-07*t**2)*FM(4)
      GKC5=(-0.00137 +1.8081e-05*t +1.2136e-07*t**2)*FM(5)
      GKC6=(-0.002   +7.7788e-06*t +1.3824e-07*t**2)*FM(6)
      GKC7=(-0.00172 +1.6565e-05*t +1.0525e-07*t**2)*FM(7)
      GKC8=(-0.00213 +1.8456e-05*t +9.4775e-08*t**2)*FM(8)
      GKC9=(-0.00655 +3.2637e-05*t +7.7150e-08*t**2)*FM(9)
      GKC10=(-0.00113 +8.1090e-06*t +9.6092e-08*t**2)*FM(10)
      GKC11=(0.01364 -4.83030e-05*t +1.4396e-07*t**2)*FM(11)
      GKC12=(-0.00812 +2.9150e-05*t +7.1085e-08*t**2)*FM(12)
      GKC13=(-0.00784 +2.7116e-05*t +7.0226e-08*t**2)*FM(13)
      GKC14=(-0.0018  +1.0242e-05*t +7.7727e-08*t**2)*FM(14)
      GKC15=(-0.00723 +2.3158e-05*t +6.7125e-08*t**2)*FM(15)
      GKC16=(-0.00671 +2.0080e-05*t +6.7235e-08*t**2)*FM(16)
      GKC17=(-0.00124 -6.3091e-06*t +8.1047e-08*t**2)*FM(17)
      GKC18=(-0.00172 +6.6775e-07*t +7.2881e-08*t**2)*FM(18)
      GKC19=(0.00153  -7.5609e-06*t +7.4184e-08*t**2)*FM(19)
      GKC20=(0.00154  -7.5268e-06*t +7.0837e-08*t**2)*FM(20)
C
      GKC21=((-2.6715e+2*t**1.0733E+0)/(1+(-6.5516E+9/t)))*FM(21)
      GKC22=((-3.0066e+2*t**1.0755E+0)/(1+(-7.7071E+9/t)))*FM(22)
      GKC23=((-2.5776e+2*t**1.0776E+0)/(1+(-6.8755E+9/t)))*FM(23)
      GKC24=((-2.4993e+2*t**1.0794E+0)/(1+(-6.9191E+9/t)))*FM(24)
      GKC25=((-2.8856e+2*t**1.0812E+0)/(1+(-8.2449E+9/t)))*FM(25)
      GKC26=((-1.7616e+2*t**1.0827E+0)/(1+(-5.2175E+9/t)))*FM(26)
      GKC27=((-1.8902e+2*t**1.0833E+0)/(1+(-5.7749E+9/t)))*FM(27)
      GKC28=((-2.0188e+2*t**1.0853E+0)/(1+(-6.3323E+9/t)))*FM(28)
      GKC29=((-2.3715e+2*t**1.08733E+0)/(1+(-6.3516E+9/t)))*FM(29)
      GKC30=((-2.7402e+2*t**1.00876E+0)/(1+(-9.0319E+9/t)))*FM(30)
C       CALCULATION OF THE AVERAGE K OF THE
C        HIDROCARBONS (OULET)
      C2H2KG=GKc1+GKc2+GKc3+GKc4+GKc5+GKc6+GKc7+GKc8+GKc9+GKc10+
     1
GKC11+GKC12+GKC13+GKC14+GKC15+GKc16+GKc17+GKc18+GKc19+GKc20
     1
+GKc21+GKc22+GKc23+GKc24+GKc25+GKc26+GKC27+GKc28+GKc29+GKc30
C     CALCULATIONS OF THERMAL CONDUC. OF THE GAS SINTESIS
(UNREACTED) AND
C       THE H2O
      KCO=(-0.012 + 1.0208e-04*T -2.2403e-08*T**2)
      KH2=8.099E-3 + 6.689E-4*T - 4.158E-7*T**2 + 1.562E-10*T**3
      KH2O=7.341E-3 - 1.013E-5*T + 1.801E-7*T**2 - 9.1E-11*T**3
      KCO2 = -7.215E-3 + 8.015E-5*T + 5.477E-9*T**2 -1.053E-11*T**3
C
      KG=(KCO*NCO*28**0.33 + KH2*NH2*2**0.33 + C2H2KG*NC2H2*NCP**0.33
     1+ KH2O*NH2O*18**0.33)/(NCO*28**0.33 + NH2*2**0.33 +NC2H2*NCP**0.33
     1  + NH2O*18**0.33)
```

```
      KG = KG*0.8598
C*************************************************************************
C     CALCULATION  COOLANT  HEAT CAPACITY ( KCAL / (KG K) )
      CPC=0.00035*TC+0.348
C*************************************************************************
C     CALCULATION OF THE COOLANT DENSITY  ( KG / CUB. M )
      DCOL=-0.4125*TC+1141.5
C*************************************************************************
C     CALCULATION OF THE COOLANT VISCOSITY ( KG / (H M) )
      UC=-0.0026*TC + 3.137
C*************************************************************************
C     COOLANT THERMAL CONDUCTIVITY ( KCAL / ( H M K ) )
      KC=-0.00005*TC + 0.1267
C*************************************************************************
C     CALCULATION  COOLANT FLUX ( KG / ( H  SQ.M ) )
C           WC = COOLANT FLOW (KG/H)
      WMC=(WC)/(3.14159/4.*(D2**2-D1**2))
C*************************************************************************
C     CALCULATION DIAMETER EQUIVALENTE
      DE=(D2**2-D1**2)/D1
C*************************************************************************
C                  CALCULATION U FROM CORRELATION
C*************************************************************************
C       CATALYST EQUIVALENT DIAMETER
      DP=0.0028
C      REYNOLDS COOLANT
      REC = 0.0015*WMC/UC
C     PRANDTL COOLANT
      PRC=CPC*UC/KC
C ************* JACKET HEAT TRANSFER PARAMETERS **********************
      HOUT=KC/0.0015*(0.203*REC**(1./3.)*PRC**(1./3.)+0.22*
     1    REC**0.8*PRC**0.4)
C      GAS FLUX
      GG=V*GASD
C     REYNOLDS GAS
      REG=DP*GG/UG
C      PRANDTL GAS
      PRG=CPGAS*UG/KG
C     EFFECTIVE DIFFUSIVITY
      DER=V*DP/(10.*(1.+19.4*(DP/(2.*R))**2))
C      PECLET GAS
      PEMR=V*DP/DER
C     EFFECTIVE THERMAL CONDUCTIVITY
      KER=KG*(6.7+PRG*REG/PEMR)
C  ************* WALL HEAT TRANSFER PARAMETER ************************
      AW= KG/DP*EXP(0.077+0.523*ALOG(REG))
C     BIOT NUMBER
      BIOT=AW*R/KER
C ************* OVERALL HEAT TRANSFER PARAMETER **********************
      U1 = 1./(1./HOUT+1./AW+R/(4.*KER))
      U=U1
```

```
c     C    CALCULATION OF COEFFICIENTS OF THE DIFFERENTIAL EQUATIONS
      A=(3.14158*R**2)
      B1=(-AHR)/(V*CPGAS*GASD)
      C=(2.0*U)/(V*CPGAS*GASD*R)
      D=(2.0*3.14159*R*U*tn)/(WC*CPC)
C*************************************************************************
C     DIFFERENTIAL EQUATIONS RESOLUTION WITH RUNGE-KUTTA
C     AXIAL STEP PROGRESSION
      ZZ=ZZ+DZ
C
      CALL RUNGE (EA,CORR1,AK10,AK30,AK40,X1,T,TC,P,NH2i,
     1    NT,ALPHA,NCO,NCOi,NH2,NC2H2,NC2H2i,NH2O,NH2Oi,OMEGA,Pt, NTi)
        X11=X1+AK10/2.0*DZ
        T1=T+AK30/2.0*DZ
        TC1=TC+AK40/2.0*DZ

C
       CALL RUNGE (EA,CORR1,AK11,AK31,AK41,X11,T1,TC1,P,
     1NH2i,NT,ALPHA,NCO,NCOi,NH2,NC2H2,NC2H2i,NH2O,NH2Oi,OMEGA,Pt,NTi)
        X12=X1+AK11/2.0*DZ
        T2=T+AK31/2.0*DZ
        TC2=TC+AK41/2.0*DZ

C
       CALL RUNGE (EA,CORR1,AK12,AK32,AK42,X12,T2,TC2,P,
     1NH2i,NT,ALPHA,NCO,NCOi,NH2,NC2H2,NC2H2i,NH2O,NH2Oi,OMEGA, Pt, NTi)
        X13=X1+AK12*DZ
        T3=T+AK32*DZ
        TC3=TC+AK42*DZ

C
       CALL RUNGE (EA,CORR1,AK13,AK33,AK43,X13,T3,TC3,P,
     1NH2i,NT,ALPHA,NCO,NCOi,NH2,NC2H2,NC2H2i,NH2O,NH2Oi,OMEGA, Pt, NTi)
C     EXTENT OF REACTION
      DX1=(DZ/6.)*(AK10+(AK11*2.0)+(AK12*2.0)+AK13)
      X1=X1+DX1
C     GAS TEMPERATURE
      DT1=(DZ/6.)*(AK30+(AK31*2.0)+(AK32*2.0)+AK33)
      T=T+DT1
C     COOLANT TEMPERATURE
      DTC=(DZ/6.)*(AK40+(AK41*2.0)+(AK42*2.0)+AK43)
      TC=TC+DTC
C     CENTER TEMPERATURE
      TCTR=T+(T-TC)*.25*BIOT/(1+0.25*BIOT)
C     TEMPERATURE CONVERSION FROM KELVIN TO CELSIUS
      CT=T-273
      CTC=TC-273
      CTCTR=TCTR-273
C
      Pco(NNN)= (NCO/NT)*P
```

```
      CONVCO(NNN) = ((NCOI-NCO)/NCOI)*100
      VCT(NNN)=CT
      VCTC(NNN)=CTC
      VTCTR(NNN)=CTCTR
      VZ(NNN)=ZZ

C       COUNTER
      IF (ZZ.LT.ZT) GOTO 9500
*************************************************************************
C     OUT PUT FILE
C*************************************************************************
      OPEN (6,FILE= 'CALOR')
      WRITE (6,6)
    6 FORMAT (///,20X, '************************************',/,20X,
     1            ' SIMULATION ONE-DIMENSIONAL MODEL',/,20X,
     1            '************************************')
      WRITE (6,11) NUM
   11 FORMAT (//,5X, 'EXPERIMENT NUMBER',I4)
      WRITE (6, 12)
   12 FORMAT (///,20X, '************************************',/,20X,
     1            ' INPUT VALUES FOR THE SIMULATION',/,20X,
     1            '************************************',//)
      WRITE (6,16) TIN
   16 FORMAT ('INITIAL TEMPERATURE OF GAS  ',20X,F6.2,'    C')
      WRITE (6,18) FLOW
   18 FORMAT ('INITIAL GAS FLOW          ',18X,F8.2,'  liter/min')
      WRITE (6,20) BETA
   20 FORMAT ('H2/CO RATIO               ',20X,F6.2)
      WRITE (6,22) P
   22 FORMAT ('TOTAL PRESSURE            ',19X,F6.1,'    MPa')
      WRITE (6,34) TCOLI
   34 FORMAT ('INITIAL TEMPERATURE OF COOLANT ',17X,F6.1, '      C' )
      WRITE (6,36) WC
   36 FORMAT ('COOLANT FLOW              ',19X,F6.1, '  Kg/h')
      WRITE (6,28) NTi
   28 FORMAT('INLET MOLES TOTAL          ',20X,F9.6, ' Kmol/hour')
      WRITE (6,30) NH2i
   30 FORMAT('INITIAL MOLES OF H2        ',20X,F9.6, ' Kmol/hour')
      WRITE (6,32) NCOi
   32 FORMAT('INITIAL MOLES OF CO        ',20X,F9.6, ' Kmol/hour')
      WRITE (6,38) AHR
   38 FORMAT ('ENTHALPY OF REACTION',25X,F9.2,' Kcal/kmol CO converted')
      WRITE (6,40) CORR1
   40 FORMAT ('K0 OF THE REACTION ',21X,E20.3,' m3/m3 cat/s',/)
      WRITE (6,42)
   42 FORMAT (///,20X,'****************************************',/,20X,
     1            ' CALCULATED VALUES DURING THE SIMULATION',/,20X,
     1            '****************************************')
      WRITE (6,50) NT
   50 FORMAT ('MOLAR FLOW                ',21X,F6.3, '  Kmol/hour')
      WRITE (6,52) GASD
```

```
  52 FORMAT('GAS DENSITY                ',20X,F6.3, '    Kg/m3')
     WRITE (6,54) V
  54 FORMAT('GAS SUPERFICIAL VELOCITY     ',13X,F15.5, ' m/h')
     WRITE (6,56) CPGAS
  56 FORMAT('GAS HEAT CAPACITY           ',19X, F8.4,'  Kcal/ C/Kg')
     WRITE (6,58) UG
  58 FORMAT('GAS VISCOSITY OUT           ',21X,F5.3, '   Kg/m/h')
     WRITE (6,60) KG
  60 FORMAT('GAS THERMAL CONDUCTIVITY OUT',21X,F7.3,'   Kcal/ C/ m/h')
     WRITE (6,70) REG
  70 FORMAT ('REYNOLDS GAS               ',19X,F10.4)
     WRITE (6,72) PRG
  72 FORMAT('PRANDTL NUMBER GAS          ',18X,F8.4)
     WRITE (6,74) PEMR
  74 FORMAT('PECLET GAS                  ',19X,F5.2)
     WRITE (6,76) BIOT
  76 FORMAT ('BIOT GAS                   ',20X,F5.2)
C
     WRITE (6,62) DCOL
  62 FORMAT('COOLANT DENSITY             ',19X, F5.1, '   Kg/m3')
     WRITE (6,64) UC
  64 FORMAT('COOLANT VISCOSITY           ',21X,F5.3, ' Kg/m/h')
     WRITE (6,66) KC
  66 FORMAT('COOLANT THERMAL CONDUCTIVITY',21X,F7.3,' Kcal/ C/ m/h')
     WRITE (6,80) REC
  80 FORMAT ('REYNOLDS COOLANT           ',19X,F5.1)
     WRITE (6,82) PRC
  82 FORMAT ('PRANDTL COOLANT            ',20X, F5.2)
C
     WRITE (6,78) KER
  78 FORMAT ('EFFECTIVE RADIAL THERMAL CONDUCTIVITY  ',11X, F6.3,' Kcal
    1/H/m/ C')
     WRITE (6,84) HOUT
  84 FORMAT('JACKET HEAT TRANSFER COEFFICIENT',16X,F8.3,' Kcal/h/m2/ C'
    1)
     WRITE (6,86) AW
  86 FORMAT('WALL HEAT TRANSFER PARAMETER  ',18X,F8.3,' Kcal/h/m2/  C')
     WRITE (6,88) U1
  88 FORMAT ('U FROM CORRELATIONS     ',23X,F8.2,'  Kcal/h/m2/  C'
    1       ////////////)
C
     WRITE (6,90)
  90 FORMAT (20X,'************************************',/,20X,
    1          '  SIMULATED TEMPERATURE PROFILE',/,20X,
    1          '************************************',//)
     WRITE (6,92) NUM
  92 FORMAT (//,15X,'RUN NUMBER    ',I4,//)
     WRITE (6,94)
     DO III = 1, NNN, 25
     WRITE(6,96)VZ(III),VCT(III),VTCTR(III),VCTC(III),Pco(III),
    1          CONVCO(III)
```

```
  96 FORMAT(2X,F8.3,6X,F6.2,6X,F6.2,6X,F6.2,6X,F9.5,6X,F9.2)
  94 FORMAT (6X, 'Z',10X, 'T',11X,'T*',10X, 'Tc',14X,'Pco',11X,'Xco',/)
     end do
     CLOSE (6)
     END
C*************************************************************************
C              SUBROUTINE RUNGE
     SUBROUTINE RUNGE (EA,CORR1,AK1,AK3,AK4,X1,T,TC,P,NH2i,
    1     NT,ALPHA,NCO,NCOi,NH2,NC2H2,NC2H2i,NH2O,NH2Oi,OMEGA,Pt,NTi)

     IMPLICIT DOUBLE PRECISION (A-H,O-Z)
     REAL AK1,AK3,AK4,X1,T,TC,NH2i,NT,ALPHA,EA,CORR1,P,PT,NTi
     REAL NCO,NCOi,NH2,NC2H2,NC2H2i,NH2O,NH2Oi,OMEGA
     REAL RCO
     DOUBLE PRECISION KCO
C
C      EA = ACTIVATION ENERGY
C      AA = PRE-EXP. KIN. FACTOR
C      KCO = KINETIC PARAMETER
     AA= (-EA/T)
KCO=(0.4*60)*CORR1*EXP(AA)
C
C     CALCULATION OF RCO
     RCO=KCO*((NH2i-ALPHA*X1)/((0.0082*T)/PT)*(NTi+(1-ALPHA)*X1))
C
      NH2=(NH2i-ALPHA*X1)
      NCO=(NCOi-OMEGA*X1)
      NC2H2=(NC2H2i+X1)
      NH2O=(NH2Oi+OMEGA*X1)

c     Calculation of Partial pressure
      pcof=((abs(nco/nt))*P)**( 0.45)
      ph2f=((nh2/nt)*P)**(0.945)
c     model 1
      Rco=Kco*pcof*ph2f

c     model 2
c.....b=38.53
c     Deno=(1+b*pcof)
c     Rco=(Kco*pcof*ph2f)/deno

c     model 3
c.....b=19.32
c     Deno=(1+b*pcof)**2
c     Rco=(Kco*pcof*ph2f)/deno

c     model 4
c.....b=12.22
c     Deno=(1+b*pcof)**3
c     Rco=(Kco*pcof*ph2f)/deno
```

```
c      model 5
c.....b=4.6
c      Deno=(1+b*pcof*ph2f)
c      Rco=(Kco*pcof*ph2f)/deno

c
       DX1DZ=A*RCO
       DTDZ=(B1*RCO)-C*(T-TC)
       DTCDZ=D*(T-TC)
       DTRCO=DTCDZ*1
C      OUTPUT
       AK1=DX1DZ
       AK3=DTDZ
       AK4=DTCDZ
       ALEX1=DTRCO
       RETURN
       END
```

APPENDIX G.2. Program for estimation the heat of reaction

```
C    PROGRAM HEAT
C*************************************************************************
C
C       THIS PROGRAM IS USED FOR CALCULATE THE HEAT OF REACTION FOR
C       THE SYNTHESIS GAS CONVERSION TO HYDROCARBONS
C
C            UPDATE 02-15-97 Version 4.0
C
C       WE USED
C          AH1= MOLES IN (EACH REACTANT) * CP IN (AVERAGE) * (T2-T1)
C          AH2= MOLES (EACH PRODUCTS)*AH for(EACH PRODUCTS)
C          AH3= MOLES OUT (EACH PRODUCTS)* CP OUT (AVERAGE) * (T3-T2)
C
C                     AHR = AH1 + AH2 + AH3 (KJ/Kmol)
C
C*************************************************************************
C
    DIMENSION NC(50)
    REAL NC, NHCT
    REAL NTi,NT,NH2i,NCOi
    REAL MOL(6)
C*************************************************************************
C                INPUT DATA
C*************************************************************************
    WRITE (6,*) 'Experiment number'
    read (6,*) num
    write (6,*) 'Temperature gas in ( C )'
    read (6,*) tgin
    write (6,*) 'Temperature gas out ( C )'
    read (6,*) tgout
    write (6,*) 'Inlet gas flow rate (Liters/minute)'
    read  (6,*) flow
    WRITE (6,*) 'CO Conversion '
    read (6,*) Conv
C
C*************************************************************************
C    INITIAL VALUES
    TGIN=TGIN+273
    TGOUT=TGOUT+273
C*************************************************************************
C
C    OPEN FILE DATA2.TXT ( MOLES OF HIDROCARBONS FROM C1 TO C30 )
C
    OPEN (5, FILE = 'DATA6.TXT')
    REWIND (5)
    I=0
    NT=0
```

```
      DO 5 I=1,30
         READ (5,10) NC(I)
   10    FORMAT(16x,F19.17)
      NHCT=NHCT+NC(I)
    5 CONTINUE
C       RATIO H2/CO
      BETA=2.0
C      INLET MOLES
      NTi=FLOW*60.0/(0.082*298.0*1000.0)
      NT=NTi
C       INLET MOLES OF CO E H2
      NCOi=NTi/(1+BETA)
      NH2i=NCOi*BETA
c      CP GAS IN
      T1=tgin
      T2=298
      CPCO=30.842-(0.012839/2)*(T1+T2)+(2.78767e-05/3)*(T1**2+
     1     T1*T2+T2**2)-(1.271e-08/4)*(T1**3+T1**2*T2+T1*T2**2+T2**2)

      CPH2=27.14+(0.009274/2)*(T1+T2)-(1.381e-05/3)*(T1**2+
     1     T1*T2+T2**2)+(7.645e-09/4)*(T1**3+T1**2*T2+T1*T2**2+T2**2)
      CPMIN=NCOI*CPCO + NH2I*CPH2
C       AH1 = AH REACTANTS
      AH1= CPMIN*(T2-T1)
C       AHF1 = AH FORMATION REACTANTS
      AHF1=-110.54*1 + 0*NH2I
C*************************************************************************************
C
C      OPEN FILE XMOL.TXT ( MOLES OF CO,H2,CO2,AND H2O)
C
      OPEN (1, FILE = 'XMOL1.TXT')
      REWIND (1)
      DO 13 N = 1,5
            READ (1,1000) MOL(N)
 1000         FORMAT(16x,F15.12)
            SMOL=SMOL+MOL(N)
   13 CONTINUE
      CLOSE (1)
C
C     AH FORMATION OF THE PRODUCTS (HYDROCARBONS)
C
      HFC1=-74.85*0.07960
      HFC2=-84.68*0.00266
      HFC3=-103.85*0.01143
      HFC4=-126.15*0.00505
      HFC5=-146.44*0.00757
      HFC6=-167.19*0.00866
      HFC7=-187.78*0.00545
      HFC8=-208.477*0.00402
      HFC9=-229.147*0.00402
      HFC10=-249.82*0.00389
```

```
      HFC11=-270.487*0.0035
      HFC12=-291.157*0.00324
      HFC13=-311.827*0.00272
      HFC14=-332.497*0.00246
      HFC15=-353.167*0.00220
      HFC16=-373.837*0.00195
      HFC17=-394.507*0.00169
      HFC18=-415.177*0.00156
      HFC19=-435.847*0.00143
      HFC20=-456.517*0.00130
      HFC21=-477.187*0.00117
      HFC22=-497.857*0.00104
      HFC23=-518.527*0.00091
      HFC24=-539.197*0.00078
      HFC25=-559.867*0.00071
      HFC26=-580.537*0.00065
      HFC27=-601.207*0.00058
      HFC28=-621.877*0.00052
      HFC29=-642.547*0.00047
      HFC30=-663.217*0.00043

      SHFC=HFC1+HFC2+HFC3+HFC4+HFC5+HFC6+HFC7+HFC8+HFC9+HFC10+
     1
HFC11+HFC12+HFC13+HFC14+HFC15+HFC16+HFC17+HFC18+HFC19+HFC20+
     1
HFC21+HFC22+HFC23+HFC24+HFC25+HFC26+HFC27+HFC28+HFC29+HFC30

C     AH FORMATION OF THE PRODUCTS
      AHF2=(-110.54*0.0)+ (0.0*1.97)  +(-393.51*0.01167)
     1          + (-241.99*0.97774) + (SHFC)
C     AH2 = AH FORMATION (PRODUCTS - REACTANTS)
      AHF1=AHF1*1000
      AHF2=AHF2*1000
      AH2=(AHF2-AHF1)*NCOi*CONV/100.0
C*****************************************************************************************************
C
C     CALCULATION OF HEAT CAPACITY
C
C
C    CALCULATION OF HEAT CAPACITY OF THE HYDROCARBONS (OULET)
C
C       HYDROCARBON GAS PHASE
C
      T2=tgout
      T1=298
      cpc1=(25.36+(168.678E-04/2)*(T1+T2)+(713.121E-07/3)*(T1**2+T1*T2
     1+T2**2)-(408.371E-10/4)*(T1**3+T1**2*T2+T1*T2**2+T2**2))*NC(1)
      cpc2=(8.181+(161.465e-03/2)*(T1+T2)-(400.710e-07/3)*(T1**2+T1*T2
     1+T2**2)-(694.209e-11/4)*(T1**3+T1**2*T2+T1*T2**2+T2**2))*NC(2)
      cpc3=(-5.338+(310.239e-03/2)*(T1+T2)-(164.64e-06/3)*(T1**2+T1+T2
     1+T2**2)+(346.908e-10/4)*(T1**3+T1**2*T2+T1*T2**2+T2**2))*NC(3)
```

```
cpc4=(-1.78+(386.961e-03/2)*(T1+T2)-(193.255e-06/3)*(T1**2+T1*T2
1+T2**2)+(348.326e-10/4)*(T1**3+T1**2*T2+T1*T2**2+T2**2))*NC(4)
cpc5=(-3.411+(485.009e-03/2)*(T1+T2)-(251.94e-06/3)*(T1**2+T1*T2
1+T2**2)+(486.767e-10/4)*(T1**3+T1**2*T2+T1*T2**2+T2**2))*NC(5)
cpc6=(-4.738+(582.41e-03/2)*(T1+T2)-(310.64e-065/3)*(T1**2+T1*T2
1+T2**2)+(629.232e-10/4)*(T1**3+T1**2*T2+T1*T2**2+T2**2))*NC(6)
cpc7=(-5.619+(676.93e-03/2)*(T1+T2)-(363.95e-06/3)*(T1**2+T1*T2
1+T2**2)+(740.735e-10/4)*(T1**3+T1**2*T2+T1*T2**2+T2**2))*NC(7)
cpc8=(-7.477+(777.47e-03/2)*(T1+T2)-(428.442e-06/3)*(T1**2+T1*T2
1+T2**2)+(917.635e-10/4)*(T1**3+T1**2*T2+T1*T2**2+T2**2))*NC(8)
cpc9=(-8.386+(872.155e-03/2)*(T1+T2)-(482.164e-06/3)*(T1**2+T1*T2
1+T2**2)+(103.11e-09/4)*(T1**3+T1**2*T2+T1*T2**2+T2**2))*NC(9)
cpc10=(-9.30+(966.713e-03/2)*(T1+T2)-(535.09e-06/3)*(T1**2+T1*T2
1+T2**2)+(113.89e-09/4)*(T1**3+T1**2*T2+T1*T2**2+T2**2))*NC(10)
cpc11=(-11.24+(106.784e-02/2)*(T1+T2)-(600.95e-06/3)*(T1**2+T1*T2
1+T2**2)+(132.4e-09/4)*(T1**3+T1**2*T2+T1*T2**2+T2**2))*NC(11)
cpc12=(-12.18+(116.265e-02/2)*(T1+T2)-(654.55e-06/3)*(T1**2+T1*T2
1+T2**2)+(143.6e-09/4)*(T1**3+T1**2*T2+T1*T2**2+T2**2))*NC(12)
cpc13=(-13.15+(125.77e-02/2)*(T1+T2)-(708.69e-06/3)*(T1**2+T1*T2
1+T2**2)+(155.1e-091/4)*(T1**3+T1**2*T2+T1*T2**2+T2**2))*NC(13)
cpc14=(-14.95+(135.79e-02/2)*(T1+T2)-(772.74e-06/3)*(T1**2+T1*T2
1+T2**2)+(172.59e-09/4)*(T1**3+T1**2*T2+T1*T2**2+T2**2))*NC(14)
cpc15=(-15.97+(145.32e-02/2)*(T1+T2)-(826.97e-06/3)*(T1**2+T1*T2
1+T2**2)+(184.07e-09/4)*(T1**3+T1**2*T2+T1*T2**2+T2**2))*NC(15)
cpc16=(-17.07+(154.83e-02/2)*(T1+T2)-(880.61e-06/3)*(T1**2+T1*T2
1+T2**2)+(195.15e-09/4)*(T1**3+T1**2*T2+T1*T2**2+T2**2))*NC(16)
cpc17=(-18.72+(164.83e-02/2)*(T1+T2)-(945.0e-06/3)*(T1**2+T1*T2
1+T2**2)+(213.020e-09/4)*(T1**3+T1**2*T2+T1*T2**2+T2**2))*NC(17)
cpc18=(-19.57+(174.25e-02/2)*(T1+T2)-(997.55e-06/3)*(T1**2+T1*T2+T
12**2)+(223.64e-09/4)*(T1**3+T1**2*T2+T1*T2**2+T2**2))*NC(18)
cpc19=(-20.5+(183.732e-02/2)*(T1+T2)-(105.14e-05/3)*(T1**2+T1*T2+
1T2**2)+(235.09e-09/4)*(T1**3+T1**2*T2+T1*T2**2+T2**2))*NC(19)
cpc20=(-22.42+(193.82e-02/2)*(T1+T2)-(111.63e-05/3)*(T1**2+T1*T2+
1T2**2)+(252.93e-09/4)*(T1**3+T1**2*T2+T1*T2**2+T2**2))*NC(20)
cpc21=(-16.201+(1.9984/2)*(T1+T2)-(0.001186/3)*(T1**2+T1*T2+
1T2**2)+(2.391e-07/4)*(T1**3+T1**2*T2+T1*T2**2+T2**2))*NC(21)
cpc22=(-17.11+(2.09384/2)*(T1+T2)-(0.001173/3)*(T1**2+T1*T2
1+T2**2)+(2.51e-07/4)*(T1**3+T1**2*T2+T1*T2**2+T2**2))*NC(22)
cpc23=(-18.019+(2.18884/2)*(T1+T2)-(0.0012274/3)*(T1**2+T1*T2
1+T2**2)+(2.629e-07/4)*(T1**3+T1**2*T2+T1*T2**2+T2**2))*NC(23)
cpc24=(-18.928+(2.28384/2)*(T1+T2)-(0.0012818/3)*(T1**2+T1*T2
1+T2**2)+(2.748e-07/4)*(T1**3+T1**2*T2+T1*T2**2+T2**2))*NC(24)
cpc25=(-19.837+(2.37884/2)*(T1+T2)-(0.0013362/3)*(T1**2+T1*T2
1+T2**2)+(2.867E-07/4)*(T1**3+T1**2*T2+T1*T2**2+T2**2))*NC(25)
cpc26=(-20.746+(2.47384/2)*(T1+T2)-(0.0013906/3)*(T1**2+T1*T2
1+T2**2)+(2.986e-07/4)*(T1**3+T1**2*T2+T1*T2**2+T2**2))*NC(26)
cpc27=(-21.655+(2.56884/2)*(T1+T2)-(0.001445/3)*(T1**2+T1*T2+
1T2**2)+(3.105e-07/4)*(T1**3+T1**2*T2+T1*T2**2+T2**2))*NC(27)
cpc28=(-22.564+(2.66384/2)*(T1+T2)-(0.0014994/3)*(T1**2+T1*T2+
1T2**2)+(3.224e-07/4)*(T1**3+T1**2*T2+T1*T2**2+T2**2))*NC(28)
cpc29=(-23.473+(2.75884/2)*(T1+T2)-(0.0015538/3)*(T1**2+T1*T2+
```

```
     1T2**2)+(3.3433e-07/4)*(T1**3+T1**2*T2+T1*T2**2+T2**2))*NC(29)
      cpc30=(-24.382+(2.85384/2)*(T1+T2)-(0.0016082/3)*(T1**2+T1*T2+
     1T2**2)+(3.462e-07/4)*(T1**3+T1**2*T2+T1*T2**2+T2**2))*NC(30)

C
C      CALCULATION OF THE AVERAGE HEAT CAPACITY OF THE
C       HIDROCARBONS (OULET)
C
      cpC2H2=cpc1+cpc2+cpc3+cpc4+cpc5+cpc6+cpc7+cpc8+cpc9+cpc10+
     1    cpc11+cpc12+cpc13+cpc14+cpc15+cpc16+cpc17+cpc18+cpc19+cpc20
     1   +cpc21+cpc22+cpc23+cpc24+cpc25+cpc26+cpc27+cpc28+cpc29+cpc30

C
C    CALCULATIONS OF HEAT CAPACITY OF THE GAS SINTESIS (unreacted),C02
AND
C     H2O
C
      CPCO=30.842-(0.012839/2)*(T1+T2)+(2.78767e-05/3)*(T1**2+
     1    T1*T2+T2**2)-(1.271e-08/4)*(T1**3+T1**2*T2+T1*T2**2+T2**2)

      CPH2=27.14+(0.009274/2)*(T1+T2)-(1.381e-05/3)*(T1**2+
     1    T1*T2+T2**2)+(7.645e-09/4)*(T1**3+T1**2*T2+T1*T2**2+T2**2)

      CPH2O=32.24+(0.00192/2)*(T1+T2)+(1.055e-05/3)*(T1**2+
     1    T1*T2+T2**2)-(3.596e-09/4)*(T1**3+T1**2*T2+T1*T2**2+T2**2)

      CPCO2=19.774+(7.344E-2/2)*(T1+T2)-(5.602E-5/3)*(T1**2+
     1    T1*T2+T2**2)+(1.715E-8/4)*(T1**3+T1**2*T2+T1*T2**2+T2**2)
C
C     CALCULATIONS OF THE AVERAGE HEAT CAPACITY (CPM OUT)
C
C
      CPMout = (CPCO*MOL(1)+ CPH2*MOL(2) + CPCO2*MOL(3)
     1          + CPH2O*MOL(4)+ CPC2H2*MOL(5) )
C     AH3 = AH OF THE PRODUCTS
      AH3= CPMOUT*(T2-T1)*2
C       AHR = AH OF THE REACTIONS
      AHR= AH1+AH2+AH3
      AHRR = (AHR*0.2389)/(NCOi*CONV/100.0)
c     OUTPUT
      open (200, file='AHR')
      write (200,200)
  200 format (////,22x,'**********************************',/,22X,
     1              '       HEAT OF REACTIONS      ',/,22X,
     1              '**********************************'//)
      WRITE (200,202) NUM
  202 FORMAT (25X,'EXPERIMENT NUMBER',I5,//)
      write(200,204) NTi
  204 format('MOLES IN',32X,F10.6,'   Kmoles/h')
      WRITE (200,230) NCOi
  230 FORMAT('MOLES CO IN',29X,F10.6,'   Kmoles/h')
```

```
   WRITE (200,240) NH2i
240 FORMAT('MOLES H2 IN',29X,F10.6,'  Kmoles/h')
   write (200,250) CPMIN
250 format('CP GAS in (mean) ',18X,F15.6,'  Kj/kmol')
   write(200,210) CPMOUT
210 format('CP PRODUCTS (mean)',17x,f15.6,'  Kj/kmol')
   write (200,220) AHF1
220 format('AH FORMATION REACTANTS',12X,F15.5,'  KJ/kmol')
   wRITE (200,260) AHF2
260 FORMAT ('AH FORMATION PRODUCTS    ',8X,F15.5, '  Kj/Kmol')
   WRITE (200,290) AH2
290 FORMAT('AH FORMATION OF THE REACTIONS',5X,F15.5,'  KJ/h')
   WRITE (200,280) AH1
280 FORMAT ('AH REACTANTS             ',6X,F15.5,'  Kj/h')
   WRITE (200,300) AH3
300 FORMAT ('AH PRODUCTS          ',10X,F15.5, '  Kj/h')
   WRITE (200,310) AHR
310 FORMAT ('AH OF THE REACTION      ',9X,F15.5, '  Kj/h')
   WRITE (200,320) AHRR
320 FORMAT ('AH OF THE REACTION      ',9X,F15.5, '  Kcal/Kmol CO CO
  1NV h')

   CLOSE (200)
   END
```

IMAGE EVALUATION
TEST TARGET (QA-3)

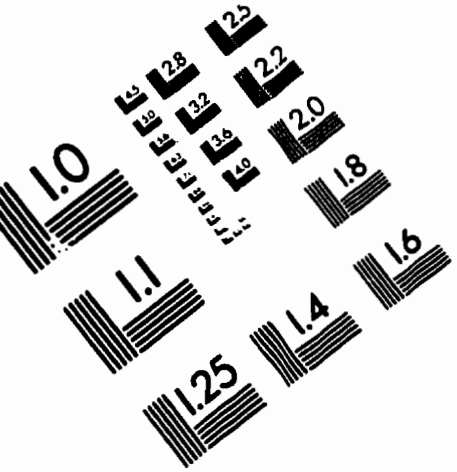

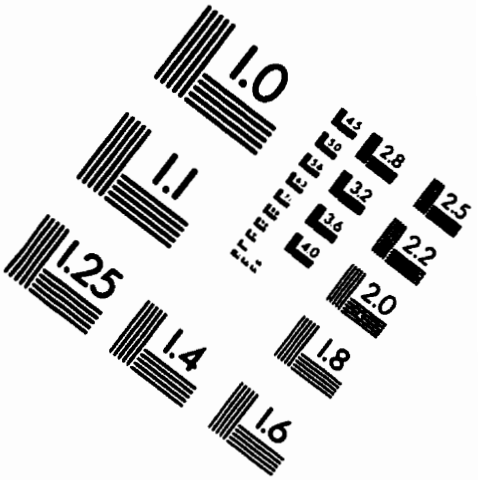

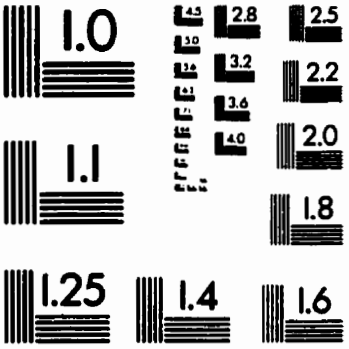

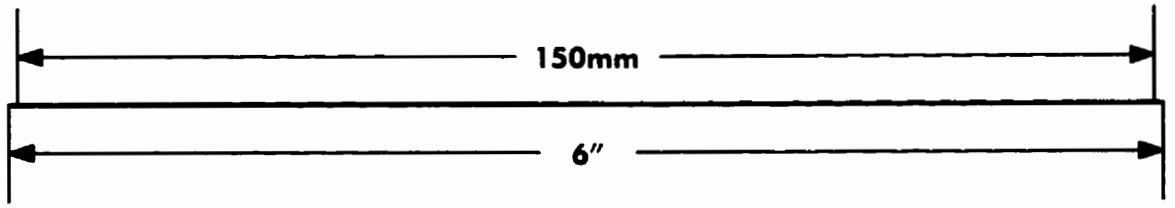

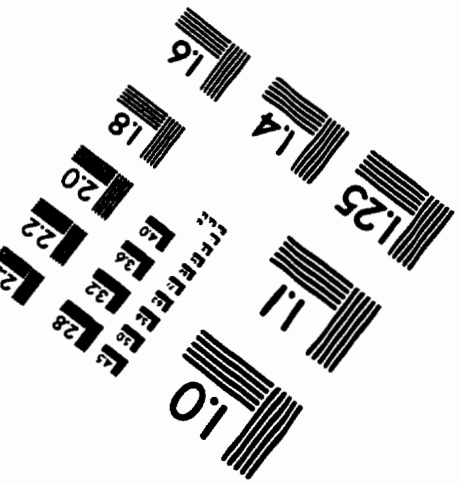

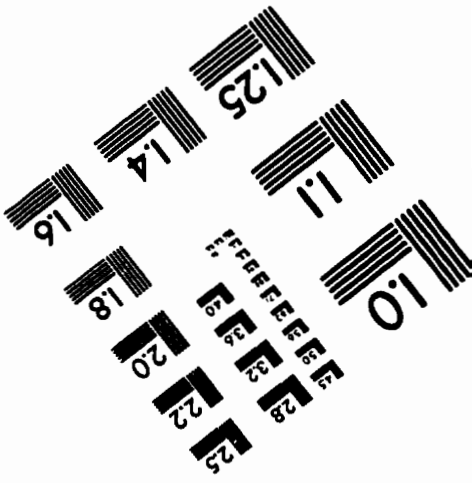

APPLIED IMAGE, Inc
1653 East Main Street
Rochester, NY 14609 USA
Phone: 716/482-0300
Fax: 716/288-5989